Title
Predictive Methods and Analysis of Time Dependent Tritium Flow Rates and Inventories in Fusion Systems

Author
riva, marco

Publication Date
2020

Peer reviewed|Thesis/dissertation

UNIVERSITY OF CALIFORNIA

Los Angeles

Predictive Methods and Analysis of Time Dependent Tritium Flow Rates and Inventories in Fusion Systems

A dissertation submitted in partial satisfaction
of the requirements for the degree
Doctor of Philosophy in Mechanical Engineering

by

Marco Riva

2020

ABSTRACT OF THE DISSERTATION

Predictive Methods and Analysis of Time Dependent Tritium Flow Rates and Inventories in Fusion Systems

by

Marco Riva
Doctor of Philosophy in Mechanical Engineering
University of California, Los Angeles, 2020
Professor Mohamed Abdou, Chair

In nuclear fusion reactors, tritium dynamics plays a dominant role. An unprecedented amount of tritium is consumed in Deuterium−Tritium (D−T) nuclear fusion reactors, ∼0.5 kg per day for 3 GW fusion power. However, tritium is radioactive, has short half-life (∼12.33 years), and is present in nature in negligible concentration. Because of tritium scarcity, future fusion power reactors must be self-sufficient, i.e. the reactor must have a closed fuel cycle where tritium is produced in greater amounts than it is consumed. Furthermore, nuclear fusion reactors must accumulate and provide tritium start-up inventory for the next generation of fusion power plants, since natural reserves of tritium are very limited. Moreover, because of its radioactive nature, tritium presents a serious hazard to the personnel and has implications to safety and nuclear licensing.

Accurate predictive models of the nuclear fusion fuel cycle are required to effectively design the fuel cycle components, understand tritium dynamics in the fusion fuel cycle, and determine the technology and physics requirements to attain tritium self-sufficiency. Moreover, accurate predictions of tritium inventories and flow rates within fusion components, and estimations of tritium releases to the environment are necessary for nuclear licensing. In this dissertation, two numerical models are developed to perform tritium transport assessment within fusion systems. First, a high fidelity numerical model is developed to simulate time-dependent tritium transport within the reactor outer fuel cycle (OFC). Detailed

(high resolution) component-level models, where constitutive transport equations are implemented in COMSOL Multiphysics and solved for various fusion sub-systems, are integrated into system-level with the use of MATLAB/Simulink S-Functions to reproduce typical OFC tritium streams. The model is applied to the KOrean Helium Cooled Ceramic Reflector Test Blanket System (KO-HCCR TBS) which will be tested in the International Thermonuclear Experimental Reactor (ITER). However, the developed model offers some flexibility and can be applied to other Test Blanket Module (TBM) designs. Second, the overall fusion fuel cycle is modeled analytically by a system of time-dependent zero-dimensional ordinary differential equations with the tritium mean residence time method. This technique yields results useful for understanding the overall fuel cycle dynamics and the importance of certain components and parameters. The analysis of tritium inventories and flow rates is extended to determine the physics and technology requirements to attain tritium self-sufficiency. In particular, the state-of-the-art plasma physics and technology parameters (e.g. tritium burn fraction, fueling efficiency, processing times, etc.) and up-to-date fuel cycle design are considered in the analysis. The tritium self-sufficiency assessment and tritium start-up inventory evaluation are performed to investigate: (i) the effect of the reactor operating scenario and availability factor, e.g. to account for random failures and ordinary maintenance, (ii) the scenarios for commercialization, e.g. risk associated with tritium reserve inventory reduction, (iii) the penetration of fusion energy into power market, e.g. effect of the doubling time, and (iv) the effect of reactor power on tritium start-up inventory, e.g. for plasma-based test facilities, DEMOnstration reactors (DEMO), and power reactors. The results highlight the physics and technology R&D requirements to attain fuel self-sufficiency in fusion reactors.

The dissertation of Marco Riva is approved.

Adrienne Lavine

Alice Ying

Laurent Pilon

Massimo Zucchetti

Mohamed Abdou, Committee Chair

University of California, Los Angeles

2020

To my family

TABLE OF CONTENTS

LIST OF FIGURES

LIST OF TABLES

ACKNOWLEDGMENTS

I wish to express my sincere gratitude to my advisor, Prof. Mohamed Abdou, for sharing his great experience with me, and encouraging and supporting me with enthusiasm and kindness. His knowledge and attention to details made me grow as a scientist and as a person, I am honored I had the chance to learn from him. I thank Dr. Alice Ying for sharing her experience on tritium transport modeling with me, and always being available for me. I am very grateful to all the members of my Doctoral Committee, Prof. Adrienne Lavine, Prof. Laurent Pilon, and Prof. Massimo Zucchetti, who contributed to improving the quality of my work with their brilliant suggestions and guidance.

Many thanks to Dr. Christian Di Sanzo and Dr. Mahmoud Youssef who taught me to use neutronics codes and perform neutronics analyses at the beginning of my journey at UCLA. In these years I shared amazing times with my lab mates and friends Dr. Jon Van Lew, Dr. Mahmoud Lotfy, Dr. Charles Kawczynski, Dr. Tyler Rhodes, Dr. Gautam Pulugundla, Dr. Jack Young, Yi Yan, Dr. Cyril Courtessol, and the other colleagues at Fusion Science and Technology Center, Dr. Neil Morley, Tom Sketchley, Dr. Hongjie Zhang. I also thank the staff members Esther Martinez, Michelle Schwartz, Erica Suh, Emily Hoffmann, and Arnoud Larousse for the kind support.

My greatest appreciation goes to my parents, Gabriella and Giuseppe, for their constant support and love which accompanied me during these years. I thank my brother, Davide, for always being there for me, in spite of the 6,000 miles that separate us. Thanks to all my friends in Italy who maintained our friendship despite the long distance between us. Finally, I am immensely grateful for Juliana for her unconditional support, love, and being the most amazing part of my life. To all these people, thank you, grazie!

This work was supported jointly by the U.S. Department of Energy Contract DE-FG03-ER52123 and by Task Agreement between UCLA-NFRI for Cooperation on R&D for Fusion Nuclear Science to Expedite the Realization of Magnetic Fusion Energy.

VITA

2008–2012 B.S. Energy Engineering, Polytechnic of Turin, Italy

2012–2014 M.S. Energy and Nuclear Engineering, Polytechnic of Turin, Italy

2015–2017 M.S. Mechanical Engineering, University of California at Los Angeles

PUBLICATIONS

- Marco Riva, Christian Di Sanzo, Mohamed Abdou & Mahmoud Youssef (2017), Reducing the Peak-to-Average-Power-Ratio in Fusion Blankets, Fusion Science and Technology, 72:3, 469-477
- Marco Riva, Alice Ying, Mohamed Abdou, Mu-Young Ahn & Seungyon Cho (2019), Impact of Outer Fuel Cycle Tritium Transport on Initial Start-Up Inventory for Next Fusion Devices, Fusion Science and Technology, 75:8, 1037-1045

CHAPTER 1

Introduction

Fusion nuclear power is considered the ultimate source of energy for mankind. D−T nuclear fusion consists in fusing nuclei of deuterium (D) and tritium (T) through the nuclear reaction 1.1 to gain a net amount of kinetic energy of 17.6 MeV per reaction (3.5 MeV carried by an α particle or ${}^4_2He$, and 14.1 MeV carried by a neutron n). The kinetic energy is then converted into heat which is extracted by a flowing coolant and used for electric production, e.g. through Rankine cycle.

$$D + T \longrightarrow \alpha\ (3.5\ \text{MeV}) + n\ (14.1\ \text{MeV}) \tag{1.1}$$

where 1 MeV $= 1.602 \times 10^{-13}$ J.

An unprecedented amount of tritium is burned in a fusion power plant. For instance, a 1000 MW_e ($\sim$ 3000 MW_t) power plant burns $\sim$ 170 kg/yr. The amount of tritium required to fuel a D−T fusion reactor is not comparable with the tritium which can be produced in fission reactors. It is estimated that $\sim$ 0.5 - 1 kg per year of tritium can be produced in Light Water Reactors (LWRs), when special designs for T production are implemented in the reactor system. Moreover, tritium production in LWRs is extremely expensive: \$84M − \$130M per kg[1]. Tritium is an unintended by-product produced by the D(n, γ)T reaction in Heavy Water Reactors (HWRs), e.g. CANada Deuterium Uranium (CANDU) reactors; however, production is limited to 130 g/yr [1]. Thus, external, non-fusion, supply of tritium cannot be the solution to provide the required tritium inventory to start new generation fusion reactors and maintain the reactor in operation throughout its life-time.

[1]per Department of Energy (DOE) Inspector General.

In fact, available tritium reserves are very limited ($\sim$27 kg peak in 2027 due to tritium accumulation in 40 years of CANDU reactor operations) and will be mostly consumed during the experimental campaign of the International Thermonuclear Experimental Reactor (ITER), which is under construction in Cadarache, France, and is projected to start D$-$T operation in 2036. If we consider that tritium decays with a half-life of 12.33 years, we can conclude that current T resources are irrelevant to serving as tritium initial start-up for DEMOnstration reactors (DEMO), which will be constructed in 20$-$30 years from now when tritium resources will be likely only a few kilograms. Thus, assuming we have a sufficient supply of tritium to start a nuclear fusion reactor, then the plant must have a closed fuel cycle, i.e. must be able to self-produce, recover, and process a sufficient amount of tritium within the reactor fuel cycle, and finally deliver it to the plasma to maintain steady operation. Therefore, fusion reactors must achieve fuel self-sufficiency. Not only should a fusion reactor self-sustain itself, i.e. produce at least the same amount of tritium that it consumes, but also it shall breed an extra amount of fuel, in a relatively short time, to compensate for potential tritium losses or radioactive decay, and to generate start-up inventories for future reactors. In particular, lithium is used to breed an adequate amount of tritium. Liquid lithium, eutectic lead-lithium, molten lithium salts, and solid lithium ceramics are proposed as candidate materials for tritium breeding in fusion breeding blankets [2]. For solid breeders, the ceramics are in the form of pebbles to allow tritium diffusion through the bed inter-porosity. In these lithium contained materials, tritium is bred through the reactions 1.2 and 1.3. Current lithium supply consumed in the breeding process described in Eqs. 1.2 and 1.3 is estimated to last for the next $\sim$ 20,000 years [3], by which time it is hoped that we will have learned how to achieve the less efficient, but tritium free, D-D fusion. After the release from pebbles, tritium is carried to the fuel cycle processing systems by a sweeping Helium purge gas. Thus, tritium is recovered and accumulated as fuel in the storage and fueling system.

$$^{6}_{3}Li + n \longrightarrow \alpha + T + 4.8MeV \tag{1.2}$$

$$^{7}_{3}Li + n \longrightarrow \alpha + T + n' - 2.5MeV \tag{1.3}$$

A schematic of a typical magnetic confined fusion reactor, i.e. the tokamak - or toroidal chamber in magnetic coils, with the aforementioned reactions of interest is shown in Fig. 1.1.

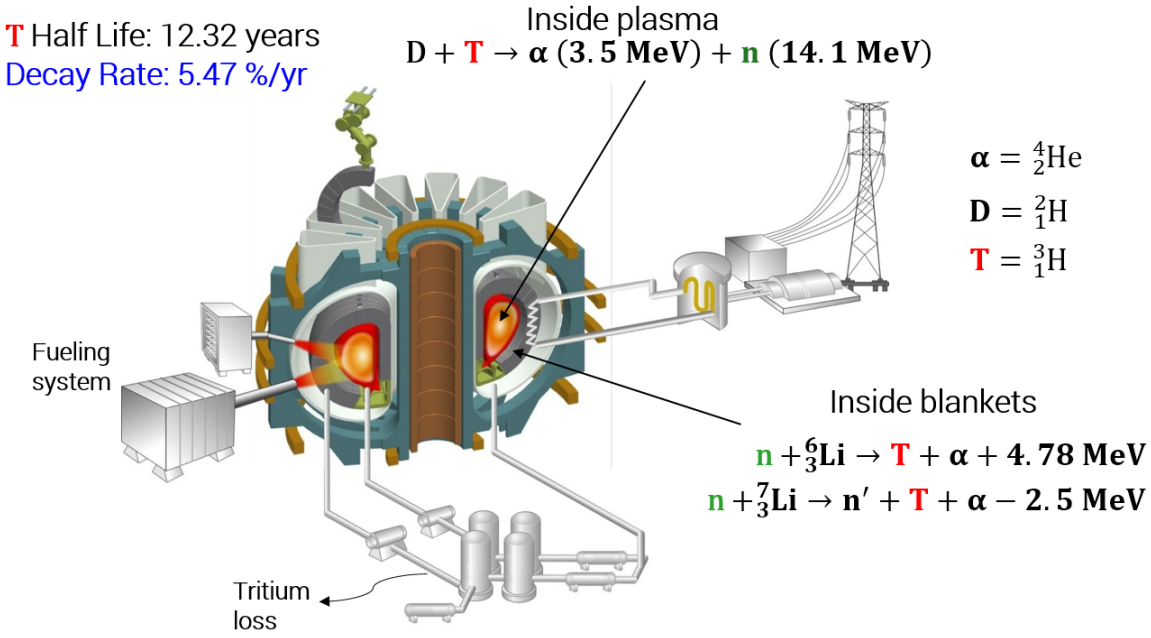

Figure 1.1: Typical tokamak reactor schematic with nuclear reactions of interest in plasma and blanket systems. Edited from [4].

At present, there are many uncertainties in assessing the required start-up inventory and self-sufficiency condition due to the complex dependence on plasma physics, fusion technology and design, nuclear data and modeling capabilities. A key aspect to assess the fuel self-sufficiency and start-up inventory and, therefore, define the tritium space phase of fusion reactors, is to determine tritium inventories and flow rates throughout the overall fuel cycle. Thus, accurate modeling of fusion plants fuel cycle is required.

Furthermore, tritium is a potential hazard: it is light, volatile, chemically reactive, and radioactive (particularly dangerous when inhaled and/or ingested due to beta minus de-

cay[2]). Tritium handling is, in fact, a very delicate task: major safety concerns and design implications arise in nuclear fusion reactors due to the tremendous volume of tritium generation and consumption. The existing tritium concentration gradient between fusion reactor components and external environment (outside the nuclear facility where the quantity of tritium dissolved in the environment is negligible) is the driving force for tritium to diffuse through structural material, e.g. bulk diffusion, and, eventually, permeate to reactor buildings (and potentially to the environment). Furthermore, tritium diffusion is strongly enhanced by the high temperatures characterizing the Plasma Facing Components (PFCs) and blanket Breeding Zone (BZ) of fusion power plants, where tritium is implanted from plasma and generated through n-Li reactions respectively. As a consequence, tritium can easily diffuse through structural materials, permeate to coolant channels of PFCs and BZ, and potentially permeate to the various rooms of the reactor building. The most important safety concerns regarding tritium transport within fusion systems are: (i) the estimation of tritium flow rates from component to component, (ii) the assessment of tritium inventory in fusion compartments, (iii) the prediction of tritium permeation to coolant systems, (iv) the chemical composition and concentration of tritium molecules in coolant and purge gas flow, (v) the tritium release to reactor buildings and environment. Moreover, determining the influence of these parameters on the requirements to attain fuel self-sufficiency, which is absolutely required, and accurately evaluating and minimizing the start-up inventory for fusion reactors of the first generation and beyond is of fundamental importance.

In light of the above, accurate predictions of time-dependent tritium transport, inventory, flow rates, permeation rates to environment, and the identification of parameters affecting tritium fuel cycle dynamics, reactor fuel self-sufficiency, and required initial start-up inventory, are fundamental in order to design, build, and operate fusion systems. Thus, extensive modeling effort and experimental campaigns must be conducted to develop accurate predictive capabilities which can simulate tritium evolution in realistic reactor-like conditions. This implies the identification of adequate mathematical formulations for tritium transport, com-

[2]In the beta minus decay a neutron is converted to a proton and an electron, or β^- particle, and an electron anti-neutrino, $\bar{\nu}_e$, are produced.

prehensive multi-physics modeling of complex fusion components (in detail and on reactor system-level), and extrapolation to start-up and self-sufficiency issues.

In this document an introduction to nuclear fusion systems and the scope of this research is given in Chapter 1. In Chapter 2 fuel cycle dynamic models available in literature for calculating time dependent tritium inventories and flow rates in fuel cycle components are described. Moreover, a summary of the main computer codes available to predict tritium evolution in fusion reactors and the mathematical formulation used to describe tritium transport within fusion system are extensively discussed. In Chapter 3, we present a new dynamic model to obtain accurate predictions of tritium transport in fusion outer fuel cycle[3]. This detailed model predicts tritium behavior in each component of the outer fuel cycle by solving constitutive transport equations with the use of COMSOL Multiphysics. Single components are then integrated to system-level, with the use of the MATLAB/Simulink software, to reproduce component-to-component tritium streams. The model is used to evaluate the permeation rates from coolant to the Port Interspace, Port Cell, and Vertical Shaft rooms of the ITER in the case of the Helium Cooled Ceramic Reflector Test Blanket System (HCCR TBS). Moreover, the effect of several parameters on the performance of the HCCR TBS is extensively discussed and analyzed in Chapter 4. In Chapter 5, the outer fuel cycle model is used to determine its impact on the initial tritium start-up inventory. Particular attention is paid to analyzing the performance of different tritium extraction system designs. In Chapter 6 an analytical model is developed to calculate inventories and flow rates of the components of the overall fusion fuel cycles (inner and outer fuel cycle) by using the mean residence time method. This analytical model offers lower fidelity compared to the detailed model developed for the outer fuel cycle in Chapter 3, but offers valuable insight regarding the overall performance of the fuel cycle and is useful to determining the R&D goals to attain tritium self-sufficiency and minimize the require tritium start-up inventory. To maintain appropriate accuracy, we use state-of-the-art plasma physics and technology parameters in the analysis. A summary of the main accomplishments of this research and future modeling work is given in Chapter 7.

[3]Inner and Outer fuel cycles are described in detail in Subsections 1.1.1 and 1.1.2

1.1 Nuclear Fusion Fuel Cycle

In Fig. 1.2 a schematic of the typical DEMO fuel cycle [2], which is subdivided into the Inner Fuel Cycle (IFC) and Outer Fuel Cycle (OFC), is shown. These sub-systems include many different components which are defined by different physics and perform different functions.

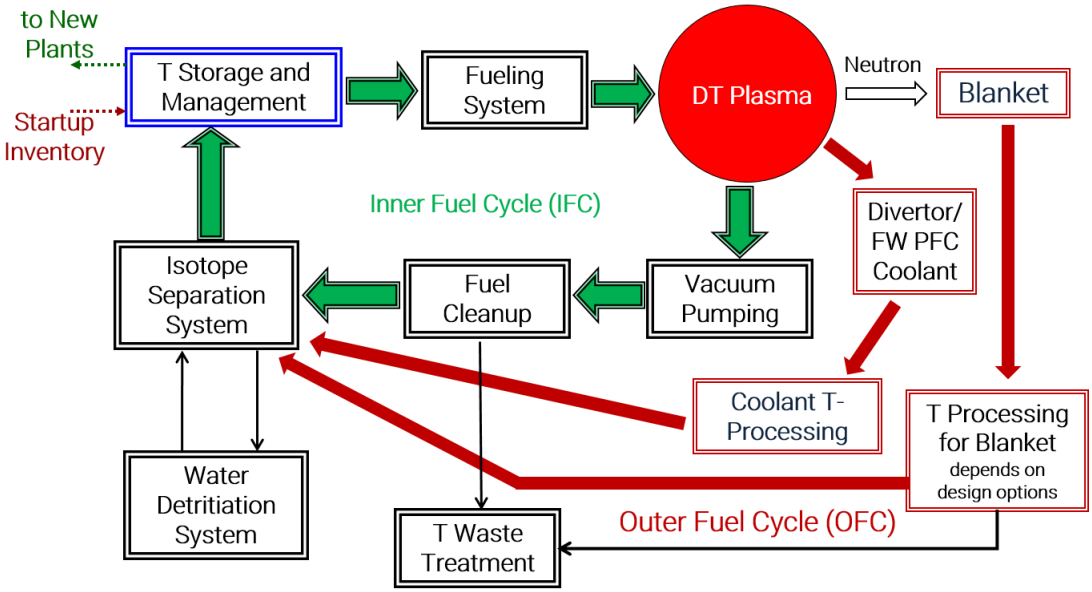

Figure 1.2: Schematic of the typical DEMO fuel cycle [2]. Components of the Outer Fuel Cycle (in red), i.e. PFC, blanket modules, coolant and blanket gas prossesing systems; components of the Inner Fuel Cycle (in black with green arrows), i.e. Vacuum Pumping, Fuel Cleanup, Isotope Separation and Water Detritiation Systems, Tritium Waste Management, tritium Storage and Management, Fueling system.

In the plasma, where hydrogen isotopes are magnetically confined by the electro-magnetic field generated through a series of toroidal and poloidal coils, and a central solenoid, the D−T reaction takes place. The tritium confinement time in plasma limited to $\sim$ 1 s, thus only a small fraction of the total tritium injected into the plasma chamber is able to fuse with deuterium during a specific confinement time, whilst the remaining fraction is exhausted through the divertor pump to the processing line of the inner fuel cycle. Then, after impurity removal, clean-up, and isotope separation, tritium is accumulated in the storage compartment.

As seen in the reaction 1.1, for every tritium nucleus burned, a neutron and an alpha

particle are produced. Alpha particles are positively charged and, therefore, confined in the plasma, where the their kinetic energy is converted into heat and contributes to maintaining the plasma at the required fusion temperature. On the contrary, the neutron, which is not confined by the magnetic field, reaches the plasma facing components (PFCs), i.e. first wall (FW) and divertor, and the blanket modules in the outer fuel cycle. Neutrons react with lithium in the breeding zones to generate tritium through the reactions 1.2 and 1.3. In particular, the tritium breeding ratio (TBR) is defined as the ratio of generation rate, $\dot{N}^{+}$, to the tritium burning rate $\dot{N}^{-}$ as shown in Eq. 1.4:

$$TBR = \frac{\dot{N}^{+}}{\dot{N}^{-}} \tag{1.4}$$

After generation in the blankets of the outer fuel Li-containing materials, tritium is extracted and processed in the tritium extraction system. Recovered tritium is then provided to the line of the inner fuel cycle.

The main components of the fusion fuel cycle are described in detail in Section 1.1.1 and 1.1.2. For the outer fuel cycle components, our description relates to solid breeder blankets concepts and extraction system for tritium removal from helium purge gas, which are modeled and analyzed in this work, although other concepts/technologies exists, e.g. liquid metal, molten lithium salts blankets, etc.

1.1.1 Inner Fuel Cycle

Due to the relatively low fueling efficiency and tritium fractional burn-up in fusion plasma, most part of tritium injected to the plasma is exhausted through the pumping duct to the processing line of the IFC. Impurities, such as Ne, Xe, Ar, which are added to plasma for control, while C and Fe particles which are present in the plasma due to plasma-matter interaction, are separated from D and T in the fuel clean-up system; different isotopes are separated with the use of the isotope separation system and accumulated in the storage and management compartment. Finally, deuterium and tritium are fed to the plasma chamber of the tokamak through the fueling system. A water detritiation system is generally connected

to the isotope separation system to treat contaminated water (tritium easily substitute hydrogen to generate tritiated water). In this section we describe the main technologies used in the IFC to re-process tritium. A more detailed description of these systems is available in [5].

1.1.1.1 Vacuum Pumping System

The vacuum pump performs extraction of fuel exhausts and impurities and transfers the gas mixture to the IFC systems for tritium re-processing. Main technology candidates for magnetic fusion devices are:

1. Cryosorption pump

   Sorption on cryogenic panels at 4 K is performed. It has the advantage of avoiding rotatory parts, which would interfere with the high magnetic field and reduce pumping efficiency. However, adsorption and regeneration phase is required, i.e. this systems work in batch-wise mode. This increases temporary tritium hold up in the pump, thus tritium is available for re-processing in downstream components after regeneration process. Depending on adsorption/regeneration dynamics, the tritium processing time and, therefore, the associated inventory in the component could increase. Thus higher tritium start-up inventory may be required to compensate for delay in exhausts recovery.

2. Turbo molecular pump

   High speed rotors are implemented to compress plasma exhausts and send the gases downstream. Due to the high magnetic fields present in the proximity of the plasma, ceramic rotors are being considered to reduce possible inefficiencies due to eddy currents generations. However, to obtain continuous operation and adequate capacity, very large rotors are necessary.

3. Roughing pump

   It is a supplementary system to the turbo molecular pump. Oil free pumps are preferable in order to avoid oil contamination due to T permeation and exchange with H

atoms.

1.1.1.2 Fuel Clean-up System

The plasma exhausts include D and T, water vapor, oxygen, carbon, and hydrocarbons generated via plasma-wall interactions, and various gases which are added to the plasma for control purpose, e.g. Ar, Ne. Hydrogen isotopes, present in molecular form Q_2 (e.g. H_2, D_2, T_2, HD HT, DT) or oxidized form Q_2O (e.g. H_2O, D_2O, T_2O, DTO, HTO), must be separated from the gas mixture before they are further processed in the Isotope Separation System, which requires high purity H gas. Thus, a *Pd-Ag* alloy is installed for H dissolution and permeation at high temperature ($\sim$ 700 K), while the other gases in the mixture do not dissolve nor permeate. Normally, the diffuser operates at ambient pressure to reduce T permeation, which is enhanced by the high temperature of the process. Tritium residuals are likely still present in the gas downstream of the diffuser, thus, further processing is performed with the use of a catalytic reactor packed with a platinum catalyst, which performs methane cracking (reaction 1.5) and water shift (reaction 1.6):

$$CH_4 \rightleftharpoons C + 2H_2 \tag{1.5}$$

$$H_2O + CO \rightleftharpoons CO_2 + 2H_2 \tag{1.6}$$

Finally, a palladium membrane is implemented to promote isotope exchange reaction between tritium impurities and H_2 as shown in reaction 1.7.

$$HTO + CH_3T + 2H_2 \rightleftharpoons CH_4 + H_2O + 2HT \tag{1.7}$$

Currently, in order to reduce carbon dust generated by methane cracking, an alternative technique based on ceramic electrolysis cell via membrane of yttrium-stabilized zirconium is being investigated and seems promising.

1.1.1.3 Isotope Separation System

After impurity removal from the exhaust gases in the fuel clean-up system the mixture has reached high purity in hydrogen isotope content, and the Q_2 stream is processed by the Isotope Separation System where cryogenic separation is performed to separate different H isotopes. Even if other separation techniques exist, e.g. gas chromatography, and thermal diffusion method, the cryogenic distillation method appears to be the preferable technology for fusion systems since it allows the treatment of huge amounts of flow rate with maintaining high separation factors.

In detail, a cascade of columns (∼3-5 m height, ∼ 0.05-0.1 m diameter for ITER) are adopted to treat streams coming from the clean-up systems ($H_2, D_2, T_2, HD, HT, DT$) and from the water detritiation system (H_2, HD, HT). Each column has a boiler at the bottom, a packed bed of adsorbent materials, e.g. Dixon Ring, in the center, and a condenser at the top to generate a Q_2 counter-current flow of liquid and gas phase. Because of the difference in the boiling point of hydrogen isotopes (∼20 K for H_2 and ∼25 K for T_2), higher boiling point isotopes, e.g. T_2, tend to accumulate at the bottom of the columns, in the boiler, whilst lower boiling point isotopes, e.g. H_2, are enriched at the top section, in the condenser.

Note that distillation column are well known and established technologies, however, extensive R&D is required when this technique is applied to realistic fusion technology scale. Main issues regarding the development of cryogenic systems are: (i) maintain low temperatures, (ii) the need of achieving high separation factors, and (iii) the necessity of minimizing the processing time to reduce local tritium inventory in the system.

1.1.1.4 Water Detritiation System

A considerable amount of tritiated water, e.g. HTO, and T_2O, is generated in the blanket systems and during tritium processing. Chemical exchange columns with organic catalyst are used for water purification and tritium removal through the exchange reaction:

$$HTO + H_2 \rightleftharpoons HT + H_2O \tag{1.8}$$

Other exchange reactions are possible, e.g. water vapor - hydrogen sulfide, and hydrogen - ammonia, but are unfavorable because of the production of chemicals HTS and NH_2T respectively.

1.1.1.5 Storage and Management System

A storage and delivery system (SMS) is required in any D−T nuclear fusion facility in order to accumulate and store tritium produced in the blankets and reprocessed in the inner fuel cycle. Furthermore, tritium inventories dissolved in fusion components are recovered through hot out-gassing process during reactor maintenance and, thus must be stored in apposite systems.

In general, tritium is stored in metal beds as hydride metals, e.g. with uranium, titanium, and zirconium, which dissociate and release hydrogen (or tritium) at high temperature, while they recombine and adsorb hydrogen at lower temperature for the same dissociation pressure. The most effective hydride currently used for tritium storage is uranium. However, for safety reasons related to the nuclear nature of uranium, nuclear regulation requirements, and the fact that fusion energy should be completely independent of and unrelated to typical nuclear fission fuels, other non-nuclear alloys are currently being developed, e.g. ZrCo, and seem promising.

1.1.1.6 Fueling System

Three main systems exist to perform plasma fueling: (i) neutral beam injection (NBI), (ii) pellet injection, and (iii) gas puffing. In a NBI, fuel particles are ionized, accelerated to energy > 1 MeV, neutralized, and injected into the plasma core. This method is also used for plasma heating via nuclei collisions and kinetic energy transfer. The pellet injection technology consists of a system of cylinders and pistons cooled by cryogenic helium where the fuel freezes, solidifies, and is shaped to the appropriate size ($\sim$ mm). Then pellets are accelerated to speed of $\sim$ km/s through centrifuge of gas gun technology. Potentially, a third acceleration technique, i.e. the rail gun, could accelerate particles to higher speed. The gas

puffing injection uses high speed electromagnetic valves installed into several different ports to provide homogeneous fueling to he plasma.

In the ITER all techniques will be tested while final DEMO strategy is under investigation, because of the higher DEMO power which translates into higher fuel flow rates and requires highest achievable fueling efficiency.

1.1.2 Outer Fuel Cycle

The Outer Fuel Cycle includes first wall, divertor, blanket modules, tritium extraction system and coolant purification systems. Tritium is directly produced from n-Li reactions 1.2 and 1.3 in the blanket modules, and recovered by using a sweeping purge gas through the porous ceramic structure of solid breeders (or by liquid metals in other blanket concepts). Part of the tritium produced in the BZ of blankets permeates to coolant loops; moreover, another source of permeation is given by high fluxes of particles that are implanted in into PFC from the plasma. In fact, in spite of the magnetic confinement of D and T in the plasma, high fluxes of particles, neutral and charged, are expected to reach the Scrape-Off Layer (SOL) region, where the magnetic field topology allows plasma-PFC interaction and consequent particle implantation in PFCs. Coolant and purge gas are treated within the Coolant Purification System (CPS) and Tritium Extraction System (TES) to recover tritium which will be further processed in the Isotope Separation system unit.

1.1.2.1 Plasma Facing Components: First Wall and Divertor

Plasma facing components (PFCs), such as the first wall (FW) and divertor, are any components which directly face the plasma. The most common structural material used for PFCs is a Reduced Activation Ferritic Martensitic steel (RAFM) with a tungsten coating layer on plasma side. The main functions of the PFCs are to (i) extract the heat generated through nuclear heating and bremsstrahlung radiation, (ii) serve as structural component to separate the plasma region from the blankets and the other outer vessel components, (iii) provide a first barrier for the radiation coming from plasma, and (iv) thermalize the 14.1

MeV virgin neutrons generated in the fusion reactors to lower energies to increase the ^{6}Li(n, α)T reaction rate. The divertor allows on-line removal of impurities and waste, e.g. helium ash, and tritium/deuterium nuclei which lose confinement and enter the SOL region.

1.1.2.2 Breeding blankets characteristics and functions

Breeding blankets with integrated first wall are one of the most critical components of nuclear fusion reactors. Blankets play a key role in fusion technology by performing: (i) tritium breeding, (ii) power multiplication and extraction, and (iii) radiation shielding.

D−T fusion fuel cycle is considered closed, assuming the reactor generates at least the same amount of tritium (see reactions 1.2 and 1.3) which is consumed in the fusion reactions. Ideally, for each tritium consumed in the reaction 1.1, i.e. for each neutron produced, a tritium atom can be breed from ^{6}Li of reaction 1.2. However, due to parasitic neutron absorption in structural material, neutron and tritium losses, a neutron multiplier is generally required to increase neutron flux intensity in the blanket and, therefore, increase tritium production. Best candidates for neutron multiplication, reaction (n, 2n), are beryllium and lead; particularly, multiplication reactions are

$$^{9}_{4}Be + n \longrightarrow 2\alpha + 2n - 1.8MeV \tag{1.9}$$

$$^{208}_{82}Pb + n \longrightarrow ^{207}_{82}Pb + 2n - 7MeV \tag{1.10}$$

It is noticeable that both reactions have an energy threshold, i.e. multiplication is possible only for interaction with fast neutrons ($\sim$ MeV). Furthermore, energy multiplication for Pb is lower that Be, because off a much higher energy threshold. Reaction $^7_3$Li(n, n', α)T generates a T atom and a thermal neutron that can potentially interact again with lithium 6; for this reason, and to reduce the cost of enriched fuel, ^{6}Li enrichment in ceramics varies from 40% to 90% depending on the blanket design.

While interacting with lithium to breed tritium, the neutron kinetic energy is converted

into heat and deposited within the blankets. Moreover, exothermic reactions, e.g. reaction 1.2, and photon heat deposition in structural material, where the photons are generated through neutron interaction with structural materials such as inelastic scattering and radiative capture reactions[4], contribute to multiplying energy within the system. This power must be extracted at high temperature for energy conversion. Finally the FW/Blankets represent the first radiation shield of the Vacuum Vessel and they are a physical boundary for the plasma.

The breeding blankets reside in an hostile nuclear and multiple-field environment. Nuclear radiation damage is caused by a remarkably hard neutron spectrum ($\sim$ 8 order of magnitude higher than fission LWRs or HWRs and $\sim$ 6 order of magnitude higher of Generation IV fast fission reactors). Blankets are characterized by the presence of sharp volumetric nuclear heat, temperature, and species concentration gradients and are subject to high magnetic field and temperature which cause considerable thermo-mechanical stresses.

As an example, we show in Fig. 1.3 the Korean Helium Cooled Ceramic Reflector (HCCR) concept [6], which will be one of the ITER Test Blanket Module (TBM) within the Test Blanket System (TBS). It is based on the ceramic pebble bed concept: the breeding ceramic

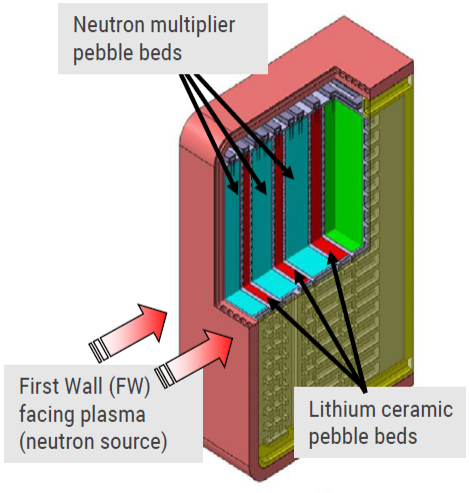

Figure 1.3: KO-HCCR ceramic breeder blankets, first wall, breeder and multiplier zones.

[4]Radiative captures reactions (n, γ) are characterized by the absorption of one neutron in the target atom and the generation of a gamma ray.

material, e.g. Li_2TiO_3 or Li_4SiO_4, and neutron multiplier, e.g. Be or $Be_{12}Ti$, in the form of pebble beds, are organized in alternating layers (sandwich configuration). A layer of graphite is positioned in the back of the module to reflect the neutrons towards the breeding region, thus, increase tritium breeding and reduce neutron radiation. Helium at low pressure ($\sim$atm) flows through the interconnected porosity of ceramic breeder and neutron multiplier the pebble beds as purge gas to extract tritium. A 0.1% vol of H_2 is typically added to the He purge gas to enhance tritium release from pebbles, in the form of HT or, rarely, T_2. Helium at high pressure ($\sim$MPa) is used as coolant in the channels of the Advanced Reduced Activation Alloy (ARAA) blanket structure. The breeder operates within a temperature window of 550 - 950 ^{o}C to enhance tritium diffusion and increase the power plant thermal efficiency; in particular, tritium residence time strongly depends on temperature and determines tritium inventories in blankets. The HCCR TBM will be used for current Dissertation modeling and development within the ITER TBS as well as Korean DEMO design.

1.1.2.3 Tritium Extraction System and Coolant Purification System

Tritium contained in He purge gas and He coolant is recovered by the tritium extraction system (TES) and coolant purification system (CPS). Tritium is mainly present in the Q_2 from, e.g. HT and T_2; however, a small amount tritium in water vapor form Q_2O, e.g. HTO and T_2O, is found because of the presence of oxygen in the lithium ceramics or if water is chosen as coolant. In both cases the main technologies adopted for tritium recovery from purge gas and coolant are (i) cryosorption, and (ii) permeation reactors.

The cryosorption process is performed in columns of porous synthesized zeolite beds. Tritium molecules carried by the He purge gas in the form of HT and T_2 are selectively adsorbed by the zeolite which is kept at cryogenic temperature by liquid nitrogen. When the bed has reached saturation of H and T content, the regeneration process performed at higher temperature enhances tritium and hydrogen desorption and recovery. Note that the efficiency of adsorption process depends on the content of H_2 in the purge gas; whether high H_2 concentration enhances tritium release from ceramics, it also complicates tritium

recovery in downstream systems. Similar techniques are used to treat HTO and T_2O; room temperature molecular sieve beds are used in this case. This technique is the known and available since it was use in other industries, e.g. oil and gas, as well as in fusion experimental facilities, e.g. JET, and are the principal choice for many TBS in ITER. However, the batch-wise mode of operation implies an increased tritium hold-up and has implications to safety. Thus, "on-line" continuous operation technologies, which minimize tritium inventory, are under investigation for future DEMOnstration power reactors. The permeation reactor with palladium diffuser used in the fuel clean-up unit of the inner fuel cycle is a candidate for on-line tritium extraction. However, its applicability to blanket system is object of debate since the tritium partial pressure in the helium purge and coolant gas are considerably lower than that in the plasma exhausts. Thus, this process may have low efficiency and should be further developed.

1.2 Objective and Scope

To predict the behavior, improve the design, and optimize the performance of tritium fuel cycle, a detailed description of the fuel cycle components is required. In this work, several components the outer fuel cycle (e.g. first wall, breeding zones, connecting pipes, etc.) are modeled in detail in COMSOL Multiphysics [7]. In particular, a rigorous mathematical model based on time dependent mass species, fluid momentum, and energy conservation constitutive equations is implemented. The models reproduce complex geometries of fusion components and prototypical fusion conditions (e.g. gradients, transients due to pulsed operation, etc.) to evaluate tritium transport in fusion components. Furthermore, a system-level model which connects the detailed component models in order to reproduce the tritium streams in the outer fuel cycle is developed in the MATLAB/Simulink environment [8]. In this work, we apply this model to the HCCR TBS in order to estimate tritium inventory in components and releases to ITER buildings. However, the same methodology can be applied to other test blanket systems, e.g. liquid-metal, and molten salt blanket concepts.

The system-level dynamic model developed for HCCR TBS is useful to provide detailed

analyses which are necessary to improve the design of specific components. However, for a more comprehensive analysis of the overall fuel cycle (including inner and outer fuel cycles), which aims to describe the overall fusion R&D requirements (e.g. in regards to attaining tritium self-sufficiency), a high level of detail is not necessary and would impact on the computational performance; thus, in this case, a different approach is preferable. In this research, a dynamic model of the overall fuel cycle is developed by using the tritium mean residence time [2, 9, 10]. In particular, the model accounts for several features that were not included in previous models, e.g. tritium processing time, tritium fueling efficiency and burn fraction, reactor availability factor, power level, etc. The analysis of tritium inventories and flow rates in the fuel cycle is extended to determine the R&D requirements to attain tritium self-sufficiency in fusion reactors and evaluate the required tritium start-up inventory.

References

1. M. Kovari *et al.*, 2018 Nucl. Fusion 58 026010

2. Abdou, M., Morley, N.B., Smolentsev, S., Ying, A., Malang, S., Rowcliffe, A., Ulrickson, M., Blanket/First wall challenges and required R&D on the pathway to DEMO, Fusion Engineering and Design, 100:2-43 (2015)

3. J. P. Freidberg. Plasma Physics and Fusion Energy. Cambridge University Press, 2007

4. https://www.iter.org/newsline/255

5. Tetsuo Tanabe, "Tritium: Fuel of Fusion Reactors", Interdisciplinary Graduate School of Engineering Sciences Kyushu University Fukuoka Japan, DOI 10.1007/978-4-431-56460-7

6. Seungyon Cho *et al.*, Fusion Engineering and Design, Volume 136, Part A,2018, Pages 190-198

7. COMSOL/Livelink: COMSOL Multiphysics with MATLAB v. 5.0. COMSOL, Inc., Burlington, MA. 2015 Livelink for MATLAB, COMSOL, Inc., Burlington, MA. 2015

8. Simulink Developing S-Functions, MATLAB & SIMULINK, R2017a, MathWorks, Inc.

9. M. ABDOU et. al., "Deuterium-Tritium Fuel self-sufficiency in Fusion Reactors", Fusion Technology, 9, 250-285 (1986)

10. M. Sawan, M. Abdou, "Physics and Technology Conditions for attaining Tritium self-sufficiency for the DT Fuel Cycle", Fusion Engineering & Design, 81 (8-14), 1131-1144 (2006)

CHAPTER 2

Literature Review

A great deal of work on tritium fuel cycle dynamic modeling is reported in literature. In a pioneering study published in 1986 by Abdou *et al.*, the authors developed an innovative methodology known as mean residence time method to compute inventories and flow rates in fusion system [1]. In this model, each component of the tritium fuel cycle is described by an ordinary differential equations, and the formulation is based on the assumption that tritium resides in each component for a characteristic residence time before it is released. In this research, findings were extrapolated to determine the conditions to achieve fuel self-sufficiency, which the authors defined as $\mathrm{TBR}_a \geq \mathrm{TBR}_r$, where a stands for achievable and r required. The achievable and required TBR have different meanings, definitions, and depend on different parameters. On the one hand, the TBR_a is defined as the ratio of tritium production rate in blankets to the tritium burning rate in plasma, $\dot{N}^+/\dot{N}^-$, and depends on fusion blanket design, technology, materials (lithium form and neutron multipliers), and physics. There are uncertainties associated with the system definition, nuclear data and numerical approximations, e.g. complex geometry effects and lack of nuclear cross sectional data for high energy neutrons ($\sim$ 10 MeV), that affect TBR_a estimations. On the other hand, the TBR_r is the result of the entire fuel cycle dynamics and, therefore, depends on overall reactor system design, technology and plasma physics, e.g. fueling efficiency η_f, tritium burn fraction f_b, processing time(s), etc. The TBR_r is required to exceed unity by a margin in order to (i) compensate for tritium losses by radioactive decay, (ii) supply tritium inventory for start-up of other reactors, and (iii) provide a "reserve" storage inventory necessary for continued reactor operation in case of failure in tritium processing line. The methodology developed in [1] was very successful and used in several studies to model the tritium fuel

cycle of various fusion reactors and analyze tritium self-sufficiency [2, 3]. The same authors of [1] further improved the methodology and expanded the analyses in several researches [4 - 6].

Starting from the '90s, thorough mathematical models describing tritium transport in material bulk and dissociation/recombination behavior at gas/structure interface were derived and validated by experimental campaigns [7 - 10]. A great effort in developing predictive models to better understand tritium transport in sub-components of fuel cycle was launched in the last thirty years. On the one hand, several tritium mapping codes were developed to evaluate tritium time evolution on system-level. These models simulate the dynamics of the entire fuel cycle by solving constitutive heat and mass transfer equations, which provides higher level of detail compared to the mean resident time approach derived in [1]; however, geometries are limited to a 1-dimensional description. Examples of these codes are the TMAP4/TMAP7 [11] developed at the Idaho National Laboratory (INL) and the FUS-TPC code [12] generated at the Karlsruhe Institute of Technology (KIT). On the other hand, detailed modeling and analyses of 2-D and 3-D fuel cycle components, e.g. blanket, first wall, tritium extraction system, etc., was performed separately, outside the system-level, with the use of PDEs commercial solvers based on the Finite Element Method (FEM) and/or Finite Volume Method (FVM). Examples of these models are available in [13 - 16] for the HCCR TBM. Most of these models use multi-physics approach, where constitutive equations are coupled in order to account for realistic fusion conditions (e.g. sharp gradients in temperature and tritium concentrations in structural material of components) and more detailed and complex geometry definition.

In the following sections the mathematical formulation of some of the tritium transport predicting tools described is given. This literature review highlight some of the advantages and deficiencies of the various available numerical techniques.

2.1 Dynamic Modeling of Fusion Fuel Cycle

The first paper describing the dynamic of the nuclear fusion fuel cycle was published in 1986 by Abdou *et al.* [1] and represents the primary reference in the field. It is a comprehensive paper that introduces the mean residence time method, derives a mathematical model describing the fuel cycle, evaluates tritium inventories and flow rates in fusion components, and explore the conditions required for achieving tritium self-sufficiency. In this work, the entire fuel cycle dynamics was modeled using a system of first-order linear differential equations, which made use of the average tritium residence time in various sub-systems to simulate tritium dynamics and compute tritium inventories in components. In particular, the differential equations derived for the fusion components have the form:

$$\frac{dI_i}{dt} = \sum_{j \neq i} \left(\frac{I_j}{\tau_j} \right)_i - (1 + \epsilon_i) \left(\frac{I_i}{\tau_i} \right) - \lambda I_i + S_i \tag{2.1}$$

where i indicates the component of interest, j the components connected to component i, I the tritium inventory, τ_i the tritium mean residence time, $(I_j/\tau_j)_i$ the tritium flow rate from component j to component i, (I_i/τ_i) and $i \neq j$, the tritium flow rate out of component i, S_i a tritium source term, and ϵ and λ the non-radioactive and radioactive losses respectively. The model was derived for all components defining the whole fuel cycle shown in Fig. 2.1.

Furthermore, in the model the authors defined the doubling time, t_d, as the time which is required for the fuel storage compartment inventory, I_5, to reach a value equaling the sum of the initial inventory, I_5^0, and the minimum or reserve inventory, I_5^m, that is:

$$I_5(t_d) = I_5^0 + I_5^m \tag{2.2}$$

where the reserve inventory is defined as the product of the tritium injection rate and the reserve time, t_r, i.e. the number of days required to supply fuel to the plasma while the plasma exhaust processing system is not available, and the initial inventory, I_5^0, is the sum of this reserve inventory and the equilibrium inventories in all reactor components. Another

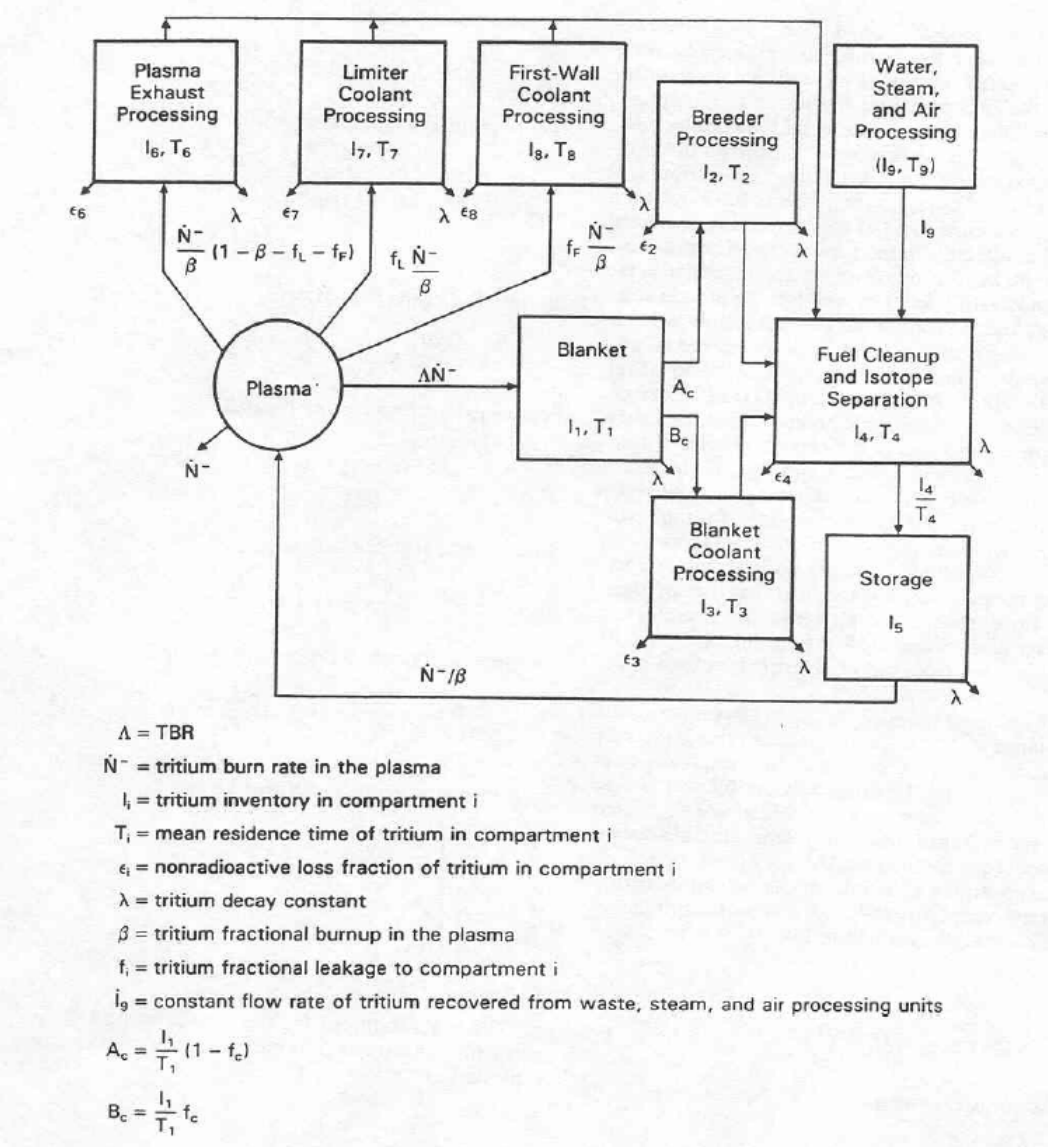

Figure 2.1: Schematic of the fuel cycle for a D−T fusion reactor used in [1].

definition of t_d commonly used in literature and addressed in the same paper is:

$$I_5(t_d) = 2I_5^0 \tag{2.3}$$

This study showed that fuel self-sufficiency assessment is a very complex problem because of the variety of plasma physics and fusion reactor technology parameters involved in the calculation, e.g. tritium burn fraction in plasma, tritium residence time, tritium reserve time, tritium doubling time, etc. In the last 30 years, several other researchers applied the

methodology developed in [1] to model the fuel cycle of specific fusion reactors, e.g. the China Fusion Engineering Test Reactor (CFETR) [2, 3]. In [4] Kuan and Abdou proposed a new approach to evaluate self-sufficiency condition and derived a more detailed formulation for the tritium start-up inventory. In particular, they integrated the analytical model of [1] with numerical results and experimental data regarding sub-components of the tritium processing systems, e.g. Impurity Separation System (ISS), and confirmed the results of [1]. Other results were also published in [5, 6].

The described models represent useful tools to describe the overall fuel cycle dynamics and offer valuable insights to defining the necessary fusion fuel cycle R&D. However, as fusion technology evolves, new features must be included in the models and the effect of different designs and parameters must be evaluated in the analyses. For instance, most part of the aforementioned models assume steady state reactor operation and ignore downtime due to random failure of scheduled maintenance, i.e. they assume an overall reactor availability factor of 100%. Thus, they neglect those times for which there is no tritium production in the fusion reactor, but tritium decays due to radioactivity. This implies that requirements on TBR could be very demanding in case of low plant availability. This if of particular concern in light of the results presented in a comprehensive paper [17], by Abdou *et al.* In particular, it was found that the availability factor of fusion reactors is expected to be particularly low in near term experimental fusion facilities fusion reactors, e.g. <30%. The analysis was based on data extrapolation from aerospace and fission industry. To conclude, there is a need of developing models that can account for state-of-the-art parameters, up-to-date fuel cycle design, and realistic reactor operational scenarios, e.g. downtime due to random failures and ordinary maintenance of various components, and their effect on the fuel cycle performance evaluated.

2.2 Tritium Transport Modeling in Fusion Systems

Tritium transport in the bulk of a solid structural material is governed by the diffusion of molecules (ceramics) or atoms (metals) in the lattice. Ricapito *et al.* [18] proposed a

comprehensive mass concentration conservation equation describing tritium dynamics in the bulk of a material with atom trapping in lattice damages:

$$\frac{\partial c_s}{\partial t} + \sum_k \frac{\partial c_s^k}{\partial t} = -\nabla \cdot \mathbf{J}_s + S_s - \lambda_s c_s - \lambda_s \sum_k c_s^k + \sum_m \left(c_m^s + \sum_k c_m^{s,k} \right) \lambda_m^s \tag{2.4}$$

where c_s = concentration of species s, c_s^k = concentration of species s in k trap, $\mathbf{J}_s$ = diffusive flux, S_s = local source rate (T generation in breeders or ion implantation in PFC), λ_s = species s decay constant, λ_m^s = decay constant of species m decaying into species s, c_m^s = concentration of atoms of species m that decay into species s, $c_m^{s,k}$ = concentration of atoms of species m in k trap that decay into species s. The diffusive term, $\nabla \cdot \mathbf{J}_s$, includes the so-called Soret effect, i.e. particle flux due to thermal gradient which is, in fusion systems, of the same order of the flux due to species concentration gradient, defined by the Fick's law. The divergence of the flux can be written as:

$$\nabla \cdot \mathbf{J}_s = \nabla \cdot \left[-D_s \left(\nabla c_s + c_s \frac{Q^*}{k_b T^2} \nabla T \right) \right] \tag{2.5}$$

and D_s is the diffusion coefficient of species s in the material, Q^* the heat of transport, k_b the Boltzmann constant, and T the temperature. The transport equation for mass can be solved to determine time-dependent concentration of hydrogen isotopes in the material. However, appropriate boundary conditions must be defined, that is, accurate representation of gas/surface interaction, i.e. gas molecules dissociation to atom form and absorption into structural material and atoms desorption, and recombination to molecular form at the gas/surface interface, must be provided. For this matter, Pick and Sonnenberg presented in [19] a detailed kinetic model for molecular/atomic hydrogen-metal interactions. Particularly, with referring to Fig. 2.2 showing the gas (or vacuum in this case) and metal interface, several hydrogen fluxes were defined:

- incident flux, f_1;
- out of surface to gas flux, f_2;

- from surface into the bulk flux, f_3;
- from the bulk to the surface flux, f_4;
- into the bulk flux due to concentration gradient, f_5.

these are, in turn, function of several parameters:

- H_2 molecules flux impinging on the surface, $\Gamma = \Gamma(p)$, and p pressure;
- sticking probability, s, i.e. the probability that hydrogen molecules impinging on the surface will dissociate and resulting hydrogen atoms will stick to the surface in chemisorption sites;
- Surface coverage, θ, i.e. the atomic fraction of hydrogen atoms to surface atoms;
- α, β, δ rate constants.

Particularly, α, β, δ, s depend on potential activation energies, e.g. dissociation E_C, absorption into bulk E_A, bulk to surface E_B, desorption for H atom E_D, bulk diffusion E_{diff}, with Boltzmann exponential law $\alpha = \alpha_0 exp(-2E_A/kT)$, $\beta = \beta_0 exp(-2E_B/kT)$, $\delta = \delta_0 exp(-2E_D/kT)$, $s = s_0 exp(-2E_C/kT)$, and α_0, β_0, δ_0, s_0 are constants. Equations for surface and bulk concentration can be obtained by balancing these fluxes. In particular, the authors of [19] found that, at equilibrium, the concentration of species s at the gas/surface interface can be expressed by the Sieverts' Law:

$$c_s = K_s p_m^{1/2} \tag{2.6}$$

where K_s is the Sieverts' constant, and p_m the partial pressure of the gas molecule m at the interface with the metal surface. Thus, for this specific case, the atom flux at the gas/metal interface shows a square root dependency with the pressure ($J_s \propto p_m^{1/2}$). This case is known in literature as diffusion-limited regime, since atom diffusion process through bulk is the limiting factor, whilst surface phenomena take place on shorter time scales.

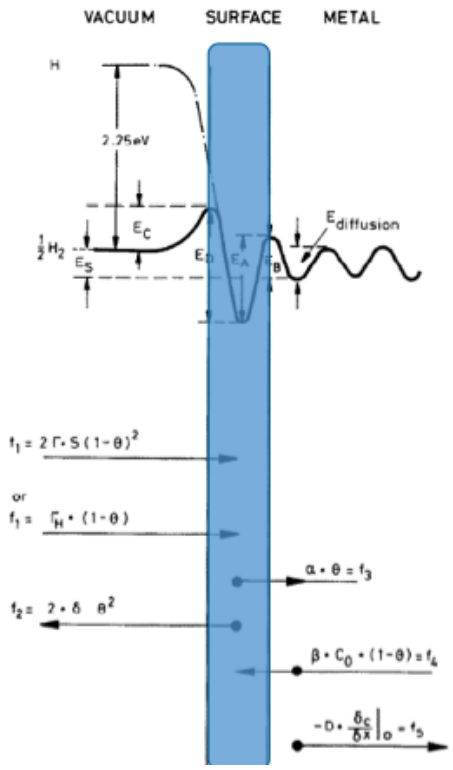

Figure 2.2: Schematic hydrogen fluxes at interface vacuum/surface - metal presented in [19]

In other situations, the surface effects can be dominant, e.g. in case of oxidation or contamination at the surface. For this case, i.e. the surface-limited regime, the atomic flux at the gas/structure interface has linear dependency with the partial pressure of the molecule in the dissolved in the gas ($J_s \propto p_m$), as shown in several experimental results [7 - 10]. The atomic flux at the surface is expressed as:

$$J_s = \sum_{m=1}^{k} a_{m_s} K_{d_m} p_m - \sum_{m=1}^{k} a_{m_s} \sum_i \sum_j K_{r_{i,j}} c_i c_j \tag{2.7}$$

where J_s = atom flux of atomic species s into the surface, a_{m_s} = number of atoms of species s in molecule of species m, K_{d_m} = dissociation coefficient for molecular species m at the surface, $K_{r_{i,j}}$ = recombination coefficient for molecular species m which consists of atomic species i and j (e.g. $s_i + s_j = m_{ij}$), p_m = partial pressure of molecular species m, c = concentration of atoms i and j which generate the molecule m. Not that the dissociation and recombination coefficients can be written as $K_{d_m} = 2\sigma k_{d_m}$, and $K_{r_{i,j}} = 2\sigma k_{r_{i,j}}$, to include

the surface roughness factor σ, i.e. the ratio of the real area to the geometrical area of the surface.

Eq. 2.7 accounts for the co-presence of various different molecules m dissolved in the gas, e.g. H_2, HT, T_2. Note that, when thermodynamic equilibrium is reached, bulk diffusion equals surface diffusion, $J_{bulk} = J_s = 0$, and from Eq. 2.7 it is possible to relate the atom concentration at the surface to the gas pressure; for instance in the case of atomic tritium ($i = j =$ T) and gas molecular tritium gas ($m =$ T_2) in a metal/gas system, we find again that concentration at the interface can be expressed in terms of Sieverts' law, $c_T = K_s\sqrt{p_{T2}}$, and $K_s = \sqrt{\frac{K_{d_{T_2}}}{K_{r_{T,T}}}}$ is the Sieverts' constant, which accurately describes the transport regime when chemisorption sites are saturated and surface effects do not play a significant role, or in case of low partial pressure. In particular, Serra and Perujo studied the effect of oxidation on MANET steel [8]. They found that bare MANET follows a diffusion-limited permeation regime whilst oxidized MANET is surface-limited. Besides, oxidation reduces permeation flux of $\sim 1-3$ orders of magnitude over the same range of partial pressures. A schematic summarizing surface-limited and diffusion-limited regimes for the case of mono-species (e.g. molecule of species m containing $i = j$ atoms, for example $m =H_2$ and $i = j =$H) is proposed in Fig. 2.3.

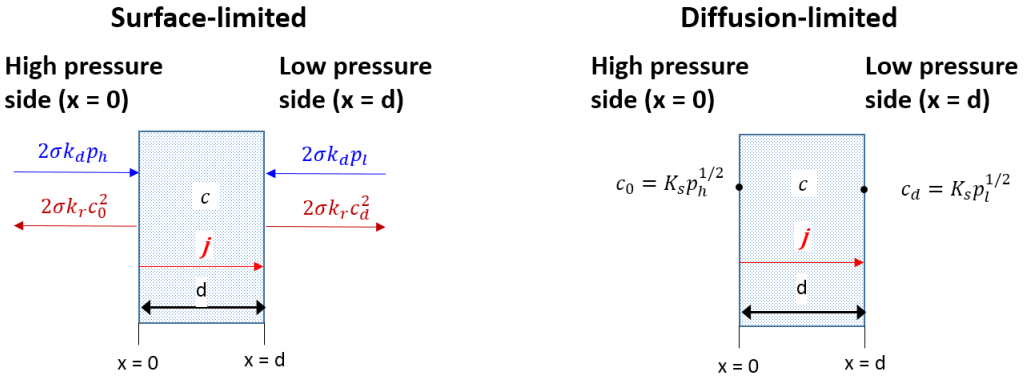

Figure 2.3: Summary of formulation of surface-limited and diffusion-limited boundary conditions for transport of a single isotope through bulk of strucutural material.

The formulation of diffusion-limited regime discussed thus far is limited to the case of transport of a single isotope. In case of co-existence of different molecules m dissolved in

the gas, e.g. H_2, D_2, T_2, HD, HT, etc., which is the case of fusion systems, a more sophisticated formulation is necessary in order to account for the contributions of all isotopes which "compete" among each other to permeate through the structural material. The modified Hickman's theory [20] relates the concentration of atomic species at the metal interface to the partial pressures of molecules dissolved in the gas by extending the mono-isotope Sieverts' law. For example, if hydrogen and deuterium molecules are dissolved in the gas, the thermodynamic equilibrium $H_2 + D_2 \rightleftharpoons HD$ is established, and H and D concentrations at the gas/surface interface at steady-state conditions can be approximated as:

$$c_H = K_{s_{H_2}} \frac{p_{H_2}}{p_{tot}^{1/2}} + \frac{1}{2} K_{s_{HD}} \frac{p_{HD}}{p_{tot}^{1/2}} \tag{2.8}$$

$$c_D = K_{s_{D_2}} \frac{p_{D_2}}{p_{tot}^{1/2}} + \frac{1}{2} K_{s_{HD}} \frac{p_{HD}}{p_{tot}^{1/2}} \tag{2.9}$$

where $p_{tot} = p_{H_2} + p_{D_2} + p_{HD}$. In fusion applications $p_{D_2} \ll p_{HD} \ll p_{H_2} \simeq p_{tot}$ thus Eqs. 2.8 and 2.9 simplify to:

$$c_H \simeq K_{s_{H_2}} p_{H_2}^{1/2} \tag{2.10}$$

$$c_D \simeq \frac{1}{2} K_{s_{HD}} \frac{p_{HD}}{p_{H_2}^{1/2}} \tag{2.11}$$

Eq. 2.11 can be written for tritium in the case of a system where the thermodynamic equilibrium is $H_2 + T_2 \rightleftharpoons HT$. A schematic of the more general case of boundary conditions to apply to a system where H_2, D_2, T_2, HD, and HT molecules are dissolved in the gas is summarized in Fig. 2.4 for the surface-limited case and in 2.5 for the diffusion-limited case.

A more detailed mathematical formulation of the co-permeation of multiple H isotopes and numerical validation with experimental results was proposed in [21]. The authors found that Eq. 2.11 can be written as $c_D \simeq K_{s_{HD}} \frac{p_{HD}}{(K_{eq} p_{H_2})^{1/2}}$, where K_{eq} is the equilibrium constant of $H_2 + D_2 \rightleftharpoons HD$. Note that K_{eq} is a function of temperature and is ~ 4 for typical temperatures of fusion systems and thus Eq. 2.9 and Eq. 2.11 are approximately equivalent lead to he same isotope concentration at gas/material interface.

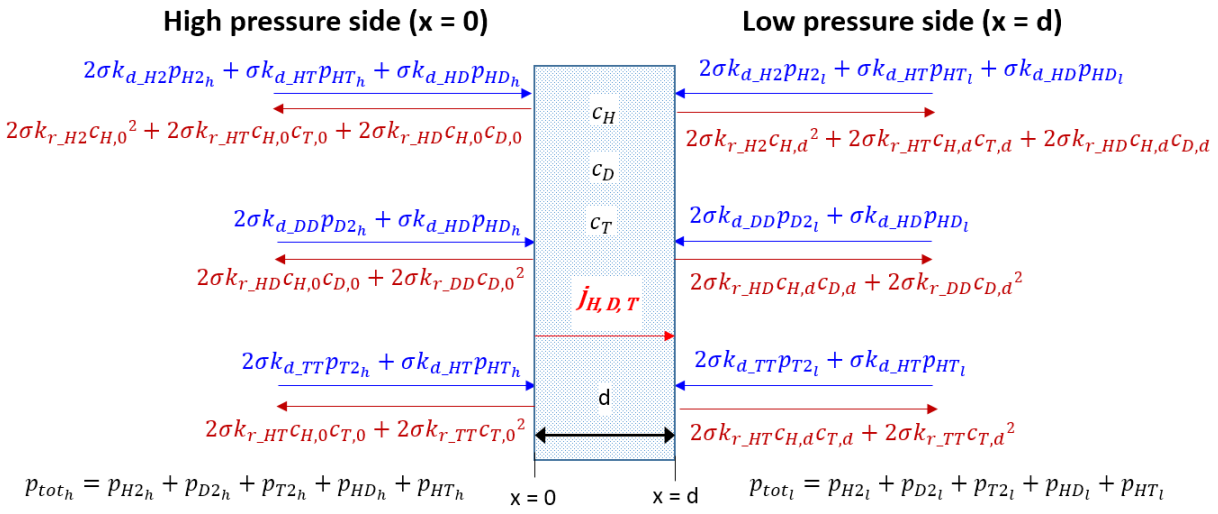

Figure 2.4: Surface-limited boundary conditions for transport of a H, D, and T isotopes through bulk of strucutural material.

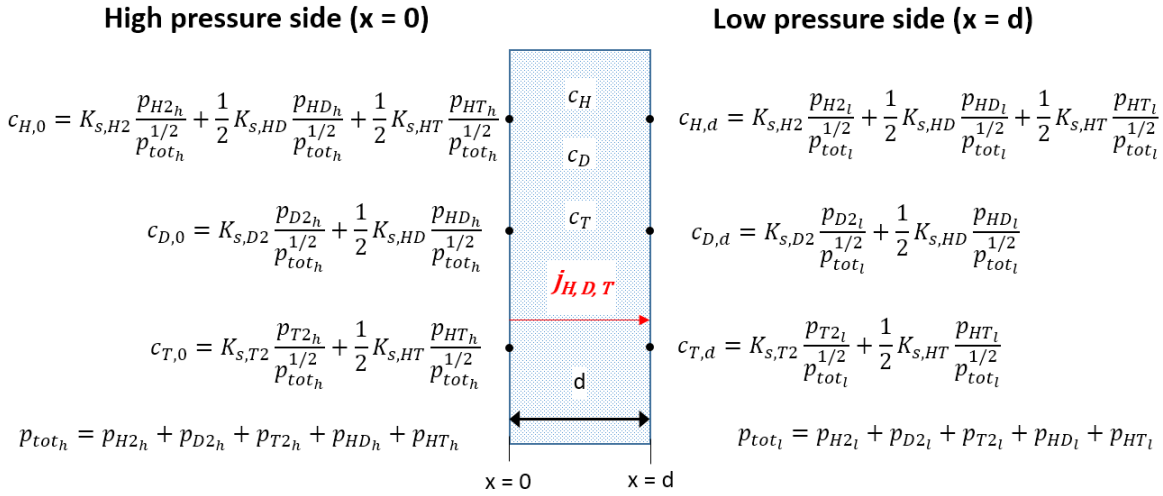

Figure 2.5: Diffusion-limited boundary conditions for transport of a H, D, and T isotopes through bulk of strucutural material.

Several experiments [21 - 30] were performed in order to determining hydrogen isotopes transport properties, e.g. diffusivity, solubility or Sieverts' constant, trapping parameters, dissociation and recombination constant rates, etc. A review of main properties for common fusion reactor materials (F82H, MANET II, BATMAN, Be, Al, Cu, W) is presented in [31]. All properties are strongly temperature dependent.

2.3 Available System-level Codes for Tritium Transport

System-level codes were developed with the main goal of estimating Q_2 (where Q = H, D, T) partial pressures build-up in coolant and purge gas gas of blanket systems, tritium inventories in fuel cycle components, and permeation rates to environment for safety purpose. The main codes for tritium analysis were developed in the US, The Tritium Migration Analysis Program (TMAP4/TMAP7) [11], at Idaho National Laboratory (INL) and in EU, FUS-TPC, at Karlsruhe Institute of Technology (KIT) [12]. These tools are described in details in the following subsections.

2.3.1 Tritium Migration Analysis Program

TMAP4 was implemented in the early '90s to simulate dynamics of gas movement through structures, between structures and adjoining gas volumes, and among gas volumes. TMAP4 was initially developed to assess tritium permeation rates during normal and accident conditions of fusion reactors but is currently used for a much wider variety of analysis. It has the capability of solving one-dimensional diffusion problems such as atoms movement through surfaces and bulk materials, as well as thermal response of structures (or *segments*). Moreover, it includes a zero-dimensional description of flows and chemical reactions between and within a control volume (or *enclosures*). In detail, TMAP4 evaluates the time dependent movement of solute species across structure surfaces, which is described by dissociation/recombination of gas molecules or atoms described in Eq. 2.7 or with the use of Sieverts' or Henry's laws. Bulk concentrations are obtained by solving Eq. 2.4, with optional atoms trapping in lattice defects, and considering the Soret effect and Fick's law, Eq 2.5. Thermal analysis of structures is critical due to the strong dependence of diffusion properties on temperature. The model relies on specified temperature, imposed heat flux or adiabatic boundary conditions to solve energy conservation:

$$\rho C_p \frac{\partial T}{\partial t} + \nabla \cdot (-k \nabla T) = S_h \tag{2.12}$$

where ρ the material density, C_p the specific heat, T the temperature, k the thermal conductivity, and S_h the local volumetric heating rate. At the surface/gas interface atomic species from the material bulk permeates the gas enclosure and the conversion between molecular species is governed by chemical reactions that in, TMAP4, are specified by the definition of reaction rates, R_c. Finally, partial pressures of gases in enclosures are calculated by solving the species conservation equation that accounts for convective flow between enclosures; the basic conservation equation for enclosures with molecular species having a concentration c_m, where an additional convection term, $\nabla \cdot c_m \mathbf{u}_m$, is added, is:

$$\frac{\partial c_m}{\partial t} + \nabla \cdot (c_m \mathbf{u} + \mathbf{J}_m) = S_{chem_m} \tag{2.13}$$

where $\mathbf{u}_m$ the velocity of molecular species m, $\mathbf{J}_m$ the diffusive flux of molecular species m, and S_{chem_m} the volumetric source of molecular species m due to chemical reactions. TMAP4, however, does not solve such equation directly but considers uniform concentrations, integrates Eq. 2.13 in the volume of the enclosure, applies Gauss' theorem to the convective term and obtains:

$$V_i \frac{\partial c_{m_i}}{\partial t} = -c_{m_i} \sum_j Q_{ij} + \sum_j c_{m_j} Q_{ji} - \sum_k A_k J_{m_k} + V_i S_{chem_m} \tag{2.14}$$

where V_i the volume of the enclosure i, c_{m_i} the concentration of molecular species m in enclosure i, j the index over all enclosures, Q_{ij} the volumetric flow rate from enclosure i to enclosures j, A_k the surface area of structure k, i.e. the physical boundary of the enclosure i, and J_{m_k} the net flux of molecular species m going into structure k surface boundary. All described equations and further details are given in [11].

An example of a simplified model for the HCCR TBS created at the Idaho National Laboratory (INL) within the collaboration INL - UCLA - NFRI (National Fusion Research Institute, South Korea) is shown in Fig. 2.6 (legend of segments and enclosures available in Fig. 2.7). TMAP4 is widely used for system-level analyses of tritium transport in fusion systems. The code has undergone a thorough validation process and it was long used in the

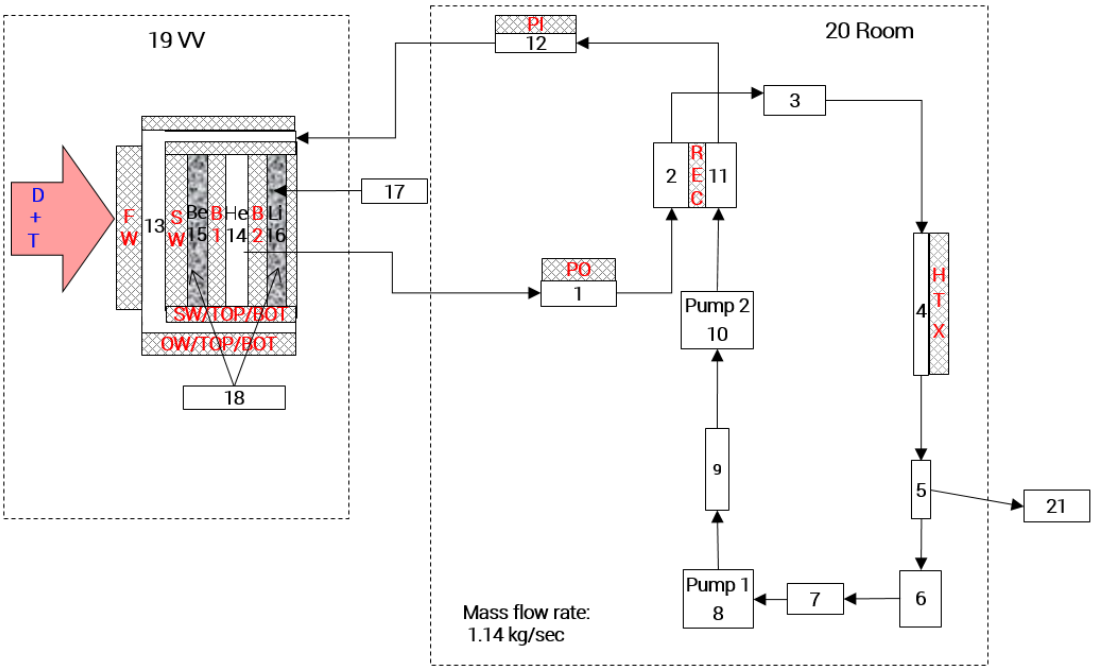

Figure 2.6: Schematic of simplified TMAP4 system-level model for HCCR TBS.

Segments (structures):

1. First Wall (FW)
2. Side Wall (SW)
3. Be Cooling (B1)
4. Breeder Cooling (B2)
5. Outlet Pipe (PO)
6. Inlet Pipe (PI)
7. HTX
8. Recuperator (REC)
9. SWI
10. SWO

Enclosures (gas volumes):

1. Outlet Pipe
2. Recuperator Outlet
3. HTX Inlet
4. HTX
5. HTX Outlet
6. Surge
7. Surge to Pump 1
8. Pump 1
9. Pump1 to Pump 2
10. Pump 2
11. Recuperator Inlet
12. Blanket Inlet
13. FW
14. Blanket He coolant
15. Blanket Be sweep gas
16. Blanket Breeder sweep gas
17. HT source
18. Tritium Extraction System (TES)
19. Vacuum Vessel (VV)
20. Room
21. CCWS
22. He clean-up

Figure 2.7: Legend of strucutres and enclosures used in the simplified TMAP4 system-level model for HCCR TBS.

last 25 years. It has the great advantage of requiring a small computational time to run ($\sim$ hours). However, many details characterizing fusion components conditions are missing. For instance, the tritium source in blankets can only be modeled as a constant inflow in the breeder zone enclosures, i.e. tritium production rate (TPR) gradients are ignored and, therefore, the temperature gradients characteristic of breeder and multiplier zones cannot be accurately reproduced. Moreover, a detailed description of the gas flow, e.g. coolant

and purge gas) is not available as volumetric average approach is used. Moreover, due to the separation of enclosures (describing gas dynamics) and segments (describing structural material dynamics), zones characterized by the coexistence of both states, e.g. breeder and multiplier pebble beds with purge gas flow, cannot be modeled in detail. Finally, the one- or zero- dimensional nature of the code simplifies noticeably the complex geometries of first wall, breeding zones, and other fusion components.

2.3.2 The FUS-TPC code

FUS-TPC [12] is a simplified fusion-devoted version of the fast-fission code SFR-TPC [32], which was primarily developed in order to evaluate tritium inventories and permeation losses from Sodium-Cooled Fast Reactors (SFRs). The FUS-TPC code, instead, predicts the hydrogen isotope concentrations and partial pressures build-up in coolant and purge gas of the Helium Cooled Pebble Bed (HCPB) blanket for EU DEMO [33]. The code is written in MATLAB and solves time-dependent zero-dimensional mass balance equations for various chemical forms of tritium molecules, e.g. T_2, HT and HTO. A simplified schematic representing tritium sources, sinks, and permeation fluxes for the HCPB in the EU DEMO design is shown in Fig. 2.8. Fig. 2.9 shows the system of equation implemented in the code while Table 2.1 gives a list of variables of interest. A more detailed description of the mathematical model, material properties, input parameters, and assumptions is available in [12]. As seen in the system of equations, in FUS-TPC uniform concentrations and average temperatures are considered. Hence, concentration and temperature gradients, which determine mass transfer and blanket/fusion system dynamics, are neglected.

Table 2.1: List of the main variables describing the FUS-TPC code [12].

Flux	**Description**
$\dot{G}_{HTO}$ [mol/s]	Total tritium generation rate inside the breeder
$\dot{G}_v^{br}$ [mol/cm^3 - s]	Local tritium generation rate inside breeder pebble beds
$\dot{G}_v^{Be}$ [mol/cm^3 - s]	Total tritium generation rate inside Beryllium pebble beds
Φ_{imp}^{FW} [mol/s]	Flux of Triton from the plasma through the FW cooling channels
Φ_{perm}^{CP} [mol/s]	HT permeated flux through CP channels
Φ_{perm}^{SG} [mol/s]	HT permeated flux through SG tubes
Φ_{TES}^{i} [mol/s]	Flux of tritium form i (i = HT, HTO) extracted by TES
Φ_{CPS}^{i} [mol/s]	Flux of tritium form i (i = HT, HTO) extracted by CPS
$\Phi_{leak,i}^{c}$ [mol/s]	Losses of tritium form i (i = HT, HTO) with coolant leakages
$\dot{\Delta}_{HTO}^{p}$ [mol/s]	HTO Isotope exchange rate inside the BU from the purge gas side
$\dot{\Delta}_{HT}^{c}$ [mol/s]	HT Isotope exchange rate inside the BU from coolant side

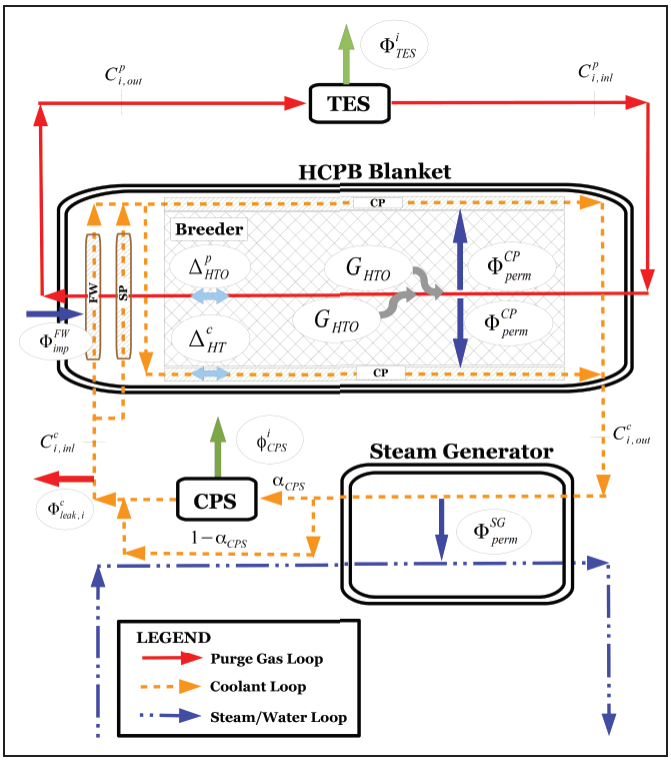

Figure 2.8: Simplified schematic of main components defininig the Outer Fuel Cycle of EU DEMO, i.e. FW, breeding zones, CPS, TES, heat exchangers [12].

Ref. 12 is the most comprehensive report regarding the FUS-TPC code; it includes a description of HCPB DEMO, the system of equations implemented, results, and discussion resulting inventories, pressure build-up in coolant loop and purge gas, and losses to environment. Other results derived with the use of the FUS-TPC code are available in [34, 35]. FUS-TPC is a useful tool for overall tritium analysis predictions but it has limitations, e.g. simplified zero-dimensional concentration equations and averaged values of flow rates and temperatures. FUS-TPC does not account for thermal response of structures.

$$
\begin{cases}
\dfrac{dC_T^{br}(t)}{dt} = \dot{G}_v^{br} - \dfrac{C_T^{br}(t)}{\tau_{res}} \\
\dfrac{dC_T^{Be}(t)}{dt} = (1-f_r)\cdot \dot{G}_v^{Be} \\
\dfrac{dC_{HT}^{p}(t)}{dt} = \dfrac{\dot{\Delta}_{HTO}^{p}(t) - \Phi_{perm}^{CP}(t) - \Phi_{TES}^{HT}(t)}{m_{He}^{p}} \\
\dfrac{dC_{HTO}^{p}(t)}{dt} = \dfrac{\dot{G}_{HTO}(t) - \dot{\Delta}_{HTO}^{p}(t) - \Phi_{TES}^{HTO}(t)}{m_{He}^{p}} \\
\dfrac{dC_{HT}^{c}(t)}{dt} = \dfrac{\Phi_{perm}^{CP}(t) + \Phi_{imp}^{FW}(t) - \Phi_{perm}^{SG}(t) - \dot{\Delta}_{HT}^{c}(t) - \Phi_{leak,HT}^{c}(t) - \Phi_{CPS}^{HT}(t)}{m_{He}^{c}} \\
\dfrac{dC_{HTO}^{c}(t)}{dt} = \dfrac{\dot{\Delta}_{HT}^{c}(t) - \Phi_{leak,HTO}^{c}(t) - \Phi_{CPS}^{HTO}(t)}{m_{He}^{c}} \\
C_i^j(0) = 0, \qquad with \quad i = T, HT, HTO, \quad j = br, Be, p, c
\end{cases}
$$

Figure 2.9: Equations implemented in the FUS-TPC model for HCPB EU DEMO system [12].

2.4 Detailed Component Modeling Efforts

In parallel with system-level codes development, many groups in the fusion community started to model single components of the fuel cycle (outside the system-level) in order to reproduce prototypical fusion conditions, and obtain a more detailed description to optimize design and performance. These mathematical models use a multi-physics approach and aim to reproduce the complex geometries of fusion components with a high degree of detail, thus these models are often referred to as "detailed components".

Various neutronics models were developed to determine the volumetric nuclear heating gradient and tritium production rate within the blanket with integrated first wall [36, 37], which serve as input parameters for detailed heat and mass transfer analysis. Robust PDE solvers, e.g. COMSOL Multiphysics, ANSYS, OpenFoam, etc., were used to implement the governing equations and perform the analyses. Particularly, several detailed 2-D and 3-D models of fusion components were developed for the HCCR TBM [13 - 16]. The analyses offered a high degree of detail by including complex geometries of fusion components and

prototypical conditions of fusion systems (e.g. gradients of concentrations, temperatures, etc.) and a multi-physics approach which solves the governing equations of mass, momentum, and heat transfer simultaneously. For example, it was found that accurate evaluation of temperature distribution in breeder zones of fusion blankets is a key parameter to accurately evaluate tritium transport dynamics, given the dependency of transport properties on temperature. Furthermore, accurate representation of coolant and purge gas flow in required to accurately determine the tritium partial pressure of dissolved Q_2 molecule in the gas, and associated concentration of Q atoms in the bulk material of structural components. As an example, we show in Fig. 2.10 and 2.11 temperature and purge gas velocity profiles of breeder (Li_2TiO_3), multiplier (Be) zones and graphite reflector of HCCR TBM calculated with detailed model [14].

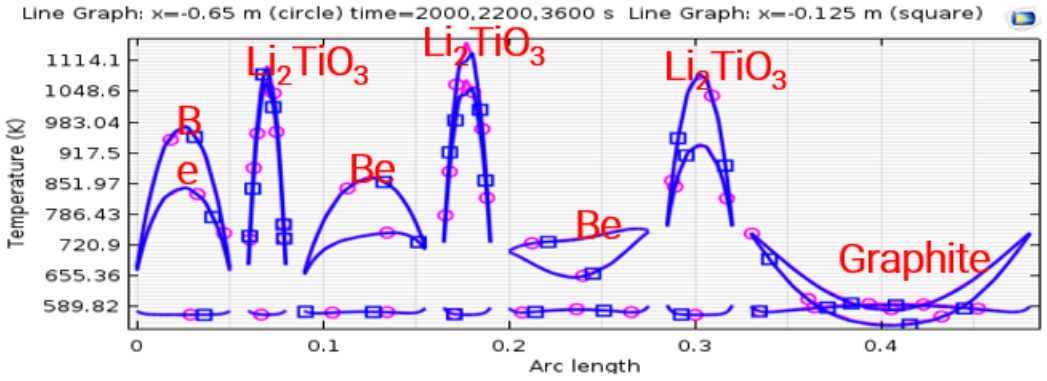

Figure 2.10: Temperature distribution in the HCCR berylium, breeder and reflector zones for different times [14].

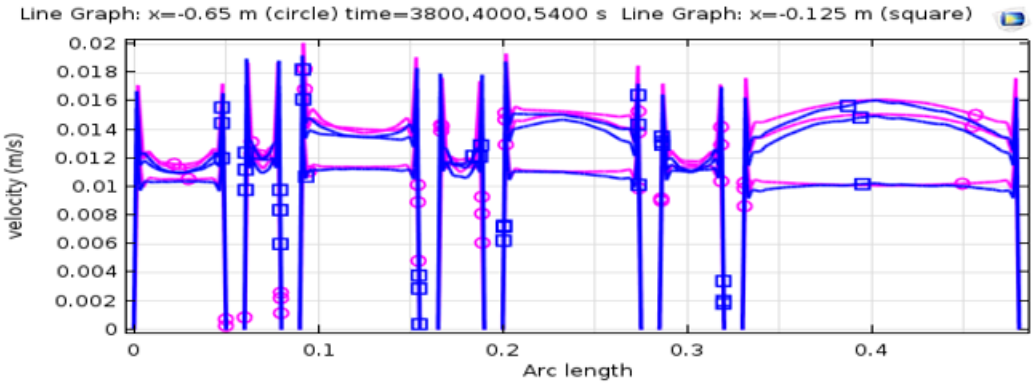

Figure 2.11: Velocity profiles of purge gas in the HCCR berylium, breeder and reflector zones for different times [14].

The level of detail achieved by these models is superior to the simplified 0-D or 1-D methodology developed in system-level models such as TMAP4 and FUS-TPC codes. However, a system level-description is required in order to evaluate the performance of the overall system, i.e. the entire fuel cycle. Thus, in order to enhance the predictive tools available for tritium transport in fusion systems, a new approach which is able to incorporate high fidelity detailed models into system-level is required. The first modeling effort to include detailed models of fusion components into system-level simulations was presented in [38]. This papers describes the methodology used to perform the coupling on detailed components models developed in COMSOL Multiphysics [39, 40] to system-level with the use of MATLAB S-Functions [41] in the MATLAB/Simulink environment [42]. The paper presents a simplified model for the HCCR TBM including first wall, breeder zone, connecting pipes and purification unit, and performs a preliminary analysis of tritium permeation rates to ITER buildings. However, the analysis is limited by the computational time required to run the code; the authors pointed out that the chosen system-level time step, dt_{SL}, drastically affects the required computational time necessary to run the code. For this preliminary analysis the author used a time step of 25 seconds on system-level. For this time-step, ten days of computation are necessary to obtain one day of simulated HCCR TBM dynamics. Furthermore, a converging of the system-level time step was not achieved: the authors showed that a simulation with dt_{SL}= 20 s causes a $\sim$5% change in pressure build-up values of Q_2 isotopes in coolant and concluded that further development was necessary in order to obtain a reliable predictive tool and perform more comprehensive analyses. This paper represents the first attempt towards developing a numerical model that can provide a higher degree of detail and accuracy by integrating detailed component models to system-level. However, the results are considered preliminary and are useful to describe some of the challenges regarding the first stage of code development. In this Dissertation, the model presented in [38] is further developed to improve the computational efficiency, obtain convergence of the time-step, and perform a comprehensive analysis regarding tritium permeation rates to the rooms of the ITER reactor and inventory build-up in the test blanket system components. The model is also used to suggest R&D of the HCCR TBS.

2.5 Literature Review Conclusions

A great deal of work on tritium self-sufficiency analysis is available in literature. However, most of these models were developed in the '80s and '90s and present outdated designs of fuel cycle and respective parameters defining their performance. Hence, new models which describe up-to-date fuel cycle design, state-of-the-art fusion parameters, e.g. tritium processing time(s), residence time(s), fueling efficiency, burn fraction, etc., and can include various reactor operational scenarios, e.g. pulsed operation, random failures, maintenance, shut down, etc., are required. Besides, a great interest in evaluating the required tritium start-up inventory for plasma based experimental facilities (e.g. FNSF[1]), DEMO(s), and future power reactor is of great interest due to the limited availability of tritium resources. The required start-up inventory for a 3 GW fusion reactor calculated in [1] is >20 kg, which is of concern given the limited resources of tritium. A recent study [43] published in 2019 presented a detailed analysis of the start-up inventory required for the specific design and parameters of the EU-DEMO. In this Dissertation a more general analyses is performed in order to define the R&D requirements to attain fuel self-sufficiency and evaluate the tritium start-up inventory in fusion reactors.

Available predictive tools for tritium transport at system-level offer high computational performance and are useful for preliminary estimation of tritium transport in fusion systems but the mathematical description of the components of the fuel cycle is limited to a 0-D or 1-D approach and details is missing. Detailed modeling of fusion components and integration into system-level offers a higher degree of detail and improves predictions of tritium transport within fusion system. A new methodology which includes detailed models into system-level was presented in [38] and is further developed in this document.

[1]Fusion Nuclear Science Facility (FNSF) is an experimental facility commissioned by the US as an intermediate step between ITER and DEMO reactors. The main goal is to provide the nuclear environment needed to develop fusion materials and components technology.

References

1. M. Abdou, et. al., "Deuterium-Tritium Fuel self-sufficiency in Fusion Reactors", Fusion Technology, 9: 250-285 (1986)

2. Lei Pan, Hongli Chen, Qin Zeng, "Sensitivity analysis of tritium breeding ratio and startup inventory for CFETR", Fusion Engineering and Design, 112 (2016) 311-316

3. Hongli Chen, Lei Pan, Zhongliang Lv, Wei Li, Qin Zeng, "Tritium fuel cycle modeling and tritium breeding analysis for CFETR", Fusion Engineering and Design 106 (2016) 17-20

4. W. Kuan and M. Abdou, "A New Approach for Assessing the Required Tritium Breeding Ratio and startup Inventory in Future Fusion Reactors", Fusion Technology, 35: 309-353 (1999)

5. M. Sawan, M. Abdou, "Physics and Technology Conditions for attaining Tritium self-sufficiency for the DT Fuel Cycle", Fusion Engineering & Design, 81:(8-14), 1131-1144 (2006)

6. Abdou, M., Morley, N.B., Smolentsev, S., Ying, A., Malang, S., Rowcliffe, A., Ulrickson, M., "Blanket/First wall challenges and required R&D on the pathway to DEMO", Fusion Engineering and Design, 100:2-43 (2015)

7. E. Serra, Hydrogen and Tritium Kinetics in Fusion Reactor Materials, Ph.D. Thesis, Department of Physics, University of Salford - UK

8. E. Serra, A. Perujo, "Influence of the surface conditions on permeation in the deuterium-MANET system", Journal of Nuclear Materials 240 (1997)215-220

9. E. Serra, A. Perujo, G. Benamati, "Influence of traps on the deuterium behaviour in the low activation martensitic steels F82H and Batman", Journal of Nuclear Materials 245 (1997) 108-114

10. E. Serra, G. Benamati, O.V. Ogorodnikova, "Hydrogen isotopes transport parameters in fusion reactor materials", Journal of Nuclear Materials 255 1998. 105-115

11. G. R. Longhurst, D. F, Holland, J. L. Jones, B. J. Merrill, "TMAP4 User's Manual, Idaho National Engineering Laboratory", Idaho Falls, ID 83415-3523

12. F. Franza, "Tritium transport analysis in HCPB DEMO blanket with the FUS-TPC code", KIT SCIENTIFIC REPORTS 7642

13. Alice Ying, Hongjie Zhang, Mu-Young Anh, Youngmin Lee, "TRITIUM TRANSPORT EVOLUTIONS IN HCCR TBM UNDER ITER INDUCTIVE OPERATIONS", FUSION SCIENCE AND TECHNOLOGY VOL. 68 SEP. 2015

14. Alice Ying, Hongjie Zhang, Brad J. Merrill, Mu-Young Ahn, "Advancement in tritium transport simulations for solid breeding blanket system", Fusion Engineering and Design Volumes 109-111, Part B, 1 November 2016, Pages 1511-1516

15. M. Zucchetti, I. Nicolotti, A. Ying, M. Abdou, "TRITIUM MODELING FOR ITER TEST BLANKET MODULE", FUSION SCIENCE AND TECHNOLOGY VOL. 68 OCT. 2015

16. Massimo Zucchetti, Marco Utili, Iuri Nicolotti, Alice Ying, Fabrizio Franza, Mohamed Abdou, "Tritium control in fusion reactor materials: A model for Tritium, Extracting System", Fusion Engineering and Design 98-99 (2015) 1885-1888

17. Mohamed A. Abdou*et al.* (1996), "Results of an International Study on a High-Volume Plasma-Based Neutron Source for Fusion Blanket Development", Fusion Technology, 29:1, 1-57, DOI: 10.13182/FST96-3

18. I. Ricapito, "Tritium transport modeling for breeding blanket: State of the art and strategy for future development in the EU fusion program", Fusion Engineering and Design 87 (2012) 793-797

19. M. A. Pick and K. Sonnenberg, "A model for atomic hydrogen-metal interacions - Application to recycling, recombination and permeation", Journal of Nuclear Materials 131 (1985) 208-220

20. Satoru Tanaka et al., J. Nucl. Sci. Technol. 16, December (1979) 923-925

21. Hongjie Zhang, Alice Ying, Mohamed Abdou, Masashi Shimada, Bob Pawelko and SeungyonCho (2017): "Characterization of Tritium Isotopic Permeation Through ARAA in Diffusion Limited and Surface Limited Regimes", Fusion Science and Technology

22. Masashi Shimada, Robert D. Kolasinski, J. Phillip Sharpe and Rion, A. Causey, "Tritium plasma experiment: Parameters and potentials for fusion plasma-wall interaction studies", REVIEW OF SCIENTIFIC INSTRUMENTS 82, 083503 (2011)

23. D. Naujoks, J. Roth, K. Krieger, G. Lieder, M. Laux, "Erosion and redeposition in the ASDEX Upgrade divertor", Journal of Nuclear Materials 210 (1994) 43-50

24. H.D. ROHRIG, R. HECKER, J. BLUMENSAAT and J. SCHAEFER, "STUDIES ON THE PERMEATION OF HYDROGEN AND TRITIUM IN NUCLEAR PROCESS HEAT INSTALLATIONS", NUCLEAR ENGINEERING AND DESIGN 34 (1975) 157-167

25. O.V. Ogorodnikova, M.A. Fuutterer, E. Serra, G. Benamati, J. F. Salavy, G. Aiello, "Hydrogen isotope permeation through and inventory in the first wall of the water cooled Pb17Li blanket for DEMO", Journal of Nuclear Materials 273 (1999) 66-78

26. G.A. Esteban, A. Perujo, K. Douglas, L.A. Sedano, "Tritium diffusive transport parameters and trapping effects in the reduced activating martensitic steel OPTIFER-Ivb", Journal of Nuclear Materials 281 (2000) 34-41

27. Hirofumi Nakamura *et al*, "Tritium permeation behavior implanted into pure tungsten and its isotope effect", Journal of Nuclear Materials 297 (2001) 285-291

28. C. San Marchi, B.P. Somerday, S.L. Robinson, "Permeability, solubility and diffusivity of hydrogen isotopes in stainless steels at high gas pressures", International Journal of Hydrogen Energy 32 (2007) 100-116

29. D.M. GRANT, D.L. CUMMINGS and D.A. BLACKBURN, "HYDROGEN IN 316 STEEL -DIFFUSION, PERMEATION AND SURFACE REACTION", Journal of Nuclear Materials 152 (1988) 139-145

30. A. Pisarev *et al.*, "Surface Effects in Diffusion Measurenments: Deuterium Permeation through Martensitic Steel", Physica Scripta. T94 121-127, 2001

31. F. Reiter, K. S. Forcey, G. Gervasini, "A Compilation of Tritium-Material Interaction Parameters in Fusion Reactor Materials", Commission of the European communities, Joint Research Centre, ISPRA Site, Institiute for Safety Technology, EUR 15217 EN

32. F. Franza, "Tritium Transport Analysis in Advanced Sodium-Cooled Fast Reactors", Thesis for a Master Degree in Nuclear Engineering, Politecnico di Torino, Italy (2011).

33. L.V. Boccaccini *et al*, "Materials and Design of the European DEMO Blankets", Journal of Nuclear Materials, 329-333 (2004) 148-155

34. F. Franza, A. Ciampichetti, I. Ricapito, M. Zucchetti, "A model for tritium transport in fusion reactor components: The FUS-TPC code", Fusion Engineering and Design 87 (2012) 299-302

35. F. Franza, L.V. Boccaccini, A. Ciampichetti, M. Zucchetti, "Tritium transport analysis in HCPB DEMO blanket with the FUS-TPC code", Fusion Engineering and Design 88 (2013) 2444-2447

36. Marco Riva, Christian Di Sanzo, Mohamed Abdou & Mahmoud Youssef (2017), "Reducing the Peak-to-Average-Power-Ratio in Fusion Blankets", Fusion Science and Technology, 72:3, 469-477

37. Seungyon Cho *et al.*, "Neutronic assessment of HCCR breeding blanket for DEMO", Fusion Engineering and Design, Volume 146, Part A, 2019, Pages 1338-1342, ISSN 0920-3796, https://doi.org/10.1016/j.fusengdes.2019.02.071.

38. Ying *et al.*, "Breeding blanket system design implications on tritium transport and permeation with high tritium ion implantation: A MATLAB/Simulink, COMSOL integrated dynamic tritium transport model for HCCR TBS", Fusion Engineering and Design, Volume 136, Part B, November 2018, Pages 1153-1160

39. COMSOL, v.5 2014. COMSOL, Inc., COMSOL Multiphysics User's Guide, Burlington, MA.

40. COMSOL/Livelink: COMSOL Multiphysics with MATLAB v. 5.0. COMSOL, Inc., Burlington, MA. 2015 Livelink for MATLAB, COMSOL, Inc., Burlington, MA. 2015

41. Simulink Developing S-Functions, MATLAB & SIMULINK, R2017a, MathWorks, Inc.

42. MATLAB and Simulink Release 2014b, MathWorks, Inc., Natick, Massachusetts, United States.

43. M. Coleman, Y. Horstensmeyer, F. Cismondi, "DEMO tritium fuel cycle: performance, parameter explorations, and design space constraints", Fusion Engineering and Design, Volume 141, 2019, Pages 79-90

CHAPTER 3

Modeling of Tritium Transport in the Helium Coolant Ceramic Reflector Test Blanket System and Analysis

In this work, an advanced numerical model is developed in order to predict time dependent tritium transport in the outer fuel cycle. In particular, the Helium Cooled Ceramic Reflector Test Blanket System (TBS) is chosen for the analysis. However, the methodology is general and can be applied to a variety of Test Blanket Modules (TBM), e.g. Dual Coolant Lead Lithium (DCLL), Water Cooled Lithium Lead (WCLL), etc. Particularly, the detailed component models of the HCCR TBS, e.g. FW, BZ, pipes, HCS/CPS, TES, etc., are developed in COMSOL Multiphysics and integrated into system-level model to reproduce the HCCR TBS coolant and purge gas streams, as shown in Fig. 3.1. This predictive tool is used to analyze tritium inventory build-up in TBS components and estimate tritium permeation rates to the buildings of the ITER. The model reproduces prototypical fusion conditions, complex geometries, and realistic plasma scenarios (e.g. pulsed operation).

In this Chapter we describe the mathematical formulation implemented in COMSOL Multiphysics [1] to generate models of first wall, breeding zone and connecting pipes of the HCCR TBS. Thus, we describe the methodology used to integrate detailed components to system-level with the use of the MATLAB/Simulink [2] and COMSOL Livelink [3] platform through S-Function blocks [4]. Finally, we perform tritium transport analysis for the HCCR TBS of the ITER. Other applications of this numerical predictive tool are presented in Chapters 4 and 5.

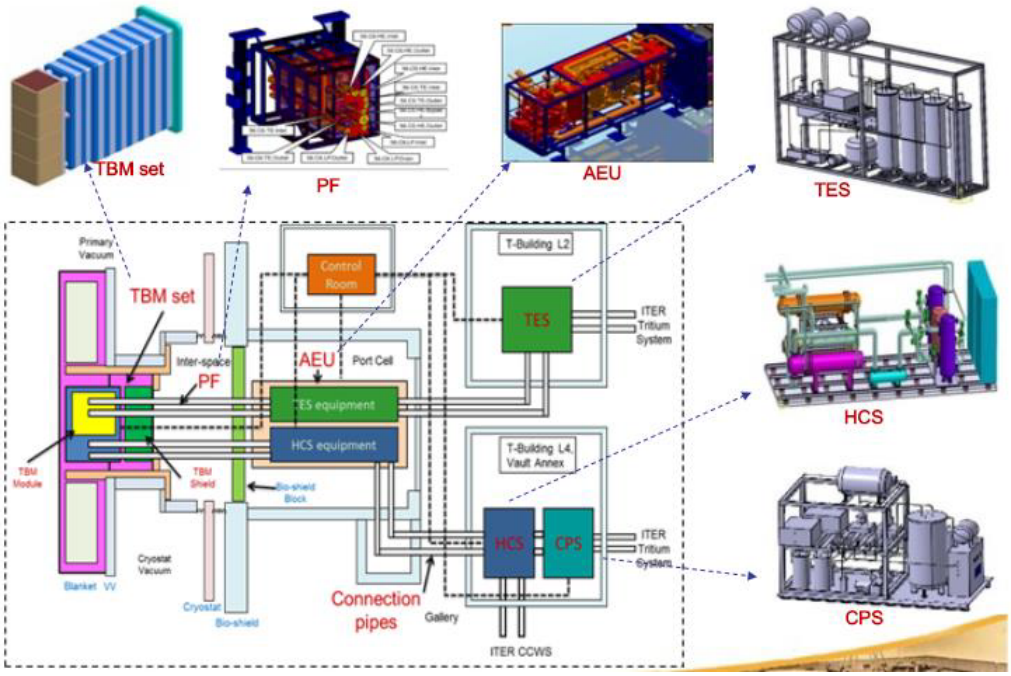

Figure 3.1: Schematic of the ITER Test Blanket System including Test Blanket Module (TBM), Pipe Forest (PF), Helium Coolant System (HCS), Coolant Purification System (CPS), Tritium Extraction System (TES).

3.1 Mathematical Formulation of Detailed Components of the HCCR TBS

In this section we describe the mathematical formulation and governing equations implemented in COMSOL Multiphysics Ver. 5.3a for each model of the HCCR TBS. The parameters and transport properties used in the analysis are listed.

3.1.1 First wall

High tritium (and deuterium) particle fluxes are expected to reach the first wall surface as particles are exhausted through the scrape-off layer (SOL) of the plasma. Thus, particles implantation into the first wall structural material occurs, implanted atoms diffuse through the bulk material, and permeate to the helium coolant channels. Furthermore, sharp temperature gradients are expected in the structural material of the first wall, due to volumetric nuclear heating and thermal radiation fluxes (e.g. bremsstrahlung radiation) on the surface

of the FW facing the plasma. Since tritium transport properties (e.g. tritium solubility in ferritic steel, dissociation and recombination rates, etc.) are strongly temperature dependent, a multi-physics approach, where heat and mass transport constitutive equations are coupled, is necessary to reproduce prototypical fusion conditions. In particular, the developed COMSOL model simulates the transport of hydrogen species and heat transfer within the Advanced Reduced Activation Alloy (ARAA) structure of the HCCR FW in the toroidal-radial plane. In particular the FW is 3 cm long in the radial direction and 25.3 cm long in the toroidal direction. However, by means of symmetry, we model only one of the eleven helium coolant channels, i.e. 2.3 cm toroidally, to reduce the computational domain and consequent computational time. The coolant channel is located at 6 mm from the first wall surface facing the plasma and is 1 cm long in the radial direction and 1.4 cm in the toroidal direction. Each channel is 77 cm wide in the poloidal direction (not simulated in the model). Further details on FW geometry are available in [5]. The mathematical formulation follows the methodology presented in [6, 7]. The governing equation for hydrogen atoms concentration dissolved in the first wall structural material c_s^{FS}, where FS implies ferritic steel (and is a convenient superscript compared to the longer ARAA), $s = H,\ D,\ T$, has the general form:

$$\frac{\partial c_s^{FS}}{\partial t} + \nabla \cdot (-D_s^{FS} \nabla c_s^{FS}) = S_s^{FS} \tag{3.1}$$

where D_s^{FS} is the diffusion coefficient of species s in FS, and S_s includes the Soret effect and ion implantation from plasma:

$$S_s^{FS} = -\nabla \cdot \left(-D_s^{FS} \frac{c_s^{FS} Q^*}{k_b (T^{FS})^2} \nabla T^{FS} \right) + (1 - r) I_0 w_d \tilde{p}(t) \tag{3.2}$$

and T^{FS} the temperature of the ferritic steel, Q^* the heat of transport, k_b the Boltzmann constant, I_0 the atomic particle flux (50% D - 50% T) from plasma into the FW, r the reflection coefficient, w_d the normalized implantation particle distribution, and $\tilde{p}(t)$ the normalized pulse function of ITER operational scenario as shown in Fig. 3.2. The implantation profile, w_d, is calculated with the use of the SRIM/TRIM Monte Carlo code [8] for the case of ARAA in Subsection 3.2.2. In this work we neglect the effect of possible defects in structural

material. Dissociation/recombination boundary conditions are implemented on plasma side

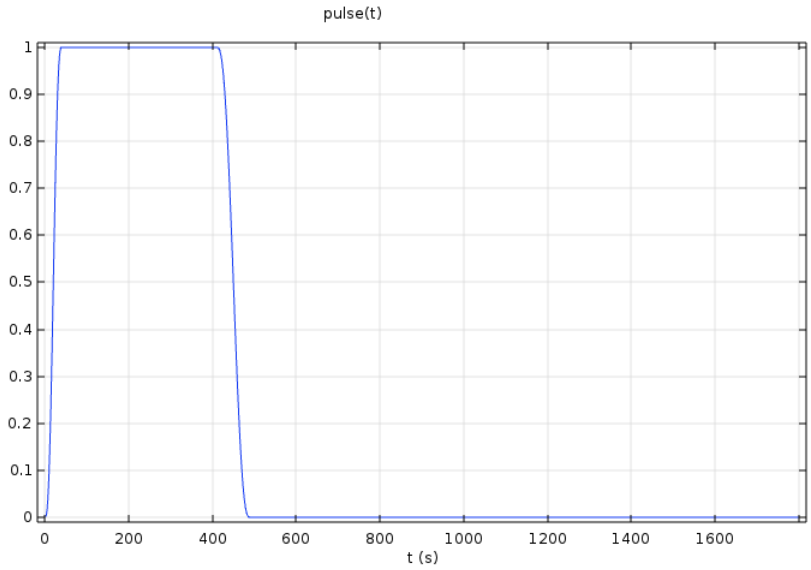

Figure 3.2: ITER pulse operational scenario: 50 s ramp-up, 350 s burn, 100 s ramp-down, 1300 s dwell time.

as described in Eq. 2.7. Thus, the atom recombination flux for D and T to plasma is:

$$J_H^{FS} = -2k_{r_{H_2}}(c_H^{FS})^2 - 2k_{r_{HD}}c_H^{FS}c_D^{FS} - 2k_{r_{HT}}c_H^{FS}c_T^{FS} \tag{3.3}$$

$$J_D^{FS} = -2k_{r_{D_2}}(c_D^{FS})^2 - 2k_{r_{DT}}c_D^{FS}c_T^{FS} - 2k_{r_{HD}}c_D^{FS}c_H^{FS} \tag{3.4}$$

$$J_T^{FS} = -2k_{r_{T_2}}(c_T^{FS})^2 - 2k_{r_{DT}}c_D^{FS}c_T^{FS} - 2k_{r_{HT}}c_T^{FS}c_H^{FS} \tag{3.5}$$

Whether it would be preferable to use different expressions for the recombination constant rate of different Q_2 molecules, in absence of more detailed experimental data we use the hydrogen recombination rate constant obtained in Ref. [9, 10] and presented in Table 3.1 for any Q_2 molecule, e.g. H_2, HT, etc. Thus Eqs. 3.3 - 3.5 simplify to:

$$J_H^{FS} = -2k_r c_H^{FS}(c_H^{FS} + c_D^{FS} + c_T^{FS}) \tag{3.6}$$

$$J_D^{FS} = -2k_r c_D^{FS}(c_H^{FS} + c_D^{FS} + c_T^{FS}) \tag{3.7}$$

$$J_T^{FS} = -2k_r c_T^{FS}(c_H^{FS} + c_D^{FS} + c_T^{FS}) \tag{3.8}$$

Note that H is not implanted in the FW but can dissolve in ferritic steel due to absorption on coolant side, where concentration of H isotopes at the gas/structure interface satisfy the Sieverts' law and the co-permeation effect is considered (see Fig. 2.5). Concentrations of H, D and T at gas/structure interface are:

$$c_H^{FS} = K_{s,H_2}\frac{p_{H_2}^{CL}}{(p_{tot}^{CL})^{1/2}} + \frac{1}{2}K_{s,HD}\frac{p_{HD}^{CL}}{(p_{tot}^{CL})^{1/2}} + \frac{1}{2}K_{s,HT}\frac{p_{HT}^{CL}}{(p_{tot}^{CL})^{1/2}} \tag{3.9}$$

$$c_D^{FS} = K_{s,D_2}\frac{p_{D_2}^{CL}}{(p_{tot}^{CL})^{1/2}} + \frac{1}{2}K_{s,HD}\frac{p_{HD}^{CL}}{(p_{tot}^{CL})^{1/2}} \tag{3.10}$$

$$c_T^{FS} = K_{s,T_2}\frac{p_{T_2}^{CL}}{(p_{tot}^{CL})^{1/2}} + \frac{1}{2}K_{s,HT}\frac{p_{HT}^{CL}}{(p_{tot}^{CL})^{1/2}} \tag{3.11}$$

where the total pressure is the sum of Q_2 partial pressures in He coolant (CL): $p_{tot}^{CL} = p_{H_2}^{CL} + p_{D_2}^{CL} + p_{T_2}^{CL} + p_{HD}^{CL} + p_{DT}^{CL} + p_{HT}^{CL}$. However, note that in fusion applications $p_{T_2} << p_{HT}$ and $p_{D_2} << p_{HD}$, thus p_{T_2} and p_{D_2} are neglected in this model. Moreover the same solubility is used for H_2, HD, and HT. Thus:

$$c_H^{FS} = K_s\frac{p_{H_2}^{CL}}{(p_{tot}^{CL})^{1/2}} + \frac{1}{2}K_s\frac{p_{HD}^{CL}}{(p_{tot}^{CL})^{1/2}} + \frac{1}{2}K_s\frac{p_{HT}^{CL}}{(p_{tot}^{CL})^{1/2}} \tag{3.12}$$

$$c_D^{FS} = \frac{1}{2}K_s\frac{p_{HD}^{CL}}{(p_{tot}^{CL})^{1/2}} \tag{3.13}$$

$$c_T^{FS} = \frac{1}{2}K_s\frac{p_{HT}^{CL}}{(p_{tot}^{CL})^{1/2}} \tag{3.14}$$

No particle flux is imposed on the other boundaries and concentrations of H, D, and T in are initially set to zero (clean FW).

The conservation of diluted species in FW structure (Eq. 3.1) is coupled with energy conservation equation:

$$\rho^{FS} C_p^{FS} \frac{\partial T^{FS}}{\partial t} + \nabla \cdot (-k^{FS} \nabla T^{FS}) = (q''')^{FS} \tilde{p}(t) \tag{3.15}$$

where ρ^{FS}, C_p^{FS}, and k^{FS} are the density, heat capacity at constant pressure, and thermal conductivity of ARAA, and the volumetric heat generation $(q''')^{FS}$ deposited during the plasma pulse, $\tilde{p}(t)$, is 4.2 MW/m^3 (calculated through detailed HCCR TBM neutronics analysis [11]) while boundary conditions are inward heat flux on plasma side (0.4 MW/m^2 during the plasma pulse), and convective heat flux on coolant side ($h_c^{FS} \sim 3750 \frac{\text{W}}{\text{m}^2-\text{K}}$ is a reference value suggested in [4]). Thermal insulation is imposed on the other boundaries. The initial temperature in the ferritic steel is 573 K. The schematic of Fig. 3.3 summarizes the simulated scenario.

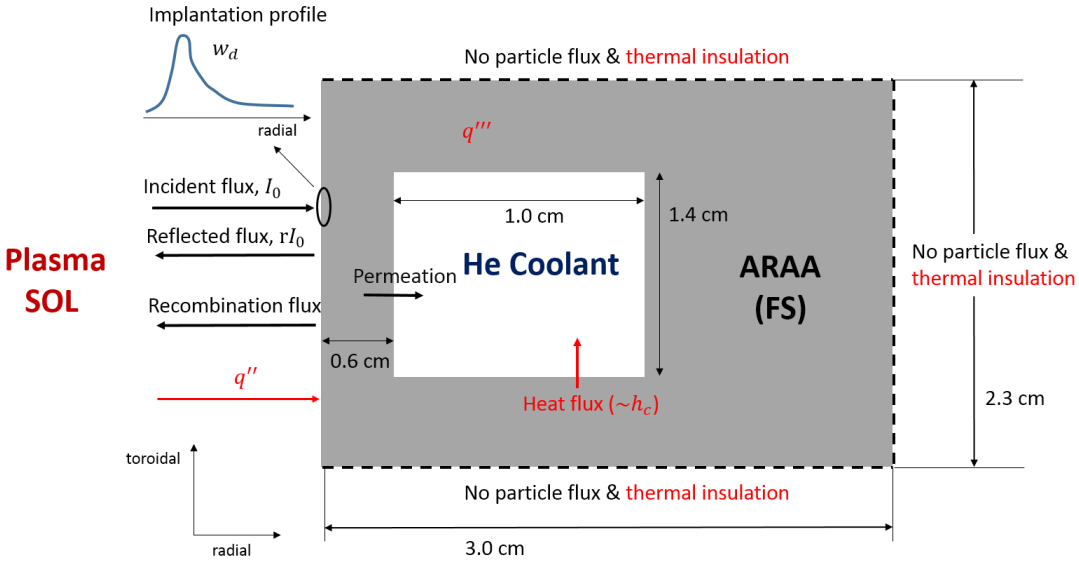

Figure 3.3: Schematic representing one helium coolant channel of HCCR FW with mass and heat fluxes, and volumetric heating of interest.

3.1.2 Breeding Zone

The breeding zone domain of one sub-module of the HCCR TBM includes three Be multiplier zones and three Li_2TiO_3 ceramic breeder zones separated by seven ARAA structural plates, each containing thirty four cooling channels, as represented in Fig. 3.4 where radial dimensions of different zones and poloidal height of the breeding zone are specified. A more detailed description is available in [12].

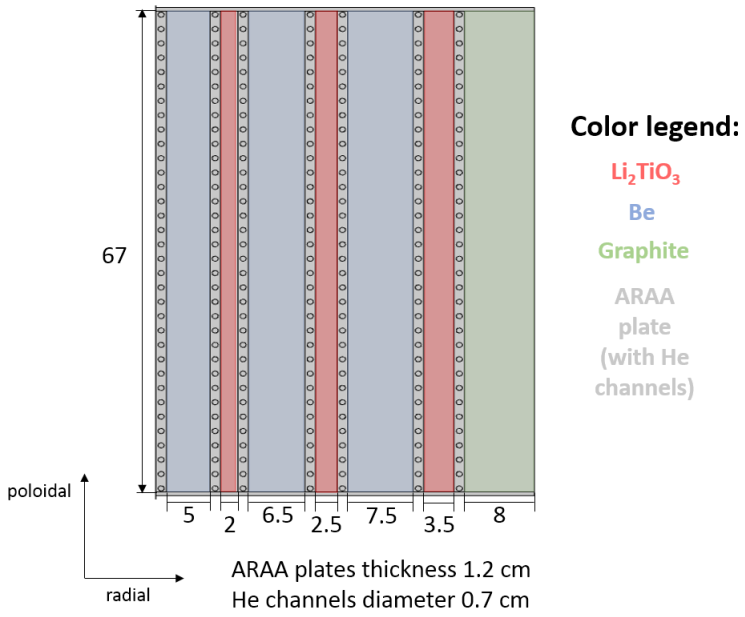

Figure 3.4: Schematic of the breeding zone of the HCCR TBM in the poloidal-radial plane with dimensions espressed in cm.

Tritium is bred in lithium ceramics (e.g. Li_2TiO_3) and released in the purge gas after a characteristic residence time τ_{res}. The purge gas is helium at atmospheric pressure with a 0.1% vol of H_2 which is added to the to enhance tritium release from pebbles and facilitate recombination of T with H to from HT molecules. Due to the presence of oxygen in the ceramics), tritiated water (HTO) molecules are formed in the purge gas. This interacts with H_2 to produce HT and H_2O. A similar discussion holds for the beryllium multiplier and purge gas zones, though tritium production rate in beryllium is several orders of magnitude smaller than the generation rate in the breeding zones and oxygen concentrations are negligible. A fraction of the tritium produced in Li_2TiO_3 and Be pebbles dissolves in the ARAA structural

plates, diffuses through the lattice, and permeates to coolant.

The numerical model implemented in the COMSOL Multiphysics includes transport of diluted species, porous media flow of purge gas through pebble beds, heat transfer in solids and porous media, and is described in detail in the following subsections.

3.1.2.1 Tritium transport in breeder, multiplier, purge gas, structural material, and reflector

The mathematical formulation of tritium transport in the breeding zone follows the methodology proposed by [6, 13−14]. In particular, the model evaluates:

- tritium concentration in ceramic breeder and beryllium multiplier pebbles (c_T^B and c_T^M);
- Concentrations of H_2, HT, HTO, and H_2O molecules in breeder purge gas (c_m^{BP}, where $m = H_2,\ HT,\ HTO,\ H_2O$);
- Concentrations of H_2 and HT molecules in beryllium multiplier purge gas (c_m^{MP}, where $m = H_2,\ HT$);
- hydrogen and tritium concentration in ARAA plates and graphite reflector (c_s^{ARAA} and c_s^G, where $s = H,\ T$).

Furthermore, heat transfer and purge gas flow through porous media (ceramics, beryllium, and graphite pebble beds) are simultaneously resolved to reproduce accurate temperature and velocity profiles. The equations implemented in the COMSOL Multiphysics Ver. 5.3a are described for the various zones of the TBM module in the following paragraphs.

Concentration of tritium in ceramic breeder and beryllium multiplier pebbles

$$\frac{\partial c_T^B}{\partial t} = \dot{G}_v^B \tilde{p}(t) - \frac{c_T^B}{\tau_{res}} \tag{3.16}$$

$$\frac{\partial c_T^M}{\partial t} = \dot{G}_v^M \tilde{p}(t)(1 - f_r) \tag{3.17}$$

where $\dot{G}_v^B$ and $\dot{G}_v^M$ are the volumetric tritium production rate in the ceramic breeder and multiplier respectively. In the breeder tritium release is governed by a characteristic tritium residence time τ_{res} while for the multiplier we assume that a fraction f_r of the tritium generated is instantaneously released, as discussed in [13].

Concentration of H_2, HT, HTO, and H_2O molecules in breeder purge gas

$$\frac{\partial c_m^{BP}}{\partial t} + \nabla \cdot (-D_m^{BP} \nabla c_m^{BP} + \mathbf{u}^{BP} c_m^{BP}) = R_m^{BP} \tag{3.18}$$

where $m = H_2, HT, HTO, H_2O$, the term $\nabla \cdot (\mathbf{u}^{BP} c_m^{BP})$ can be expanded as $\mathbf{u}^{BP} \cdot \nabla c_m^{BP} + c_m^{BP} \nabla \cdot \mathbf{u}^{BP}$, which includes the advection term $(\mathbf{u}^{BP} \cdot \nabla)$ and the divergence of the velocity field $(\nabla \cdot \mathbf{u}^{BP})$ to account for compressible behavior, and $m = H_2,\ HT,\ HTO,\ H_2O$. The term R_m^{BP} is a reaction rate that accounts for HT and HTO formation in the purge gas. In particular, we assume that tritium is released to the He purge gas in the HT and HTO molecular form with a 50% HT - 50% HTO ratio. Thus, per each mole of tritium atoms released, half a mole of molecules HT and HTO are formed, and half a mole of hydrogen molecules is consumed. Here we assume oxygen is release when two lithium nuclei are consumed. Hence, the reaction rate per unit of purge gas volume is:

$$R_{H_2}^{BP} = -\frac{1}{2} \frac{c_T^B}{\tau_{res}} \frac{V^B}{V^{BP}} \tag{3.19}$$

$$R_{HT}^{BP} = \frac{1}{2} \frac{c_T^B}{\tau_{res}} \frac{V^B}{V^{BP}} \tag{3.20}$$

$$R_{HTO}^{BP} = \frac{1}{2} \frac{c_T^B}{\tau_{res}} \frac{V^B}{V^{BP}} \tag{3.21}$$

$$R_{H_2O}^{BP} = 0 \tag{3.22}$$

where c_T^B/τ_{res} is the release rate from Li_2TiO_3, c_T^B is calculated in Eq. 3.16 and expressed

in moles of tritium atoms per unit of breeder volume, V^B is the breeder volume, and V^{BP} the volume of purge gas. Hence, HTO is reduced to HT due to the chemical reaction with H_2 which generates H_2O: $HT + H_2O \rightleftharpoons HTO + H_2$. The equilibrium constant rate can be expressed as:

$$K_{eq} = \frac{[HTO][H_2]}{[HT][H_2O]} \tag{3.23}$$

and was experimentally found to be a function of temperature [15]:

$$logK_{eq} = 0.292\ logT^{BP} + \frac{336.5}{T^{BP}} - 1.055 \tag{3.24}$$

and T^{BP} is the temperature of the purge gas. COMSOL Multiphysics provides a built-in reaction solution function which evaluates the molecule concentrations in a dynamic fashion based on the formulation of the equilibrium constant given in Eq. 3.24.

Diffusion-limited boundary conditions are implemented at the purge gas and cooling plates interface, as described in Eqs. 2.8 and 2.11 applied to H and T:

$$c_H^{FS} = K_{s_{H_2}} \frac{p_{H_2}^{BP}}{p_{tot}^{BP\,1/2}} + \frac{1}{2} K_{s_{HT}} \frac{p_{HT}^{BP}}{p_{tot}^{BP\,1/2}} \tag{3.25}$$

$$c_T^{FS} = \frac{1}{2} K_{s_{HT}} \frac{p_{HT}^{BP}}{p_{tot}^{BP\,1/2}} \tag{3.26}$$

where c_H^{FS} and c_T^{FS} are hydrogen and tritium concentrations dissolved in the ARAA ferritic steel at the purge gas and cooling plates interface (solution of Eq. 3.32), $p_{H_2}^{BP}$ and p_{HT}^{BP} are the partial pressures of H_2 and HT respectively ($p_{tot}^{BP} = p_{H_2}^{BP} + p_{HT}^{BP}$ is the total pressure in the purge gas), and relate to the concentrations $c_{H_2}^{BP}$ and c_{HT}^{BP} through the ideal gas law:

$$p_{H_2}^{BP} = c_{H_2}^{BP} R T^{BP} \tag{3.27}$$

$$p_{HT}^{BP} = c_{HT}^{BP} R T^{BP} \tag{3.28}$$

A stiff-spring condition ensures flux continuity gas/metal interface. No flux boundary con-

dition is imposed for HTO and H_2O, since these molecules do not permeate to at the cooling plates. The concentrations at the purge gas channel inlet are derived through the ideal gas law as in 3.27 and 3.28 while outflow boundary condition ($-\mathbf{n} \cdot D_m^{BP} \nabla c_m^{BP} = 0$) is imposed at the channel outlet. The initial concentration of H_2 is calculated by using Eq. 3.27 for a partial pressure of 100 Pa of H_2 while HT, HTO, and H_2O are not initially present in the gas.

Concentration of H_2 and HT in beryllium multiplier purge gas

$$\frac{\partial c_m^{MP}}{\partial t} + \nabla \cdot (-D_m^{MP} \nabla c_m^{MP} + \mathbf{u}^{MP} c_m^{MP}) = R_m^{MP} \tag{3.29}$$

and $m = H_2,\ HT$. Eq. 3.29 has the same form of Eq. 3.18, thus a similar discussion holds. Here, we assume that the tritium produced in the beryllium multiplier is released in the molecular form HT; hence, for each mole of tritium atoms released a mole of HT molecules is formed and half a mole of H_2 molecules is consumed contained in the purge gas:

$$R_{H_2}^{BM} = -\frac{1}{2} \dot{G}_v^M f_r \tilde{p}(t) \frac{V^M}{V^{MP}} \tag{3.30}$$

$$R_{HT}^{BM} = \dot{G}_v^M f_r \tilde{p}(t) \frac{V^M}{V^{MP}} \tag{3.31}$$

where $\dot{G}_v^M f_r \tilde{p}(t)$ is the release rate from Be pebbles, V^M is the multiplier volume, and V^{MP} the volume of purge gas in the multiplier region. The presence of oxygen impurities due to Be nuclear transmutation is assumed to be negligible, thus formation of HTO and H_2O is not evaluated. The boundary conditions applied at the purge gas and cooling plates are the same as in Eqs. 3.25−3.28 where instead of the superscript BP (breeder purge) we use MP (multiplier purge). Similarly, the same inflow and outflow boundary conditions chosen for the breeder purge are used for the multiplier purge. There is no initial concentration of HT and H_2 in the multiplier purge gas.

Concentration of hydrogen and tritium in ARAA plates and graphite reflector

$$\frac{\partial c_s^{FS}}{\partial t} + \nabla \cdot (-D_s^{FS} \nabla c_s^{FS}) = 0 \tag{3.32}$$

$$\frac{\partial c_s^{G}}{\partial t} + \nabla \cdot (-D_s^{G} \nabla c_s^{G}) = 0 \tag{3.33}$$

where $s = H, T$. The boundary conditions of Eq. 3.32 are the same as equations 3.25 - 3.26 on breeder purge side, and equations 3.12 - 3.14 on coolant side. Instead, for Eq. 3.33 we use flux continuity at the cooling plate and graphite reflector interface, i.e. $-\mathbf{n} \cdot D_s^G \nabla c_s^G = J_s^{FS}$ where J_s^{FS} is the desorption/recombination flux from the cooling plate:

$$J_H^{FS} = 2\sigma k_{d_{H_2}} (c_H^{FS})^2 + 2\sigma k_{d_{HT}} c_H^{FS} c_T^{FS} \tag{3.34}$$

$$J_T^{FS} = 2\sigma k_{d_{T_2}} (c_T^{FS})^2 + 2\sigma k_{d_{HT}} c_H^{FS} c_T^{FS} \tag{3.35}$$

No flux boundary conditions are applied on the other boundaries of the graphite domain and the initial H and T concentrations in the graphite are zero.

3.1.2.2 Flow of purge gas through porous media

The purge gas flow through the pebble bed, is modeled by the Brinkman equations [16], i.e. an extended version of the Darcy's law which accounts for dissipation of kinetic energy by viscous shear, in a similar fashion to Navier-Stokes, and applies to fast-moving fluids through porous media. These equations are based on the volume averaging technique introduced by Whitaker [17]. The COMSOL physical model chosen for the fluid description is compressible flow (Ma<0.3). The fluid density is defined empirically as a function of temperature while the Brinkman equations are solved to obtain the velocity field $\mathbf{u}^i$ and pressure p^i in the

breeder and multiplier zones:

$$\frac{\rho^i}{\epsilon_p^j}\left(\frac{\partial \mathbf{u}^i}{\partial t}+(\mathbf{u}^i\cdot\nabla)\frac{\mathbf{u}^i}{\epsilon_p^j}\right)=\nabla\cdot\left[-p^i\mathbf{I}+\frac{\mu^i}{\epsilon_p^j}\left(\nabla\mathbf{u}^i+(\nabla\mathbf{u}^i)^T\right)-\frac{2}{3}\frac{\mu^i}{\epsilon_p^j}(\nabla\cdot\mathbf{u}^i)\mathbf{I}\right]-\frac{\mu^i}{\kappa^j}\mathbf{u}^i \quad (3.36)$$

$$\frac{\partial(\epsilon_p^j\rho^i)}{\partial t}+\nabla\cdot(\rho^i\mathbf{u}^i)=0 \quad (3.37)$$

where ρ^i and μ^i are the density and dynamic viscosity of helium purge gases ($i=BP,MP$), while ϵ_p^j and κ^j are the porosity and permeability of the pebble beds in the breeding and multiplier zones respectively, i.e. $j=BZ$ for $i=BP$ and $j=MZ$ for $i=MP$. No slip boundary condition is imposed at the walls, average inlet velocity is chosen as inlet condition, while backflow is suppressed at the channel outlet. The fluid is initially at rest.

3.1.2.3 Heat transfer in solids and porous media

Porous media: lithium metatitanate and beryllium pebble beds

In this work, the heat transfer analysis in breeding and multiplier zones is performed by using the COMSOL *Heat transfer in porous media* module, which treats the porous bed with helium purge gas as an homogeneous medium where characteristic properties are averaged based on the porosity (ϵ_p) and volume fraction ($1-\epsilon_p$) of the pebble beds in the breeder zone (BZ) and multiplier zone (MZ). Thus the energy equation for the breeder and multiplier pebble beds can be written as:

$$(\rho C_p)_{eff}^j\frac{\partial T^j}{\partial t}+\rho^i C_p^i\mathbf{u}^i\cdot\nabla T^j+\nabla\cdot(-k_{eff}^j\nabla T^j)=(q^{'''})^j\tilde{p}(t) \quad (3.38)$$

and:

$$(\rho C_p)_{eff}^{BZ}=\epsilon_p^{BZ}\rho^{BP}C_p^{BP}+(1-\epsilon_p^{BZ})\rho^B C_p^B \quad (3.39)$$

$$(\rho C_p)_{eff}^{MZ}=\epsilon_p^{MZ}\rho^{MP}C_p^{MP}+(1-\epsilon_p^{MZ})\rho^M C_p^M \quad (3.40)$$

where $j = BZ$ for $i = BP$ and $j = MZ$ for $i = MP$, BZ the breeder zone, BP the breeder purge, B the breeder, MZ the multiplier zone, MP the multiplier purge, and M the multiplier. For the effective thermal conductivity (k^j_{eff}) we use the empirical correlation [18] shown in Table 3.1. Heat flux continuity is implemented at the interface between the solids (ARAA) and porous media (i.e. Li_2TiO_3 or Be pebble beds), and between ARAA and graphite. Temperature boundary condition is imposed at the channel inlet while outflow boundary conditions is applied at the outlet of the channel. The BZ and MZ are initially at temperature of 573 K.

Solids: ARAA cooling plates and graphite

The heat transfer equations describing the cooling plates and the graphite reflector are:

$$\rho^{FS} C_p^{FS} \frac{\partial T^{FS}}{\partial t} + \nabla \cdot (-k^{FS} \nabla T^{FS}) = (q^{'''})^{FS} \tilde{p}(t) \tag{3.41}$$

$$\rho^{G} C_p^{G} \frac{\partial T^{G}}{\partial t} + \nabla \cdot (-k^{G} \nabla T^{G}) = (q^{'''})^{G} \tilde{p}(t) \tag{3.42}$$

where the meaning of the various terms has been previously discussed for Eq. 3.15, which has identical form. In this model conjugate heat transfer and thermo-fluid modeling of the purge gas and coolant is not considered. Instead, a convective heat transfer boundary condition, where the heat transfer coefficient is calculated analytically, is applied at the coolant/structure (CS) interface ($h_c^{CS} = 3750 \frac{W}{m^2 - K}$) since this method was proven to be effective [14] in representing prototypical BZ condition and a more detailed analysis is not of interest. Boundary conditions have been discussed in the previous section and the initial temperature is 573 K.

3.1.3 Connecting Pipes

The COMSOL module *Transport of Diluted Species* is used to model hydrogen isotopes transport in connecting pipes of the HCS and TES in ITER's rooms Port Interspace (PI), Port Cell (PC), and Vertical Shaft (VS). A 2-D axisymmetric model is used to describe the

mass transfer in the gas (He coolant and purge gas) and bulk structural material (SS316L). A schematic describing a section of the computational domain, geometrical parameters, and typical fluxes in shown in Fig. 3.5. The transport governing equation of hydrogen species

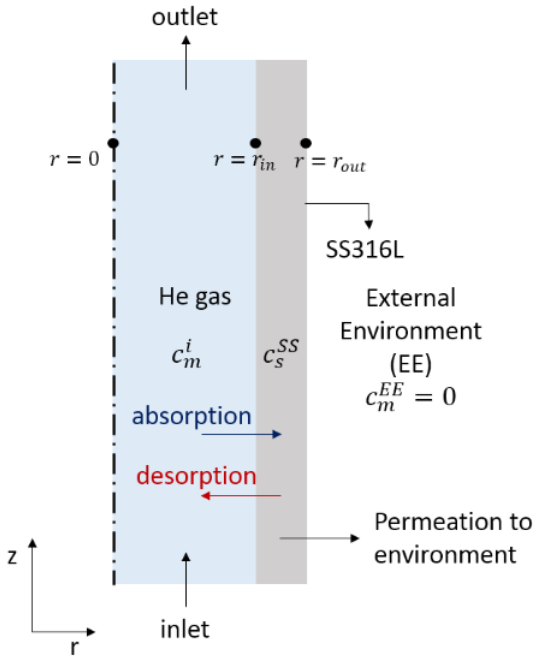

Figure 3.5: Schematic of gas and stainless steel domains of the pipe model implemented in COMSOL Multiphysics with concentrations of molecules $m = H_2,\ HD,\ HT$ dissolved in gas $i = CL, PG$, atom species $s = H,\ D,\ T$ dissolved in structural material, and various permeation fluxes.

in the He gases, i.e. coolant gas (CL) and purge gas (PG), and stainless steel (SS) regions are:

$$\frac{\partial c_m^i}{\partial t} + \nabla \cdot (-D_m^i \nabla c_m^i) + \mathbf{u}^i \cdot \nabla c_m^i = 0 \tag{3.43}$$

$$\frac{\partial c_s^{SS}}{\partial t} + \nabla \cdot (-D_s^{SS} \nabla c_s^{SS}) = 0 \tag{3.44}$$

where the molecules dissolved in the gas domain are $m = H_2,\ HD,\ HT$ for $i = CL$ and $m = H_2,\ HT,\ HTO,\ H_2O$ for $i = PG$, and the atoms dissolved in the stainless steel are $s = H,\ D,\ T$. Boundary conditions at the coolant gas/metal interface are typical diffusion

limited equations:

$$c_H^{SS} = K_{s_{H_2}} \frac{p_{H_2}^{CL}}{p_{tot}^{CL\,1/2}} + \frac{1}{2} K_{s_{HD}} \frac{p_{HD}^{CL}}{p_{tot}^{CL\,1/2}} + \frac{1}{2} K_{s_{HT}} \frac{p_{HT}^{CL}}{p_{tot}^{CL\,1/2}} \tag{3.45}$$

$$c_D^{SS} = \frac{1}{2} K_{s_{HD}} \frac{p_{HD}^{CL}}{p_{tot}^{CL\,1/2}} \tag{3.46}$$

$$c_T^{SS} = \frac{1}{2} K_{s_{HT}} \frac{p_{HT}^{CL}}{p_{tot}^{CL\,1/2}} \tag{3.47}$$

and similarly, for the purge gas we have:

$$c_H^{SS} = K_{s_{H_2}} \frac{p_{H_2}^{PG}}{p_{tot}^{PG\,1/2}} + \frac{1}{2} K_{s_{HT}} \frac{p_{HT}^{PG}}{p_{tot}^{PG\,1/2}} \tag{3.48}$$

$$c_T^{SS} = \frac{1}{2} K_{s_{HT}} \frac{p_{HT}^{PG}}{p_{tot}^{PG\,1/2}} \tag{3.49}$$

where c_H^{SS}, c_D^{SS}, and c_T^{SS} are hydrogen, deuterium, and tritium concentrations dissolved in SS316L at the purge gas and cooling plates interface (solution of Eq. 3.44), $p_{H_2}^{CL}$, p_{HD}^{CL}, and p_{HT}^{CL} are the partial pressures of H_2, HD, and HT in the coolant gas respectively ($p_{tot}^{CL} = p_{H_2}^{CL} + p_{HD}^{CL} + p_{HT}^{CL}$ is the total pressure in the coolant), $p_{H_2}^{PG}$, and p_{HT}^{PG} are the partial pressures of H_2, and HT in the purge gas respectively ($p_{tot}^{PG} = p_{H_2}^{PG} + p_{HT}^{PG}$ is the total pressure in the purge gas), and relate to the concentrations c_m^i through the ideal gas law: $p_m^i = c_m^i R T^i$. A stiff-spring condition ensures flux continuity at gas/solid interface. For the gas region, the inlet boundary conditions are inflow with constant molecules m concentration constraint ($c_m^i = p_m^i / R T^i$) and the outlet boundary condition is outflow $-\mathbf{n} \cdot D_m^i \nabla c_m^i = 0$. For the stainless steel region, the same Eqs. 3.45 - 3.47 apply to the gas/solid interface, while constant concentration $c_s^{SS} = 0$ is applied to the solid boundary in contact with the external environment, where we assume ^{1}H, ^{2}H, and ^{3}H are present in negligible fractions.

Heat transfer is simultaneously resolved in the gas and stainless steel regions by using

the COMSOL Multiphysics modules *Heat Transfer in Fluids* and *Heat Transfer in Solids*:

$$\rho^i C_p^i \frac{\partial T^i}{\partial t} + \rho^i C_p^i \mathbf{u}^i \cdot \nabla T^i + \nabla \cdot (-k^i \nabla T^i) = 0 \tag{3.50}$$

$$\rho^{SS} C_p^{SS} \frac{\partial T^{SS}}{\partial t} + \nabla \cdot (-k^{SS} \nabla T^{SS}) = 0 \tag{3.51}$$

where $i = CL, PG$, and SS is stainless steel SS316L. The pipes are externally thermally insulated while a characteristic heat transfer coefficient is applied at the gas/steel interface, $h_c^{CL/SS} = 2900$ W m^{-2} K^{-1} and $h_c^{PG/SS} = 25$ W m^{-2} K^{-1}. Inlet temperature condition is the coolant or purge gas temperature, while outflow is imposed at the pipe outlet, $-\mathbf{n} \cdot (-k^i \nabla T^i)$.

In this models we do not solve the momentum equation to determine the flow velocity distribution. Instead, we implement a fully developed velocity distribution with: (i) the "one-seventh power low", i.e. an accurate description of turbulent flow in helium coolant circular pipes ($Re^{CG} \sim 10^5$), and (ii) a parabolic distribution for the laminar helium purge gas flow ($Re^{PG} \sim 10^2$):

$$\frac{\mathbf{u}^{CL}}{U_{avg}^{CG}} = \left(1 - \frac{r}{r_{in}}\right)^{1/7} \tag{3.52}$$

$$\frac{\mathbf{u}^{PG}}{U_{max}^{PG}} = \left(1 - \frac{r}{r_{in}}\right)^{2} \tag{3.53}$$

where $U_{avg}^{CL} = \frac{7}{8} U_{max}^{CL}$, and r the radial coordinate varying from 0 to r_{in}, i.e. from the axis of symmetry and the inner radius of the pipe as shown in Fig. 3.5.

3.1.4 Other Components

Other components of the TBS, e.g. the Coolant Purification System and the Room Temperature Molecular Sieve, are not modeled in detail. Instead, an analytical formulation based on characteristic extraction process efficiency is implemented in the Simulink S-Functions as described in Subsection 3.3.1.

3.1.5 Transport properties and parameters used in the analysis

The correlations of transport parameters and properties used in the analysis are shown in Table 3.1, further detail can be found in [9, 10, 18, 19, 20]. In the absence of specific correlation for ARAA, we use data available for Eurofer and F82H which have similar chemical composition to ARAA.

Table 3.1: Transport properties used in the analysis.

Property	**Material**	**Correlation**	**Units**
Diffusivity	Eurofer	$4.57 \times 10^{-7} exp(-22300/R/T)$	$m^2\ s^{-1}$
Solubility	Eurofer	$2.25 \times 10^{-2} exp(-15100/R/T)$	$mol\ m^{-3}\ Pa^{-1/2}$
Q^*	Eurofer	$-0.77[eV] + 5.5 \times 10^{-4}[eV/K]T$	eV
Rec. Const. (clean plasma)	F82H	$2.89 \times 10^{-5} exp(0.48/k_b/T)$	$m^4\ mol^{-1}\ s^{-1}$
Rec. Const. (dirty plasma)	F82H	$7.83 \times 10^{-7} exp(0.68/k_b/T)$	$m^4\ mol^{-1}\ s^{-1}$
Density	Eurofer	$7732 - 1.92 \times 10^{-1}T - 3.64 \times 10^{-4}T^2 + 2.56 \times 10^{-7}T^3$	$kg\ m^{-3}$
Spec. Heat	Eurofer	$444.86 + 0.43T - 4.13 \times 10^{-4}T^2 + 9.25 \times 10^{-7}T^3$	$J\ kg^{-1}\ K^{-1}$
Conductivity	Eurofer	$25.77 + 1.34 \times 10^{-2}T - 7.46 \times 10^{-6}T^2 - 1.24 \times 10^{-8}T^3$	$W\ m^{-1}\ K^{-1}$
Diffusivity	SS316L	$7.66 \times 10^{-8} exp(-42500/R/T)$	$m^2\ s^{-1}$
Solubility	SS316L	$1.47 exp(-20600/R/T)$	$mol\ m^{-3}\ Pa^{-1/2}$
Density	Li_2TiO_3	1927	$kg\ m^{-3}$
Spec. Heat	Li_2TiO_3	$1062 + 0.9205T - 3.11 \times 10^{-4}T^2 + 1.56 \times 10^{-12}T^3$	$J\ kg^{-1}\ K^{-1}$
Conductivity	Li_2TiO_3	$1.0763 + 1.1354 \times 10^{-4}T$	$W\ m^{-1}\ K^{-1}$
T Res. Time	Li_2TiO_3	$1.28 \times 10^{-5} exp(9729/T)$	hr
Density	Be	1147	$kg\ m^{-3}$
Spec. Heat	Be	$1741 + 3.34T - 3.11 \times 10^{-3}T^2 + 1.27 \times 10^{-6}T^3$	$J\ kg^{-1}\ K^{-1}$
Conductivity	Be	2.5	$W\ m^{-1}\ K^{-1}$
Density	Graphite	1770	$kg\ m^{-3}$
Spec. Heat	Graphite	1500	$J\ kg^{-1}\ K^{-1}$
Conductivity	Graphite	80	$W\ m^{-1}\ K^{-1}$

where T is in K, the gas constant $R = 8.314 J\ kg^{-1}\ mol^{-1}$, and the Boltzmann constant $k_b = 8.617 \times 10^{-5} eV\ K^{-1}$. Unless otherwise specified, the analyses performed in Chapters 3−5 use the parameters of Table 3.1. Diffusivity coefficients for D and T in bulk structural

materials such as ARAA or SS316L are calculated as the hydrogen diffusivity multiplied by the square root of the ratio of H and T (or D) atomic masses, e.g. $D_T = D_H\sqrt{\frac{m_H}{m_T}}$ and $D_D = D_H\sqrt{\frac{m_H}{m_D}}$, as derived in [21].

3.1.6 Validation of the mathematical formulation of tritium co-permeation

The validation of the co-permeation mathematical model used in this work (see Eq. 3.11) is performed by comparing the tritium permeation rates simulated in COMSOL Multiphysics and the results of a recent Tritium Gas Absorption Permeation (TGAP) experimental campaign performed at the Idaho National Laboratory (INL) [22]. In the experiment, tritium permeation rates for Korean ARAA circular samples were calculated over a wide range of HT partial pressures, i.e., from 10^{-5} to 10^{1} Pa, and for H-T thermodynamics equilibrium conditions. Our calculation shows perfect agreement between experimental results and predicted values over the entire range of HT pressure, as shown in Fig. 4.6. We found linear dependency of tritium permeation rate with HT partial pressure and square root dependency with T_2 partial pressure (plotted in the range 10^{-5} to 10^{1} Pa).

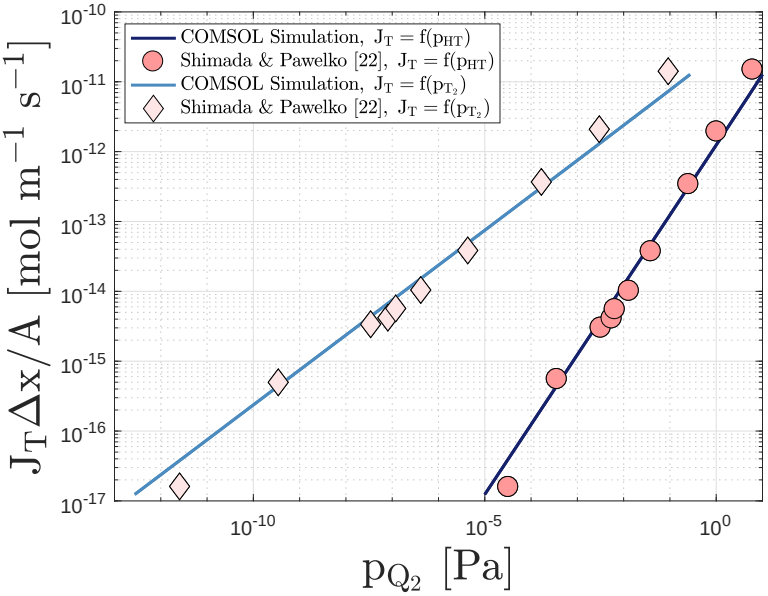

Figure 3.6: Comparison of tritium permeation rates predicted with COMSOL Multiphysics and INL's experimental results [22]. Permeation rates are plotted as a function of Q_2 partial pressure, where Q_2 = HT, T_2.

3.2 Neutronics Analysis of the HCCR TBM and Assessment of Particle Implantation into the First Wall

In this section we perform neutronics analysis of the HCCR TBM with the use of the MCNP code to calculate volumetric nuclear heating and tritium production rate in breeding materials of the blanket. Furthermore, we evaluate the first wall implantation particle flux profile for ion energy range 200 - 400 eV with the use of the SRIM/TRIM code. These parameters serve as input values to the HCCR TBS dynamic model described in Section 3.1, thus they need to be evaluated before performing the assessment of tritium inventory and release to ITER's rooms.

3.2.1 Neutronics assessment of HCCR breeding blanket with integrated first wall

Blankets play a key role in fusion technology by performing power extraction, tritium breeding and shielding. A peculiar characteristic of the fusion environment is the presence of steep nuclear heating gradients and tritium production rate due to the exothermic nuclear reaction ^{6}Li(n, α)T and the high intensity neutron flux in the proximity of the first wall and beryllium zones, where neutron multiplication takes place as ^{9}Be(n, 2n)2α. Moreover, the steep bulk nuclear heating gradient generates sharp temperature gradients affecting tritium transport and generating thermal-mechanical stresses that can compromise performance and integrity of components. Accurate evaluation of nuclear heating and tritium production rates is necessary to provide input to FEM models and perform thermal and mass transport analysis.

This study analyzes the Korean HCCR ceramic breeder blanket TBM [23] that will be tested in the International Thermonuclear Experimental Reactor. Neutronics simulations are performed with the use of MCNP6 1.0 [24] neutron transport code with ENDFB/VII.0 cross section library. For convenience, blankets are simulated in a simplified ITER-like wedge reactor model (Fig. 3.7) with reflective boundary conditions in the azimuthal and z directions and a peak neutron wall loading (NWL) of 0.78 MW/m^2, which is representative of the ITER equatorial port where the HCCR is placed. The wedge's height is equal to the

height of the blankets, the wideness is defined by blankets width while radial dimensions and materials are sum up in Table 3.2.

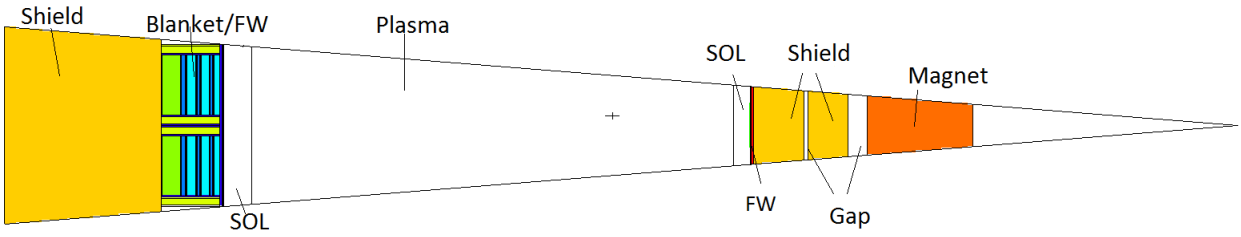

Figure 3.7: MCNP ITER-like reactor wedge model.

The HCCR is 1670 mm height, 462 mm width and 520 mm thick. It is subdivided into four sub-modules as shown in Fig. 3.8. The components of each sub-module are: First Wall (FW), Side Wall (SW), Breeding Zone (BZ), Multiplier Zone (MZ), Graphite Reflector (GR). The back of each sub-module is connected to a commune Back Manifold (BM).

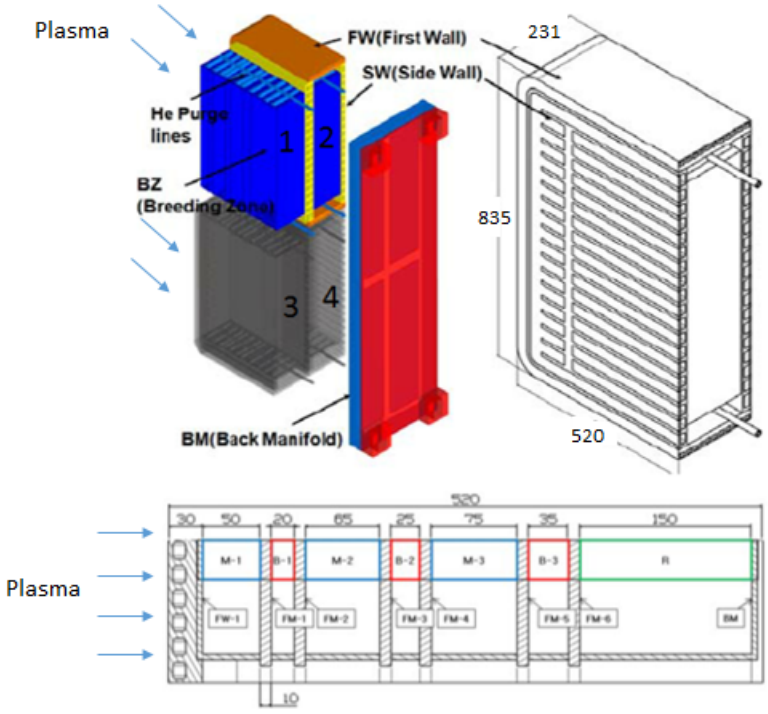

Figure 3.8: KO HCCR TBM and its sub-modules. The numbers in the figure indicate each HCCR sub-module. (Edited by [25])

The breeder is Li_2TiO_3 and the purge gas is helium. The neutron multiplier is pure beryllium in form of pebbles. The structural material for FW and SW is Advanced Reduced

Table 3.2: ITER-like model material compositions and dimensions.

Component	**Radial Thickness [cm]**	**Material**	**% vol**
Magnet	87.5	SS316	47%
		Epoxy	13.3%
		Cu	12%
		Nb_3Sn	3%
		He Liquid	17.2%
		Bronze	7.5%
Gap	16	Void	-
Shield	33.5	SS316	75%
		H_2O	25%
Gap	3	Void	-
Shield	33.5	SS316	75%
		H_2O	25%
FW	2	Cu	70%
		H_2O	20%
		SS316	10%
FW coating	1	Be	100%
SOL	14	Void	-
Plasma	400	Void	-
SOL	24.8	Void	-
BLANKET+FW: HCCR	52		
Shield	33.5	SS316	75%
		H_2O	25%

Activation Alloy (ARAA) with helium cooling ducts. The FW is modeled by three layers of different materials: FW front channel (100% F82H), cooling channel (83% He, 17% F82H), back plate (100% F82H).

3.2.1.1 HCCR nuclear volumetric heating assessment

Neutronics simulations have been performed for the HCCR breeding blanket. The reference design has 70% enrichment in ^{6}Li and uses lithium meta-titanate pebbles with 0.64 packing fraction. A considerable part of the neutron current passing through the FW is at lower energy than 14.58 MeV because of neutron back-scattering in the inboard region of the reactor. The total nuclear heating in the TBM is 0.661 MW. Nuclear heating gradient in sub-module 1 (Fig. 3.8) is shown in Fig. 3.9. It is found that the most of the nuclear heating is due to neutrons energy deposition while photons contribution is negligible. 2-D plots of nuclear heating are shown in Fig. 3.10.

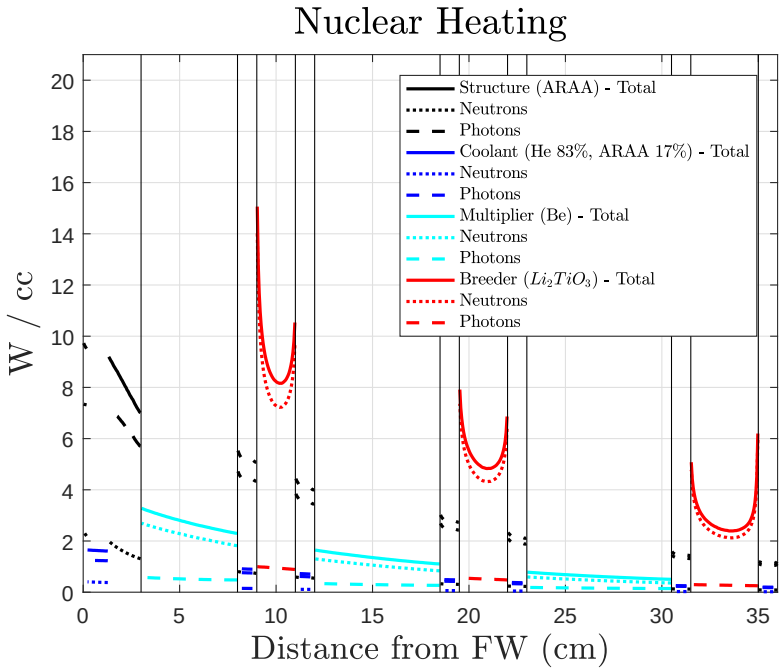

Figure 3.9: Radial nuclear heating deposition for HCCR sub-module 1. Graphite reflector is not shown.

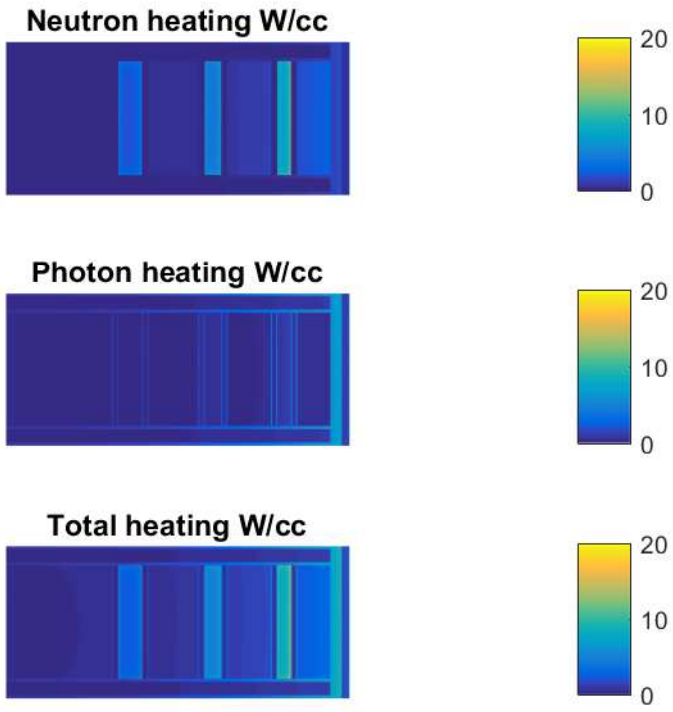

Figure 3.10: Nuclear heating deposition for HCCR sub-module 1.

3.2.1.2 HCCR tritium production rate assessment

The local TBR in the whole blanket (four sub-modules) is 0.86 for a total tritium production rate of 1.147×10^{-6} g/s, i.e. 99.1 mg/day. The TPR profiles are shown in Fig. 3.11. Tritium production is enhanced in proximity of the cooling plates, due to the effect of the neutron multiplication in beryllium, which resides in the adjacent zones.

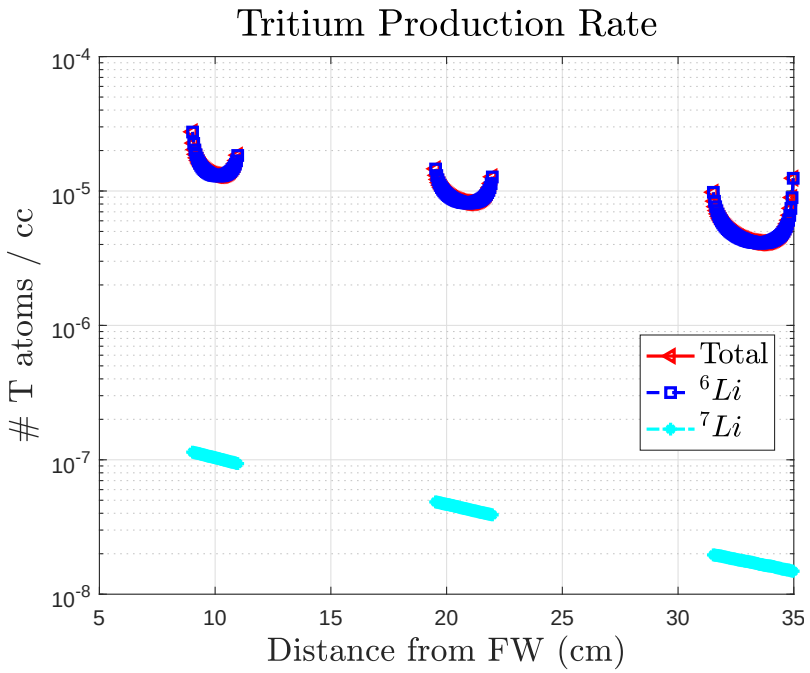

Figure 3.11: Tritium production rate in breeding material for HCCR sub-module 1.

3.2.2 Assessment of first wall implantation particle flux profile with ion flux energy range 200 eV, 400 eV, 600 eV

The FW is subject to a high deuterium-tritium ion flux from plasma which diffuses from the ferritic steel structure and, ultimately, permeates to the helium coolant loop. For ITER, the D−T flux is expected to be of the order of 10^{21} atoms/m^2-s and corresponds to $\sim$ 25 times of HCCR TBM calculated tritium generation rate. The ion energy spectrum is expected to be between 200 to 600 eV [26]. Accuracy in defining the deuterium-tritium source in Plasma Facing Components, e.g. FW and divertor, is of fundamental importance to determine the correct D, and T permeation rate to coolant, particularly because tritium permeation to coolant from FW is the dominant process, while tritium permeation to coolant from the BZ is reduced by the presence of a 0.1% vol of H_2 in the purge gas. Analysis regarding the energy spectrum of the ion particle implanted into the FW is performed with the use of the Monte Carlo code Stopping and Range of Ions in Matter (SRIM) [8] for D and T ions at energies E = 200, 400, 600 eV colliding with a 300 Angstrom target of Advanced Reduced Activation Alloy (ARAA), whose composition is shown in Table 3.3. The resulting ion distributions and

estimated reflection coefficients for different ion energies are shown in Fig. 3.12 and Table 3.4.

Table 3.3: Chemical composition of ARAA.

Element	**Unit**	**ARAA**
C	wt%	0.08 - 0.12
Si	wt%	0.05 - 0.15
Mn	wt%	0.30 - 0.60
Cr	wt%	8.70 - 9.30
W	wt%	1.00 - 1.40
V	wt%	0.05 - 0.30
Ta	wt%	0.005 - 0.09
N	wt%	0.005 - 0.015
B	wt%	< 0.002
Ti	wt%	0.005 - 0.020
Zr	wt%	0.005 - 0.020
S	ppm	< 50
P	ppm	< 50
O	ppm	< 100
H	ppm	< 10
Cu	ppm	< 100
Ni	ppm	< 100
Mo	ppm	< 50
Nb	ppm	< 50
Al	ppm	< 100
Co	ppm	< 100
As + Sn + Sb	ppm	< 50

It can be seen from the normalized fluxed distribution that to higher energies corresponds deeper penetration into the target. Moreover, no particles are expected to penetrate further than 30 nm, not even for particle energy of 600 eV. Given the magnitude of the region

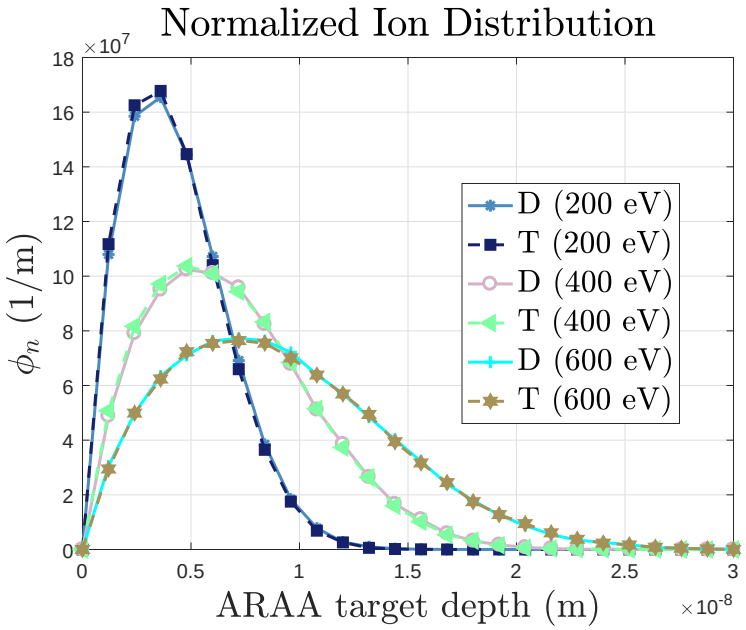

Figure 3.12: SRIM ion distribution for different energies.

Table 3.4: Reflection factor r for D, T at different energies.

Ion	**E = 200 eV**	**E = 400 eV**	**E = 600 eV**
D	0.335	0.303	0.282
T	0.334	0.305	0.286

of D, T implantation, small changes are expected to be noticed in terms of permeation to coolant rate for different energy range. The implantation profile is modeled in COMSOL as a Weibull probability density function:

$$w(x|a,b) = \frac{a}{b}\left(\frac{x}{b}\right)^{a-1} exp\left[-\left(\frac{x}{b}\right)^{a}\right] \tag{3.54}$$

where $a > 0$ and $b > 0$ are the shape and scale factors respectively. Values of shape and scale factors were found with the use of the MATLAB function *wblfit*. As an example, we show in Fig. 3.13 the SRIM normalized ion distribution and relative Weibull distribution for tritium at 400 eV.

Fig. 3.14 shows the calculated tritium permeation rate to coolant. The impact of the energy level of the implanted fluxes on tritium transport and permeation rate to coolant is

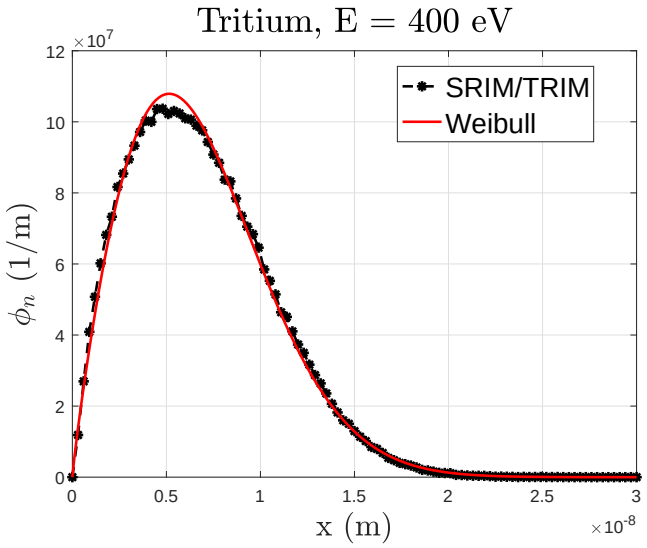

Figure 3.13: SRIM ion distribution for 400 eV incoming flux.

almost insignificant since ion deposition occurs only at a region < 30 nm. In the absence of detailed energy spectrum data, 400 eV as average value is used for ion implantation energy. More accurate characterization of ion implantation profile and subsequent inventory and permeation rate to coolant will be performed upon energy spectrum data is availability.

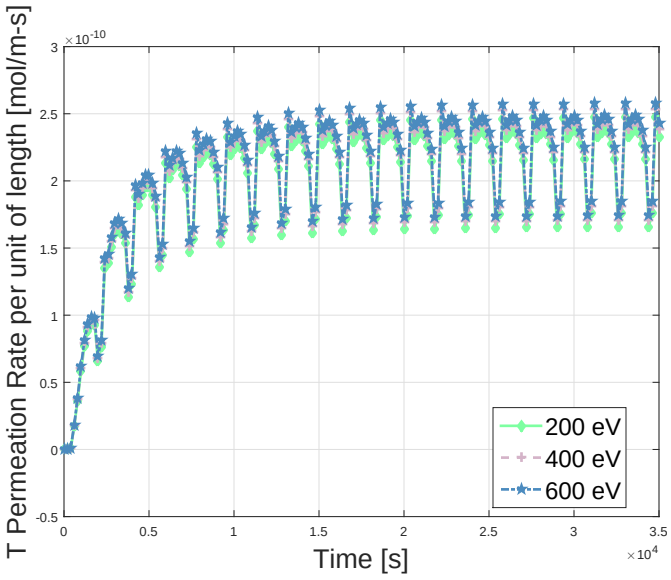

Figure 3.14: Tritium permeation rate to coolant per unit of length for ion implantation energies of 200, 400, 600 eV.

3.3 HCCR TBS System-level Dynamic Modeling

In this section, a detailed description of the of the mathematical formulation derived in order to estimate of the Q_2 and Q_2O partial pressures in the coolant gas and purge gas is provided. A system-level model representing tritium streams in the HCCR TBS is necessary to evaluate tritium content in He coolant and purge gas, which depends on the tritium permeation rate from FW and BZ (tritium sources) to He gas, and on the performance of purification and extraction systems (tritium sinks), i.e. CPS and TES. Accurate evaluation of Q_2 molecule concentrations (or partial pressures) in coolant and purge gas is particularly important to determine the tritium inventory build-up in connecting pipes and the tritium permeation rate to the environment. These operations are performed through MATLAB functions, i.e. System Functions (or S-Functions). The mathematical formulation implemented in the MATLAB S-Functions to compute Q_2 and Q_2O partial pressure in gas streams is given in detail in Subsection 3.3.1.

S-Functions are a computer language description of a Simulink block written in MATLAB (or C/C++), that can perform a variety of tasks. Especially, S-Functions are very powerful tools for data transfer between components of the system: within the integrated system-level approach, each S-Function provides the virtual representation of a detailed component by generating a link between the COMSOL detailed models and the Simulink system-level description. A generic S-Function is shown in Fig. 3.15. It is divided into three sub-functions: (i) *mdlInitializeSizes* receives the input $\mathbf{u}$ and returns the size, initial conditions, and sample times; (ii) *mdlUpdate* returns the updated states $\mathbf{x}$; (iii) *mdlOutputs* returns the block outputs $\mathbf{y} = f(t,\ \mathbf{x},\ \mathbf{u})$.

Within one system-level time step dt_{sys}, the S-Function calls the COMSOL application, i.e. a detailed model of the HCCR TBS, and runs it for a time interval $[t_i,\ t_{i+1}]$, where $dt_{sys} = t_{i+1} - t_i$. During this run, COMSOL uses appropriate detailed component model time step (dt_{DC}) in order to meet the time convergence criteria of the finite element problem and uses the states $\mathbf{x}(t_i)$, e.g. H, D, and T concentrations, temperature profiles, etc., as initial conditions while the boundary conditions are defined in the inputs $\mathbf{u}(t_i)$, e.g. these

are the partial pressures of Q_2 and Q_2O in the coolant and purge gas. Finally, the output $\mathbf{y} = f(t,\ \mathbf{x},\ \mathbf{u})$ is generated and transferred to the next component, which will interpret this as an input for the next time step $[t_{i+1},\ t_{i+2}]$. With the use of S-Functions it is possible

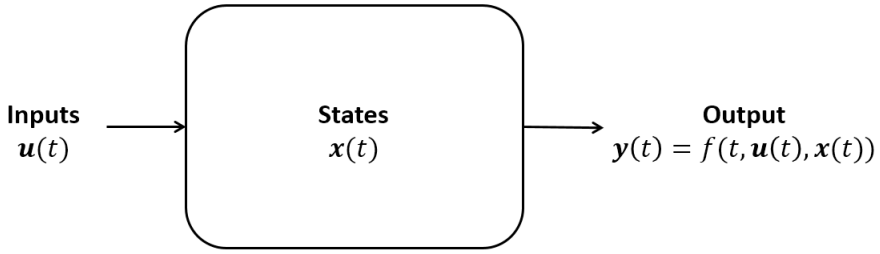

Figure 3.15: Schematic of a generic S-Function.

to model a circuit which accurately reproduces tritium flow rates on system level and, at the same time, maintain a high degree of accuracy in each component, which is accurately resolved by COMSOL solver. This approach is superior to previous system-level codes, e.g. TMAP4/TMAP7 or FUS-TPC, where the high fidelity of detailed component is missing in favor of a system-level description.

The generated HCCR TBS system-level model is shown in Fig. 3.16. In particular, the He coolant removes heat generated in the FW and BZ sub-modules and reaches the heat exchanger (HX) through the connecting pipes (hot leg) located in PI, PC, and VS rooms. A fraction α_{CPS} of the total He flow rate is by-passed to the coolant purification system (CPS) where tritium removal from gas is performed, with an efficiency η_{CPS}. Finally, the purified He coolant stream returns to the FW and BZ sub-modules through connecting pipes (cold leg) of PI, PC, and VS rooms. In parallel, the He purge gas, which includes a 0.1% addition of H_2 to enhance tritium extraction from pebbles, is processed by the tritium extraction system (TES) which comprehends the Cryogenic Molecular Sieve Bed (CMSB), and the Room Temperature Molecular Sieve (RTMS).

The objective of the system-level model is to accurately capture the TBS dynamics, with particular interest regarding the Q_2 and Q_2O concentrations in the coolant and purge gas, which determine the boundary conditions at the gas/structure interface of FW, BZ, and pipes. In particular the following operations are performed:

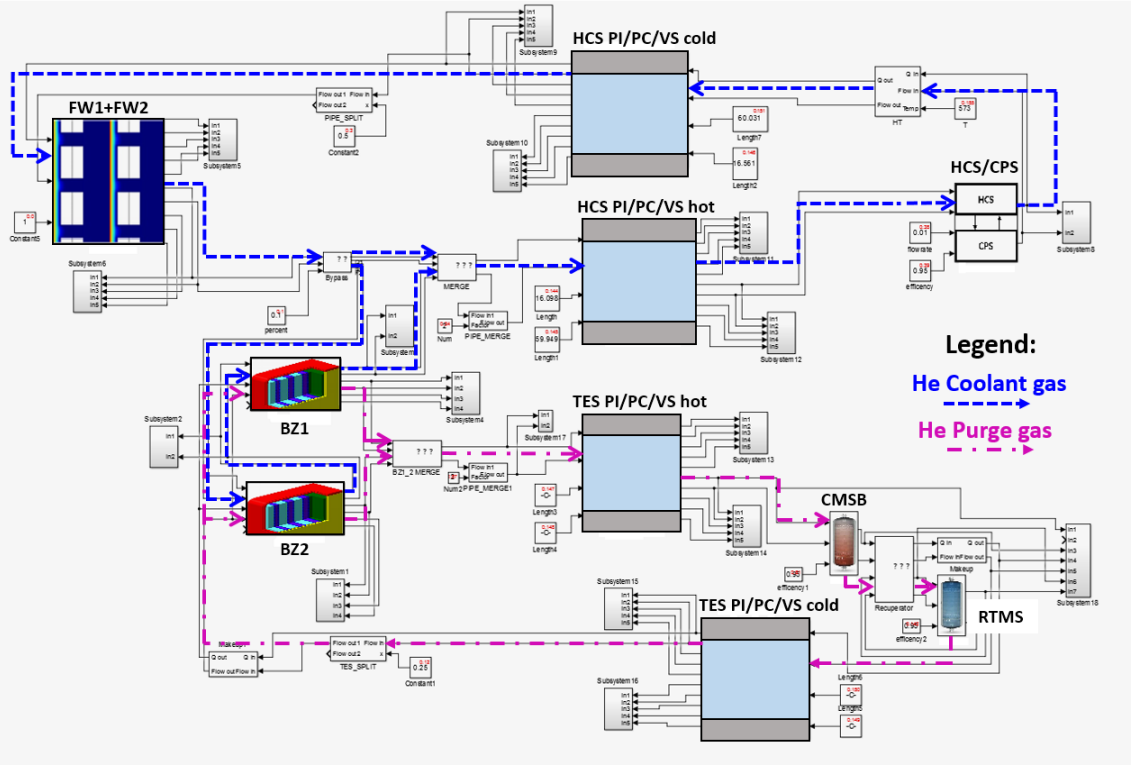

Figure 3.16: Schematic of the HCCR TBS modeled in the Simulink: each block is described by a specific S-Function.

- calculation of ^{1}H, ^{2}H, and ^{3}H permeation rates from BZ and FW to coolant gas;
- evaluation of Q_2 and Q_2O partial pressures in coolant and purge gas;
- definition of boundary condition to be used in the COMSOL calculation;
- COMSOL run;
- data post-processing, e.g. evaluation of permeation rates to buildings, inventories of fuel cycle components, etc.;
- storing of results and outputs.

3.3.1 Mathematical formulation implemented in the S-Functions developed for the HCCR TBS

Concentrations of HT (and other Q_2 molecules) in the coolant gas are due to tritium (and other Q atoms) permeation to coolant from the breeding zones, where tritium in bred in the ceramics and $\sim$100$-$300 Pa of H_2 are present in the purge gas, and from the first wall, where tritium and deuterium are implanted in the structural material because of the high particle fluxes at the first wall surface from the plasma. In order to determine the partial pressures of Q_2 molecules in the coolant, it is necessary to evaluate the Q permeation rates from FW and BZ. The S-Functions of both FW and BZ calculate the total permeation rate of species s into coolant, $J_s^{i\rightarrow CL}$ $(mol\ s^{-1})$, from component i, where $i = FW, BZ$, by integrating the atomic flux of species s, N_s $(mol\ m^{-2}\ s^{-1})$, over the surface area of the coolant channels, A_{CL} (m^2):

$$J_s^{i\rightarrow CL} = \int_{A_{CL}} N_s dA \tag{3.55}$$

where $N_s = -D_s \nabla c_s$, s = H, D, T, and i = BZ, FW. The concentrations of HD and HT molecules in the coolant at the BZ and FW outlet are obtained by summing the ratio of the calculated permeation rates, J_s, to the volumetric helium coolant flow rate, Q^{CL} $(m^3 s^{-1})$, to the concentrations of HD and HT in the coolant at the BZ and FW inlet:

$$c_{m,out}^{i,CL} = c_{m,in}^{i,CL} + \frac{J_s^{i\rightarrow CL}}{Q^{CL}} \tag{3.56}$$

where m = HD, and HT. Hence, since each D and T atoms consumes respectively one H atom, the H_2 concentration in the coolant is:

$$c_{H_2,out}^{i,CL} = c_{H_2,in}^{i,CL} + \frac{1}{2}\frac{J_H^{i\rightarrow CL} - J_D^{i\rightarrow CL} - J_T^{i\rightarrow CL}}{Q^{CL}} \tag{3.57}$$

and $m = H_2$, HD, and HT.

In the HCCR TBS, tritium (and other Q atoms) removal form coolant gas is performed in the coolant purification system (CPS), which we modeled analytically in the CPS S-Function by assuming that a fraction (α_{CPS}) of the total coolant flow rate is processed with

an efficiency η_{CPS}. Thus, the concentration at the CPS outlet is:

$$c_{m,out}^{CPS} = c_{m,in}^{CPS}(1 - \alpha_{CPS}\eta_{CPS}) \tag{3.58}$$

Concentration can then be converted into pressures by means of ideal gas law. The purge gas dynamics is simulated in COMSOL; thus, in this case, the S-Functions are only used to output the Q_2 and Q_2O concentrations at specific locations. However, an analytical description of the tritium extraction system (TES) is used to model CMSB, in a similar fashion to Eq. 3.58:

$$c_{m,out}^{CMSB} = c_{m,in}^{CMSB}(1 - \eta_{CMSB}) \tag{3.59}$$

where $m = H_2$, HT, η_{CMSB} is the extraction efficiency of the CMSB. For the RTMS:

$$c_{m,out}^{RTMS} = c_{m,in}^{RTMS}(1 - \eta_{RTMS}) \tag{3.60}$$

where $m = H_2O$, HTO, η_{RTMS} is the extraction efficiency of the CMSB.

As the purge gas and coolant gas flow through the pipe forest, Q atoms permeates into the pipe structural material and are released to the buildings. The tritium permeation rates to building are calculated by integrating the tritium flux over the outer surface of the pipes:

$$J_s^{i \to rooms} = \int_{A_P} N_s dA \tag{3.61}$$

where $N_s = -D_s \nabla c_s$, s = H, D, T, and i = PI, PC, and VS pipes for both CPS and TES lines (PI, PC, and VS are the Port Interspace, Port Cell, and Vertical Shaft of the ITER rooms, respectively).

3.3.2 Optimization of the Simulink setup

3.3.2.1 Reduction of S-Function calls and use of combined COMSOL models

The computational efficiency of the dynamic tritium transport model for HCCR TBS is limited by the presence of several S-Functions which, at each time step, generate a COMSOL

object and run it. The presence of n S-Functions generate and run n COMSOL objects with n components (e.g. First Wall, Breeding Zones, pipes, etc.). To minimize the number of S-Function calls, which have a detrimental effect of computational time, multi-component COMSOL models were generated by including different components (e.g. PI and PC pipes) in a single COMSOL file. Hence, with a single S-Function call, more components can run simultaneously in the same COMSOL file. For instance, if every COMSOL file contains 2 components, S-Function calls are cut in half: $n/2$ S-Functions generate and run $n/2$ COMSOL objects with n components. In particular, we reduced the overall number of S-Functions from 12 (one per each COMSOL model) to 7 (by using multi-component COMSOL models for FW and pipes combined) and obtained an overall reduction of the computational time of $\sim 20\%$.

3.3.2.2 Investigation of COMSOL minimum time-step and multi-core cluster option

An effort was launched to optimize the computational performance of the COMSOL solver. As far as COMSOL is concerned, a new simulation is run at each system level time-step (defined in the Simulink model). Therefore, to achieve convergence the numerical solver of COMSOL imposes the default minimum time-step (Solver Configuration $\rightarrow$ Time Stepping). We found that this default time step is, in most cases, too strict therefore making the simulation computational time longer than needed. In other words, the converging of the time step can be found for larger time-steps which reduce the computational time required to run the model. A parametric study on the maximum COMSOL stepsizes that ensures numerical convergence was performed for each component and different stepsizes, depending on the component nature and physics simulated, were implemented in different models. For instance, the most expensive COMSOL model in terms of computational time was the breeding zone; the minimum time step was increased from 10^{-4} to 10^{-1} and the use of the Fully Coupled solver was chosen. This procedure reduced the computational time required to run the breeding zone model by more than a half, resulting in an overall reduction the system-level computational time of $\sim 20\%$.

In parallel, the model was tested on the UCLA Hoffman2 cluster for a one-month trial period using different cluster nodes with 12, 16, 24 cores at a speed of 2.20 GHz. Even for the best case (24 cores), the required computational time was similar (slightly reduced) to the one found for a computer with 12 cores and 2.67 GHz. This is due to the nature of time-dependent problems that are "completely serial", because of the dependence of subsequent parts of the solution on previously computed values, (even if the COMSOL solver is "partially parallel" when solving the matrix for each time-step). Thus, the cluster option does not offer better performances and therefore will not be considered.

3.4 Benchmark Activity of the HCCR TBS Simulink/COMSOL Dynamic Model

3.4.1 Study on the converging of the system-level time step

A converging of the system-level time step study was performed for the HCCR TBS model in order to define the smaller time step which ensures convergence of results (i.e. time step independence) and, simultaneously, reduces the computational time needed to run the full model. The HT pressure evolution with time is shown in Fig. 3.17 for system level time step of 2, 4, and 10 s. For this simulation we used the design values of the CPS and TES lines, i.e. $\eta_{CPS} = 95\%$, $\alpha_{CPS} = 1\%$, $Q^{CL} = 1.14$ kg/s, $\eta_{CMSB} = 95\%$, $\eta_{RTMS} = 95\%$, $Q^{PG} = 1$ g/s. We found that the time step choice affects transient behavior while same equilibrium pressure is found for all time steps, as in typical sink/source problems.

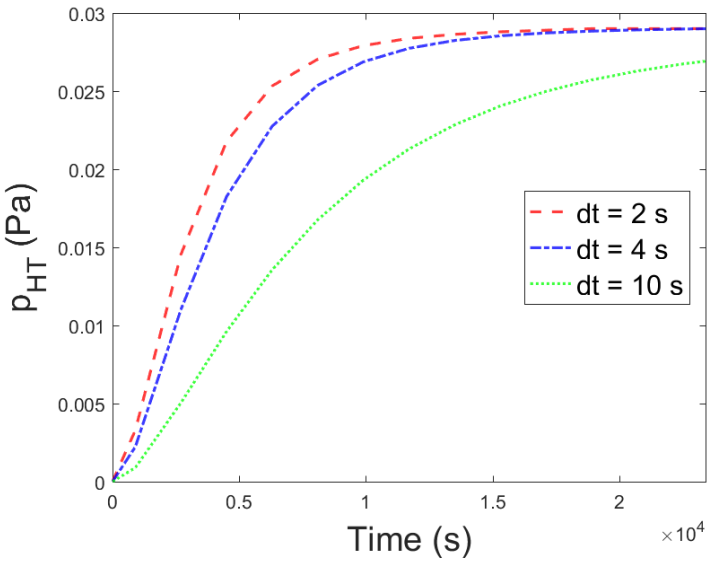

Figure 3.17: Average values (per ITER pulse) of HT partial pressure time evolution for system-level time step of 2, 4, and 10 s.

We did not run any simulation with a time step smaller than 2 s, since the computational time would increase to unacceptable values (e.g. one month of computational time or more to run up to quasi-equilibrium state - i.e. about 8 ITER pulses of 1800 s each) we believe that a 2 s time step is adequate in term of convergence of the time step. In fact, there is

small difference between the pressures obtained for time step of 2 s and 4 s during the initial transient. Moreover, the coolant pressures are in quasi-equilibrium after ∼8 ITER pulses, i.e. ∼14.4×10^3 s, while tritium permeation from pipes to rooms starts after more than two days of pulsed operation (the permeation is delayed due to dwell time where temperatures are low and tritium is mainly re-emitted within the pipes to the He coolant). Thus, small inaccuracy in the coolant pressure transient during the first 8 pulses has a negligible effect on tritium permeation from pipes to rooms, which occurs after more than 100 pulses. The computational time needed to run the model until the system is in quasi-equilibrium for time step of 2, 4, and 10 s is shown in Fig. 3.18.

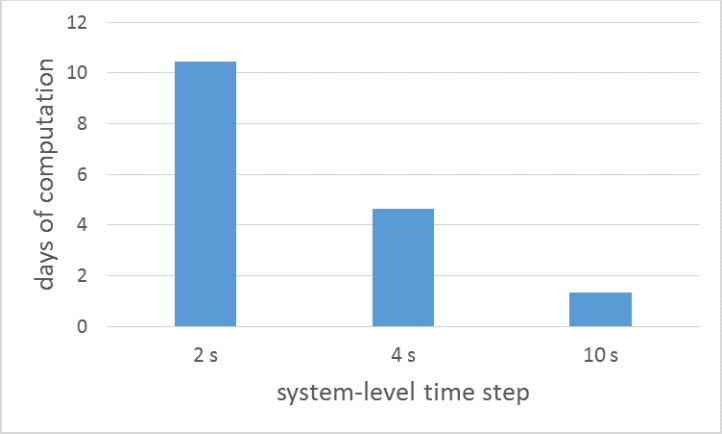

Figure 3.18: Computational time required to obtain quasi-equilibrium values of coolant partial pressure for various system-level time steps.

3.4.2 Verification of mass conservation in the HCS of the the HCCR TBS dynamic model

This verification study is based on the fact that, if an equilibrium state is obtained in the coolant partial pressures, then, because of mass conservation, the tritium permeation rate from FW and BZ to coolant must be equal to the the tritium flow rate extracted by the CPS units. We performed a mass conservation verification study to ensure that tritium permeated into the coolant from FW and BZ is entirely removed by the CPS at equilibrium. The design parameters of the CPS and TES lines are used in the analysis, i.e. $\eta_{CPS} = 95\%$, $\alpha_{CPS} = 1\%$, $Q^{CL} = 1.14$ kg/s, $\eta_{CMSB} = 95\%$, $\eta_{RTMS} = 95\%$, $Q^{PG} = 1$ g/s. Results of the

calculation are shown in Fig. 3.19 (the simulation is performed on a time step of 10 s). It is

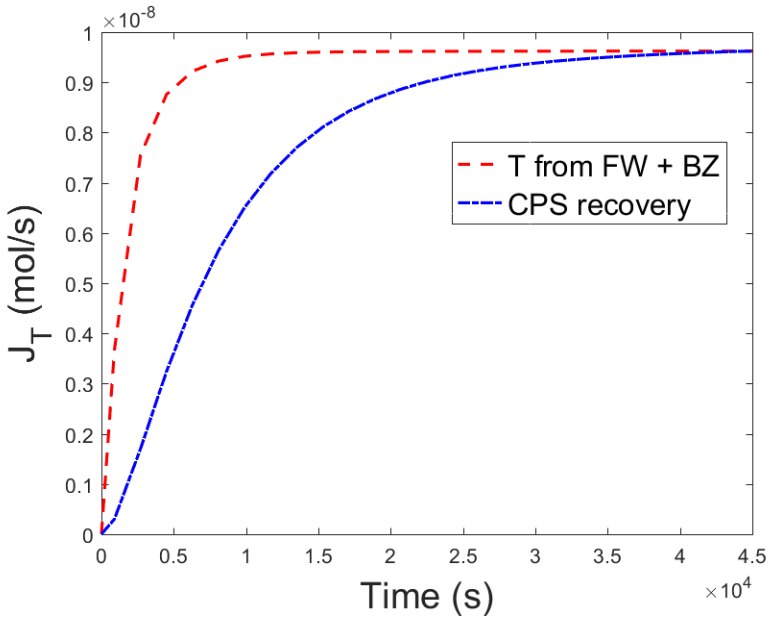

Figure 3.19: Average values (per ITER pulse) of tritium permeation rate to coolant from FW and CPS recovery flow rate evolution with time.

seen that, when equilibrium is reached, the tritium recovered by the CPS unit matches the tritium permeated into coolant from FW and BZ. To conclude, we have confirmed that the systems dynamics is correctly implemented, and mass is conserved.

3.4.3 Validation of the HCCR TBS dynamic model

3.4.3.1 Comparison between tritium release to ITER's room obtained with the HCCR TBS dynamic model and pre-existing models developed by NFRI

A first effort to evaluate tritium permeation to ITER rooms for the HCCR TBS was started by the National Fusion Research Institute (NFRI) team in 2017 [27]. In this section we validate the HCCR dynamic model described in Sections 3.1, 3.2, and 3.3 by running the model under the same conditions of [27] and comparing the obtained results of tritium release to the ITER's rooms. In particular, the calculation follows the following conservative assumptions:

- steady-state approach for tritium production (25.9 mg/day for each HCCR submodule - total of 4 submodules);
- bulk-diffusion for transport mechanism through structural materials and diffusion-limited regime;
- only tritium is considered (co-permeation of H and D is neglected);
- average temperature for hot and cold legs of HCS pipes: hot leg at 450 °C and cold leg 300 °C.

Note that neglecting H and D species in the coolant gas implies that tritium exists in the form of T_2, and the diffusion-limited regime defines tritium concentration at the metal and gas interface as $C_T = K_{S_T}\sqrt{p_{T_2}}$, where K_{S_T} is the Sieverts' constant (or solubility) of tritium dissolved in the bulk of SS316L (or ferritic steel ARAA). In the analysis we assume $K_{S_T} = K_{S_H}$ to be consistent with the calculation of [27]. The analysis is performed for the design parameters presented in Table 3.5 and uses the properties listed in Table 3.6.

Table 3.5: Design parameters of HCS and CPS.

Sub-system	**HCS**	**CPS**
Fluid	Helium Coolant	Helium Coolant
Pressure	8 MPa	8 MPa
Flow rate	1.14 kg/s	1% of HCS flow rate
Tritium processing efficiency	-	95%

Table 3.6: Properties used in the validation calculation.

Property	**Correlation**	**Units**
Diffusivity Eurofer	$4.57 \times 10^{-7} exp(-22300/R/T)$	$m^2\ s^{-1}$
Solubility Eurofer	$2.25 \times 10^{-2} exp(-15100/R/T)$	$mol\ m^{-3}\ Pa^{-1/2}$
Diffusivity SS316L	$7.66 \times 10^{-8} exp(-42500/R/T)$	$m^2\ s^{-1}$
Solubility SS316L	$1.47 exp(-20600/R/T)$	$mol\ m^{-3}\ Pa^{-1/2}$

Tritium release to ITER rooms by permeation is calculated for the tritium dissolved in the coolant of the HCS at equilibrium, i.e. for a pressure of 0.0104 Pa. The calculated tritium release rate to ITER rooms is shown in Table 3.7 in detail for the hot and cold legs of the HCS. The total release rate (sum of hot and cold leg contributes) is summarized in Table 3.8, together with the results of the calculation presented in [27], and the relative error between the two calculations. The permeation rates obtained by using the HCCR TBS dynamic model are in good agreement with the results presented in [27], when the same assumptions are considered. The relative error between the two calculations is below 0.5% in all ITER HCS locations with the only exception of room 14-L4-21 (relative error of 1.68%).

Table 3.7: Equilibrium tritium release to ITER's rooms calculated with the dynamic model of HCCR TBS assuming constant temperatures of 300 °C for cold leg and 450 °C for hot leg and tritium partial pressure of 0.01 Pa.

Location in HCS	**Pipe length (m)**	**T release (mg/day)**
Cold Leg		
PI	10.51	1.81E-03
11-L1-C18	6.05	1.21E-03
11-L1-V18	5.51	1.10E-03
11-L2-V18	4.58	9.16E-04
11-L3-03E	11.42	2.28E-03
11-L4-04	16.6	3.32E-03
14-L4-21	4.87	9.74E-04
14-L4-20	30.68	6.13E-03
Hot Leg		
PI	9.63	2.91E-02
11-L1-C18	6.47	2.26E-02
11-L1-V18	4.6	1.61E-02
11-L2-V18	4.58	1.60E-02
11-L3-03E	10.76	3.76E-02
11-L4-04	19.04	6.65E-02
14-L4-21	1.41	4.93E-03
14-L4-20	29.87	1.04E-01

Table 3.8: Comparison of total tritium permeation release to ITER's rooms at equilibrium from both hot and cold leg calculated with the dynamic model of HCCR TBS and comparison with results of [27].

Location in HCS	**T release (mg/day) calculated in [27]**	**T release (mg/day) dynamic model**	**Relative Error (%)**
PI	3.10E-02	3.09E-02	0.35
11-L1-C18	2.39E-02	2.38E-02	0.37
11-L1-V18	1.72E-02	1.72E-02	0.17
11-L2-V18	1.70E-02	1.69E-02	0.50
11-L3-03E	4.00E-02	3.99E-02	0.32
11-L4-04	7.00E-02	6.98E-02	0.24
14-L4-21	6.00E-03	5.90E-03	1.68
14-L4-20	1.11E-01	1.10E-01	0.47

3.4.3.2 Code-to-code validation of HCCR TBS dynamic models

A simplified HCCR TBS model was developed with the use of the TMAP4 code by INL under the INL-UCLA-NFRI collaboration for Cooperation on R&D for Fusion Nuclear Science to Expedite the Realization of Magnetic Fusion Energy. A code-to-code comparison is proposed to validate the COMSOL/Simulink numerical model developed in this Dissertation. The properties and parameters chosen for the calculation are summarized in Tables 3.9 and 3.10. The plasma pulse includes a 50 s ramp-up, 400 s flat-top, 50 s ramp-down, 1800 s dwell time. The Soret effect and distribution profile of FW implantation flux are neglected in the simulations.

Table 3.9: Parameters of HCS and CPS used in the simulations for the code-to-code validation.

Sub-system	**HCS**	**CPS**
Fluid	Helium Coolant	Helium Coolant
Pressure	8 MPa	8 MPa
Flow rate	1.14 kg/s	3% of HCS flow rate
Tritium processing efficiency	-	95%

Table 3.10: Properties used in the simulations for the code-to-code validation [9, 10].

Property	**Correlation**	**Units**
Diffusivity	$7.50 \times 10^{-8} exp(-0.14/k_b/T)$	$m^2\ s^{-1}$
Solubility	$3.10 \times 10^{-1} exp(-0.25/k_b/T)$	$mol\ m^{-3}\ Pa^{-1/2}$
Recombination Const.	$0.25 \times 7.83 \times 10^{-7} exp(-0.68/k_b/T)$	$m^4\ mol^{-1}\ s^{-1}$

The HT concentration in the helium coolant calculated with the TMAP4 and COMSOL/Simulink models is presented in Fig. 3.20. The HT build-up presents the same dynamics and numerical results are in agreement within a <5% relative difference. At equilibrium the COMSOL/Simulink model computes an HT concentration <1% lower than TMAP4.

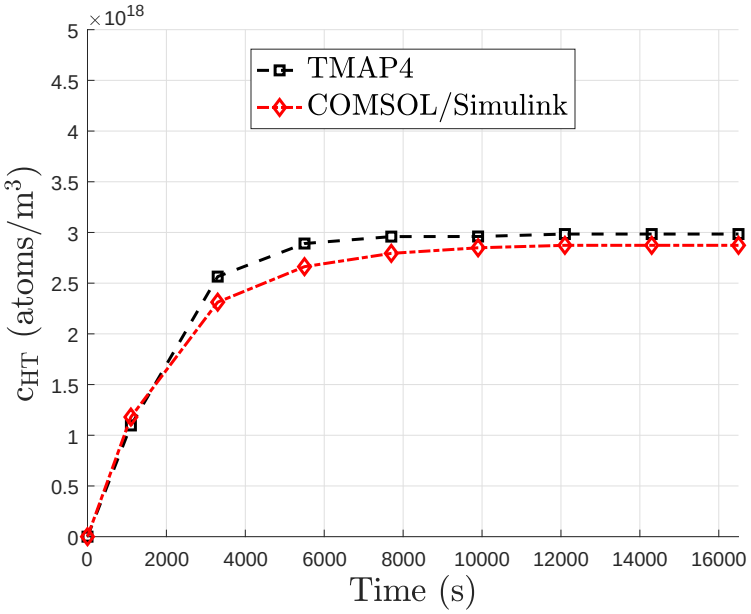

Figure 3.20: Average values (per pulse of 2200 s) of HT concentration in coolant calculated with TMAP4 and the COMSOL/Simulink HCCR TBS dynamic model developed in this Dissertation.

3.5 Analysis of Tritium Transport in the HCCR TBS

For nuclear safety and licensing, the ITER Organization (IO) requires accurate evaluation of tritium inventory build up in TBS components and permeation rates to buildings. In this section we use the HCCR TBS dynamic model developed in the COMSOL and Simulink environment to perform tritium inventory and permeation rate evaluation for the HCCR TBS. Compared to the previous study on tritium permeation and inventory assessment for the Korean HCCR TBS [27], the current methodology accounts for ITER pulsed operation, which consists in a burn-time of 400 s (including 50 s rump-up and rump-down) and a dwell-time of 1400 s for a total pulse period of 1800 s, and includes the co-permeation effect by tracking the evolution of H, D, and T atoms in bulk material, and H_2, HD, and HT in helium coolant. Furthermore, accurate evaluations of tritium production rate in blanket and tritium implantation into first wall structural material derived in Subsections 3.2.1 and 3.2.2, respectively, are used in the analysis.

In detail, we perform a concentrated analysis of tritium evolution in the HCCR TBS with the goal of providing further outer fuel cycle tritium R&D guidance from an integrated point of view. A calculation of tritium permeation rate to ITER's rooms Port Interspace, Port Cell, and Vertical Shaft, is performed for the updated design of pipe forest as defined in Spec. of EN13480 (DN100 Sch., DN80 for HCS). Multi-physics simulations accounting for ITER pulsed operation (burn and dwell times), realistic temperature estimation, and co-permeation effect, show that tritium permeation rate to ITER's rooms is $\sim$1 order of magnitude lower than that evaluated with the simplified approach of [27], which neglects the co-permeation effect, ignores temperature and concentration gradients by using a zero-dimensional model, and assumes steady operation. The analysis is presented in the following subsections

3.5.1 Operating temperature and tritium concentration profiles in the first wall and breeding zones

The mathematical formulation describing the first wall and breeding zone models presented in Section 3.1 for the HCCR TBM was derived by Ying *et al.* in [6, 7, 14]. The same authors performed numerical validation and extensive analysis of the performance of these components, thus a thorough discussion of first wall and breeding zone is omitted here. Instead, this research starts from the work of [6, 7, 14] and extends the modeling effort and analysis to the system level, i.e. a numerical model which connects the various HCCR components is generated in order to analyze the entire Test Blanket System. However, before we proceed with the analysis of tritium permeation rates in the pipe forest of the HCCR TBS, we show here the characteristic temperature and tritium concentration profiles in the first wall and breeding zones. These results are consistent with those of [6, 7, 14] (refer to those studies for a more detailed analysis of first wall and breeding zones).

In Fig. 3.21, we report tritium concentration in the first wall structural material at different instants of time during the fifth ITER pulse (at times of 7400 s, 7600 s, 8000 s, and 9000 s). As tritium is implanted in the FW, it diffuses towards the coolant channel driven by concentration and thermal gradients. During the dwell time the tritium concentration in the structure decreases as tritium permeation to coolant continues at a lower rate in the absence of a tritium implantation source. The temperature distribution during the plasma pulse is shown in Fig. 3.22. It is seen that the FW has a maximum temperature of 775 K on the plasma facing surface, which is below the material limit of 823 K. After the pulse the temperature decreases to 573 K with a quick transient ($\sim$ 50 s) due to the high thermal conductivity of ARAA ($\sim$28 W/m/K).

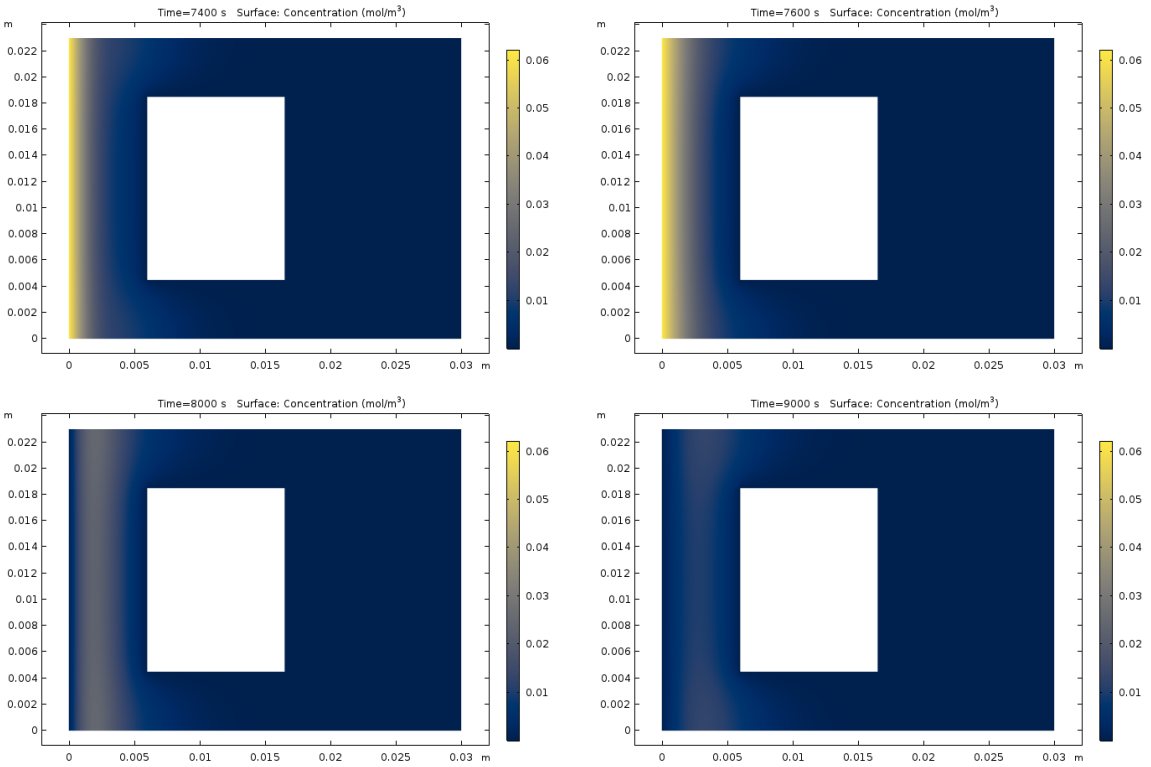

Figure 3.21: Tritium concentration in FW structure [mol/m^3] during the 5^{th} plasma pulse. Top left: t = 7400 s (200 s from beginning of 5^{th} plasma pulse); top right: t = 7600 s (end of the burn time of the 5^{th} plasma pulse); bottom left: t = 8000 s (during dwell time of 5^{th} plasma pulse); bottom right: t = 9000 s (end of 5^{th} plasma pulse).

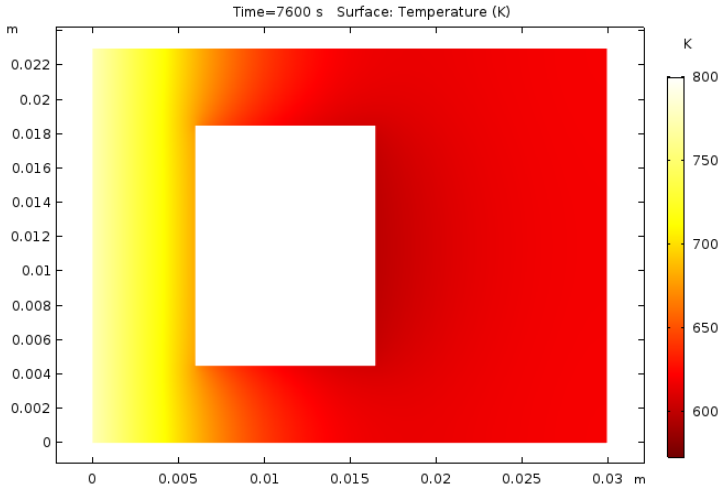

Figure 3.22: Temperature of structural material in the first wall at the end of burn time of the 5^{th} plasma pulse.

The tritium concentration in various domains of the breeding blanket is shown in Fig. 3.23. The tritium concentration in the breeder zone (top left of Fig. 3.23) is higher near the coolant plates because of: (i) a higher tritium generation rate in the region close to the cooling plates (see Fig. 3.11), and (ii) a lower breeder temperature in the proximity of the coolant plates compared to the middle of the breeder channel (as seen in Fig. 3.25 showing the temperature profiles in the breeder region), and thus a longer tritium residence time which reduces local tritium release from breeder to purge gas and increases the inventory in the breeder pebbles. A similar discussion holds for the multiplier region (top right of Fig. 3.23), but tritium concentrations are at least 2 orders of magnitude lower, due to a lower tritium generation rate in the multiplier. The HT concentration in the breeder and multiplier purge gases is shown at the bottom left and bottom right of Fig. 3.23, respectively. We notice that HT content in the gases increases as the purge gas flows upward in the channels and collects the tritium released from the pebbles. The left side of Fig. 3.24 presents the tritium concentration in the cooling plates while the right side of the same figure is the zoom of the structural material separating the first breeder channel, the first multiplier channel, and the second breeder channel. Tritium concentration is higher next to the breeder zones and decreases to zero at the cooling channels surface. We also notice that tritium concentration in the cooling plates increases along with the flow direction, as the HT concentration in the purge gas increases.

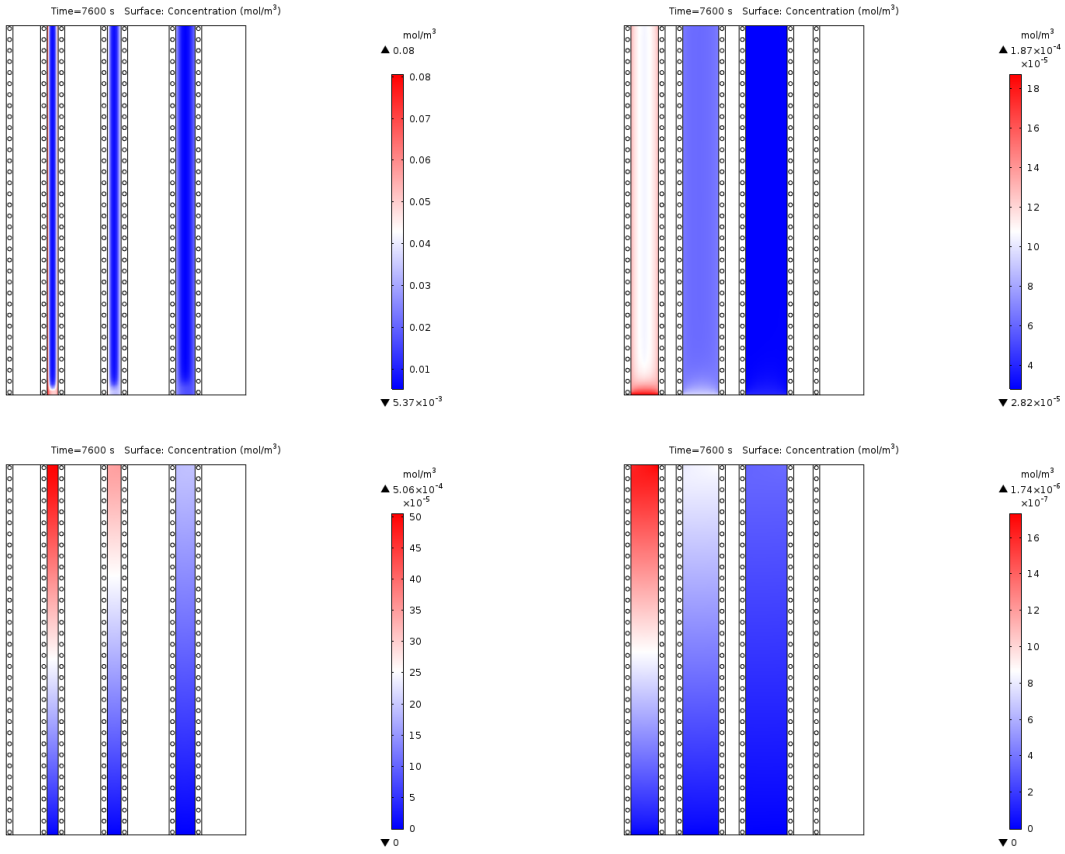

Figure 3.23: Tritium concentration in breeder and multiplier pebbles, and HT concentration in breeder purge gas and multiplier purge gas (mol/m^3) at the end of the burning time of the 5^{th} plasma pulse, t = 7600 s. Top left: tritium concentration in the breeder; top right: tritium concentration in the multiplier; bottom left: HT concentration in the breeder purge gas; bottom right: HT concentration in in the multiplier purge gas.

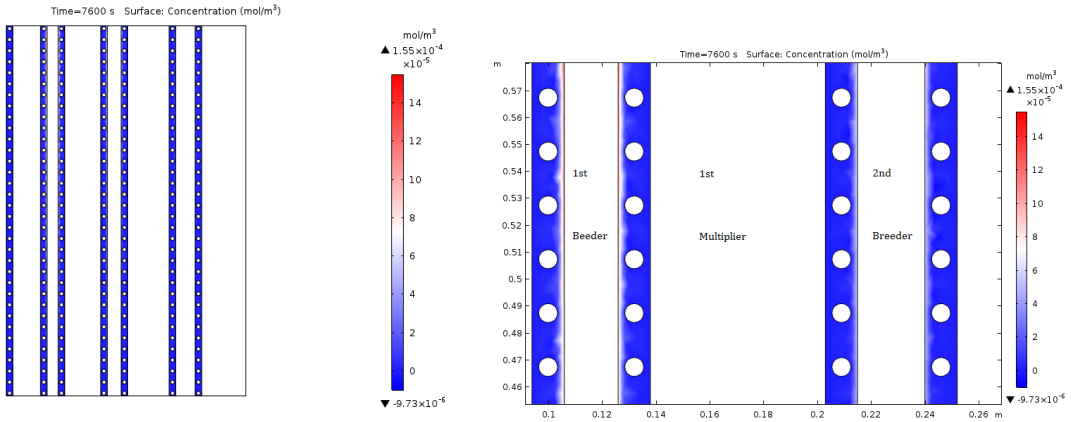

Figure 3.24: Tritium concentration in ARAAcooling plates (mol/m^3) at the end of the burning time of the 5^{th} plasma pulse, t = 7600 s. Top left: tritium concentration in the structural material; top right: zoom of the cooling plates delimiting the first and second breeder channels.

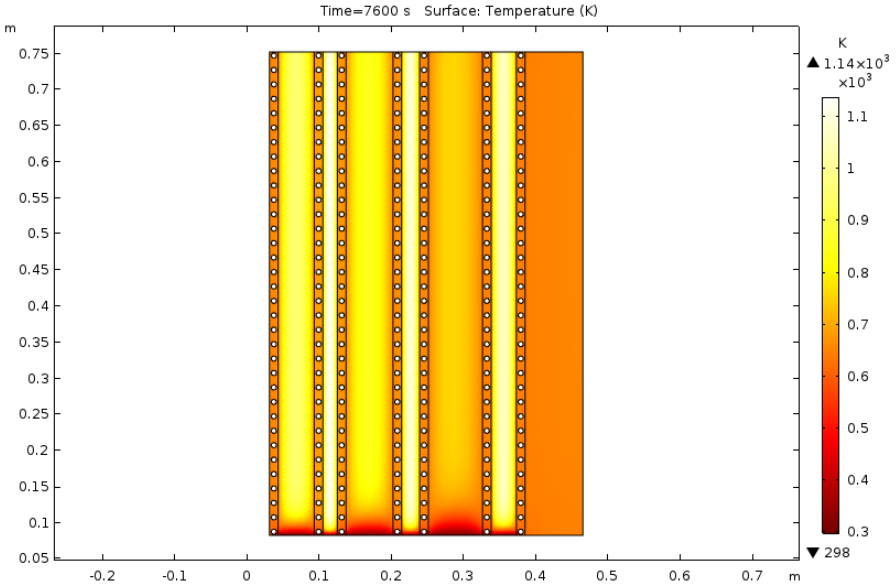

Figure 3.25: Temperature of cooling plates, breeder, and multiplier in the breeding zone at the end of burning time of the 5^{th} plasma pulse.

3.5.2 Analysis of tritium release to ITER's rooms and evaluation of tritium inventory build-up in the pipe forest of the HCCR TBS

3.5.2.1 Tritium release to ITER's rooms and pipe inventory for nominal design parameters of the HCCR TBS

The HCCR TBS tritium transport dynamic model was run to compute pressures of Q_2 species in the coolant loop of the HCCR TBS under ITER inductive operation conditions (400 s burn and 1800 s per cycle) for the suggested design parameters, $\eta_{CPS} = 95\%$, $\alpha_{CPS} = 1\%$, $Q^{CL} = 1.14$ kg/s, $\eta_{CMSB} = 95\%$, $\eta_{RTMS} = 95\%$, $Q^{PG} = 1$ g/s. Calculated H, D, and T permeation rates from FW and BZ to coolant are shown in Fig. 3.26. In this simulation we assume a perfectly clean first wall surface on plasma side, and we use the recombination coefficient derived by Zhou *et al.* in [9] and reported in Table 3.1. The effect of the presence of impurities on the first wall surface on tritium permeation rate to coolant is discussed in Subsection 3.5.2.2. It is seen that, for a clean FW surface on the plasma side, the tritium permeation rate from FW to the coolant channels reaches a quasi-equilibrium state in a handful of ITER pulses and is ∼2 orders of magnitude higher than the tritium permeation rate from the BZ. The lower tritium permeation rate from the BZ is a consequence of the co-permeation effect: the presence of 0.1% H_2 in He purge gas at atmospheric pressure reduces tritium permeation. Furthermore, the permeation of hydrogen from BZ to the coolant is significant. The presence of some concentration of H_2 in the coolant is beneficial to reduce tritium permeation rates from connecting pipes to ITER's rooms, as we will show in detail in Chapter 4.

Tritium concentration in the coolant builds up as coolant continuously circulates through the first wall and blanket to extract heat from the structural material. The coolant purification system (CPS) removes a fraction of tritium from the coolant as coolant circulates around the loop. In Fig. 3.27 we present the time evolution of the partial pressures of H_2, HD, and HT dissolved inside the coolant. It is found that the system reaches a quasi-equilibrium state in ∼6−8 plasma pulses, in agreement with the temporal evolution of permeation rates expressed in Fig. 3.26.

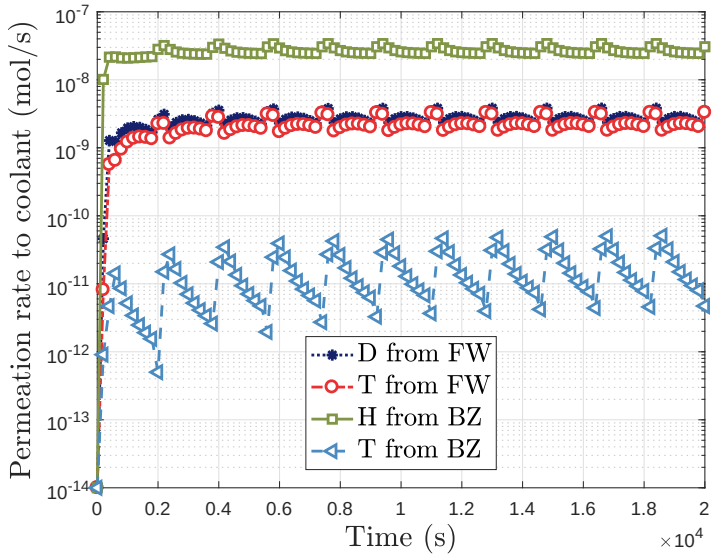

Figure 3.26: H, D, and T permeation rates from first wall and breeding zones to coolant channels.

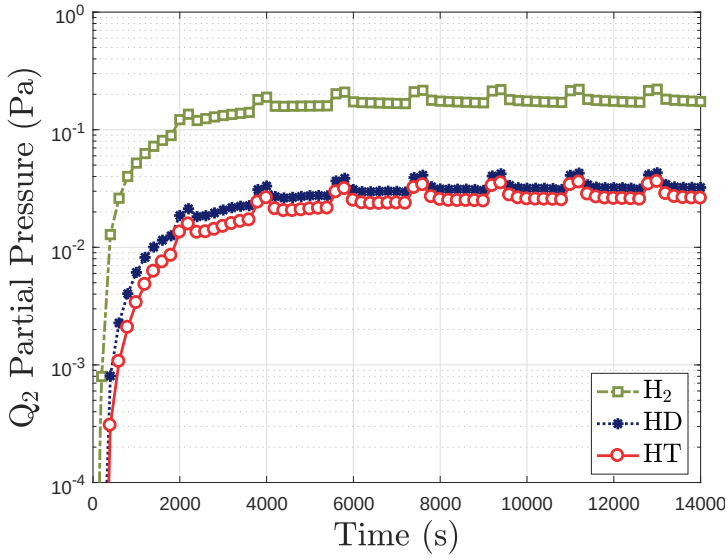

Figure 3.27: Q_2 partial pressure time-evolution in He coolant.

As the coolant circulates in the loop, part of its tritium content is absorbed in the SS316L structural material of the connecting pipes, thus tritium inventory in the pipes increases. Hence, tritium diffuses through the structural material of the pipes until it reaches the outer surface, and is released to the external environment. In Figs. 3.28 - 3.31 we show the obtained tritium inventories and permeation rates in the ITER's Port Interspace (PI), Port Cell (PC), and Vertical Shaft (VS) for the hot leg and the cold leg of the helium coolant

system (HCS). The values are averaged over one ITER pulse (1800 s). Table 3.11 summarizes the dimensions of the pipes used in the analysis. Note that differences in permeation rates between hot and cold legs of HCS are due to temperature effects. In particular in Fig. 3.32 we display the temperature behavior of gas and structural material of the PI pipe. Conversely, the cold leg is kept at constant temperature of 573 K.

Table 3.11: Lengths of the hot and cold legs of pipes in the Port Interspace, Port Cell, and Vertical Shaft rooms of the ITER.

	Length (m)		**Diameter (m)**	
Room	**Hot Leg**	**Cold Leg**	**Inner**	**Outer**
PI	11.8	10.5	0.0737	0.0892
PC	12.3	12.3	0.0978	0.1145
VS	71.9	75.3	0.0978	0.1145

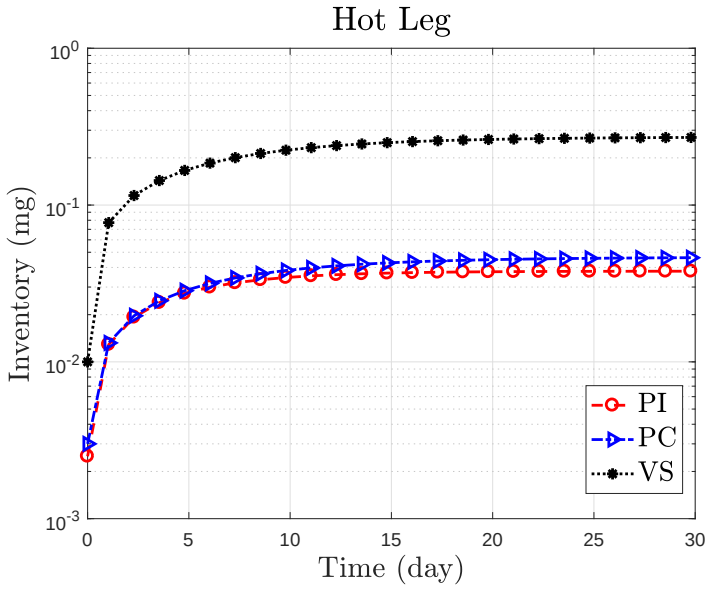

Figure 3.28: Tritium inventory build-up in hot leg of PI, PC, and VS rooms. Values are averaged over a ITER pulse of 1800 s.

Finally, we present the inventory and permeation values (in red) in detail for every sub-location of PI, PC, and VS rooms (VS includes: 11-L1-V18, 11-L2-V18, 11-L3-03E, 11-L4-04, 11-L4-21, 11-L4-20, and 14-L4-21) in Figs. 3.33 and 3.34. We also report, as a comparison, the values of inventory and permeation rates (in blue) found by the NFRI team using a simplified approach (steady state, no co-permeation, 723 K for hot leg and 573 K

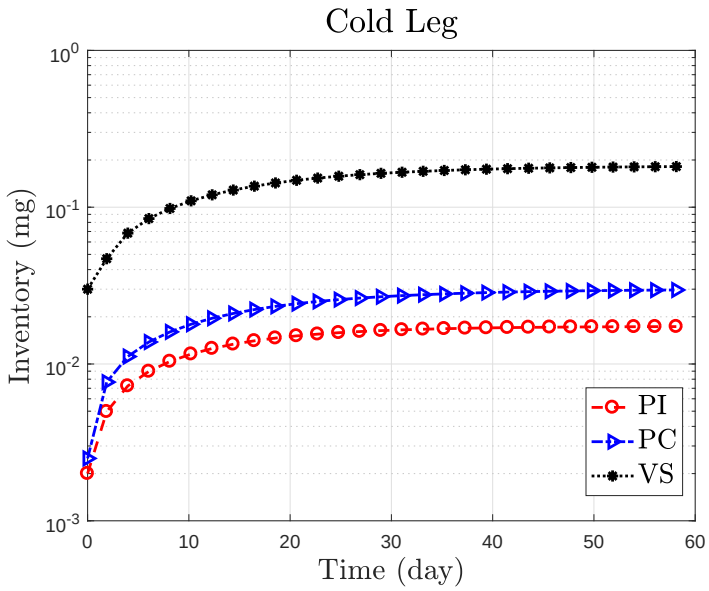

Figure 3.29: Tritium inventory build-up in cold leg of PI, PC, and VS rooms. Values are averaged over a ITER pulse of 1800 s.

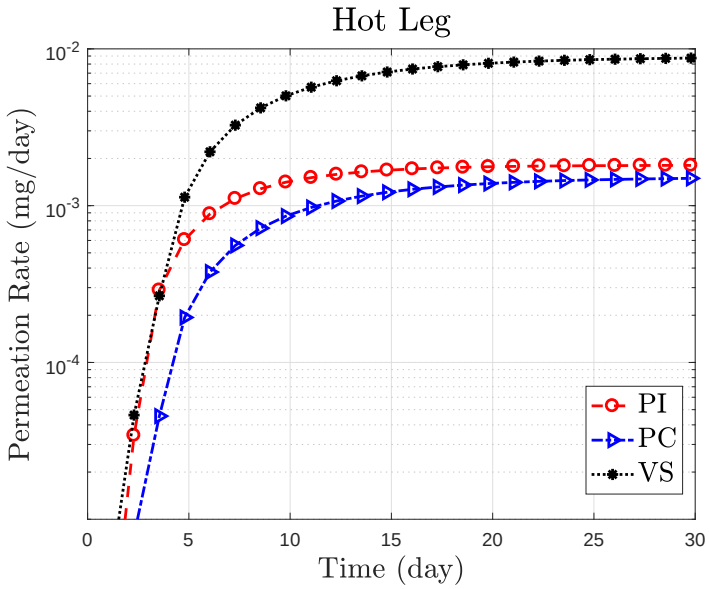

Figure 3.30: Tritium permeation rate to environment in hot leg of PI, PC, and VS rooms. Values are averaged over a ITER pulse of 1800 s.

for cold leg). The use of the HCCR TBS dynamic simulation tool gives ∼19 times lower tritium inventory (0.444 mg versus 8.6 mg in CPS components) and ∼23 times lower tritium permeation rate (total permeation rate from HCS CPS: 1.11×10^{-2} mg/d versus 2.60×10^{-1} mg/d) which could be released in case of fire. In this study we did not consider the permeation rates to buildings from the tritium extraction system (TES) pipes. However, as shown in the

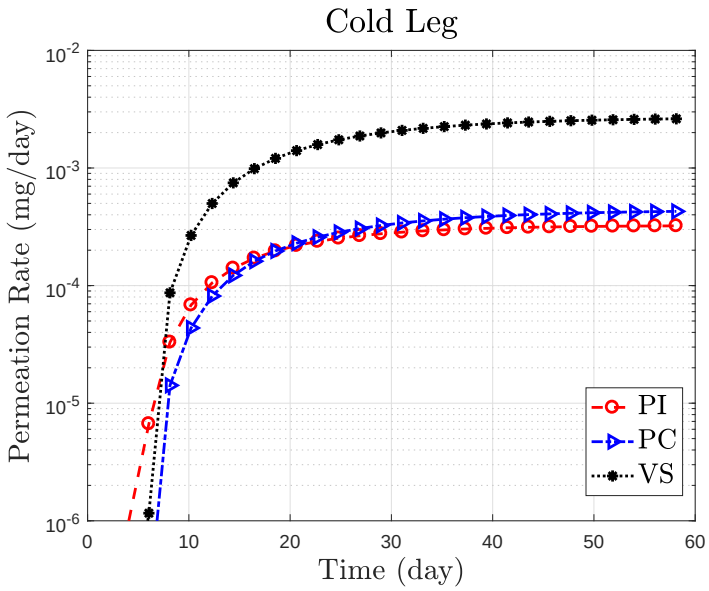

Figure 3.31: Tritium permeation rate to environment in cold leg of PI, PC, and VS rooms. Values are averaged over a ITER pulse of 1800 s.

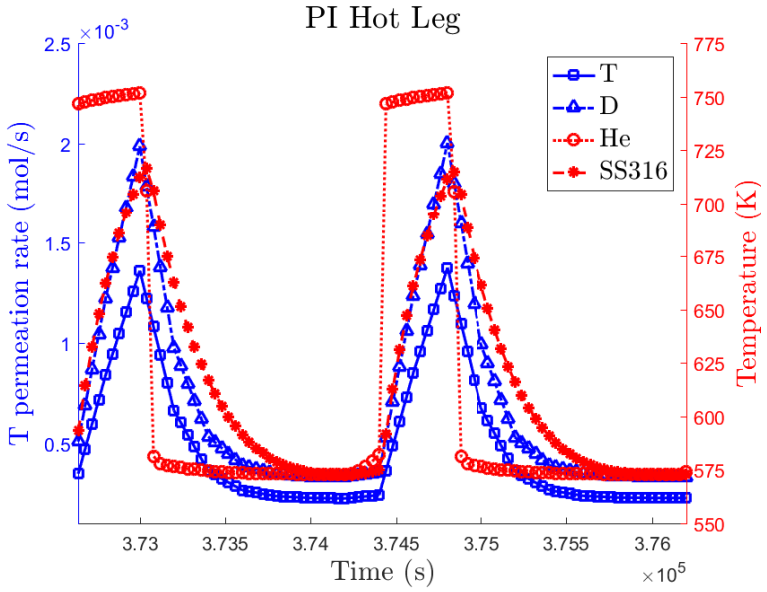

Figure 3.32: Detail of tritium and deuterium permeation to buildings, and temperature evolution in He coolant gas and SS316 structural material of PI hot leg pipe. Two ITER pulses are shown.

preliminary calculation (blue values in Figs. 3.33 and 3.34) tritium permeation rates from TES line are predicted to be ∼6-7 orders of magnitude lowers than those from the HCS. The reason for this discrepancy is attributed to the low temperature on the TES pipes, i.e. 573 K, due to a purge gas flow rate of only 0.1 g/s at 0.1 MPa compared to an HCS coolant

flow rate of 1.14 kg/s at 8 MPa. Fig. 3.35 summarizes tritium and hydrogen inventory and permeation (release) to ITER's rooms.

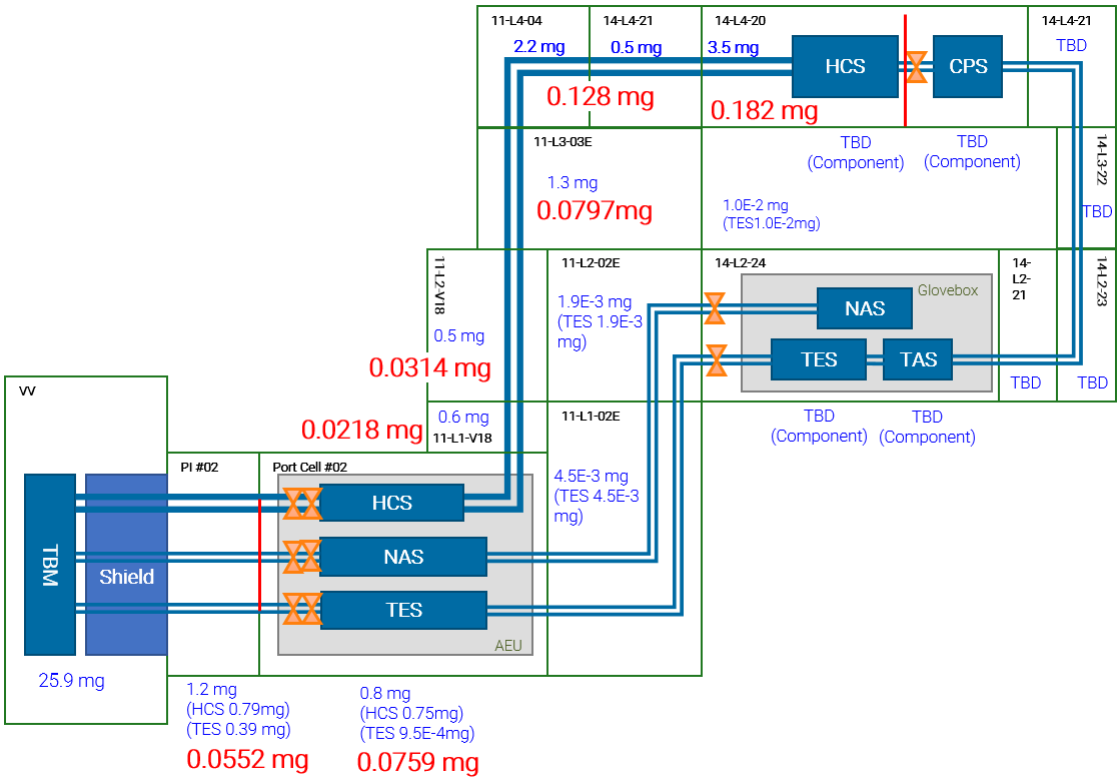

Figure 3.33: Schematic of TBS with values of equilibrium tritium inventory in the HCS pipes of the PI, PC, and VS rooms. Red values refer to the results obtained with the dynamic model for HCCR TBM while blue values are obtained by the NFRI team in [27].

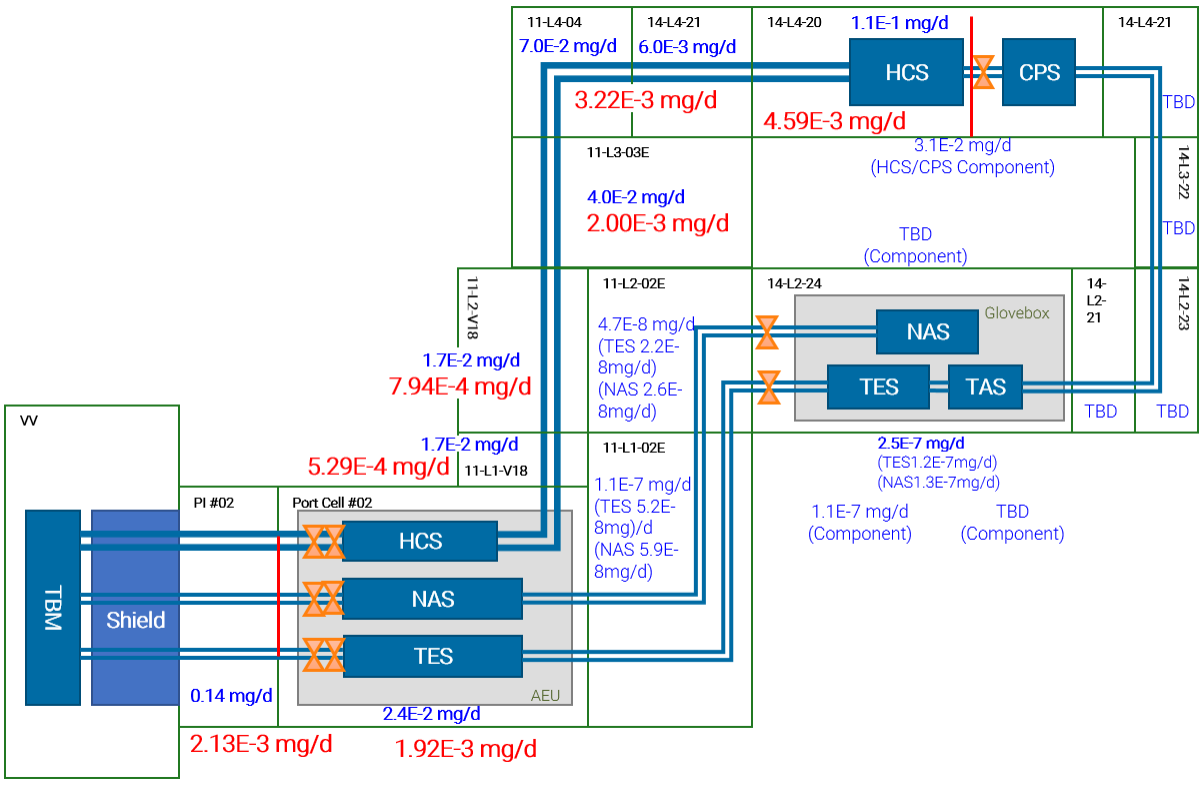

Figure 3.34: Schematic of TBS with values of equilibrium tritium permeation rates to the PI, PC, and VS rooms for the HCS line. Red values refer to the results obtained with the dynamic model for HCCR TBM while blue values are obtained by the NFRI team in [27].

Location **HCS CPS**	Description	Length-Pipe [m]	Tritium release by permeation [mg/day]	Hydrogen release by permeation [mg/day]	Tritium dissolved in structures [mg]	Hydrogen dissolved in structures [mg]	Tritium content in He gas [mg]	Hydrogen content in He gas [mg]
PI (PF)	Cold line in PF	1.05E+01	3.22E-04	2.19E-03	1.73E-02	6.77E-02	7.89E-04	3.90E-03
PC (AEU)	Cold line in AEU (in the enclosure)	1.23E+01	4.30E-04	2.95E-03	2.97E-02	1.17E-01	1.61E-03	7.96E-03
11-L1-C18	Cold CP (outside the enclosure)	1.34E+00	4.69E-05	3.22E-04	3.24E-03	1.28E-02	1.76E-04	8.68E-04
11-L1-V18	Cold CP	4.09E+00	1.43E-04	9.81E-04	9.88E-03	3.89E-02	5.35E-04	2.64E-03
11-L2-V18	Cold CP	5.09E+00	1.78E-04	1.22E-03	1.23E-02	4.84E-02	6.66E-04	3.29E-03
11-L3-03E	Cold CP	1.33E+01	4.65E-04	3.19E-03	3.21E-02	1.27E-01	1.74E-03	8.60E-03
11-L4-04	Cold CP	2.15E+01	7.49E-04	5.14E-03	5.18E-02	2.04E-01	2.81E-03	1.39E-02
14-L4-21	Cold CP							
14-L4-20	Cold CP	3.00E+01	1.05E-03	7.19E-03	7.24E-02	2.85E-01	3.92E-03	1.94E-02
PI (PF)	Hot line in PF	1.18E+01	1.81E-03	1.27E-02	3.79E-02	1.53E-01	8.61E-04	4.31E-03
PC (AEU)	Hot line in AEU (in the enclosure)	1.23E+01	1.49E-03	1.06E-02	4.62E-02	1.86E-01	1.56E-03	7.82E-03
11-L1-C18	Hot CP (outside the enclosure)	1.34E+00	1.63E-04	1.15E-03	5.04E-03	2.03E-02	1.71E-04	8.53E-04
11-L1-V18	Hot CP	3.19E+00	3.86E-04	2.73E-03	1.20E-02	4.82E-02	4.05E-04	2.03E-03
11-L2-V18	Hot CP	5.09E+00	6.16E-04	4.36E-03	1.91E-02	7.70E-02	6.47E-04	3.23E-03
11-L3-03E	Hot CP	1.27E+01	1.53E-03	1.09E-02	4.75E-02	1.92E-01	1.61E-03	8.04E-03
11-L4-04	Hot CP	2.04E+01	2.47E-03	1.75E-02	7.66E-02	3.09E-01	2.59E-03	1.30E-02
14-L4-21	Hot CP							
14-L4-20	Hot CP	2.92E+01	3.54E-03	2.51E-02	1.10E-01	4.42E-01	3.71E-03	1.86E-02
TOTAL			1.54E-02	1.08E-01	5.83E-01	2.33E+00	2.38E-02	1.18E-01

Figure 3.35: Summary of hydrogen and tritium release to buildings (permeation rates) and inventory build up in structural material SS316L of PI, PC, and VS connecting pipes and in He coolant gas at equilibrium.

3.5.2.2 Effect of first wall surface condition and CPS unit performance on tritium release by permeation to the ITER's rooms

It is known that the surface conditions of the structural material of fusion components, e.g. RAFM, stainless steel, etc., have a major effect on the recombination process of desorbed atoms at the gas/metal interface. For instance, the recombination coefficients reported in literature for stainless steel vary between several orders of magnitude [28]. Zhou *et al.* derived two empirical correlations for the recombination coefficient of hydrogen in ferritic steel F82H by conducting plasma-driven permeation (PDP) experiments for the case of (i) "clean" F82H sample surface [9] and (ii) "dirty" F82H sample surface [10] on plasma side. For the experiment of [9], the clean surface was obtained by performing argon plasma bombardment on the F82H sample performed for 10 min at -50 V in order to remove contamination due to air exposure. The obtained recombination coefficients are plotted in function of the reciprocal temperature in Fig. 3.36.

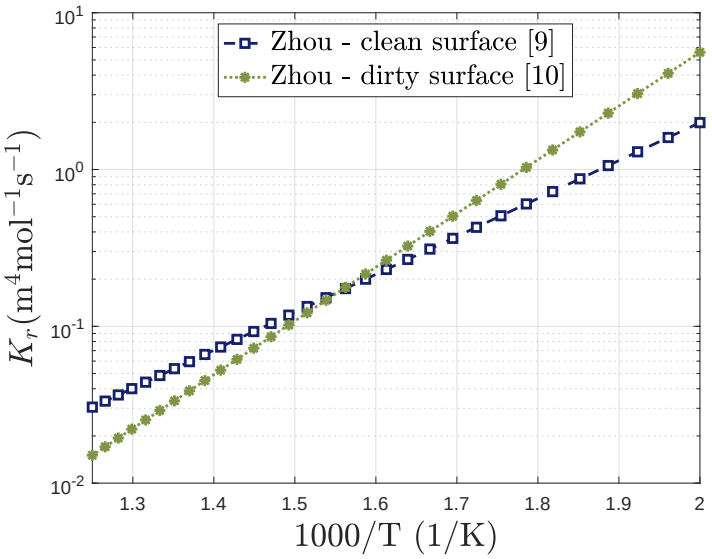

Figure 3.36: Hydrogen recombination coefficient for clean and dirty surface of F82H ferritic steel in function of the reciprocal temperature.

For the typical temperatures of the FW during the plasma pulse (∼800 K), the recombination coefficient for a clean surface facing the plasma is about two times greater than the one for a dirty surface on plasma side. Thus, higher tritium inventory in RAFM structure is found in case of dirty FW surface and, as a consequence, the tritium permeation rate to

coolant increases, as shown in Fig. 3.37 (left: tritium inventory in one FW sub-module; right: tritium permeation rate to coolant from one FW sub-module). In this calculation the particle flux from plasma (I_0) is 10^{21} atoms/m^2-s of D and T (assuming 50% D - 50% T) and the reflective coefficient (r) is 0.3, as we derived in Subsection 3.2.2.

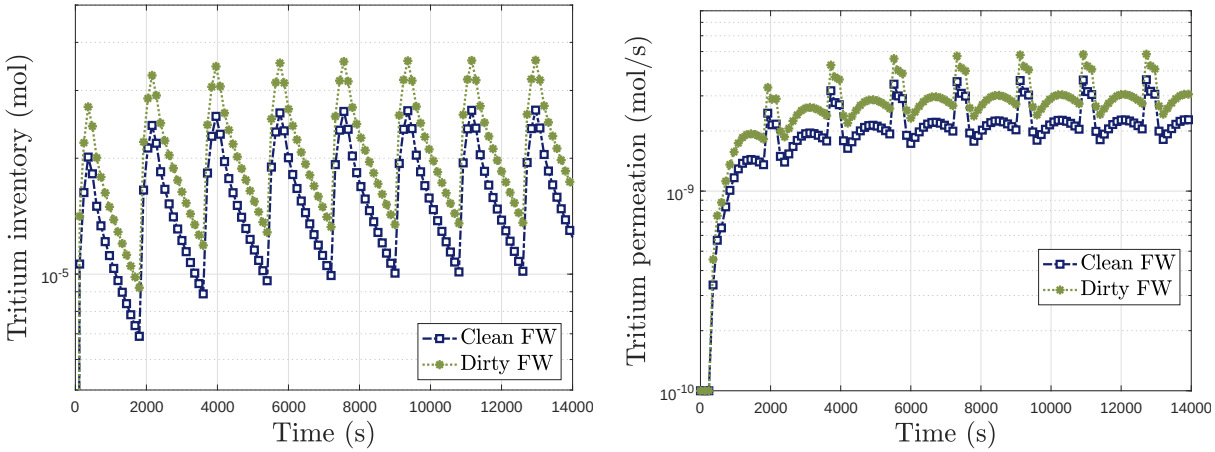

Figure 3.37: Tritium inventory in one FW sub-module (left) and tritium permeation rate to coolant from one FW sub-module (right) in case of clean and dirty FW surface on plasma side.

In Fig. 3.38 we present the evaluated HT (left) and H_2 (right) partial pressures in the coolant for clean and dirty FW surface on plasma side, and nominal design parameters of the CPS, i.e. tritium processing efficiency $\eta_{CPS} = 95\%$ and flow rate fraction $\alpha_{CPS} = 1\%$. In order to examine the CPS performance, we also evaluated the effect of an increased flow rate fraction ($\alpha_{CPS} = 2\%$); for this case, a reduction in the CPS processing efficiency is assumed ($\eta_{CPS} = 80\%$). The results show that the HT partial pressure in the coolant is higher in the case of a FW with dirty surface on plasma side for nominal CPS design parameters. For the same case, the hydrogen partial pressure in the coolant decreases of ~10% compared to the case of clean FW surface, as more hydrogen is consumed to form HT (and HD). In spite of a decrease of the CPS efficiency to 80%, increasing the fractional flow rate to 2% has a major effect in reducing the HT and H_2 pressures in the helium coolant (overall reduction of ~40% compared to the nominal parameters of CPS for clean first wall).

The equilibrium tritium releases from the HCS pipe forest to the ITER's rooms for the three cases presented in Fig. 3.38 are summarized in Table 3.12; the values are averaged

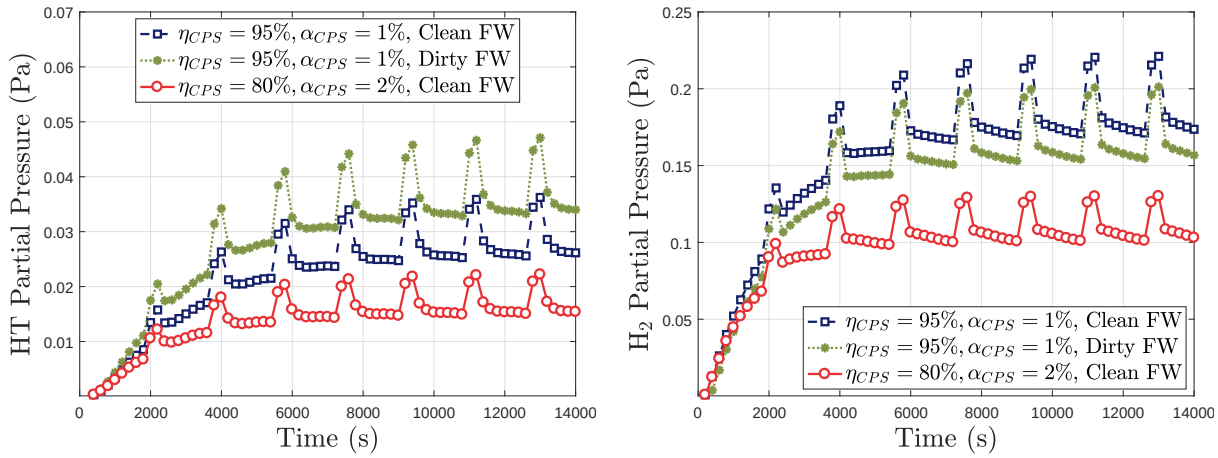

Figure 3.38: Time evolution of HT (left) and H_2 (right) partial pressures in helium coolant of the HCS/CPS line of HCCR TBS. Simulations for nominal values of CPS efficiency (η_{CPS} = 95%) and flow rate fraction (α_{CPS} = 1%) for clean and dirty FW surface on plasma side, and for increased CPS flow rate fraction (α_{CPS} = 2%) with lower efficiency (η_{CPS} = 80%) for clean FW surface on plasma side.

over the plasma pulse (1800 s). The tritium release for contaminated FW surface is 1.3 times higher than the release for clean FW surface (increase of ∼32%). An increased CPS fractional flow rate to 2% (with efficiency of CPS decreased to 80%) reduces the tritium release to the rooms of ∼20% compared to the reference CPS parameters (fractional flow rate of 1% and efficiency of 95%). Note that as the CPS reduces HT content in coolant, it also decreases the amount of H_2, thus limiting the benefits of the co-permeation effect, i.e. a reduced tritium permeation in case of the presence of other hydrogen species. In this sense, adding some hydrogen to the coolant to increase the H_2 of a few Pa can be beneficial to further reduce tritium permeation to the reactor buildings.

Table 3.12: Equilibrium tritium release to ITER's rooms calculated with the dynamic model of HCCR TBS in case of clean and dirty first wall surface and nominal CPS parameters ($\alpha_{CPS} = 1\%$, $\eta_{CPS} = 95\%$), and in case of clean first wall surface, increased CPS fractional flow rate $\alpha_{CPS} = 2\%$, and reduced CPS efficiency $\eta_{CPS} = 80\%$.

Location in HCS	**Pipe length (m)**	**T release (mg/day) Clean FW** $\alpha_{CPS} = 1\%$ $\eta_{CPS} = 95\%$	**T release (mg/day) Dirty FW** $\alpha_{CPS} = 1\%$ $\eta_{CPS} = 95\%$	**T release (mg/day) Clean FW** $\alpha_{CPS} = 2\%$ $\eta_{CPS} = 80\%$
		Cold Leg		
PI	10.5	3.22E-04	4.26E-04	2.53E-04
PC	12.3	4.30E-04	5.68E-04	3.38E-04
11-L1-C18	1.34	4.69E-05	6.20E-05	3.69E-05
11-L1-V18	4.09	1.43E-04	1.89E-04	1.12E-04
11-L2-V18	5.09	1.78E-04	2.35E-04	1.40E-04
11-L3-03E	13.3	4.65E-04	6.14E-04	3.65E-04
11-L4-04	21.5	7.49E-04	9.90E-04	5.89E-04
14-L4-20	30.0	1.05E-03	1.39E-03	8.25E-04
		Hot Leg		
PI	11.8	1.81E-03	2.39E-03	1.42E-03
PC	12.3	1.49E-03	1.97E-03	1.17E-03
11-L1-C18	1.34	1.63E-04	2.15E-04	1.28E-04
11-L1-V18	3.19	3.86E-04	5.10E-04	3.03E-04
11-L2-V18	5.09	6.16E-04	8.14E-04	4.84E-04
11-L3-03E	12.7	1.53E-03	2.02E-03	1.20E-03
11-L4-04	20.4	2.47E-03	3.26E-03	1.94E-03
14-L4-20	29.2	3.54E-03	4.68E-03	2.78E-03
	Total	1.54E-02	2.03E-02	1.21E-02

3.6 Conclusions

The HCCR TBS tritium transport dynamic model was developed to improve the design of TBS components, assess safety and nuclear licensing, and to perform maintenance assessment. The model integrates pre-existing detailed component models of the HCCR TBM, e.g. FW and BZ [6, 7, 14], and other newly developed models, e.g. connecting pipes, developed in COMSOL Multiphysics to system-level, with the use of Simulink S-functions. The system-level model was validated by comparing partial pressures and permeation rate results with previous calculations [27] and by performing code-to-code validation, i.e. comparison with TMAP4. Thus, we used the code to perform assessment of tritium (and hydrogen) inventory in pipes and permeation rate from pipes to the ITER's PI, PC, and VS rooms for the HCS stream. The study shows that permeation from HCS to environment is mainly driven by the tritium fluxes implanted into the FW from plasma and by the CPS performance. Thus, accurate estimations of ion fluxes in the Scrape-off Layer of the plasma are key to predict tritium permeation to coolant and, then, releases to rooms. Most tritium produced in the BZ is carried to the TES by the purge gas, however a considerable amount of hydrogen permeates from the BZ to the coolant channels, because of the high concentration of H_2 in the breeder purge gas.

The results show that 2.13×10^{-3} mg/day, 1.92×10^{-3} mg/day, and 1.11×10^{-2} mg/day of tritium are released in the PI, PC, and VS rooms, respectively, for a pulsed reactor with 50 s ramp-up, 400 s burn time, 50 s ramp-down, 1700 s of dwell time. These values are $\sim$20 times lower than previous results obtained with a simplified model [27] that did not account for pulsed operation, co-permeation of hydrogen isotopes, accurate temperature profiles, realistic spatial distribution (gradients) of ion implantation in FW and tritium production rate in BZ. Moreover, the effect of the contamination of the FW surface on plasma side was investigated. It was found that a dirty FW surface reduces the atom recombination flux of to plasma and causes an increase of tritium inventory in the FW structure and, therefore, of tritium permeation rate to coolant, when the same particle flux at the FW surface is considered. As a consequence, the tritium release to ITER's rooms increases by $\sim$32%.

Furthermore, this model can be used to determine the performance requirements of the CPS and other extraction systems in order to reduce the permeation rates to acceptable limits. In our case, we considered the effect of an increase in the CPS fractional flow rate to 2% followed by a reduction in the CPS efficiency to 80%. For these parameters, the tritium release to ITER's room is decreased by ∼20% compared to the nominal CPS parameters ($\alpha_{CPS} = 1\%$ and $\eta_{CPS} = 95\%$). Increasing the CPS flow rate fraction is therefore beneficial to reducing the tritium release to the environment.

References

1. COMSOL Multiphysics v. 5.3a. www.comsol.com

2. MATLAB and Simulink Release 2014b, MathWorks, Inc., Natick, Massachusetts, United States.

3. COMSOL/Livelink: COMSOL Multiphysics with MATLAB v. 5.0. COMSOL, Inc., Burlington, MA. 2015 Livelink for MATLAB, COMSOL, Inc., Burlington, MA. 2015.

4. Simulink Developing S-Functions, MATLAB & SIMULINK, R2017a, MathWorks, Inc.

5. S. Y. CHO, et al., "Design and R&D progress of Korean HCCR TBM," Fusion Engineering and Design, 89, 1137-1143 (2014); http://dx.doi.org/10.1016/j.fusengdes.2014.01.032.

6. Ying *et al.*, "TRITIUM TRANSPORT EVOLUTIONS IN HCCR TBM UNDER ITER INDUCTIVE OPERATIONS", Fusion Science and Technology, Vol. 68, Sep. 2015, http://dx.doi.org/10.13182/FST14-908.

7. Ying *et al.*, "Analysis of Tritium Retention and Permeation in FW/Divertor Including Geometric and Temperature Operating Features", Fusion Science and Technology, Vol. 64, 303-308, 2013.

8. Ziegler, J. F.; Biersack, J. P.; Littmark, U. (1985). The Stopping and Range of Ions in Matter. New York: Pergamon Press. ISBN 978-0-08-021607-2

9. H. Zhou *et al.*, "Gas- and plasma-driven hydrogen permeation through a reduced activation ferritic steel alloy F82H", Journal of Nuclear Materials 455 (2014) 470-474

10. H. Zhou *et al.*, "First Wall Particle Flux Measurements by an F82H Permeation Probe in QUEST", Plasma and Fusion Research: Regular Articles, Volume 9, 3405041 (2014), DOI: 10.1585/pfr.9.3405041

11. Seungyon Cho *et al.*, "Neutronic assessment of HCCR breeding blanket for DEMO", Fusion Engineering and Design, Volume 146, Part A, 2019, Pages 1338-1342, ISSN 0920-3796, https://doi.org/10.1016/j.fusengdes.2019.02.071.

12. Seungyon Cho *et al.*, Fusion Engineering and Design, Volume 136, Part A,2018, Pages 190-198

13. F. Franza, "Tritium transport analysis in HCPB DEMO blanket with the FUS-TPC code", KIT SCIENTIFIC REPORTS 7642

14. A. YING, H. ZHANG, B. J. MERRIL, M. Y. AHN, "Advancement in tritium transport simulations for solid breeding blanket system", Fusion Engineering and Design, 109-111, Part B, 1511-1516, (2016)

15. C. H. Oh, E. S. Kim, September 2009, Development and Verification of Tritium Analyses Code for a Very High Temperature Reactor, INL/EXT-09-16743.

16. Zhongying Shi, Xia Wang, "Comparison of Darcys Law, the Brinkman Equation, the Modified N-S Equation and the Pure Diffusion Equation in PEM Fuel Cell Modeling", Excerpt from the Proceedings of the COMSOL Conference 2007, Boston

17. Whitaker, S., "Fluid Motion in Porous Media", Ind. Eng. Chem., 61(12), pp.14-28(1969)

18. S. Pupeschi *et al.*, Effective thermal conductivity of advanced ceramic breeder pebble beds, Fusion Engineering and Design 116:73-80 March 2017

19. G. A. Esteban *et al.*, Journal of Nuclear Materials, 367-370 (2007) 473-477

20. K. S. Forcey *et al.*, Journal of Nuclear Materials, 160 (1988) 117-124

21. C. San Marchi, B.P. Somerday, S.L. Robinson, "Permeability, solubility anddiffusivity of hydrogen isotopes in stainless steels at high gas pressures", Int. J. Hydrog. Energy 32 (2007) 100-116.

22. M. Shimada, R.J. Pawelko, "Tritium permeability measurement in hydrogen-tritium system", Fusion Engineering and Design 129 (2018) 134-139

23. S. CHO et al., "Overview of Helium Cooled Ceramic Reflector Test Blanket Module development in Korea," *Fusion Engineering and Design*, **88**, *6-8*, 621 (2012).

24. J.T. Goorley, *et al.*, "Initial MCNP6 Release Overview - MCNP6 version 1.0", LA-UR-13-22934 (2013).

25. D. WON LEE et al., "Functional components design and analysis of a Korean HCCR TBM in ITER," *2013 IEEE 25th Symposium on Fusion Engineering (SOFE)*, 10-14 June 2013, San Francisco, CA, 10.1109/SOFE.2013.6635374

26. Task Force on TBM Program Safety Demonstration -WM25, June 7-9, 2017 -2016, ITER Organization

27. NFRI KO TBM Team, Technical Meeting - 3^{rd} Consolidation of Specification for the TBS CPs System, ITER Headquarter, St Paul Lez Durance Jun. 13, 2017.

28. W. Moller, J. Roth, "Physics of Plasma-Wall-Interactions in Controlled Fusion", Plenum Press, New York, 1986.

CHAPTER 4

Recent Advances in Tritium Modeling and its Implications on Tritium Management for Outer Fuel Cycle

Recent advances in tritium transport modeling of helium cooled ceramic breeding blankets systems has shined light into some tritium management issues. A detailed component model accounting for multi-physics, design, and operational features is necessary to provide accurate estimations of tritium permeation rates to the building/environment, a safety and licensing concern for a fusion nuclear reactor. We found that tritium permeation to buildings can be reduced of ∼20 times when H_2 is increased from ∼0.2 Pa to 100 Pa in coolant streams due to the effect of H and T co-permeation. Similarly, the practice of adding about 0.1% vol of H_2 into the helium purge gas to promote tritium release can also reduce permeation from breeding zones to coolant systems. However, high H_2 partial pressure in helium purge gas further complicates tritium extraction methodology, and may compromise extraction efficiency.

4.1 Introduction

The necessity for accurate predictions of tritium permeation rates to buildings and tritium inventory requested by the ITER Organization (IO) for each Test Blanket System (TBS) has led to advancements and renewed interest in tritium transport modeling. IO's requirements offer the opportunity to develop an advanced simulation predictive capability, while evaluating the state-of-the-art of the tritium transport, properties, and management from

an integrated point of view. Tritium systems are complex and include a variety of components, e.g., first wall (FW), divertor, blankets, primary cooling sub-systems with purification components, connecting pipes, tritium extraction system, etc., which execute different tasks, operate at different operational condition (e.g. temperatures, pressures, flow rates, etc.), but are interconnected, and affect each other's performance and tritium dynamics. Thus, tritium quantities must be analyzed for the "integrated system" of connected components in which tritium evolves.

However, the subject itself is complicated by the variety of phenomena, operational conditions, and physics involved. For instance, ITER's pulsed operations imply dynamics effect in tritium transport due to temperature transients, FW and divertor are subject to high D-T charge-exchange neutrals and ions implantation, tritium transport regime may be determined by diffusion phenomena ("diffusion-limited regime") or by surface effects ("surface-limited regime") depending on material properties, surface oxidation, and structure thickness, H_2 addition in coolant and purge gas streams, Co- and Counter- permeation effects, chosen tritium extraction technique, etc. In order to predict precise tritium behavior, components of fusion systems must be analyzed in an interconnected manner. In the last half decade the authors of this paper have developed various high fidelity detailed models of tritium components [1-5] to reproduce tritium streams characteristic of the Korean Helium Cooled Ceramic Reflector (HCCR) TBS [6]. This modeling approach offers an accurate evaluation of tritium inventory, flow rates, and permeation rates, and leads to a better understanding of design requirements and improvements. Moreover, results were extrapolated to future DEMO conditions to evaluate the impact of the outer fuel cycle on the initial start-up tritium inventory [7].

Other examples of detailed and system-level modeling with different mathematical approach are available in [8-9]. These models treat main components of tritium plant as black boxes characterized by certain flow rates, surface areas, volumes and temperatures, which requires lower computational power but miss the accuracy that a dimensional detailed analysis can offer, especially for a delicate task such as tritium transport and permeation.

In this research we analyze performances of tritium systems, evaluate tritium permeation

rates, identify critical parameters and physics that most impact tritium transport prediction, and propose tritium management strategies by using the models we developed over time. In particular, we focus our attention on the interconnected behavior of tritium components within a system with the goal of identifying how a functional requirement of a component may result in a contradictory requirement for another component or may further enhance performances to achieve an optimal tritium management scheme for the outer blanket fuel cycle system. Moreover, we offer some example of the planned experimental programs developed at NFRI and KIT to further verify and benchmark simulation platforms.

4.2 Intrinsic Complexities of Tritium Transport and the Need of an Integrated Multiphysics Computational Model

4.2.1 Pre-analysis of tritium transport regime

It is known that tritium transport regime is diffusion-limited, i.e. tritium diffusion through bulk is the limiting factor for transport, at high tritium pressure whilst it is surface-limited, i.e. surface processes such as molecule dissociation, atoms adsorption, recombination, and desorption at the gas/metal interface are the limiting factor for transport when diffusion process is faster, at low tritium pressure [10]. Moreover, the presence of isotopes other than T_2, e.g., H_2, D_2, HD, HT, etc., which are present in fusion environments, affects tritium permeation due to co- and counter- permeation effects [11]. Given the number of complexities associated with tritium transport in fusion components a pre-analysis of temperature-dependent properties, operational pressures, and geometric parameters is beneficial to identify which transport regime is more likely to occur and determine appropriate boundary conditions at the gas/structure interface. The dimensionless permeation number W is a measure of the expected permeation behavior. Here we use a generalized permeation number [12], to account for the presence of multi-species (e.g. H_2, HT, HD, etc.) in gas and their co-permeation effect as:

$$W = \frac{\sigma k_1 d}{\phi} \sqrt{p_{TOT}} \tag{4.1}$$

and:

$$p_{TOT} = p_{H_2} + p_{HT} + p_{T_2} \tag{4.2}$$

where σ the surface roughness factor, k_1 the adsorption constant, d the membrane thickness, ϕ the permeability of the material. $W >> 1$ implies a diffusion-limited regime where atom concentrations at metal surface are in equilibrium with their gas phases and the permeation flux for slab geometry is:

$$J_T = \frac{\phi}{d} \frac{p_T}{\sqrt{p_{TOT}}} \tag{4.3}$$

$$p_T = \frac{1}{2} p_{HT} + p_{T_2} \tag{4.4}$$

while W $\ll 1$ denotes a surface-limited regime where diffusion occurs on a much faster scale than recombination/adsorption surface processes and permeation flux for slab geometry is:

$$J_T = \frac{1}{2} \sigma k_1 p_T \tag{4.5}$$

The outer fuel cycle system involves components with different hydrogen isotopes and tritium transport regimes. In Fig. 4.1 we show the generalized W calculated for breeding zone and helium cooling system (HCS) coolant pipes.

On one hand, the Reduced Activation Ferritic Steel (RAFS) structural material of HCCR is characterized by an intermediate transport regime. On the other hand, the SS316L of He coolant connection pipes (DN100 and DN80) has low diffusivity, and fall into the diffusion-limited regime. Based on these results, we performed permeation evaluation by using: (i) diffusion-limited boundary conditions on gas/structure interface of coolant pipes and (ii) surface-limited boundary conditions on gas/metal interface of breeding zones (BZ) to enforce a linear proportionality between partial pressure and permeation rate (see Equation 4.5), even though an intermediate regime is likely more characteristic.

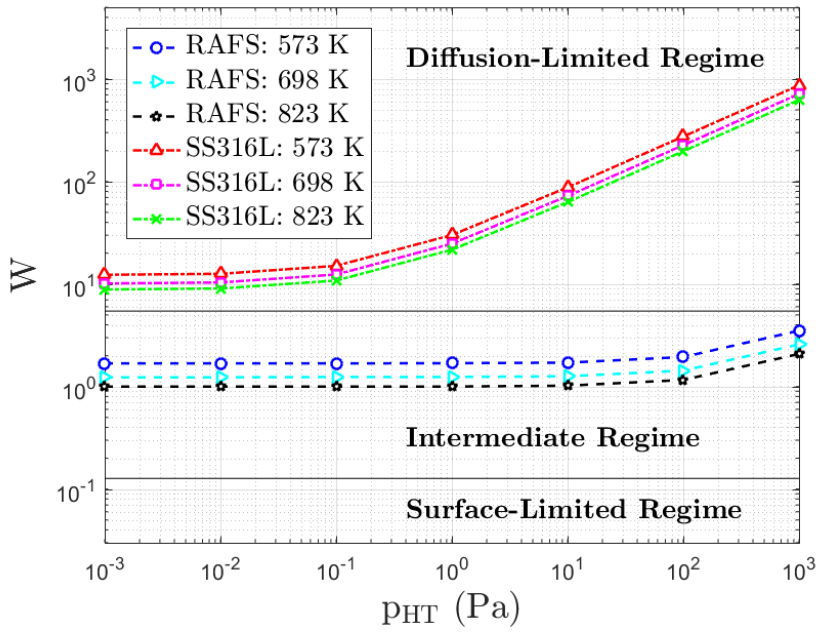

Figure 4.1: Generalized permeation number calculated for the RAFS structural material of the HCCR TBM (300 Pa H_2) and for SS316L structural material of TBS coolant system connection pipes (DN80 and DN100) (0.2 Pa H_2) at various temperatures.

4.2.2 Features and requirements for tritium transport modeling: a complex multi-physics multi-component simulation platform

The complexity involved in predicting the tritium behavior requires a dynamic, multi-physics simulation in a multi-material, prototypical geometric configuration. The curves shown in Fig. 4.2 are the calculated integrated tritium permeation rates over 238 coolant channel surfaces of a HCCR sub-module as a function of time over one ITER cycle for different primary/upstream side purge gas compositions and secondary/downstream side He coolant gas conditions. The solid lines show the permeation evolution for various H_2 pressure in purge gas (circles: 30 Pa; squares: 300 Pa; stars: 3000 Pa. Pressure of 300 Pa is considered the reference value) when surface processes take place on the purge gas and metal interface while a clean coolant (zero concentration) is assumed on the coolant/metal interface. The dotted line represents the reference case on purge side (300 Pa of H_2) and includes surface effects on coolant side for He containing 0.187 Pa of H_2, 0.035 Pa of HD, and 0.029 Pa of HT. These equilibrium pressures are calculated with the HCCR TBS model presented in

Chapter 3, with purge gas containing 300 Pa of H_2 and a FW controlled by diffusion-limited regime, a clean plasma side, and an implantation flux of 10^{21} atoms/m^2-s (50% D - 50% T). The dashed lines represent a coolant with the same amount of HD and HT (0.035 Pa and 0.029 Pa respectively) but H_2 content is increased to 10 Pa (red line with asterisk markers) and 100 Pa (light blue line with triangle markers).

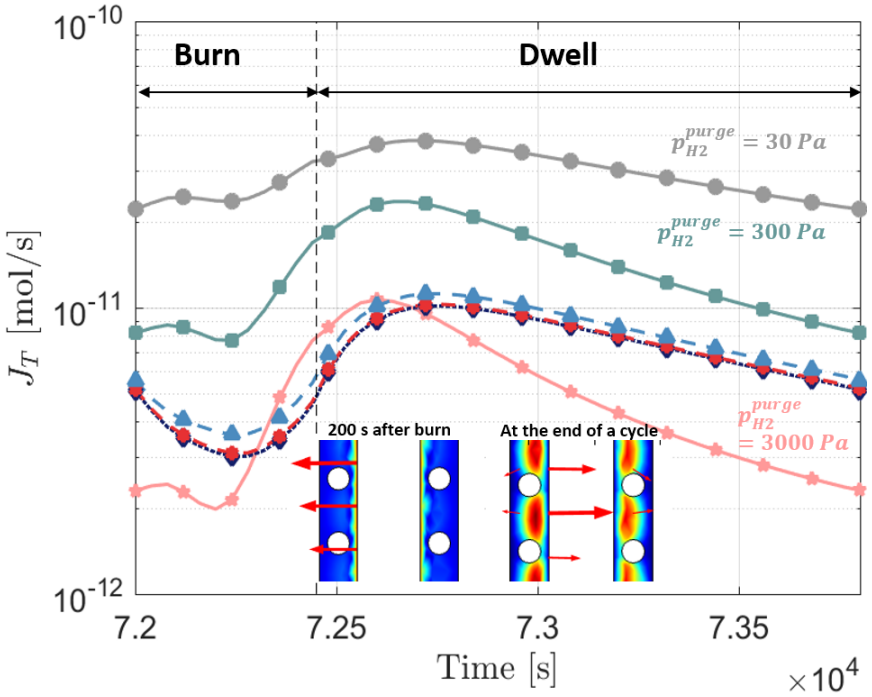

Figure 4.2: Tritium permeation rate over all the coolant surfaces of the breeding zones of a HCCR sub-module. (Insert figure: tritium concentrations in coolant containing structures, and HT flux across the boundaries).

As we expected, a multitude of parameters and operational conditions concur to determine the amount of tritium permeation to the coolant. The permeation evolution is strongly affected by RAFS thermal and concentration gradients driven by the plasma pulse. In particular, the permeation rate does not increase immediately following the plasma burn since the newly dissolved tritium is diffusing through the bulk and has not reached the coolant surface yet. The tritium concentration at the coolant surface decreases for about 200 s, which reduces the tritium permeation rate even further, until the newly dissolved tritium reaches the coolant channel surface and the permeation rate begins to increase. The tritium permeation rate continues to increase, until the tritium concentration reverses its profile which causes

tritium to recombine back to the breeder zone, and tritium permeation rate to the coolant decreases. Between the coolant channels, we see that tritium can diffuse beyond the coolant channel and leak to the neighboring Beryllium region where tritium concentration is lower.

An increase in H_2 content in the purge gas implies a reduction in permeation ($\sim$3 times lower when H_2 is increased from 300 Pa to 3000 Pa). However, variation of the purge gas pressure and H_2 content may affect tritium release from ceramics and tritium extraction system (TES) performance. When the isotopes in coolant reach equilibrium pressures the permeation rate is reduced due to tritium adsorption into structure on the coolant side, which reduces the net tritium flux released at the interface (the net flux is given by the difference between recombination and adsorption flux). An addition of H_2 in coolant (e.g. 100 Pa of H_2 to reduce tritium permeation from pipes to rooms as a result of the co-permeation effect) has the downside of enhancing T release from structure to coolant due to higher concentrations of H_2 on the gas/metal interface which facilitates tritium recombination and desorption. However, the increase of permeation to coolant is small compared to the reduction in tritium permeation to rooms as we show in Subsection 4.2.3.

Even with a simpler geometry such as the coolant connection pipes, the tritium permeation behavior to the building is complicated by the pulsed operations which result in thermal transients in both the coolant gas and SS-316L structural material of the pipes and impose implications on mass transfer. Use of the pulsed average values of temperatures to estimate transport properties has led to an underestimation of tritium permeation rate of up to 50%, while using steady state burn temperature led to overestimating a release rate by a factor of 10 [13]. Thus, accurate coupling of heat transfer with species transport is required to eliminate unnecessary uncertainties in the estimations.

4.2.3 Co-permeation effect in presence of multi-isotopes on tritium permeation rates to ITER buildings

As validated with experimental results [11], tritium permeation under diffusion-limited regime in the presence of multi-isotopes is inversely proportional to the square root of the total pressure contained in a gas (co-permeation effect) [14]. For the purge gas, higher H_2 pressure reduces permeation from breeding zones to coolant, as shown in Fig. 4.2.

Similarly, for the HCS the presence of H_2 in higher concentrations than HT (and HD) represents a natural barrier limiting permeation to reactor rooms. As shown in Fig. 4.3 the permeation rates to ITER's PI (Port Interspace), PC (Port Cell), and VS (Vertical Shaft) for the reference case (coolant pressures: 0.187 Pa of H_2, 0.035 Pa of HD, and 0.029 Pa of HT) and for H_2 pressure increased to 10, and 100 Pa. The analysis shows that higher H_2 content in He coolant has major benefits for reducing tritium losses to buildings. An increase from the reference value 0.187 Pa to 100 Pa reduces permeation rate by a factor of ~20.

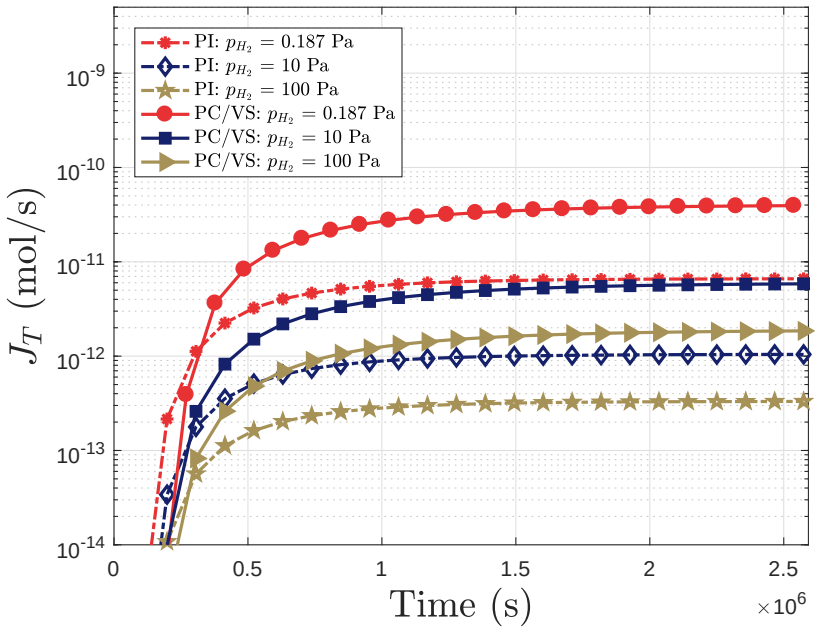

Figure 4.3: Integrated tritium permeation rates (time averaged over ITER 1800 s cycle) to PI, PC, and VS buildings.

However, in addition to tritium generation in the ceramics, implantation fluxes from plasma into the FW represents another tritium source for the permeation in the outer part

of fuel cycle. It was found that 99.99% of implanted tritium into the FW is re-emitted to plasma while only 0.01% diffuses through structural material and permeates to coolant loop. Even though a small fraction of the total implanted flux, this quantity represents the main contribution to tritium build-up in coolant, since permeation rates form BZ were found to be approximately 2 orders of magnitude lower. When diffusion-limited regime governs tritium transport, permeation rates from FW to coolant are 9.61×10^{-9} mol/s and 1.29×10^{-8} mol/s respectively for clean and dirty plasma side independently of H_2 content in coolant. In fact, for this case the effective tritium pressure in coolant, p_T, at equilibrium is much smaller than the total pressure, p_{TOT}, regardless of H_2 addition (see Eq. 4.3). If we assume a surface-limited regime we notice that the presence of H_2 in coolant slightly enhances tritium release from FW to coolant due to the counter-permeation effect as seen in Table 4.1. Moreover, a dirty FW surface on plasma side reduces re-emission to plasma and, thus, increases the permeation rate on the coolant side. As seen from Fig. 4.2 and Table 4.1, we find that tritium permeation to coolant increase only of $\sim$1%. Thus, H_2 addition could be considered as an active way to control and reduce tritium permeation to buildings and environment if necessary.

Table 4.1: Tritium permeation rates from FW to coolant under surface-limited regime for various H_2 contents in coolant and clean/dirty FW surface facing the plasma.

H_2 (Pa)	J_T (mol/s) - Clean plasma side	J_T (mol/s) - Dirty plasma side
0.187	7.61×10^{-9}	1.05×10^{-8}
10	7.68×10^{-9}	1.06×10^{-8}
100	8.01×10^{-9}	1.09×10^{-8}

4.2.4 Analysis of hot out-gassing in connection pipes during short-term maintenance period

The planned ITER operational scenario expects an 11-day period of continuous pulses followed by a 3-day short term maintenance time. Out-gassing procedure could be performed as a short term maintenance activity to recover tritium contained in pipes and other com-

ponents, lower inventories, and reduce subsequent permeation to buildings.

An out-gassing calculation is performed for the hot legs of the HCS/CPS including PI, PC, and VS connection pipes. We assume pure He flows at 623, 723, and 773 K to enhance tritium release from the inner surface of the pipe. Note that, some concentrations of H_2, HD, and HT will be present in He depending on the inventory release rates from various components. However, here we only focus on evaluating the tritium released inside the connection pipes (recovered amount), and outside (losses to buildings), and the time response characteristics. Figs. 4.4 and 4.5 show the tritium permeation rate to buildings and inventory characteristics during the first 11 days of pulsed operation followed by 6 days of hot out-gassing process. On one hand, we note a faster decrease in the inventory as the temperature

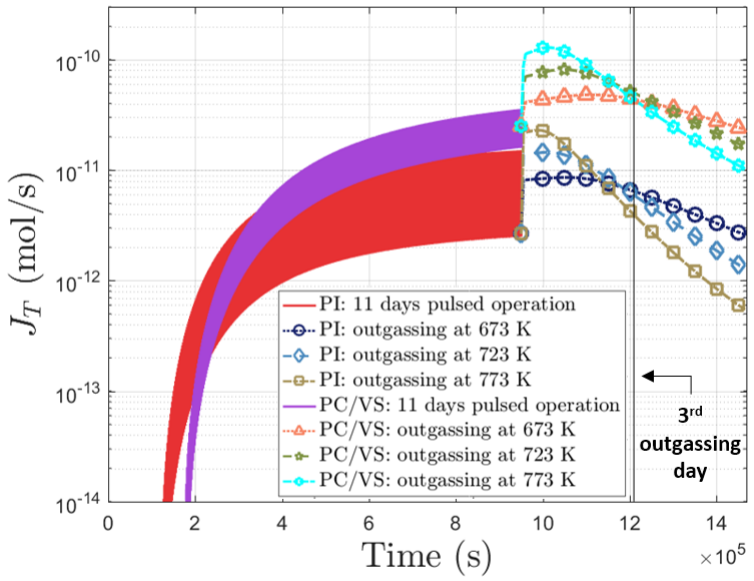

Figure 4.4: Tritium permeation rates to buildings from pipes of ITER's HCS/CPS hot leg PI, PC, and VS for first 11 days of ITER pulsed operations and 6 days of hot out-gassing.

is increased from 623 to 773 K. On the other hand, higher temperatures cause an increase in the permeation to buildings during the out-gassing time. This effect is due to the higher and constant temperatures of the pipes during out-gassing compared to the pulsed scenario where temperatures oscillates between 573 and 730 K. Despite this increase in tritium loss to building, major amounts of recovered tritium are found for the 773 K case (∼60% for the PI pipe and ∼56% for PC/VS pipes). It should also be noted that, though lower temperatures

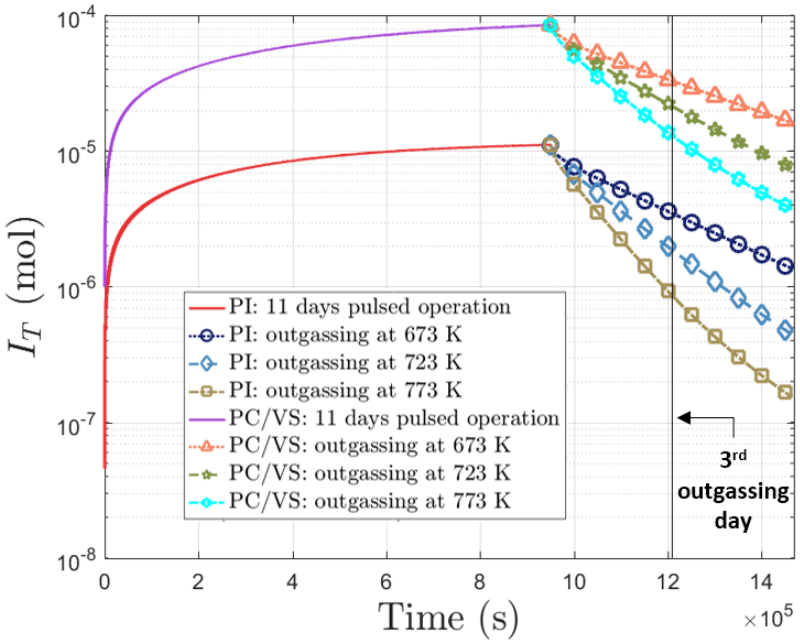

Figure 4.5: Tritium inventory for first 11 days of ITER pulsed operations and 6 days of hot out-gassing in ITER's HCS/CPS hot leg PI, PC, and VS connecting pipes.

give overall lower tritium recovery, they also reduce permeation to rooms and offer a better recovery performance, i.e., the ratio of released tritium to He to the total released amount (sum of tritium released to helium and to buildings) is higher for lower temperatures: 73%, 68%, and 65% for PI, and 77%, 71%, and 66% for PC/VS respectively for 623, 723, and 773 K. The inventories in pipes decrease by ∼92% for PI, and ∼85% for PV/VS at day 3 of the out-gassing, and if out-gassing period is prolonged to six days inventories in pipes are decreased by ∼2 orders. The analysis suggests that if an out-gassing is to be performed for removing the tritium inventory in the pipe components, the sudden increase in the tritium release to the buildings/environments would need to be taken into account in designing the detritation systems to meet the allowable dose rate in the maintenance period.

4.3 Experimental Activities to Support the Benchmark Activity of Tritium Transport Modeling Tools

Accompanying with the development of tritium transport simulation predictive capabilities, experimental programs had also been launched to verify and enhance our understanding of tritium behavior in the blanket outer fuel cycle systems and serve as validating tools for tritium transport numerical modeling. Until now, two sets of validations have been performed.

The first set of comparison was validation of the co-permeation mathematical model used in this work [11]. We performed modeling validation by comparing the calculated tritium permeation rates with the results of a recent Tritium Gas Absorption Permeation (TGAP) experimental campaign performed at the Idaho National Laboratory (INL) [14]. In the experiment, tritium permeation rates for KO-RAFM circular samples were calculated over a wide range of HT partial pressures, i.e., from 10^{-5} to 10^{1} Pa, and for H-T thermodynamics equilibrium conditions. Our calculation shows perfect agreement between experimental and predicted values over the entire range of HT pressure, as shown in Fig. 4.6. We found linear dependency of tritium permeation rate with HT partial pressure and square root dependency with T_2 partial pressure (plotted in the range 10^{-5} to 10^{1} Pa). This validation effort expands the model validity over a wider pressure range than the one considered in [11], which was limited to HT partial pressure $\sim 10^{-2}$ - 10^{-1} Pa.

The other validation concerns the hydrogen adsorption characteristic of a large-scale CMSB installed at the PGLoop at NFRI [15]. The PGLoop CMSB uses 50.7 kg of MS5A as the adsorbent. Experiments with different swamping ratios, flow rates, and total pressures in the range of hydrogen partial pressures from 100 Pa to 700 Pa were conducted. The MS5A adsorption amount at the breakthrough was calculated based on the theory presented in [16], where the concentrations of the adsorbate in the gas phase and in the adsorbent are expressed as a function of the axial length from the inlet of the CMSB, z, and time, t. The comparison shows performance of the experiments is around 90% compared to the computation, which can be attributed to the scale-up effect.

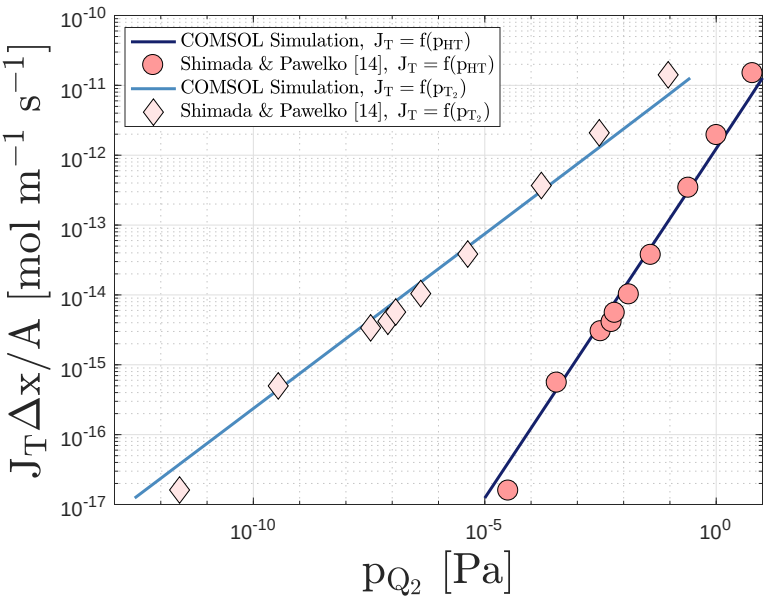

Figure 4.6: Comparison of tritium permeation rates predicted with COMSOL Multiphysics and INL's experimental [14]. Permeation rates are plotted as a function of Q_2 partial pressure, where Q_2 = HT, T_2.

The planned experimental activities using the PGLoop CMSB module include a hydrogen adsorption and desorption experiment as well as multicomponent hydrogen isotopes adsorption experiments. The multicomponent hydrogen isotopes experiment is particularly useful to verify CMSB capacity of the HT extraction/adsorption with respect to the coexistence of the hydrogen partial pressures. This data set will guide and optimize CMSB design and subsequent adsorption/desorption operations.

Considering the quantification of tritium permeation in the breeding blanket systems is of high importance from the safety point of view and in the definition of the interfaces between various subsystems, several experimental configurations to serve as validating tools for tritium transport numerical modeling are being constructed by KIT and CIEMAT. The aim is to develop experimental set-ups that will include various measuring cells designed to characterize the permeation parameters that cover both needs of WCLL and HCPB. Two dedicated experimental rigs are under construction and commissioning at TLK to benchmark the modeling tool, in which experimental rig relevant to the HCPB is described here. For the HCPB case tritium will permeate from purge gas to He coolant and from He coolant to water. The experimental set-up will be operated with He and tritium on one side and He

with hydrogen/deuterium at various partial pressures on the other side. This will allow to evaluate the tritium permeation from purge gas to cooling gas. The experimental set-up will incorporate enough sampling points and required instrumentation to quantify the dynamics of tritium permeation from one side to another. The measuring cell is designed to allow easy dismantling in view of the physical characterization of the permeation surface that may influence dissociation and recombination coefficients. The experiments will be continued for long term operation with hydrogen and deuterium in order to understand the surface dynamics and give references concerning the possibilities for eventual chemical treatment of the surface. The experiments will be carried out at pressures and temperatures that are relevant for DEMO applications.

KIT will develop the configuration of the measuring cell based on the outcome of the simulation of tritium permeation performed at CIEMAT. The aim of the modeling activities at CIEMAT is to define the main characteristics of the measuring cell, e.g., amount of tritium required, thickness of the permeation plate, etc. and to develop the experimental procedure needed to measure the parameters that are necessary for the calibration of the modeling tool. In summary, these experimental activities are expected to enhance our understanding of tritium behavior in a system and enable us to achieve precise numerical simulations.

4.4 Conclusions

In this Chapter we showed the outer fuel cycle tritium performance parameters with pulsed operations are in transient states. A time-dependent dynamic multi-physics simulation in a multi-material, prototypical and geometric configuration is necessary to capture the realistic effects. A higher amount of H_2 in the purge gas stream leads to faster tritium releases from breeding materials but a less efficient use of tritium extraction system. We then propose a new perspective using an integrated system point of view to identify and evaluate the complex relationship between different components of the tritium outer fuel cycle.

In order to achieve an optimal configuration, tritium management should not remain stagnant. On the contrary, periodical tuning of key operating parameters, e.g., H_2 in coolant

and purge gas, out-gassing temperature, etc., can serve as an active means to dynamically control and enhance the performance of tritium systems. In view of H_2 amount on TES efficiency, we recommend a systematical study of the impact of H_2 (or H_2O if a wet purge gas is considered) on tritium residence time and tritium extraction economy for the candidate breeder materials.

This Chapter also summarizes the main progress in the tritium transport modeling activity and main experimental set-ups designed for validation purpose. Experimental activities are being conducted in KIT, NFRI, and other institutions to enhance our understanding of tritium behavior in a system and achieve precise numerical simulations.

References

1. A. YING, H. ZHANG, M. Y. ANH, Y. LEE, "Tritium Transport Evolutions in HCCR TBM under ITER Inductive Operations", Fusion Sci. Technol., 68, 2, 346-352 (2015)

2. A. YING, H. ZHANG, B. J. MERRIL, M. Y. AHN, "Advancement in tritium transport simulations for solid breeding blanket system", Fusion Engineering and Design, 109-111, Part B, 1511-1516, (2016)

3. A. YING, H. LIU, M. ADBOU, "Analysis of Tritium Retention and Permeation in FW/Divertor Including Geometric and Temperature Operating Features," Fusion Sci. Technol., 64, 2, 303-308 (2013)

4. COMSOL Multiphysics v. 5.3a. www.comsol.com

5. Ying *et al.*, "Breeding blanket system design implications on tritium transport and permeation with high tritium ion implantation: A MATLAB/Simulink, COMSOL integrated dynamic tritium transport model for HCCR TBS", Fusion Engineering and Design, Volume 136, Part B, November 2018, Pages 1153-1160

6. Seungyon Cho *et al.*, Fusion Engineering and Design, Volume 136, Part A, 2018, Pages 190-198

7. Marco Riva *et al.*, [2019] Impact of Outer Fuel Cycle Tritium Transport on Initial Start-Up Inventory for Next Fusion Devices, Fusion Sci. Technol., DOI: 10.1080/15361055.2019.1643691

8. E. Carella *et al.*, (2017) Tritium Behavior in HCPB Breeder Blanket Unit: Modeling and Experiments, Fusion Sci. Technol., 71:3, 357-362

9. F. Franza *et al.*, "Tritium transport analysis in HCPB DEMO blanket with the FUS-TPC code", Fusion Engineering and Design, Volume 88, Issues 9-10, 2013, Pages 2444-2447

10. E. Serra and A. Perujo, Journal of Nuclear Materials 223 (1995) 157-162

11. H. ZHANG *et al.*, "Characterization of Tritium Isotopic Permeation Through ARAA in Diffusion Limited and Surface Limited Regimes", Fusion Sci. Technol., 72, 416-425 (2017)

12. Paul Humrickhouse, "Tritium Transport, Permeation, and Control", 4th IAEA DEMO Programme Workshop, Karlsruhe Institute of Technology, November 15, 2016

13. M. Ahn *et al.*, "Status of Tritium Permeation Assessment from KO TBM Team", TBM-PT Information Meeting on Tritium Transport Modelling, ITER Headquarter, June 21, 2019

14. M. Shimada, R.J. Pawelko, "Tritium permeability measurement in hydrogen-tritium system", Fusion Engineering and Design 129 (2018) 134-139

15. Soon Chang Park *et al.*, "Hydrogen adsorption performance for large-scale cryogenic molecular sieve bed", Fusion Engineering and Design, Volume 146, Part B, 2019, Pages 1863-1867

16. K. Tanaka, M. Uetake, M. Nishikawa, Calculation of breakthrough curve of multicomponent hydrogen isotopes using cryosorption column, Fusion Sci. Technol., 33 (1996) 492-503

CHAPTER 5

Impact of Outer Fuel Cycle Tritium Transport on Initial start-up Inventory for Next Fusion Devices

5.1 Introduction

Accurate estimation of time-dependent tritium inventories and flow rates in fusion reactor components is critical to meet nuclear licensing criteria and safety regulations. Moreover, reserves of natural tritium are very limited and the fuel very precious. For tritium economy and fusion commercialization a balanced budget is critical.

A great deal of work on tritium fuel cycle dynamic modeling was reported in literature. Most studies are based on the residence-time approach, i.e. the average time tritium stays in a component before it is released. In these studies, the overall fusion fuel cycle is modeled by systems of time-dependent zero-dimensional ordinary differential equations describing tritium flow rates [1-4]. Kuan and Abdou proposed a new modeling approach by introducing more physics for each fuel cycle component and accounting for more realistic operation parameters [5]. However, due to the lack of detailed reactor design and limited computational capabilities, the model still used a 0-D description for fusion subsystems. With the development of finite element solvers several research groups started to model fusion fuel cycle detailed components [6-9], i.e. considering $2-D/3-D$ complex geometries and solving constitutive equations. Recently, an effort was launched to incorporate high resolution detailed models to system-level to reproduce the fuel cycle dynamic. A dynamic tritium transport model [10], where detailed components modeled with COMSOL Multiphysics [11] are integrated to system-level through the MATLAB/Simulink computational platform [12], was presented for the Helium Coolant Ceramic Reflector Tritium Breeding System (HCCR

TBS). The mathematical formulation was described in detail in Chapter 3.

Analysis and assessment of tritium inventories and flow rates through system level models can be extended to determining key parameters impacting fusion technology feasibility and economy such as the Initial Start-up Tritium Inventory ($ISTI$) and Required Tritium Breeding Ratio (TBR_{r}), as seen in Ref. 1 - 5. The fuel cycle comprehends several subsystems characterized by different functions, requirements, conditions, and physics. We can divide the overall fuel cycle into (i) Inner Fuel Cycle (IFC), i.e. Plasma Exhaust, Fuel Clean-up, Isotope Separation and Delivery Systems, and (ii) Outer Fuel Cycle (OFC), i.e. First Wall/Divertor, Blanket, Coolant and Purge Gas Processing Systems. Current experimental fusion reactors are characterized by relatively low fueling efficiency ($< 50\%$) and tritium fractional burn-up ($\sim 0.35\%$ calculated for ITER [13]). Therefore, a large part of tritium contained in the vacuum vessel is exhausted through the pumping duct to the processing line of the IFC. In particular, ISTI is driven by the tritium fractional burn-up (f_b), fueling efficiency (η_f), and processing time (t_p) of tritium recovery systems: for $f_b \times \eta_f < 2\%$ and $t_p > 6$ h, $ISTI > 10$ kg [4]. In this case the IFC is dominant, since most inventories are found within the IFC. However, IFC impact on ISTI can be reduced if the product $f_b \times \eta_f$ increases to values higher than 2% and processing times of IFC components are reduced, as seen in Ref. 4. Recently, Day *et al.*, proposed the so-called Direct Internal Recycling (DIR) concept [14], which aims to recycle tritium exhausted through the pumping duct directly to plasma, to further minimize tritium retention in IFC compartments, and found that IFC inventory drops to ~ 1 kg (as seen in [15]). In all these cases ($f_b \times \eta_f > 2\%$ and low processing times or use of the DIR), the OFC becomes dominant for $ISTI$ assessment since most tritium inventory resides in the OFC.

In detail, this paper aims to evaluate the Outer Fuel Cycle (OFC) impact on $ISTI$. The analysis is performed to assess the effect of (i) ceramic breeder tritium residence time (τ_{res}), e.g. extrusion-spheronisation sintering processed Li_2TiO_3 and melt spray Li_4SiO_4 - these are examples of breeders with distinct difference in residence time due to different fabrication technique, (ii) tritium processing time of tritium extraction systems (τ_p), e.g. on-line (continuous) technology such as membrane reactors and PERMCAT [16] and batch-

wise mode of adsorption/regeneration columns [17], and (iii) material choices of PFCs, e.g. pure Advanced Reduced Activation Alloy (ARAA) and ARAA with tungsten coating (2 mm thickness). We define the OFC attributed $ISTI$ as the initial amount of tritium that we need to prepare to run the reactor in question until tritium produced in its blankets is recovered and available on-line (assessment of tritium accumulation to start-up following reactors and required TBR assessment are beyond the scope of this research).

A mathematical formulation for OFC attributed $ISTI$ is derived through control volume analysis on tritium flow rates interesting the OFC in Section 5.2. These flow rates are computed with the tritium transport dynamic model presented in Chapter 3. With this innovative approach, it is possible to evaluate $ISTI$ for specific fuel cycle designs under prototypical fusion environment, which never was addressed with previous 0-D lumped models.

5.2 Definition of the Problem

5.2.1 Inner and Outer Fuel Cycle contributes to ISTI

The OFC includes two main processing lines: (i) Tritium Extraction System (TES), (ii) Helium Coolant System (HCS). On the one hand, the HCS main goal is to maintain OFC within the nominal temperature range by extracting heat generated in PFCs and blanket systems. Because of Charge Exchange Neutrals (CXN) and ion fluxes at PFCs surface, tritium implantation into PFCs and permeation to coolant occurs. Tritium content in coolant gas is controlled with the Coolant Purification System (CPS). Therefore, the $ISTI$ must account for the inventories of HCS/CPS components. On the other hand, the TES processes tritium produced in blanket systems, which will be accumulated to fuel the plasma. Therefore, the $ISTI$ problem for TES line results in the determination of the effective tritium extraction time (τ_{eff}^{TES}), which we define as the time needed for tritium flow rates extracted from TES ($\dot{m}_{out}^{TES}$) to match the value of tritium burning rate in plasma ($\dot{N}^{-}$), i.e. $\tau_{eff}^{TES} = t$: $\dot{m}_{out}^{TES} = \dot{N}^{-}$.

A schematic of a typical OFC scheme, representing main components and tritium flow rates, is presented in Fig. 5.1 while variables of interest are listed in Table 5.1.

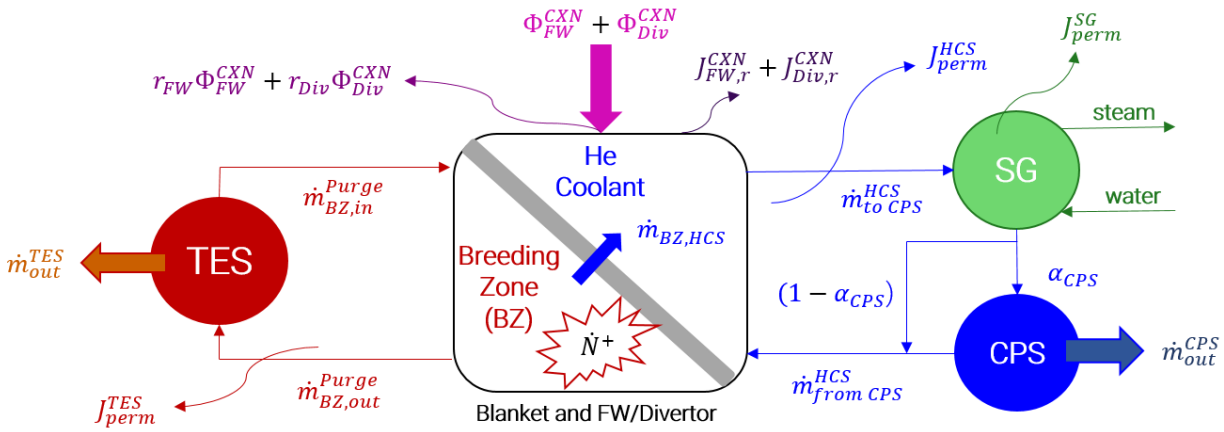

Figure 5.1: Schematic of OFC main components and tritium flow rates.

To quantify the OFC impact on $ISTI$ a control volume analysis for the system of Fig. 5.1 is proposed. The rate of inventory change in the OFC is:

$$\begin{aligned}\frac{dI_{OFC}}{dt} = \dot{N}^+ + \Phi_{FW}^{CXN}A_{FW} + \Phi_{Div}^{CXN}A_{Div} - J_{perm}^{TES} - \dot{m}_{out}^{TES} - r_{FW}\Phi_{FW}^{CXN}A_{FW} \\ -r_{Div}\Phi_{Div}^{CXN}A_{Div} - J_{FW,r}^{CXN} - J_{Div,r}^{CXN} - J_{perm}^{SG} - J_{perm}^{HCS} - \dot{m}_{out}^{CPS}\end{aligned} \tag{5.1}$$

where A_{FW} and A_{Div} are the surface areas of FW and Divertor. The total amount of tritium inventory build-up in the OFC, i.e. TES and HCS lines, can be found by integrating Eq. 5.1 in time. By summing and subtracting $\dot{m}_{BZ,HCS}$ to the right hand side of Eq. 5.1 we can separate the contributions of TES, I_{OFC}^{TES}, and HCS, I_{OFC}^{HCS}, lines as follow:

$$\frac{dI_{OFC}^{TES}}{dt} = \dot{N}^+ - \dot{m}_{out}^{TES} - J_{perm}^{TES} - \dot{m}_{BZ,HCS} \tag{5.2}$$

$$\begin{aligned}\frac{dI_{OFC}^{HCS}}{dt} = (1-r_{FW})\Phi_{FW}^{CXN}A_{FW} + (1-r_{Div})\Phi_{Div}^{CXN}A_{Div} \\ +\dot{m}_{BZ,HCS} - J_{FW,r}^{CXN} - J_{Div,r}^{CXN} - J_{perm}^{SG} - J_{perm}^{HCS} - \dot{m}_{out}^{CPS}\end{aligned} \tag{5.3}$$

Noting that $\dot{N}^+ = TBR \times \dot{N}^- = \dot{N}^- + (TBR-1)\dot{N}^-$, integrating Eq. 5.2 with respect to

Table 5.1: List of variables used to describe OFC tritium flow rates.

Variable	Unit	Description
$\dot{N}^{+}$	kg/s	Tritium production rate
$\dot{m}_{BZ,out}^{Purge}$	kg/s	Purge gas flow rate BZ outlet
$\dot{m}_{BZ,in}^{Purge}$	kg/s	Purge gas flow rate BZ inlet
$\dot{m}_{out}^{TES}$	kg/s	Tritium flow rate extracted from TES
J_{perm}^{TES}	kg/s	TES Tritium losses to building via permeation
$\dot{m}_{BZ,HCS}$	kg/s	Tritium flow rate permeated to coolant from BZ
Φ_{FW}^{CXN}	kg/m^2-s	CXN flux to FW
Φ_{Div}^{CXN}	kg/m^2-s	CXN flux to Divertor
r_{FW}	-	FW reflection coefficient
r_{Div}	-	Divertor reflection coefficient
$J_{FW,r}^{CXN}$	kg/s	FW CXN re-emission to plasma flux
$J_{Div,r}^{CXN}$	kg/s	Divertor CXN re-emission to plasma flux
$\dot{m}_{to\,CPS}^{HCS}$	kg/s	Tritium flow rate in coolant to CPS
$\dot{m}_{from\,CPS}^{HCS}$	kg/s	Tritium flow rate in coolant from CPS
α_{CPS}	-	Fraction of total coolant flow rate treated in CPS
$\dot{m}_{out}^{CPS}$	kg/s	Tritium flow rate extracted from CPS
J_{perm}^{HCS}	kg/s	HCS Tritium losses to building via permeation
J_{perm}^{SG}	kg/s	HCS Tritium losses to SG via permeation

time and rearranging, we obtain:

$$I_{OFC}^{HCS}(t) = \int_0^t (\dot{N}^- - \dot{m}_{out}^{TES})d\tilde{t} + \int_0^t (TBR-1)\dot{N}^- d\tilde{t} - \int_0^t (J_{perm}^{TES} + \dot{m}_{BZ,HCS})d\tilde{t} \qquad (5.4)$$

The first term on the right hand side of Eq. 5.4 represents the difference between the amount of tritium burned in the plasma and extracted from the TES. This can be further split in the intervals [0, τ_{eff}^{TES}], where $\dot{N}^- > \dot{m}_{out}^{TES}$, and tritium must be supplied to the reactor from an external source, i.e. during TES processing when bred tritium is not available, and [τ_{eff}^{TES}, t], for which $\dot{m}_{out}^{TES} > \dot{N}^-$ and tritium accumulation can begin. Therefore, Eq. 5.4 is rewritten as:

$$\begin{aligned} I_{OFC}^{HCS}(t) = &\int_0^{\tau_{eff}^{TES}} (\dot{N}^- - \dot{m}_{out}^{TES})d\tilde{t} + \int_{\tau_{eff}^{TES}}^t (\dot{N}^- - \dot{m}_{out}^{TES})d\tilde{t} \\ &+ \int_0^t (TBR-1)\dot{N}^- d\tilde{t} - \int_0^t (J_{perm}^{TES} + \dot{m}_{BZ,HCS})d\tilde{t} \end{aligned} \qquad (5.5)$$

Considering the right hand side of Eq. 5.5, we define the first term as the OFC TES attributed $ISTI$, the second term (negative in the balance) represents the amount of tritium which is extracted from the TES at the net of tritium burning rate in plasma, i.e. the tritium which can be accumulated to generate fuel reserve and start-up inventory for other reactors, the third term is the extra amount of tritium produced due to TBR margin, i.e. $\dot{N}^+ - \dot{N}^-$, and, finally, the last term represents the tritium lost via permeation to coolant line and buildings. Note that the tritium permeation losses from TES line are not included in the $ISTI$ definition; in fact, tritium streams flowing in TES line are generated within the breeding blanket and not directly subtracted from the plasma vacuum chamber. To conclude, the OFC TES attributed $ISTI$ is:

$$ISTI_{OFC}^{TES} = \int_0^{\tau_{eff}^{TES}} (\dot{N}^- - \dot{m}_{out}^{TES})d\tilde{t} \qquad (5.6)$$

The OFC HCS total inventory is given by integrating Eq. 5.3 with respect to time:

$$I_{OFC}^{HCS} = \int_0^t [(1-r_{FW})\Phi_{FW}^{CXN} A_{FW} + (1-r_{Div})\Phi_{Div}^{CXN} A_{Div} + \dot{m}_{BZ,HCS} - J_{FW,r}^{CXN} - J_{Div,r}^{CXN} - J_{perm}^{SG} - J_{perm}^{HCS} - \dot{m}_{out}^{CPS}]d\tilde{t} \tag{5.7}$$

The initial start-up inventory for OFC HCS line ($ISTI_{OFC}^{HCS}$) should include components inventory (Eq. 5.7) and tritium losses due to permeation to building, i.e. J_{perm}^{SG} and J_{perm}^{HCS}, since both contributes are tritium sinks subtracting fuel to plasma, evaluated in the "Short-Term", i.e. for $t = \tau_{eff}^{TES}$. In fact, after such time, tritium produced in blanket modules is available and TBR margin compensates for losses. Furthermore, the term $\dot{m}_{BZ,HCS}$ should not be included in $ISTI_{OFC}^{HCS}$ since this is tritium coming from TES line and not from plasma. Hence:

$$ISTI_{OFC}^{HCS} = I_{OFC}^{HCS}(t = \tau_{eff}^{TES}) + \int_0^{\tau_{eff}^{TES}} (J_{perm}^{SG} - J_{perm}^{HCS} - \dot{m}_{BZ,HCS}^{CPS})d\tilde{t} \tag{5.8}$$

Moreover, to be conservative, we also neglect tritium recovered from CPS, which is expected to process very small fractions of total coolant flow rate, e.g. $\alpha_{CPS} = 0.1\% - 1\%$, and longer times could be required. Therefore:

$$ISTI_{OFC}^{HCS} = \int_0^{\tau_{eff}^{TES}} [(1-r_{FW})\Phi_{FW}^{CXN} A_{FW} + (1-r_{Div})\Phi_{Div}^{CXN} A_{Div} - J_{FW,r}^{CXN} - J_{Div,r}^{CXN}]d\tilde{t} \tag{5.9}$$

Eq. 5.9 corresponds to the total amount of tritium implanted into PFCs which will generate inventory in PFCs (I_{PFC}) and thus permeation to coolant ($J_{PFC}^{Coolant}$). Finally, the OFC attributed $ISTI$ ($ISTI_{OFC}$) is the sum of contributions from TES (Eq. 5.6) and HCS (Eq. 5.9): $ISTI_{OFC} = ISTI_{OFC}^{TES} + ISTI_{OFC}^{HCS}$.

5.2.2 Computational model

The computational model used in this analysis is an updated version of the dynamic COMSOL-MATLAB/Simulink for OFC tritium transport presented in [10], which was described in detail in Chapter 3. The model comprises (i) TES line, i.e. Breeding Zone (BZ), extraction systems, heat exchanger, H_2 make-up units, connecting pipes (DN15/40S), and (ii) HCS line, i.e. FW/Divertor, CPS, connecting pipes (DN80/80S). The physics implemented in the model includes tritium mass transport, isotope swamping effect, chemical reactions, heat transfer and compressible purge gas flow through porous media. Details of the mathematical formulation is available in [6 - 8, 18]. The Simulink setup and COMSOL convergence was optimized to allow higher computational performance; computational time was reduced by one half compared to the model presented in [10].

For TES modeling, an analytical formulation is adopted for the On-line (continuous operation) case; particularly, TES is characterized by an extraction efficiency, η_{TES}, and $\dot{m}_{out}^{TES} = \eta_{TES}\dot{m}_{in}^{TES}$. In case of batch-wise operation, detailed modeling of Cryogenic Molecular Sieve Bed (CMSB) was performed; the constitutive equations implemented are presented in [19]. The sieve bed adopted is Zeolite 5A, particle diameter is 2.0×10^{-3}, packing of bed 58%, column height and internal diameter are 0.86 m and 0.31 m respectively. Adsorption is performed at 77 K while regeneration at 100 K to enhance tritium release and reduce processing time of regeneration phase. Note that CMSB only treats molecular hydrogen isotopes, i.e. H_2, HT, while oxidized molecules, i.e. HTO, are treated in a different unit, e.g. Room Temperature Molecular Sieve (RTMS) followed by water detritiation process. However for HCCR blanket, HT represents >95% of tritium content in purge gas at BZ outlet, which controls the availability of bred tritium for use in fueling.

Note that, $ISTI_{OFC}$ problem interests Short-Term inventories, i.e. inventories characteristic of the system at time equal to τ_{eff}^{TES}, which falls within the range 1 h - 5 days depending on technology used for tritium extraction. For this time scale, i.e. reactor beginning of life, the reactor is subject to low irradiation dose (<0.3 dpa), therefore, tritium retention due to ion- and neutron- induced trapping does not have a significant effect on start-up

problems (while it affects Long-Term tritium retention). Moreover, due to the low trapping energies, i.e. 0.85 eV [20] tritium retained in intrinsic traps is de-trapped at typical PFCs temperatures [8] and is not influential for $ISTI$ characterization. For these reasons, inventory build-up in PFC due to trapping is insignificant and not calculated in this study. Similarly, radioactive decay losses are negligible on $ISTI$ time scales, and not accounted in the proposed calculation.

5.3 Initial Start-up Tritium Inventory Assessment and Discussion

5.3.1 Tritium Extraction System line - TES

Tritium flow rates recovered by TES ($\dot{m}_{out}^{TES}$) were evaluated for different tritium breeder residence time, i.e. Li_4SiO_4 and Li_2TiO_3 (correlations given in [21]). OFC TES line attributed $ISTI$ results are extrapolated to typical DEMO or future commercial reactors power of 3 GW_{fus}, i.e. $\dot{N}^- \sim 0.459$ kg/day, and different TBR values, i.e. 1.05 - 1.20. As an example, Fig. 5.2 shows the flow rates at TES outlet normalized by $\dot{N}^-$ for On-line (continuous) TES mode, TBR = 1.10, and TES efficiency of 85% and 95%, and Fig. 5.3 shows the respective OFC TES attributed $ISTI$, calculated with Eq. 5.6.

We found that τ_{eff}^{TES} is less than ∼0.5 day for lithium orthosilicate while ∼2 days are required for lithium metatitanate when efficiency is 95%. For lower TES efficiency, 85%, longer times are required, i.e. ∼1 days for Li_4SiO_4 and ∼4.5 days for Li_2TiO_3. Note that in this case $\tau_{eff}^{TES} \sim \tau_{res}$ since $\tau_p \sim 0$. Longer residence time (Li_2TiO_3) increases the OFC TES attributed $ISTI$ of one order of magnitude (0.10 kg $< ISTI <$ 0.25 kg) compared to shorter (Li_4SiO_4) residence time (0.01 kg $< ISTI <$ 0.025 kg) while TES efficiency reduction from 95% to 85% is less impactful. However, results suggest that if TES efficiency falls below 90% and TBR is ∼1.05 the tritium extracted from TES is slightly smaller than the tritium burning rate in plasma. Hence, further extraction must be performed downstream TES at very low partial pressure to ensure break-even between tritium extraction and consumption in the plasma.

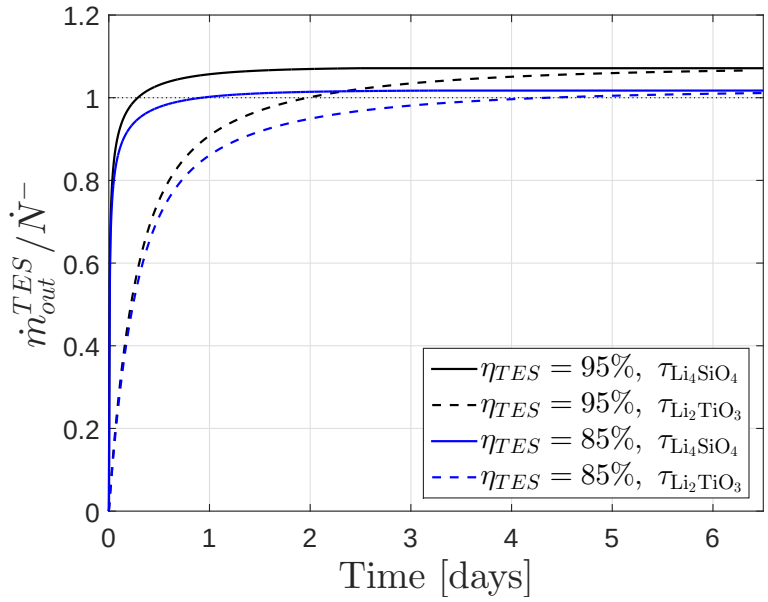

Figure 5.2: Normalized tritium flow rates at TES outlet for On-line mode and TBR=1.10.

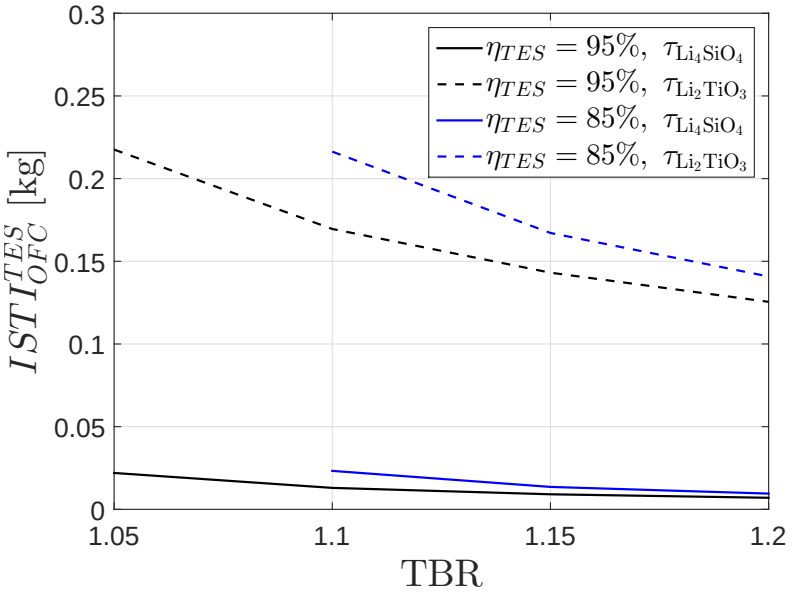

Figure 5.3: OFC TES attributed ISTI for TES On-line mode.

In case of batch-wise operation, the total processing time of adsorption/regeneration columns can be calculated as $\tau_p = \tau_{ad} + \tau_{reg}$, where τ_{ad} adsorption time and τ_{reg} regeneration time. This parameter varies depending on column capacity, dimensions, operating temperature, and TBR. In our case, for the parameters given in Subsection 5.2.2, we found that the adsorption time calculated at column saturation, i.e. when tritium concentrations at CMSB

outlet are equal to 0.1% of concentration at inlet, is ∼134 h (∼5.6 days) for Li_4SiO_4 and ∼137.2 h (∼5.7 days) for Li_2TiO_3 (values calculated for TBR=1.10). The time delay between breeders is due to the different tritium residence time of tritium in ceramics. Regeneration time is ∼1 day, when performed at 100 K, however only ∼1.5 h are needed to provide flow rates that overcome tritium burning rate in the plasma, as shown in Fig. 5.4. Due to the long times required to reach saturation in the column during the adsorption process, the TBR effect is less noticeable compared to the on-line case, e.g. Li_4SiO_4 with TBR=1.20 (best case scenario) gives adsorption time 3 h smaller than Li_2TiO_3 with TBR=1.05 (worst case scenario).

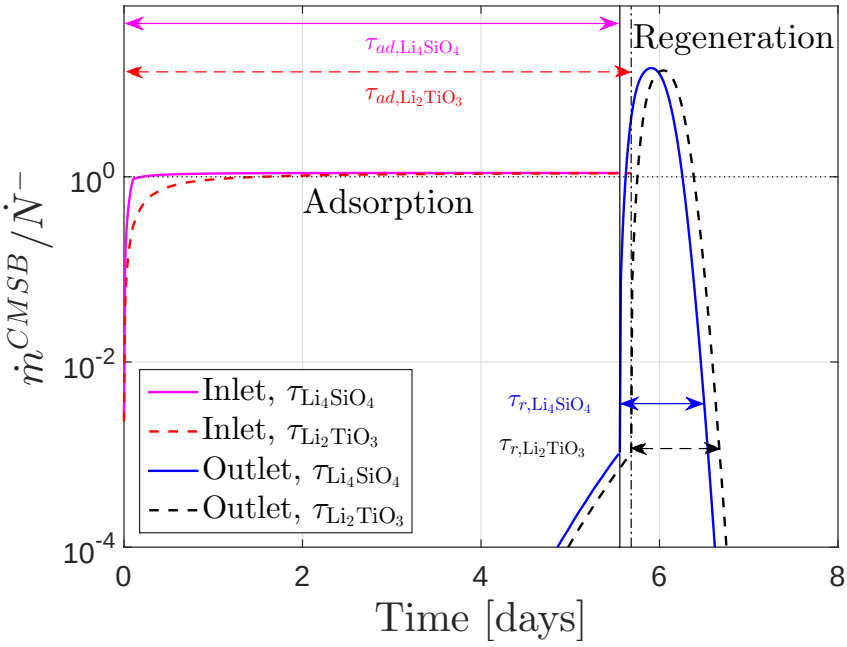

Figure 5.4: CMSB inlet/outlet flow rates for Li_4SiO_4 and Li_2TiO_3.

We show in Table 5.2 the $ISTI_{OFC}^{TES}$ calculated using Eq. 5.6. The range is 2.55 - 2.64 kg depending on breeding material and TBR. As observed, adsorption time is dominant in defining the effective extraction time, i.e. $\tau_{eff}^{TES} \sim \tau_{ad}$, attenuating the effect of breeder choice and TBR, which accounts for ∼90 g difference inventory.

Table 5.2: OFC TES attributed ISTI for TES operated in batch-wise mode.

$ISTI_{OFC}^{TES}$	TBR=1.05	TBR=1.10	TBR=1.15	TBR=1.20
Li_4SiO_4	2.58	2.57	2.56	2.55
Li_2TiO_3	2.64	2.63	2.62	2.61

5.3.2 Helium Coolant System line - HCS

Tritium inventory build-up in HCS components and permeation to coolant depend on CXN implantation into PFCs. In general, CXN magnitude varies depending on several parameters, e.g. physics regime, scrape off layer and edge fueling. The presented results are obtained for CXN tritium flux at FW calculated for ITER HCCR TBM port 22, i.e. 10^{21} atoms/m^2-s (50% D - 50% T) at energy of 400 eV. This choice is considered representative of average implantation into PFCs in the absence of data for specific DEMO design. We considered different PFC structural materials: (i) pure Advanced Reduced Activation Alloy (ARAA), and (ii) ARAA with tungsten coating layer (2 mm thickness). CXN implantation spatial distribution profile in ARAA and W are derived with the SRIM/TRIM code. Reflection coefficients of ARAA and W are ∼0.3 and ∼0.45 respectively. We found that tungsten coating reduces inventory build-up and permeation to coolant of about 1 - 2 orders of magnitude compared with the case of pure ARAA as seen in Figs. 5.5 and 5.6. The HCS attributed $ISTI$ calculated with Eq. 5.9 for K-DEMO [23] PFCs design with $\dot{N}^- \sim 0.459$ kg/day and using representative τ_{eff}^{TES} of each extraction technology, material and TBR, is shown in Fig. 5.7 for on-line operation, and in Table 5.3 for the batch-wise case.

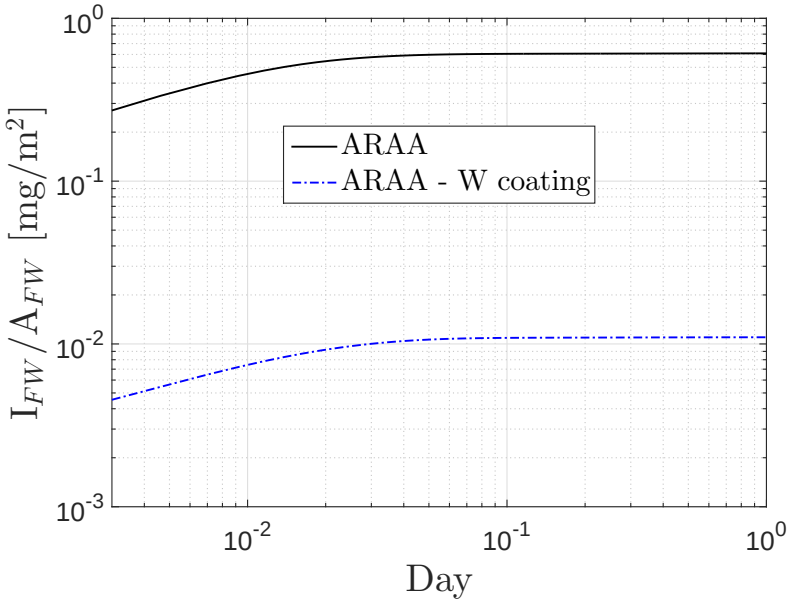

Figure 5.5: Tritium inventory per unit of FW surface area.

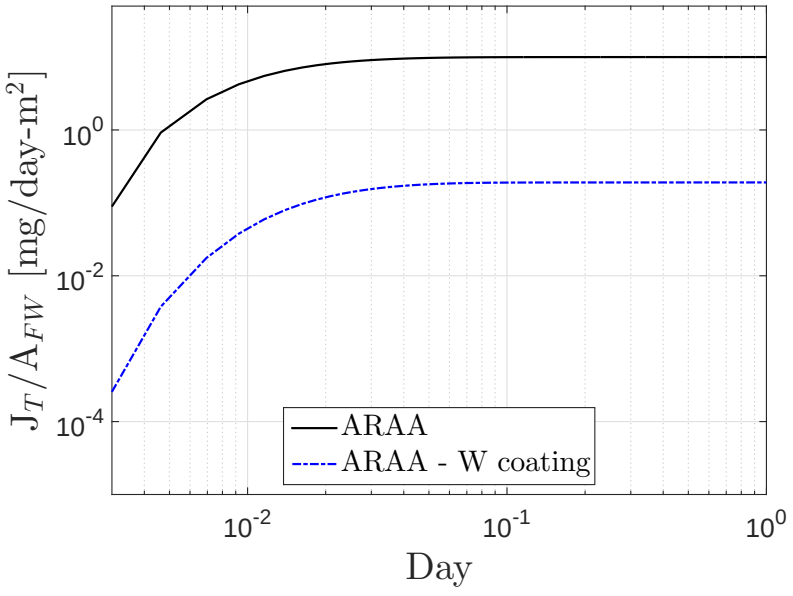

Figure 5.6: Tritium permeation to coolant per unit of FW surface area.

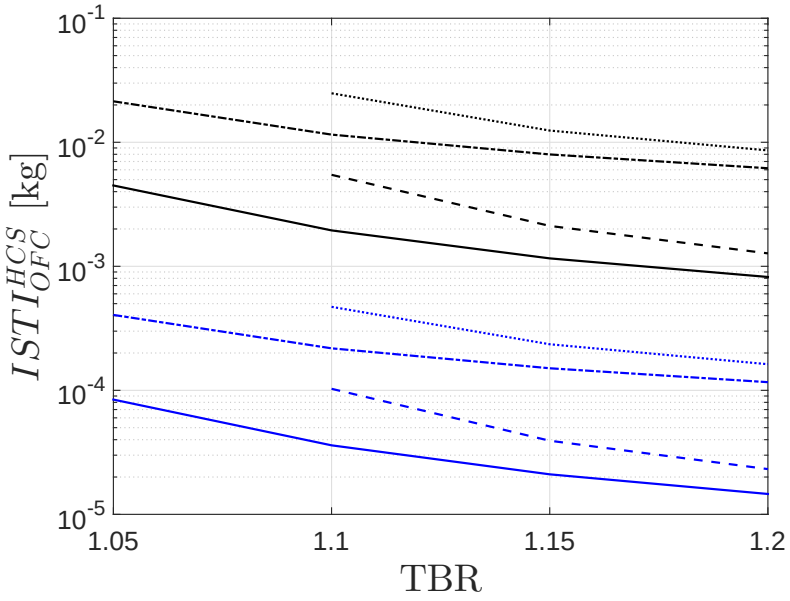

Figure 5.7: OFC HCS attributed $ISTI$ for continuous operation of TES. Black: ARAA PFCs; blue: ARAA with W coating PFCs; solid line: Li_4SiO_4, $\eta_{TES} = 0.95$; dashed line: Li_4SiO_4, $\eta_{TES} = 0.85$; dash-dot line: Li_2TiO_3, $\eta_{TES} = 0.95$; dotted line: Li_2TiO_3, $\eta_{TES} = 0.85$.

Table 5.3: OFC HCS attributed ISTI for TES operated in batch-wise mode.

$ISTI_{OFC}^{HCS}$	TBR=1.05	TBR=1.10	TBR=1.15	TBR=1.20
		ARAA		
Li_4SiO_4	3.21×10^{-2}	3.20×10^{-2}	3.19×10^{-2}	3.17×10^{-2}
Li_2TiO_3	3.29×10^{-2}	3.27×10^{-2}	3.26×10^{-2}	3.25×10^{-2}
		ARAA - W coating		
Li_4SiO_4	6.08×10^{-4}	6.06×10^{-4}	6.04×10^{-4}	6.01×10^{-4}
Li_2TiO_3	6.23×10^{-4}	6.20×10^{-4}	6.18×10^{-4}	6.16×10^{-4}

5.4 Conclusions

A control volume analytical method has been derived to incorporate tritium flow rates calculated from an improved dynamic integrated model for tritium initial start-up tritium inventory analysis. $ISTI$ was evaluated for different breeder material residence times, TES operational modes, efficiency, and PFC surface materials. The analysis shows that the TES line is dominant in determining the OFC impact to $ISTI$. Most important parameters are the residence time of tritium in the breeders and the processing time of tritium extraction technologies, which contribute to defining the effective tritium extraction time. OFC attributed $ISTI$ is minimum when continuous extraction technologies are implemented ($\sim$10$-$250 g) while it is considerably higher ($\sim$2.6 kg) when adsorption/regeneration columns are the extraction technique. In this case the processing time ($\sim$5.5 days) has a dominant effect over breeder residence time ($\sim$hours). If batch-wise operation mode will be further developed and/or considered for future commercial reactors, R&D should focus on reducing adsorption time, and therefore total processing time, to a minimum. This implies finding the optimal column capacity/dimension and adsorption capability. The HCS attributed $ISTI$ is less significant, particularly when W coating is implemented ($ISTI_{OFC}^{HCS} \sim 10^{-5} - 10^{-3}$ kg). However, for nuclear regulation and safety, the integrated dynamic model developed and improved in this study provides means to predict, control, and minimize HCS tritium inventories and permeation rates to the environment.

References

1. M. ABDOU et. al., "Deuterium-Tritium Fuel self-sufficiency in Fusion Reactors", Fusion Technology, 9, 250-285 (1986)

2. L. PAN, H. CHEN, Q. ZENG, "Sensitivity analysis of tritium breeding ratio and startup inventory for CFETR", Fusion Engineering and Design, 112, 311-316 (2016)

3. H. CHEN, *et al.*, "Tritium fuel cycle modeling and tritium breeding analysis for CFETR", Fusion Engineering and Design, 106, 17-20 (2016)

4. M. ABDOU et. al., "Blanket/first wall challenges and required R&D on the pathway to DEMO", Fusion Engineering and Design, 100, 2-43 (2015)

5. W. KUAN and M. ABDOU, "A New Approach for Assessing the Required Tritium Breeding Ratio and startup Inventory in Future Fusion Reactors", Fusion Technology, 35, 309-353 (1999)

6. A. YING, H. ZHANG, M. Y. ANH, Y. LEE, "Tritium Transport Evolutions in HCCR TBM under ITER Inductive Operations", Fusion Sci. Technol., 68, 2, 346-352 (2015)

7. A. YING, H. ZHANG, B. J. MERRIL, M. Y. AHN, "Advancement in tritium transport simulations for solid breeding blanket system", Fusion Engineering and Design, 109-111, Part B, 1511-1516, (2016)

8. A. YING, H. LIU, M. ADBOU, "Analysis of Tritium Retention and Permeation in FW/Divertor Including Geometric and Temperature Operating Features," Fusion Science and Technology, 64, 2, 303-308 (2013)

9. M. ZUCCHETTI, I. NICOLOTTI, A. YING, M. ABDOU, "Tritium Modeling for ITER Test Blanket Module", Fusion Sci. Technol., 68 (2015)

10. A. YING *et al.*, "Breeding Blanket System Design Implications on Tritium Transport and Permeation with High Tritium Ion Implantation: A MATLAB/Simulink,

COMSOL Integrated Dynamic Tritium Transport Model for HCCR TBS", Fusion Engineering and Design (2018), https://doi.org/10.1016/j.fusengdes.2018.04.093

11. COMSOL/Livelink: COMSOL Multiphysics with MATLAB v. 5.0. COMSOL, Inc., Burlington, MA. 2015 Livelink for MATLAB, COMSOL, Inc., Burlington, MA. 2015

12. Simulink Developing S-Functions, MATLAB & SIMULINK, R2017a, MathWorks, Inc.

13. M. ABDOU, "Tritium Fuel Cycle, Tritium Inventories, and Physics and Technology R&D Challenges for: 1) Enabling the startup of DEMO and future Power Plants AND 2) Attaining Tritium self-sufficiency in Fusion Reactors", 13th International symposium on Fusion Nuclear Technology (ISFNT-13) September 25th - 29th, 2017, Kyoto, Japan

14. C. DAY, T. GIEGERICH, "The Direct Internal Recycling Concept to Simplify the Fuel Cycle of a Fusion Power Plant", Fusion Engineering and Design, 88, 616-620 (2013)

15. C. DAY, "A Smart Architecture for the DEMO Fuel Cycle", 30th Symposium on Fusion Technology, Sept. 16-21, 2018, Italy

16. D. DEMANGE *et al.*, "Zeolite membranes and palladium membrane reactor for tritium extraction from the breeder blankets of ITER and DEMO", Fusion Engineering and Design, 88, 2396-2399 (2013)

17. M. ZUCCHETTI *et al.*, "Tritium control in fusion reactor materials: A model for Tritium Extracting System", Fusion Engineering and Design, 98-99, 1885-1888 (2015)

18. H. ZHANG *et al.*, "Characterization of Tritium Isotopic Permeation Through ARAA in Diffusion Limited and Surface Limited Regimes", Fusion Science and Technology, 72, 416-425 (2017)

19. K. TANAKA, M. UETAKE, M. NISHIKAWA, "Calculation of Breakthrough Curve of Multicomponent Hydrogen Isotopes Using Cryosorption Column", Journal of Nuclear Science and Technology, 33, 6, 492-503 (1996)

20. O. V. OGORODNIKOVA *et al.*, "Deuterium Retention in Tungsten in Dependence of the Surface Conditions", J. Nucl. Mater., 313-316, 469-477 (2003)

21. J.G. LAAN *et al.*, "Tritium release data for ceramic breeder materials: compilation of results from EXOTIV-7,-7 and -8", 7th International workshop on Ceramic Breeder Blanket Interaction, Pelten, 16 - 16 September 1998

22. Task Force on TBM Program Safety Demonstration -WM25, June 7-9, 2017 -2016, ITER Organization

23. S. CHO *et al.*, "Investigation of technical gaps between DEMO blanket and HCCR TBM", Fus. Eng. & Des. (2018), article in press

CHAPTER 6

Quantitative Physics and Technology Requirements for Realizing Tritium Self-sufficiency in Fusion Reactors

6.1 Introduction

Tritium dynamics in fusion systems with deuterium-tritium (D−T) fuel cycle plays a key role. Tritium and deuterium consumption in nuclear fusion systems is unprecedented: a total of ∼111.6 kg of tritium and deuterium (∼55.8 kg per isotope) is consumed in nuclear fusion reactions per 1000 MW fusion power per year. Deuterium can be extracted in great amounts from the Earth's oceans. Conversely, due to its radioactive nature and relatively short half-life of 12.33 *years*, tritium is rarely found in nature in significant concentrations. Instead, tritium can artificially be produced in nuclear reactors through neutron-lithium interactions. However, tritium consumption in fusion reactors is huge, but its production from non-fusion systems is very limited. For instance, tritium production in light water reactors (LWR) is ∼0.5−1 kg/year, it requires special tritium breeding systems, and it is expensive. In addition, tritium permeation is of concern and has safety implications. The CANDU (Canada Deuterium Uranium) reactors produce ∼130 g per year from n−D reaction and represent the only reliable source of tritium. It has been estimated that the available tritium inventory will peak to ∼27 kg in 2027, due to CANDU accumulation over forty years of operation [1, 2, 3]. However, after the ITER D−T experimental campaign planned to start in 2036 and consuming ∼0.9 kg of tritium per year, only a few kilograms of tritium (<5 kg) will be available to provide initial start-up inventory for any major D−T fusion facility. Thus, for fusion feasibility and attractiveness, future generation nuclear fusion D−T demonstration (DEMO) reactors and beyond, e.g. power reactors, have the imperative of

achieving tritium self-sufficiency. Hence, a fusion reactor must have a closed fuel cycle where tritium is bred in appropriate amounts and efficiently extracted to fuel the burning plasma. Furthermore, tritium production must be suitable to accumulate extra amounts of tritium which can provide the required inventories for the initial startup of other fusion facilities. In fact, current reserves are irrelevant in a temporal horizon of 20−30 years, as tritium quickly decays. Finally, efficient tritium management in fusion systems is absolutely necessary in light of the the biological hazards of tritium, for safety and nuclear licensing.

Modelling and analyzing tritium transport dynamics in fusion fuel cycle is key to successfully develop a feasible and attractive fusion technology. In this paper we derive a mathematical model which describes the dynamics of the fusion fuel cycle. The model is used to evaluate tritium flow rates into and out of fuel cycle components and calculate tritium inventory build-up in fuel cycle components. Furthermore, we perform a comprehensive analysis of the fusion fuel cycle in order to define the requirements for achieving tritium self-sufficiency and guide the fuel cycle R&D. Finally, an assessment of the availability of external tritium supply for start-up of near and long term fusion facilities and the calculation of the required start-up tritium inventory for a wide range of parameters, reactor powers, and operating conditions, is discussed in great detail. Note that some authors [4, 5] have argued that a tritium start-up inventory is not required at beginning of life (BOL) of fusion reactors. Instead, they propose to start operations under D−D mode, and breed tritium by using the soft neutrons released in the D(n, $^3_2$He)D reaction and the tritium generated in the plasma via D(p, T)D reaction. However, this strategy presents noticeable difficulties: (i) fusion in D−D plasmas is more challenging to be achieved and knowledge of D−D plasmas is limited, and (ii) tritium production per neutron absorption is ∼0.67, which implies long times could be needed to produce considerable amounts of tritium. Thus, the D−D option seems unpractical, would pose additional tokamak physics and technological problems, delay power production by years, and is not economically sensible.

6.1.1 Literature survey and objectives of the study

A great deal of research on tritium transport modeling, self-sufficiency analysis, and start-up inventory assessment is available in literature. The first and primary reference in the field is a comprehensive paper published in 1986 by Abdou *et al.* [6]. In this paper, the authors derived an analytical dynamic model to predict time-dependent tritium flow rates and inventories in the components of the fusion fuel cycle, and discussed the physics and technology requirements to attain tritium self-sufficiency in fusion reactors. Moreover, neutronics analysis of a wide range of breeding blankets design and materials was performed to estimate the achievable tritium breeding ratio (TBR). The authors also developed a statistical model to evaluate and quantify uncertainties regarding numerical modeling techniques, experimental data, and cross sections. This paper motivated many initiatives in physics, fusion technology, tritium processing technology in the US, EU, and Japan over three decades and recently sparked new research in China, Korea, and India. This dynamic modeling technique and analysis went through major improvements in the course of the years. In [7] Kuan and Abdou developed detailed models for all sub-components of the tritium processing systems (e.g. Impurity Separation, Isotope Separation System, etc.) to derive expressions for the tritium mean residence time and their analysis confirmed results of [6]. In 2006 Sawan and Abdou [8] summarized the results of [6] and [7], and added specific evaluation of the achievable TBR in several blanket concepts. In [9] Abdou *et al.* presented a comprehensive paper discussing various key technical issues, challenges, and required R&D of blanket and first wall technology on the pathway to DEMO. In the paper, a short section describes the effect of variable processing time on the tritium self-sufficiency and start-up inventory. Many other studies [10−13] adopted the methodology presented in [6−9] to perform dynamic modeling and analysis of specific fusion reactors (e.g. ITER, CFETR, etc.). Recently, Coleman *et al.* [14] performed start-up inventory analysis for the EU-DEMO considering the effect of low reactor load factors (∼15−45%) and the recently proposed Direct Internal Recycling[1] (DIR)

[1]DIR is a novel tokamak exhaust gas pumping system based on superpermeation principle which works in a continuous matter to reduce tritium residence time and potentially replace the batch-wise cryogenic pumps, thus reducing inventory hold-up in inner part of fuel cycle. Further information on the superpermeation concept and DIR technology can be found in [17].

technology [15, 16]. The authors of [14] also performed parametric sensitivity studies where the main design parameters were varied within a certain range in order to find the conditions that minimize tritium start-up inventory and doubling time. The results presented describe the effect of DIR, global availability, and other parameters on EU-DEMO start-up inventory requirement and doubling time for EU-DEMO fusion power of 2037 MW. The authors' main findings confirmed the importance of parameters such as tritium burn fraction and fueling efficiency on start-up inventory, as it was previously shown [9]. However, self-sufficiency analysis was not performed while the authors assumed a representative TBR value of 1.10 for EU-DEMO and then varied it in the range (1.03−1.08) to determine its effect on fuel cycle performances.

In this paper we aim to use a similar model to the one developed in [6−9] and extend the analysis to incorporate other features that were not considered in the pre-existing models and studies. The objective of this study is to determine the quantitative physics and technology requirements for realizing tritium self-sufficiency and minimizing tritium start-up inventory in fusion reactors during different stages of fusion technology development. In particular, in this research we:

1. derive an up-to-date fusion fuel cycle model describing tritium flow rates and inventories in fusion components with the use of the mean residence time method proposed in [6−9];

2. include in the model the capability of describing tritium dynamics for different plasma scenarios, e.g. burn and dwell time, shut-down due to random failures, and for scheduled maintenance;

3. evaluate the effect of physics parameters (e.g. tritium burn fraction in plasma, fueling efficiency, etc.), technology parameters (e.g. tritium processing time), and other key parameters (e.g. tritium reserve and doubling time, reactor availability factor, power level, etc.) on tritium self-sufficiency and start-up inventory;

4. evaluate the tritium start-up inventory for various reactors with different designs and

powers (e.g. ITER, FNSF, CFETR, DEMO, and power reactors);

5. define the R&D goals regarding the physics and technology requirements to attain self-sufficiency and reduce the required tritium start-up inventory.

6.2 Description of the Fusion Fuel Cycle

The fuel cycle of a fusion reactor includes two sub-cycles: (1) the Inner Fuel Cycle (IFC), i.e. Plasma Exhaust , Fuel Clean-up, Isotope Separation, Water Detritiation, Storage and Matter Injection, and Fueling Systems, and (2) the Outer Fuel Cycle (OFC), i.e. First Wall, Divertor, Breeding Zone, Coolant Processing and Tritium Extraction System. The schematic of a typical fusion fuel cycle is shown in the block diagram of Fig. 6.1. The next two subsections will discuss details of the inner and outer fuel cycles, respectively.

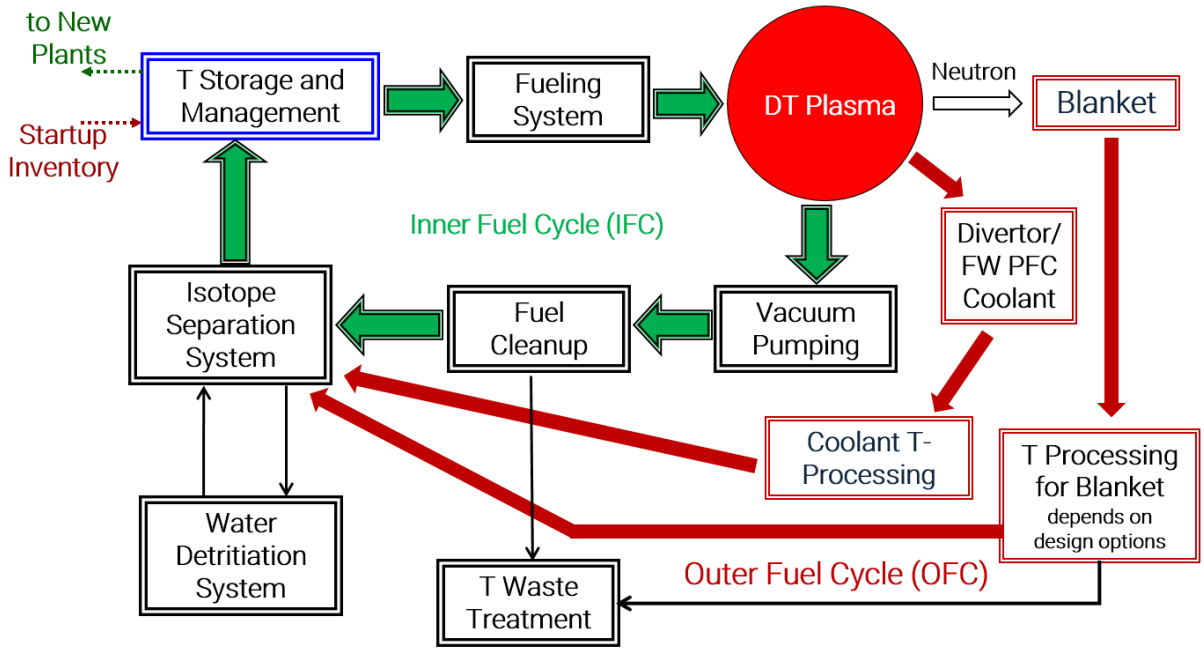

Figure 6.1: Schematic of main components of fusion inner and outer fuel cycles showing main tritium flow rates in fusion systems.

6.2.1 Inner fuel cycle: tritium storage, fueling, exhaust, fuel clean-up and processing systems

A tritium start-up inventory is necessary to start D−T reactor operation. Tritium in the form hydrides is initially stored in apposite metal beds (e.g. uranium). The storage system is connected to the fueling system where D and T are prepared to fuel the plasma. Most common techniques are: (i) injection of frozen pellets at high speed − pellet velocity of ∼1000 m/s is necessary reach the plasma core more efficiently, and (ii) gas puffing. Note that only a fraction of the injected fuel particles, proportional to the fueling efficiency, reaches the plasma core where particles are confined for a characteristic confinement time and nuclear fusion reactions occur. The fraction of the fuel that does not reach the core, or is not burned in the core, is eventually exhausted through the Scrape-off Layer (SOL) to the vacuum pump. In the IFC tritium fluxes exhausted from the plasma through the vacuum pump are processed in order to obtain the adequate level of purity, physical form, and required D−T ratio to fuel the plasma. In particular, exhausted fluxes from plasma are pumped to the fuel clean-up compartments where Plasma Enhancement Gases, e.g. Ar, Ne, N, etc., and helium ashes are separated from hydrogenic species with the use of diffusers, e.g. Pd-Ag alloy, and catalytic reactors with Pd membrane. After the clean-up process, hydrogen isotopologues (e.g. H_2, D_2, T_2, HD, HT, and DT) reach the isotope separation system (ISS). This is a cryogenic distillation column which performs isotope separation exploiting a sensible difference in the boiling points of H_2, and T_2, respectively 20 and 25 K. This technology is the most promising among the candidates (e.g. gas chromatography, thermal diffusion method, etc.) because it can process large flow rates and maintain high separation factor, but has the downside of holding tritium for long times (∼hours) thus increasing the tritium inventory in the component. The ISS is connected to the Water Detritiation System (WDS), which executes tritium removal from tritiated water through several chemical exchange columns (e.g. water vapor/HT), and to the storage and fueling systems.

6.2.2 Outer fuel cycle: tritium extraction systems from blanket, plasma facing components, and coolant

Two lines characterize the OFC: (i) Tritium Extraction System (TES) and (ii) Coolant Purification System (CPS). Tritium generated in the breeding zones of blankets is released from lithium containing materials (ceramics, liquid metals, or molten salt) and carried to the TES unit where tritium is separated from its carrier, e.g. helium purge gas for ceramic breeders or eutectic Lithium-Lead for liquid metal concepts. At the same time, high tritium fluxes from plasma, in the form of Charge eXchange Neutrals (CXN) and ions, are implanted into the Plasma Facing Components (PFCs), i.e. first wall and divertor. Driven by concentration and thermal gradients, tritium diffuses through structural material of PFCs and permeates to the coolant channels. Thus, the coolant is processed in the Coolant Purification System (CPS) units. Tritium permeation from the coolant loop to the reactor buildings is of particular concern in fusion systems, thus design optimization of the CPS unit is critical. Finally, the hydrogenic species recovered by the TES and CPS units reunite and are further processed in the inner fuel cycle.

6.3 Dynamic Fuel Cycle Model to Determine Time-dependent Tritium Flow Rates and Inventories, and Perform Self-sufficiency Analysis and Start-up Assessment

6.3.1 The tritium self-sufficiency condition

Due to the scarcity of tritium resources, fusion reactors must breed and efficiently extract tritium in self-sufficient amounts. According to [6−9], the self-sufficiency condition is defined as:

$$TBR_A \geq TBR_R \tag{6.1}$$

where the achievable TBR (TBR_A) is determined by the breeding design, technology, physics, and material choices. Neutronics studies [8] have shown that the achievable TBR is in the range 1−1.15. However, the authors pointed out that there are various uncertainties in the calculations due to:

1. system definition and design (e.g. breeding configuration, breeder to structure volume ratio);
2. complexity of modeling accurate tokamak toroidal 3−D geometry with detailed FW/Blankets and other ports in vacuum vessel (e.g. diagnostics ports);
3. nuclear cross sections multi-group data library (e.g. uncertainties in the measured cross sections, energy and angle of secondary neutrons).

Recently an effort was launched by the fusion neutronics community to develop more realistic models capable of representing a 3-D sector of DEMO reactors, e.g. in [18−20] various blanket concepts designed for the EU-DEMO were simulated with the use of the MCNP nuclear code. Results have shown achievable TBR in the range 1.10−1.30. However, the higher values are consequence of a reduced volume of structural material in the blankets which is not feasible in practice. When realistic design were considered, achievable TBR <1.15 were obtained.

The required TBR (TBR_R) is defined as $TBR_R = 1+\Delta$, where Δ is the margin exceeding unity which is needed to:

1. compensate for losses by radioactive decay (5.47% per year) during time between production and use, and during fusion system shutdown;

2. supply tritium inventory for start-up of other reactors (for a specified doubling time);

3. provide a "reserve" storage inventory necessary for continued reactor operation under certain conditions (e.g. a failure in a tritium processing line).

The magnitude Δ depends on the dynamics of the entire fuel cycle which is characterized by a handful of physics constraints and technology parameters.

Attaining tritium self-sufficiency is absolutely necessary for D−T fusion energy systems to be feasible, since tritium is no-longer a natural element present in nature and reserves are extremely limited, and depends on complex interactions of plasma physics and fusion technology parameters. In order to perform tritium self-sufficiency analysis and start-up inventory evaluation, accurate models of the fusion fuel cycle are required. The mathematical model developed in this work is described in the following subsection.

6.3.2 System level simulation modeling of fuel cycle

6.3.2.1 The mean residence time method

In this work, the fuel cycle is modeled by using the mean resident time method proposed in [6−9]. The overall fusion fuel cycle is described by a system of time-dependent zero-dimensional ordinary differential equations (ODEs). Each equation describes the tritium dynamics of a particular component of the fuel cycle. The tritium flow rates in and out of the component and the component inventory are determined by the tritium residence time of that specific component, i.e. a measure of how long tritium resides in a certain component before it is released. Each component i is characterized by a tritium inventory, I_i, a tritium residence time, τ_i, a tritium flow rate from component j to component i, $(I_j/\tau_j)_i$ and $j \neq i$,

and a tritium flow rate out of component i, (I_i/τ_i). Thus, the the rate of change of tritium inventory in component i is determined by the tritium flow rates into and out of component i:

$$\frac{dI_i}{dt} = \sum_{j \neq i} \left(\frac{I_j}{\tau_j}\right)_i - (1+\epsilon_i)\left(\frac{I_i}{\tau_i}\right) - \lambda I_i + S_i \tag{6.2}$$

where S_i is a tritium source term in component i (tritium generation is normally only in blanket modules), and ϵ_i and λ the non-radioactive and radioactive losses respectively. The numerical dynamic model reproduces the typical fusion fuel cycle, which we present in Fig. 6.2. In particular, each tritium flow rate is summarized in Tables 6.1 and 6.2 for the outer and inner fuel cycles, respectively.

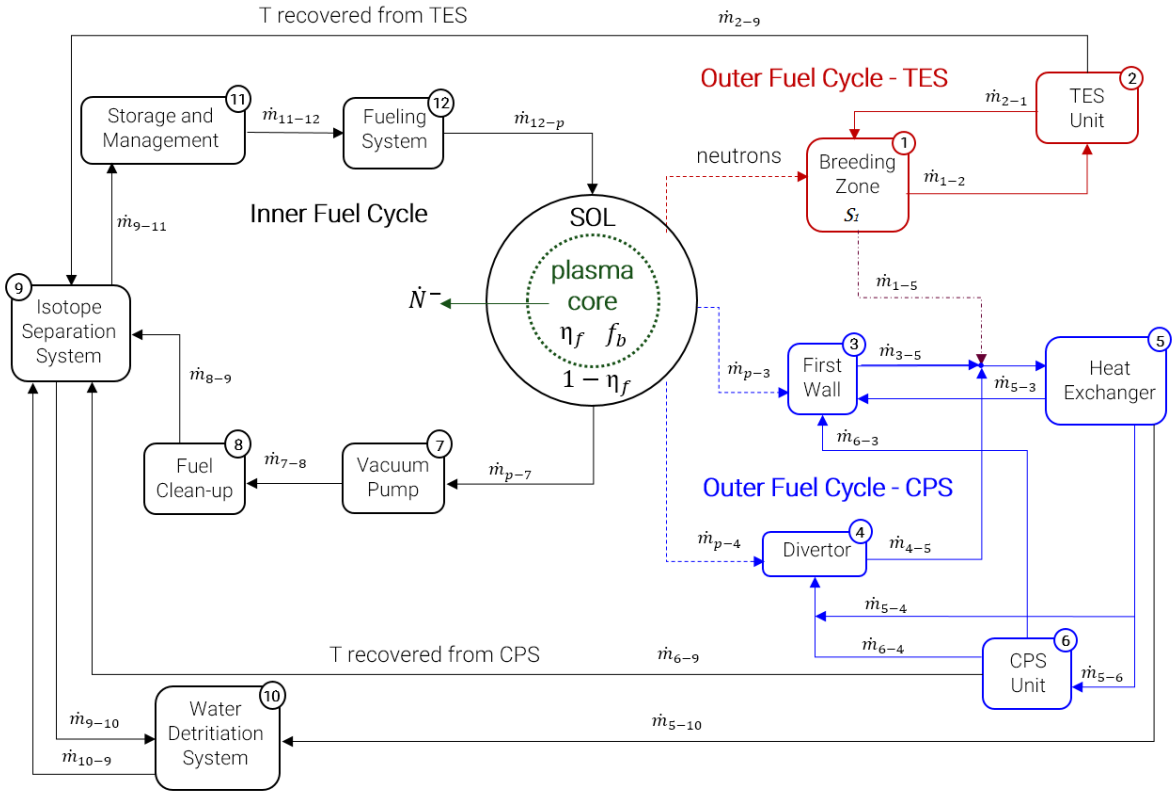

Figure 6.2: Detailed schematic of fusion inner and outer fuel cycles with tritium flow rates used to build the dynamic numerical model.

Table 6.1: Tritium flow rates in the outer fuel cycle of Fig. 6.1.

Component	Flow rate	Mathematical formulation
1	S_1	$\Lambda\dot{N}^-$
	$\dot{m}_{2-1}$	$(1-\eta_2)\frac{I_2}{\tau_2}$
	$\dot{m}_{1-2}$	$-(1-f_{1-5})\frac{I_1}{\tau_1}$
	$\dot{m}_{1-5}$	$-f_{1-5}\frac{I_1}{\tau_1}$
	losses	$-\epsilon_1\frac{I_1}{\tau_1}-\lambda I_1$
2	$\dot{m}_{1-2}$	$(1-f_{1-5})\frac{I_1}{\tau_1}$
	$\dot{m}_{2-12}$	$-\eta_2\frac{I_2}{\tau_2}$
	$\dot{m}_{2-1}$	$-(1-\eta_2)\frac{I_2}{\tau_2}$
	losses	$-\epsilon_2\frac{I_2}{\tau_2}-\lambda I_2$
3	$\dot{m}_{p-3}$	$f_{p-3}\frac{\dot{N}^-}{\eta_f f_b}$
	$\dot{m}_{5-3}$	$f_{5-3}(1-f_{5-6})(1-f_{5-10})\frac{I_5}{\tau_5}$
	$\dot{m}_{6-3}$	$f_{6-3}(1-\eta_6)\frac{I_6}{\tau_6}$
	$\dot{m}_{3-5}$	$-\frac{I_3}{\tau_3}$
	losses	$-\epsilon_3\frac{I_3}{\tau_3}-\lambda I_3$
4	$\dot{m}_{p-4}$	$f_{p-4}\frac{\dot{N}^-}{\eta_f f_b}$
	$\dot{m}_{5-4}$	$(1-f_{5-3})(1-f_{5-6})(1-f_{5-10})\frac{I_5}{\tau_5}$
	$\dot{m}_{6-4}$	$(1-f_{6-3})(1-\eta_6)\frac{I_6}{\tau_6}$
	$\dot{m}_{4-5}$	$-\frac{I_4}{\tau_4}$
	losses	$-\epsilon_4\frac{I_4}{\tau_4}-\lambda I_4$
5	$\dot{m}_{1-5}$	$f_{1-5}\frac{I_1}{\tau_1}$
	$\dot{m}_{3-5}$	$\frac{I_3}{\tau_3}$
	$\dot{m}_{4-5}$	$\frac{I_4}{\tau_4}$
	$\dot{m}_{5-3}$	$-f_{5-3}(1-f_{5-6})(1-f_{5-10})\frac{I_5}{\tau_5}$
	$\dot{m}_{5-4}$	$-(1-f_{5-3})(1-f_{5-6})(1-f_{5-10})\frac{I_5}{\tau_5}$
	$\dot{m}_{5-6}$	$-f_{5-6}(1-f_{5-10})\frac{I_5}{\tau_5}$
	$\dot{m}_{5-10}$	$-f_{5-10}\frac{I_5}{\tau_5}$
	losses	$-\epsilon_5\frac{I_5}{\tau_5}-\lambda I_5$
6	$\dot{m}_{5-6}$	$f_{5-6}(1-f_{5-10})\frac{I_5}{\tau_5}$
	$\dot{m}_{6-3}$	$-f_{6-3}(1-\eta_6)\frac{I_6}{\tau_6}$
	$\dot{m}_{6-4}$	$-(1-f_{6-3})(1-\eta_6)\frac{I_6}{\tau_6}$
	$\dot{m}_{6-12}$	$-\eta_6\frac{I_6}{\tau_6}$
	losses	$-\epsilon_6\frac{I_6}{\tau_6}-\lambda I_6$

Table 6.2: Tritium flow rates in the inner fuel cycle of Fig. 6.1.

Component	Flow rate	Mathematical formulation
7	$\dot{m}_{p-7}$	$(1-\eta_f f_b - f_{p-3} - f_{p-4})\frac{\dot{N}^-}{\eta_f f_b}$
	$\dot{m}_{7-8}$	$-\frac{I_7}{\tau_7}$
	losses	$-\epsilon_7\frac{I_7}{\tau_7} - \lambda I_7$
8	$\dot{m}_{7-8}$	$\frac{I_7}{\tau_7}$
	$\dot{m}_{8-9}$	$-\frac{I_8}{\tau_8}$
	losses	$-\epsilon_8\frac{I_8}{\tau_8} - \lambda I_8$
9	$\dot{m}_{2-9}$	$\eta_2\frac{I_2}{\tau_2}$
	$\dot{m}_{6-9}$	$\eta_6\frac{I_6}{\tau_6}$
	$\dot{m}_{8-9}$	$\frac{I_8}{\tau_8}$
	$\dot{m}_{10-9}$	$\frac{I_{10}}{\tau_{10}}$
	$\dot{m}_{9-10}$	$-f_{9-10}\frac{I_9}{\tau_9}$
	$\dot{m}_{9-11}$	$-(1-f_{9-10})\frac{I_9}{\tau_9}$
	losses	$-\epsilon_9\frac{I_9}{\tau_9} - \lambda I_9$
10	$\dot{m}_{5-10}$	$f_{5-10}\frac{I_5}{\tau_5}$
	$\dot{m}_{9-10}$	$f_{9-10}\frac{I_9}{\tau_9}$
	$\dot{m}_{10-9}$	$-\frac{I_{10}}{\tau_{10}}$
	losses	$-\epsilon_{10}\frac{I_{10}}{\tau_{10}} - \lambda I_{10}$
11	$\dot{m}_{9-11}$	$(1-f_{9-10})\frac{I_9}{\tau_9}$
	$\dot{m}_{11-p}$	$-\frac{\dot{N}^-}{\eta_f f_b}$
	losses	$-\lambda I_{11}$
12	$\dot{m}_{11-12}$	$-\frac{\dot{N}^-}{\eta_f f_b}$
	$\dot{m}_{12-p}$	$\frac{\dot{N}^-}{\eta_f f_b}$

In these tables, Λ is the required TBR, f_{j-i} the fraction of the total flow rate out of component j to component i, η_i is the efficiency of tritium processing system in component i, e.g. for components such as the TES and CPS units, $\dot{N}^-$ the tritium burning rate in the plasma, η_f the fueling efficiency, and f_b the tritium burn fraction. Further detail regarding η_f and f_b definition and their effect on self-sufficiency is given in Section 6.4.

The system of ODEs representing the overall fuel cycle is:

$$\frac{dI_1}{dt} = \Lambda\dot{N}^- + (1-\eta_2)\frac{I_2}{\tau_2} - \frac{I_1}{T_1} \tag{6.3}$$

$$\frac{dI_2}{dt} = (1-f_{1-5})\frac{I_1}{\tau_1} - \frac{I_2}{T_2} \tag{6.4}$$

$$\frac{dI_3}{dt} = f_{p-3}\frac{\dot{N}^-}{\eta_f f_b} + f_{5-3}(1-f_{5-6})(1-f_{5-10})\frac{I_5}{\tau_5} + f_{6-3}(1-\eta_6)\frac{I_6}{\tau_6} - \frac{I_3}{T_3} \tag{6.5}$$

$$\frac{dI_4}{dt} = f_{p-4}\frac{\dot{N}^-}{\eta_f f_b} + (1-f_{5-3})(1-f_{5-6})(1-f_{5-10})\frac{I_5}{\tau_5} + (1-f_{6-3})(1-\eta_6)\frac{I_6}{\tau_6} - \frac{I_4}{T_4} \tag{6.6}$$

$$\frac{dI_5}{dt} = f_{1-5}\frac{I_1}{\tau_1} + \frac{I_3}{\tau_3} + \frac{I_4}{\tau_4} - \frac{I_5}{T_5} \tag{6.7}$$

$$\frac{dI_6}{dt} = f_{5-6}(1-f_{5-10})\frac{I_5}{\tau_5} - \frac{I_6}{T_6} \tag{6.8}$$

$$\frac{dI_7}{dt} = (1-\eta_f f_b - f_{p-3} - f_{p-4})\frac{\dot{N}^-}{\eta_f f_b} - \frac{I_7}{T_7} \tag{6.9}$$

$$\frac{dI_8}{dt} = \frac{I_7}{\tau_7} - \frac{I_8}{T_8} \tag{6.10}$$

$$\frac{dI_9}{dt} = \frac{I_8}{\tau_8} + \frac{I_{10}}{\tau_{10}} + \eta_2\frac{I_2}{\tau_2} + \eta_6\frac{I_6}{\tau_6} - \frac{I_9}{T_9} \tag{6.11}$$

$$\frac{dI_{10}}{dt} = f_{9-10}\frac{I_9}{\tau_9} + f_{5-10}\frac{I_5}{\tau_5} - \frac{I_{10}}{T_{10}} \tag{6.12}$$

$$\frac{dI_{11}}{dt} = (1-f_{9-10})\frac{I_9}{\tau_9} - \frac{\dot{N}^-}{\eta_f f_b} - \lambda I_{11} \tag{6.13}$$

$$\dot{m}_{12-p} = \frac{\dot{N}^-}{\eta_f f_b} \tag{6.14}$$

where $\frac{1}{T_i} = \frac{1+\epsilon_i}{\tau_i} + \lambda$, and the initial conditions are:

- $I_i(t=0) = I_{i,0} = 0$ for $i = 1, 2, ..., 10$;
- $I_{11}(t=0) = I_{11}^0$ is the initial start-up inventory.

This system of equations was numerically implemented with the use of the MATLAB/Simulink computing environment. The Simulink ODE solvers offer efficient computational perfor-

mance, and the scope blocks allow on-line tracking of inventories and flow rates time evolution. Moreover, Simulink's library includes several predefined signal blocks which can be used to model the plasma operating scenario which determines the reactor availability factor, e.g. through the pulse generator block. The model tracks tritium inventory build-up and tritium flow rates into and out of the fuel cycle components. The performance of each component is modeled by a handful of characteristic parameters (e.g. residence and processing times, tritium extraction and fueling efficiency, etc.) representative of each technology. No effort is spent to solve any transport phenomena and/or chemical balance in detail with typical numerical method used for dimensional modeling. Instead, our modeling technique can be classified as system-level simulation (SLS), i.e. a simulation where the level of detail is adjusted to the practical simulation of large and complex systems which comprehend various components that are not completely defined. Thus, the model does not require a detailed knowledge of each part of the system and can serve as a precious tool to investigate the performance of the overall system in the early stages of conceptual design. This choice allows overcoming some challenging issues of fuel cycle modeling:

1. self-sufficiency analysis requires a computational technique which ensures simulations of reactor performances over a reactor lifetime, i.e. $\sim$30 years. Thus, the computational technique must ensure acceptable computational times;

2. several components of fuel cycle system are still in conceptual design phase. Therefore detailed modeling may not be practical. Modeling of components as black boxes, with an associated residence time, is more practical and yields results useful to understanding the overall system behavior and the importance of certain components and parameters.

Our model may also be used for sensitivity analyses and gives helpful information back to the system level designers, e.g. on acceptable residence times, and hence directly influences technology choices. Note that detailed models of fuel cycle components, where constitutive governing equations are numerically solved, exist in literature, e.g. for the Helium Coolant Ceramic Reflector Test Blanket Module (HCCR$-$TBM) [22$-$25]. Further advancement of

outer fuel cycle modeling was shown in [26] and [27], where the authors integrated the detailed model to system level in order to represent typical tritium streams. Despite the improvements in the computational technique used for this kind of modeling, high fidelity models require a significant computational power. Thus, simulations are possible only on short time scales, e.g. a few days, and are therefore unpractical for extending the analysis over the reactors lifetime. However, the higher fidelity of these models provides various data, e.g. processing times, permeation rates, losses to environment, etc., which constitutes precious input to the system-level model and helps to maintain a high accuracy in the residence time models.

6.3.2.2 Evaluation of start-up inventory and required TBR

The storage system dynamics was accurately described by Kuan and Abdou in Ref. 7 and is summarized in Fig. 6.3. The tritium inventory initially contained in the storage system (I_S^0) characterizes the start-up inventory. As reactor operation begins, the tritium inventory in the storage decreases, as tritium is provided to the fueling system and, ultimately, to the plasma. Thus, after it reaches a minimum, the storage inventory starts to increase as a result of the extraction and accumulation of tritium coming from the outer fuel cycle (i.e. the tritium bred in blanket modules and extracted by the tritium extraction systems) and due to the re-circulation of tritium processed in the inner fuel cycle (i.e. the tritium contained in the plasma exhaust). In particular, the storage inventory must include a reserve inventory (I_r) in order to allow continuous reactor operation in case of any malfunctions due to random failures in a part of any tritium processing line. This reserve inventory is critical to ensure high level of plant reliability and availability, which has direct implications to the competitiveness of fusion technology. In this work, we specify the minimum storage inventory as:

$$I_S^{min} = I_r \tag{6.15}$$

$$I_r = \frac{\dot{N}^-}{\eta_f f_b} t_r q \tag{6.16}$$

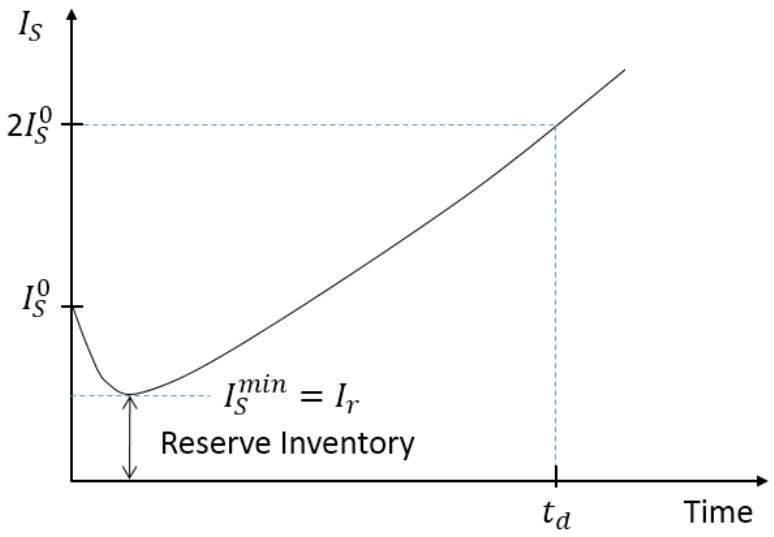

Figure 6.3: Qualitative description of the storage system tritium inventory dynamics.

where t_r is the reserve time, i.e. the period of tritium supply kept in reserve storage to maintain the plasma and the power plant operational in case of any malfunction in a fraction q of any tritium processing system. This implies that the storage system is able to provide the necessary tritium injection rate to the plasma $\dot{N}^-/\eta_f f_b$ for a time t_r when a fraction q of the fuel cycle fails. The definition of burn fraction, fueling efficiency, and tritium injection rate is given in Section 6.4.

After a doubling time (t_d) the storage system inventory reaches a value equal to twice the initial inventory:

$$I_S(t_d) = 2I_S^0 \tag{6.17}$$

Thus, in a doubling time, the reactor generates a sufficient start-up inventory to start a second reactor. Here we assume this second reactor has the same technology and characteristic parameters of the original first reactor, hence the same start-up inventory is needed. However, this assumption is conservative since in times of $\sim t_d$ (which is several years) technology may advance, and lower start-up may be sufficient. Note that an alternative definition of Eq. 6.17 is available in various previous researches [6−9] as $I_S(t_d) = I_S^0 + I_S^{min}$. However, Eq. 6.17 is slightly more conservative (see TBR_R values reported in TABLE II of [6]) and

we believe more appropriate at this state of knowledge of fusion technology.

The required TBR (TBR_R) and tritium start-up inventory (I_S^0) are mutually dependent and neither of them is known in the beginning of the calculation. Therefore, the code calculates the required TBR and tritium start-up inventory through iterations. Given the weak dependency of start-up inventory on required TBR, convergence with a degree of accuracy of 0.01% is found for Eq. 6.17 in a few iterations.

6.3.2.3 Reactor availability factor modeling

In order to account for ordinary maintenance period and/or unexpected shutdown due to random failures, we introduced in the model an overall reactor duty or availability factor (AF), which was originally defined in [21], and can be written as:

$$AF = \frac{MTBF}{MTBF + MTTR} = \frac{1}{1 + \frac{MTTR}{MTBF}} \tag{6.18}$$

where $MTBF$ is the mean time between failures (plasma on) and $MTTR$ the mean time to repair (plasma off). A switch operator which turns the plasma on and off according to the $MTBF$ and $MTTR$ periods is implemented in the numerical model in order to account for the availability factor of the plant.

Analyses have shown that, in order to obtain an overall availability factor $> 50\%$ for a DEMO reactor, the blanket/divertor system shall require $MTBF > 10\ years$ and $MTTR < 1\ month$, giving a blanket/divertor availability factor of $\sim 87\%$ [21]. Extrapolation from other technologies, e.g. aerospace and fission industry, shows expected $MTBF$ for fusion blankets/divertor as short as $\sim hours - days$, and $MTTR \sim months$ denoting a significant difference between requirements and expectations. The fundamental reasons which lead to short $MTBF$, long $MTTR$, and low expected availability in current fusion confinement systems reside in the necessary choice of locating the Blanket/FW/Divertor inside the vacuum vessel[2], which is a low fault tolerance domain and requires immediate shutdown in case of

[2]The decision to insert the blanket inside the vacuum vessel is necessary to protect the vacuum vessel, which must be robust and cannot be in high radiation, temperature, stress state facing the plasma.

various failures (e.g. coolant leak). Furthermore, due to limited physical space and other considerations, no redundancy is possible. Long $MTTR$ is due to the difficulties in accessing the nuclear components inside the vacuum vessel. Repair and replacement require breaking the vacuum seal, many connects/disconnects, and many operations in the limited access space of tokamaks, stellerators, and other "toroidal/closed" configurations. Large surface area of the first wall results in high failure rate for a given unit failure rate per unit length of piping, welds, and joints, determining short $MTBF$.

Low availability factors could have tremendous consequences on tritium economy and self-sufficiency: during the reactor downtime (i.e. during the $MTTR$) tritium production in blankets is interrupted whilst tritium is continuously lost by radioactive decay. Thus, the TBR requirements could become more demanding in case of low availability factor. In the fusion development pathway there are three different stages of reactor development:

1. Near tern plasma-based experimental facilities (e.g. FNSF, VNS, CTF, etc.);
2. DEMO reactors (e.g. EU-DEMO, K-DEMO, etc.);
3. Power reactors.

These facilities will have different performance, reliability, and availability. Near-term facilities are expected to have availability factor $<30\%$, DEMO should reach availability of $\sim 30-50\%$, whereas high availability factors ($>80\%$) are needed in future commercial fusion power plants to ensure competitiveness and establishment of fusion technology as a reliable energy source. In this study, we perform self-sufficiency analysis to assess the effect of availability factors on required TBR for the different stages of fusion technology and suggest ideas to enable compensation for shortfall in tritium breeding of near term devices.

6.3.3 Parameters and tritium processing times of various subsystems

A literature survey was performed to determine the parameters to use in the analysis which we summarize in Tables 6.3, 6.4, and 6.5 − refer to the underlined value in case multiple parameters are shown for the same technology as some discrepancies were found among the data reported in literature.

Table 6.3: Main parameters for the reference case.

Parameter	**Value**	**Reference/Explanation**
$\dot{N}^{-}$	0.459 kg/day	Burning rate for 3 GW fusion plant
f_b	<u>0.35%</u>	State-of-the-art (ITER) [3]
	1.5%	Expected for first DEMOs [14]
η_f	<u>50%</u>	Barry, DEMO 2016 [3]
	70%	Coleman *et al.* [14]

Table 6.4: Inner fuel cycle processing times chosen for the reference case.

Component	**Processing Time**	**Reference**
Vacuum Pump	<u>600 s</u>	Day *et al.* [15]
	150 s	Coleman *et al.* [14]
	1 day	Abdou *et al.* [6]
	0.1 day	Abdou *et al.* [9]
Fuel Clean-up & Isotope Separation System	1.3 h	Day *et al.* [15]
	5 h	Coleman *et al.* [14]
	0.1 day	Abdou *et al.* [6]
	1 - 24 h	Abdou *et al.* [9]
	<u>4 h</u>	Chosen for analysis
Water Detritiation System	<u>1 h</u>	Day *et al.* [15]
	20 h	Coleman *et al.* [14]

Table 6.5: Outer fuel cycle processing times (and residence times) chosen for the reference case.

Component	**Processing Time**	**Reference**
Breeding Zone	10 days	Abdou *et al.* [6]
	0.1 - 1 day	EXOTIC -6, -7, -8 [28]
TES	1 day	Abdou *et al.* [6,9]
	Negligible (on-line)	Demange *et al.* [29]
	1-5 days (batch-wise)	Riva *et al.* [27]
CPS	100 days	Abdou *et al.* [6,9]
	10 days	Chosen for analysis
FW	1000 s	Riva *et al.* [27]
Divertor	1000 s	Riva *et al.* [27]
Steam Generator	1000 s	Chosen for analysis

Table 6.6: Flow rates fractions and component efficiency assumed for the reference case.

Flow Rate Fraction	**Value**
f_{1-5}	10^{-2}
f_{p-3}	10^{-4}
f_{p-4}	10^{-4}
f_{5-3}	0.6
f_{5-6}	10^{-2}
f_{5-10}	10^{-4}
f_{6-3}	0.6
f_{9-10}	10^{-1}
η_2	0.95
η_6	0.95

Note that the CPS processing time is chosen to be 10 days arbitrarily to account for the slow recovery process expected in coolant systems, given the early stage of this technology, and to be conservative. Finally, we summarize in Table 6.6 the values of flow rate fractions (f_{j-i}), which indicate the fraction of the flow rate from component j which flows to component i, and tritium processing efficiency (η_i), e.g. for components such as TES and CPS units. All losses to environment ϵ_i are set to 10^{-4} arbitrarily. We assume there are no direct losses to environment from the blanket and PFCs, since these components are in the vacuum vessel, and from the storage and fueling system, since the fuel is stored and processed at low temperature ($\epsilon_1 = \epsilon_3 = \epsilon_4 = \epsilon_{11} = \epsilon_{12} = 0$).

6.4 Analysis and Discussion

Tritium inventory dynamics and hence self-sufficiency are complex functions of plasma physics, technology, fuel cycle design, and operating parameters. The key parameters affecting tritium inventories and required TBR are summarized in Table 6.7.

Table 6.7: Key parameters affecting tritium inventories, and hence, required TBR.

1. Tritium burn fraction in the plasma (f_b)
2. Fueling efficiency (η_f)
3. Time(s) required for tritium processing of various tritium-containing streams, e.g. plasma exhaust, tritium-extraction fluids from the blanket (t_p)
4. Availability factor (AF) of the power plant
5. Reserve Time (t_r), i.e. period of tritium supply kept in reserve storage to keep plasma and plant operational in case of any malfunction in a part (q) of any tritium processing system
6. Parameters and conditions that lead to significant trapped inventories in reactor components (e.g. in divertor, FW); and Blanket inventory caused by bred tritium released at a rate much slower than the T processing time
7. Inefficiencies (fraction of T not usefully recoverable) in various tritium processing schemes (ϵ_i)
8. Doubling time (t_d) for fusion power plants (time to accumulate surplus tritium inventory sufficient to start another power plant)

The tritium burn fraction (f_b) is a measure of the amount of tritium burned in the plasma before confinement is lost and particles diffuse through the Scape-off Layer (SOL). It is defined as the ratio of the tritium burning rate ($\dot{N}^-$) to the tritium fueling rate ($\dot{T}_f$) as shown in Eq. 6.19:

$$f_b = \frac{\dot{N}^-}{\dot{T}_f} \tag{6.19}$$

The tritium fueling rate ($\dot{T}_f$) is the fraction of tritium injection rate ($\dot{T}_i$) that has penetrated the plasma and reached the core region. In particular, the fueling efficiency is defined as the

ratio of the tritium fueling rate to the tritium injection rate:

$$\eta_f = \frac{\dot{T}_f}{\dot{T}_i} \tag{6.20}$$

Combining Eqs. 6.19 and 6.20 we obtain an expression for the tritium injection rate as:

$$\dot{T}_i = \frac{\dot{T}_f}{\eta_f} = \frac{\dot{N}^-}{\eta_f f_b} \tag{6.21}$$

Thus, in order to minimize the tritium injection rate, one needs to maximize the tritium fueling efficiency and burn fraction. Assuming a $50\% - 50\%$ D $-$ T mixture, where tritium and deuterium density is $n_T = n_D = n$, an expression for f_b can be derived as:

$$f_b = \frac{< \sigma v > n\tau^*}{2 + < \sigma v > n\tau^*} \tag{6.22}$$

where $< \sigma v >$ the product of energy-dependent cross section (σ) for the D-T reaction, (v) the velocity, and τ^* the effective particle confinement time, which is defined as:

$$\tau^* \simeq \frac{\tau}{1 - R} \tag{6.23}$$

where τ the confinement time and R is the recycling coefficient (from the edge). Since the 1980s, reactor studies assumed $R = 0.95$, with no theoretical or experimental evidence, in order to obtain very high f_b, e.g. $30-40\%$. Recent experimental results showed that gas fueling is highly inefficient ($R \sim 0$), leading to very low values of burn fraction and fueling efficiency. Detailed analysis of extrapolation of the state-of-the-art in plasma physics and fusion technology, represented by ITER with burn fraction of 0.35% and fueling efficiency <50%, to future DEMO and power plants showed that serious programs of R&D are required. These critical issues were addressed in several publications over the years. Even though substantial progress has been made in several areas of plasma physics, technology, and design, nevertheless there is a number of challenges that have not been resolved yet. In this paper, we propose a detailed analysis of the fuel cycle performance and aim to stimulate new ideas

and approaches toward fulfilling the principal requirements of the tritium fuel cycle.

6.4.1 Calculation of tritium inventory in various systems as function of key physics and technology parameters

The time evolution of tritium inventories in various components of the fuel cycle are presented in Fig. 6.4. These inventories refer to a reactor producing 3 GW of fusion power and are calculated for steady-state reactor operation, i.e. in this analysis we do not consider shut-down periods due to random failures or ordinary maintenance. In particular, we evaluate the tritium inventories for different values of burn fraction and fueling efficiency product, i.e. for the ITER state-of-the-art parameters f_b =0.35% and η_f optimistically assumed to be 50% (black lines), $\eta_f f_b$ =1% (blue lines), and $\eta_f f_b$ =5% (magenta lines).

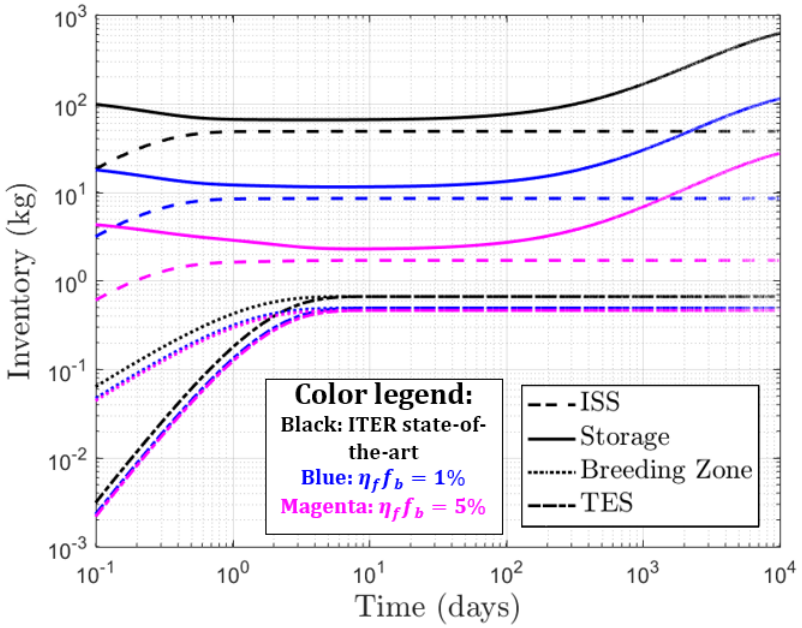

Figure 6.4: Tritium inventory evolution in various systems. The black lines represent extrapolation of ITER state-of-the-art (f_b =0.35% and η_f optimistically assumed to be 50%), the blue lines show $\eta_f f_b$ =1%, and the magenta show $\eta_f f_b$ =5%. Parameters used in the analysis: ISS processing time = 4 h, Breeding Zone residence time = 1 day, Tritium Extraction System processing time = 1 day, availability factor = 100%, fusion power = 3 GW, reserve time = 24 h, fraction failing = 25%, doubling time = 5 years.

As noted in the figure, the storage inventory decreases from its initial value to a minimum, as tritium inventory builds up in the other components, and then, it starts to rapidly increase, as inventory build-up in components reaches saturation. In particular, the minimum inventory in the storage system is found after $\sim$6$-$8 days. The isotope separation system (ISS) is the most demanding component in terms of inventory build-up. The equilibrium value of tritium inventory in ISS is found after $\sim$1 day of operation. Note that the ISS inventory and the storage inventory are very sensitive to the burn fraction and fueling efficiency product, which determine the amount of tritium exhausted to the inner fuel cycle line. Instead, the breeding zone (BZ) and tritium extraction system (TES) do not directly depend on the burn fraction and fueling efficiency; however, slight differences in the BZ and TES inventories are seen for different values of $\eta_f f_b$ due to the different required TBR obtained for each $\eta_f f_b$ considered. A reactor that operates with ITER state-of-the-art parameters has a required TBR of 1.46, which is impossible to achieve in practice, whilst values of $\eta_f f_b$ of 1% and 5% require a TBR of 1.08 and 1.02, respectively.

In Subsection 6.4.2 we perform tritium self-sufficiency analysis to explore the performance of the fuel cycle under a wide range of parameters. The tritium start-up inventory assessment is presented in Subsection 6.4.3.

6.4.2 Physics and technology parameters window for tritium self-sufficiency

We start our analysis with presenting in Table 6.8 the calculated TBR_R for various availability factors (AF=10%, 30%, 50%, 90%, calculated by maintain the $MTBF$ fixed at 7 days and varying the $MTTR$), and two cases of tritium burn fraction ($f_b = 0.35\%$ representing the state-of-the-art value for ITER, and $f_b = 1.5\%$ which is considered a reasonable assumption for first DEMO [14]). The parameters used in the analysis are presented in Tables $6.3 - 6.6$; we summarize here the most important ones: the processing time in ISS ($\tau_9 = t_p$) is 4 h, the tritium residence time in blanket (τ_1) and processing time in TES (τ_2) are both 1 day, the reserve time (t_r) is 1 day, the doubling time (t_d) is 5 years, the fraction of system failing (q) is 25%, and the reactor power is 3 GW corresponding to a tritium burning rate ($\dot{N}^-$) of

0.459 kg/day.

Table 6.8: Calculated values of required TBR using ITER and DEMO expected burn fraction values, i.e. f_b =0.35% and f_b =1.5% respectively, and fueling efficiency assumed to be 50%. Availability factors of 10%, 30%, 50%, and 90% are considered. Parameters used in the analysis: ISS processing time = 4 h, Breeding Zone residence time = 1 day, Tritium Extraction System processing time = 1 day, fusion power = 3 GW, reserve time = 24 h, fraction failing = 25%, doubling time = 5 years.

	f_b = 0.35% (ITER)				f_b = 1.5% (DEMO)			
AF	10%	30%	50%	90%	10%	30%	50%	90%
TBR_R	3.56	2.01	1.70	1.53	1.52	1.21	1.14	1.11

With current state-of-the-art plasma physics and technology requirements, represented by ITER with f_b =0.35% and η_f <50%, self-sufficiency cannot be attained as $TBR_R > TBR_A$ as shown in Table 6.8. Moreover, initial start-up tritium inventory would be ∼140 kg for a 3000 MW reactor, when ITER state-of-the-art values are used in the analysis. An increase in the tritium burn fraction to the value of 1.5% improves the scenario noticeably and offers a concrete window of possible self-sufficiency: $TBR_R \leq 1.15$ for $AF > 50\%$. Table 6.8 also shows a critical dependence of the required TBR on the availability factor: as AF decreases TBR_R increases dramatically.

Further details and analyses are proposed in the following sub-sections where we explore the effect of various parameters on the required TBR in order to define the phase space of tritium self-sufficiency. Due to the uncertainties in predicting the achievable TBR, which is expected to be in the range 1.05−1.15, we attribute different levels of confidence in attaining tritium self-sufficiency to different values of required TBR. In particular, we consider attaining self-sufficiency:

- unlikely: if $TBR_R > 1.15$;
- Possible: if $1.05 < TBR_R < 1.15$ (represented by the area shown in light green in the plots presented in the following subsections);
- Possible with high confidence: if $TBR_R < 1.05$ (represented by the area shown in dark

green in the plots presented in the following subsections).

6.4.2.1 Effect of tritium burn fraction, fueling efficiency, and tritium processing time on tritium self-sufficiency

Figure 6.5 shows the required TBR variation as a function of the fueling efficiency and burn fraction product ($\eta_f f_b$). Furthermore, the plot shows the effect of the tritium processing time of the Isotope Separation System (t_p) on the required TBR. Representative processing times of 1, 4, and 12 hours are used in the analysis. The required TBR is plotted for availability factors of 50%.

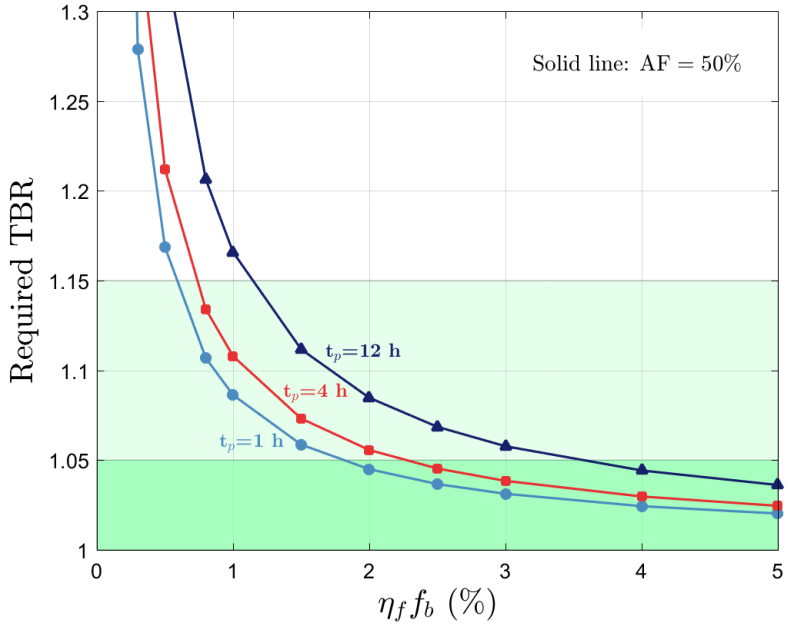

Figure 6.5: Required TBR as a function of the product of tritium burn fraction and fueling efficiency for various tritium processing times in the Isotope Separation System (1, 4, and 12 h) and availability factor of 50%. Fixed parameters used in the analysis: Breeding Zone residence time = 1 day, Tritium Extraction System processing time = 1 day, availability factor = 50%, fusion power = 3 GW, reserve time = 24 h, fraction failing = 25%, doubling time = 5 years.

It is seen that the TBR_R increases slightly if the product of tritium burn fraction and fueling efficiency decreases from 5% to 3%, largely if $\eta_f f_b$ decreases from 3% to 1%, and dramatically if $\eta_f f_b$ is lower than 1%. Thus, burn fraction and fueling efficiency represent

dominant parameters towards realizing tritium self-sufficiency. However, the results of Fig. 6.5 suggest that reducing the tritium processing time in the inner fuel cycle (i.e. in the ISS in particular) has major impact on reducing the required TBR, especially at low $\eta_f f_b$. Conversely, if tritium processing time is high (∼12 h), self-sufficiency is impossible at $\eta_f f_b$ <1%. Required TBR in the 1.05−1.15 range is observed if 0.7% < $\eta_f f_b$ <2% and the processing time is less than 4 hours. Furthermore, a wide region of possible self-sufficiency with high confidence is seen for $\eta_f f_b$ >2% at processing time of 1−4 hours. Hence, major effort should be made to develop efficient processing units in the inner fuel cycle to minimize the required processing time as major improvements are needed for attaining tritium self-sufficiency with higher confidence level. The suggested R&D goals are to achieve a product of fueling efficiency and tritium burn fraction greater than 5% (or, at least not lower than 2%) and tritium processing time shorter than 4 hours.

6.4.2.2 Self-sufficiency analysis during different stages of nuclear fusion development: the effect of reactor availability factor

In this section we explore the effect of the reactor availability factors on self-sufficiency. Figure 6.6 shows that the availability factor has a significant effect on the TBR_R. In detail, the required TBR increases slightly when AF is reduced from 80% to 60%, significantly when AF is reduced from 60% to 30%, largely when AF is reduced from 30% to 10%, and dramatically when AF is less than 10%. In fact, low availability factor implies long times when tritium generation does not occurs (i.e. during $MTTR$) but tritium is lost due to radioactive decay. Thus, higher TBR is required during reactor operation in order to meet the requirements expressed in Eq. 6.17. Hence, the self-sufficiency problem is affected by the "Long-Term" system dynamics, i.e. for times $\sim t_d$ which are comparable to the tritium half-life. Conversely, the start-up inventory is practically not affected by the reactor availability since the tritium inventory in the storage system starts to increase in a few days, as explained in Paragraph 6.3.2.2. Thus, the start-up inventory depends on the "Short-Term" system dynamics, when losses by radioactive decay are small.

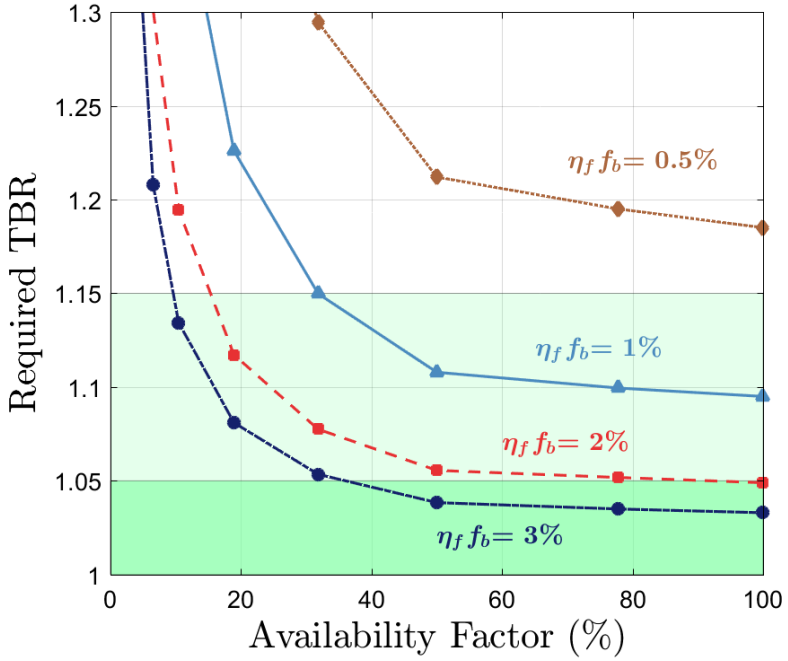

Figure 6.6: Required TBR as a function of reactor availability factor for various tritium burn fraction and fueling efficiency products. Parameters used in the analysis: ISS processing time = 4 h, Breeding Zone residence time = 1 day, Tritium Extraction System processing time = 1 day, fusion power = 3 GW, reserve time = 24 h, fraction failing = 25%, doubling time = 5 years.

Low reactor availability factor is expected in the early stage of fusion technology development, e.g. for experimental facilities and DEMO reactors, due to frequent random failures (short $MTBF$) and long times needed to repair/replace components (long $MTTR$). As physics and technology improve, the fusion systems will reach higher degree of maturity and longer availability factors will be achieved. Thus, these results imply that attaining tritium self-sufficiency in near-term fusion experimental facilities (e.g. FNSF, VNS, CTF,etc.) could be impossible in light of the predicted low availability factor [21]. Therefore, near-term facilities should have low power in order to:

1. Reduce the required tritium start-up inventory (non-fusion sources are not available);

2. Enable compensation for shortfall in tritium breeding.

On the other hand, we found that there only is a marginal change in the TBR_R if $AF > 60\%$ for specific values of $\eta_f f_b$. Thus, attaining tritium self-sufficiency in power reactors, which

have AF >80%, will be less challenging and will depend on the performance of fusion fuel cycle and advances in plasma confinement. To summarize, tritium self-sufficiency is:

- impossible if AF <10% for any $\eta_f f_b$;
- impossible if $\eta_f f_b$ <0.5% for any availability factor;
- possible if 10%< AF <30% and $\eta_f f_b$ >2%;
- possible if AF > 30% and 1%≤ $\eta_f f_b$ ≤2%;
- possible with high confidence if AF >50% and $\eta_f f_b$ > 2%.

Results suggest that obtaining high availability factor in fusion reactors is absolutely necessary to achieve fuel self-sufficiency and accomplish a competitive alternative to conventional power plants. In order to improve the fuel cycle design and reliability, near-term experimental facilities should be constructed. Main goals of these facilities should be (i) identifying random failure types, (ii) evaluating the random failure rates, and (iii) performing blankets and fuel cycle R&D, (iv) obtaining higher fuel cycle reliability and reactor availability factor, and (v) investigating other issues that affect the likelihood of attaining tritium self-sufficiency. These near-term devices must be designed to have small fusion powers in order to enable mitigation for shortfall in tritium breeding.

6.4.2.3 Penetration of fusion energy into power market

In this subsection we analyze the effect of the doubling time on the required TBR for a fusion near-term facility with modest availability factor of 30% (Fig. 6.7), and a mature power reactor with high availability factor of 80% (Fig. 6.8). The doubling time is 1, 3, 5, and 7 years for both cases. As shown in Fig. 6.7, self-sufficiency is possible if $\eta_f f_b$ >1% for doubling time of ∼5−7 years and for shorter doubling time, i.e. t_d =3 years when $\eta_f f_b$ =1.5%. It is impossible to obtain a required TBR lower than 1.15 for short doubling time of 1 year. Fig. 6.8 shows lower required TBR values for the same burn fraction, fueling efficiency, and doubling time due to an increase of the availability factor from 30% to 80%.

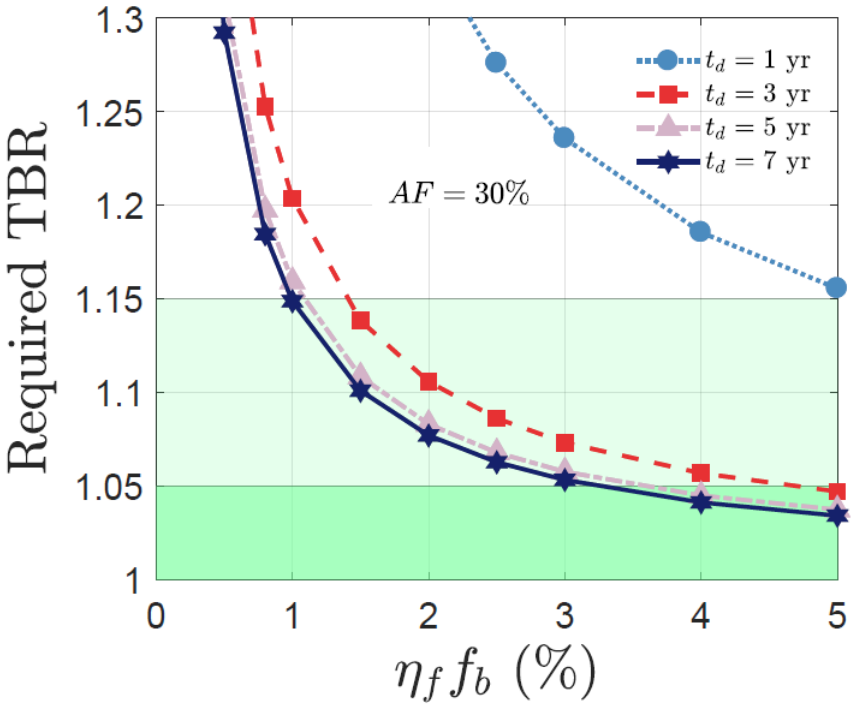

Figure 6.7: Required TBR as a function of the product of tritium burn fraction and fueling efficiency for various doubling times (1, 3, 5, and 7 years) for availability factor of 30%. Parameters used in the analysis: ISS processing time = 4 h, Breeding Zone residence time = 1 day, Tritium Extraction System processing time = 1 day, fusion power = 3 GW, reserve time = 24 h, fraction failing = 25%, availability factor = 30%.

Due to the scarcity of tritium resources and the inadequacy of non-fusion facilities to provide the required amounts of tritium to fusion facilities, the penetration of fusion technology

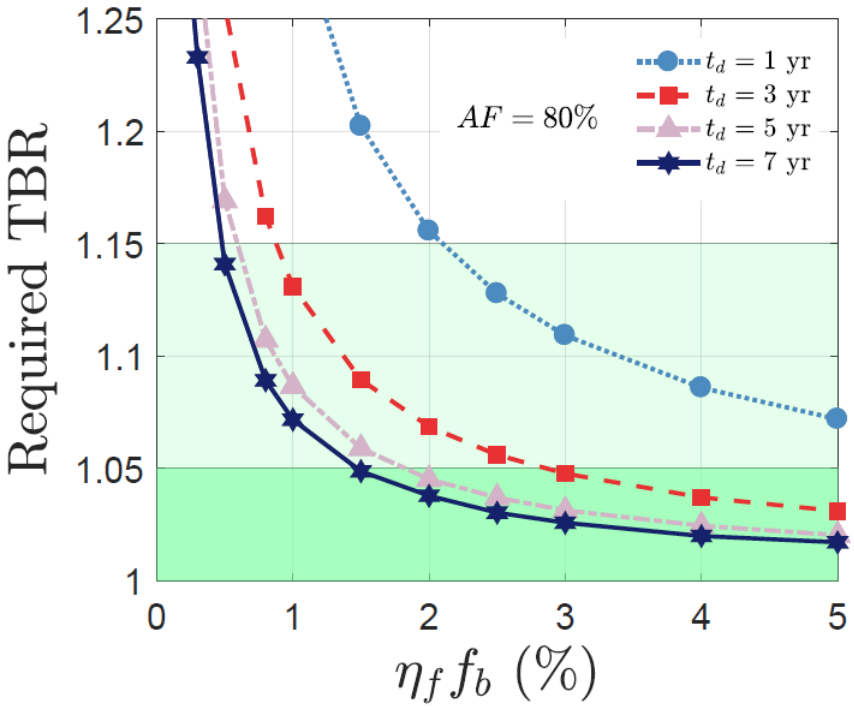

Figure 6.8: Required TBR as a function of the product of tritium burn fraction and fueling efficiency for various doubling times (1, 3, 5, and 7 years) for availability factor of 80%. Parameters used in the analysis: ISS processing time = 4 h, Breeding Zone residence time = 1 day, Tritium Extraction System processing time = 1 day, fusion power = 3 GW, reserve time = 24 h, fraction failing = 25%, availability factor = 80%.

into the energy market will be strongly affected by the capability of the fusion reactors to achieve self-sufficiency and generate appropriate start-up inventory to begin operation of new reactors in short times. Typical doubling time of mature power industry, e.g. conventional power plants, fission reactors, etc., is 5−7 years. However, for fusion technology a shorter doubling time, e.g. ∼1−3 years, is highly desirable because of the lack of tritium resources. The analysis shows that it is possible to attain tritium self-sufficiency for doubling time as short as 3−5 years at low availability factors, which would allow the generation of tritium start-up inventory for several DEMO reactors in reasonable times, but major improvements regarding tritium burn fraction and fueling efficiency must be accommodated. For power reactors self-sufficiency is less challenging and can be achieved for a wide range of parameters.

6.4.3 Assessment of the availability of external tritium supply for start-up of near and long term fusion facilities and calculation of the required start-up tritium inventory

The issue of external tritium supply from non-fusion sources is serious and has major implications on fusion development pathway. As discussed in Section 6.1 DEMO and future generation power plants require ∼55.8 kg of T per 1000 MW of fusion power per year. Tritium production rate in fission reactors is much smaller than the tritium consumption rate in fusion reactors: tritium production in light water reactors (LWR) is limited to ∼0.5−1 kg/year whilst CANDU reactors produce ∼130 g per GWe per fpy from n−D reaction. Future supply from CANDU depends on whether current reactors can be licensed to extend life by 20 years after refurbishment; however, there are political, national policy, and practical issues, e.g. implies tritium permeation and safety issues. Furthermore, tritium generation in fission reactors requires special tritium breeding systems and is very expensive (∼80M−130M per kg, per DOE Inspector General). Other non-fission sources, e.g. proton accelerator (APT), were proved to be uneconomical. Because of the relatively short life of tritium, which decays at a rate of ∼5.5% per year (12.32 years half-life), and the issues and limitations of tritium production in fission systems, tritium resources available now from non-fusion sources are irrelevant to evaluating availability of tritium for start-up of DEMO or FNSF which will be constructed after 2040.

The time evolution of tritium inventory available to provide start-up for fusion reactors is presented in Fig. 6.9 [30]. With production and decay over 40 years of operation of CANDU reactors, tritium supply peaks at 27 kg in 2027. A successful ITER D−T campaign starting in 2036 will leave only a few kg of tritium (<5 kg in 2050) left to provide a start-up inventory for any major D−T fusion facility. With many independent countries currently designing their own DEMO reactors, e.g. EU-DEMO, K-DEMO, etc., and planning operation to begin after 2040, it is necessary to accurately evaluate the tritium start-up inventory necessary to start DEMO(s), since tritium resources could be exhausted or not sufficient. Hence, minimizing the tritium start-up inventory is key developing a sustainable and economic fusion technology,

which can be competitive in the energy market without further delay.

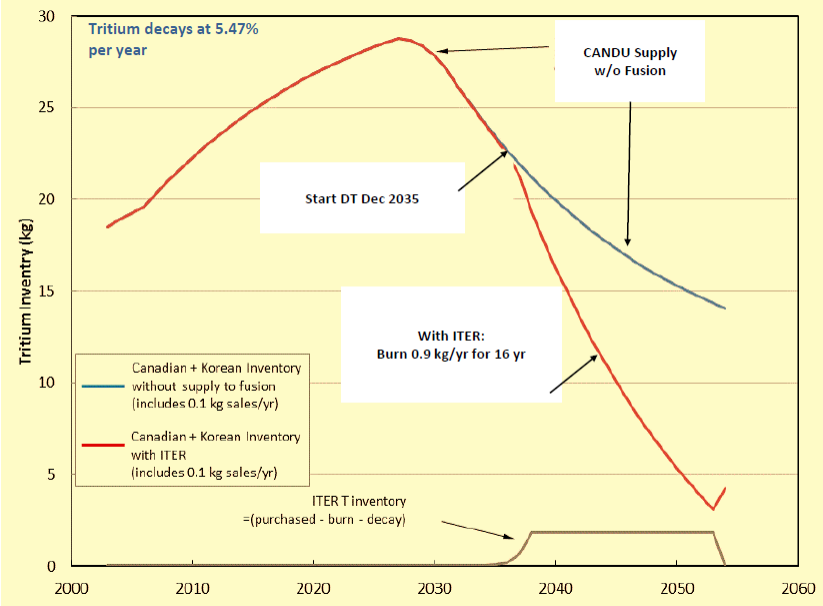

Figure 6.9: Tritium inventory available to provide start-up inventory in the temporal window 2000−2060 [30].

In the following subsections we perform tritium start-up inventory evaluation for different reactor powers and technology parameters. Our analysis shows that the tritium start-up inventory depends mainly on the fusion power, the amount of reserve inventory kept in the storage system to supply tritium in case of partial failures in the fuel cycle (see Eq. 6.16), and the tritium processing time.

6.4.3.1 Implications of tritium processing time on start-up inventory

The effect of tritium processing time on start-up inventory is shown in Fig. 6.10 for a reactor of 3000 MW of fusion power. In the simulation we account for a reserve time of 24 h and a fraction of the fuel cycle failing of 25%. Fig. 6.10 shows that a processing time reduction from 12 hours to 1 hour corresponds to a start-up inventory decrease from ∼39 kg to ∼16 kg, i.e. difference of ∼23 kg, when $\eta_f f_b$=1%, while a reduction from ∼14 kg to ∼6 kg, i.e. a difference of 8 kg, is obtained if $\eta_f f_b$=3%. Thus, reducing the processing time is particularly useful at low to mid $\eta_f f_b$. For a 3 GW fusion power reactor the tritium initial start-up

inventory is <10 kg when t_p <4 hours and if the product of the tritium burn fraction and fueling efficiency is >2%. Start-up inventories smaller than 5 kg are only possible for higher burn fraction and fueling efficiency, $\eta_f f_b$ >4%, and shorter processing times, t_p <4 hours.

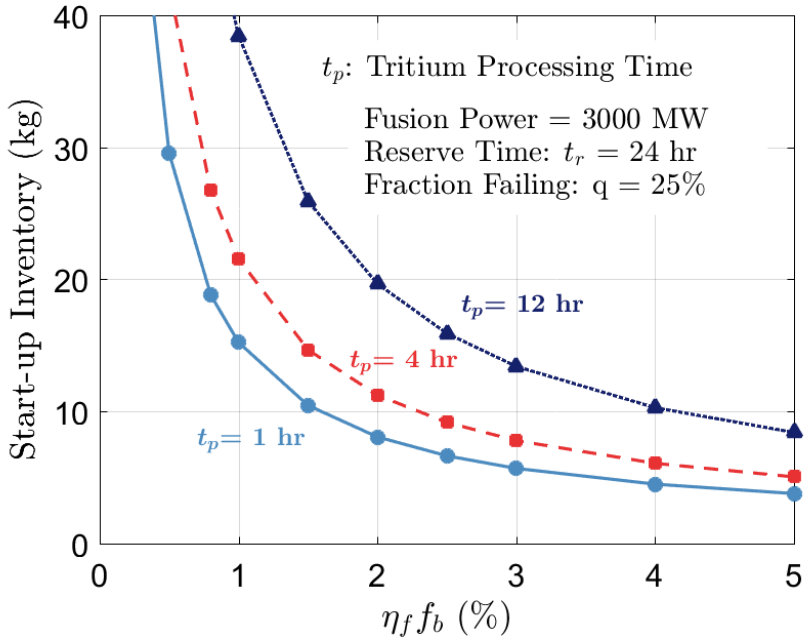

Figure 6.10: Start-up inventory as a function of tritium burn fraction and fueling efficiency product for tritium processing time in ISS of 1, 4, and 12 hours. Parameters used in the analysis: Breeding Zone residence time = 1 day, Tritium Extraction System processing time = 1 day, fusion power = 3 GW, reserve time = 24 h, fraction failing = 25%, doubling time = 5 years.

Since most part of the tritium in the plasma is exhausted to the inner fuel cycle processing line, an efficient and fast tritium processing system must be designed in order to recover tritium and inject it into the plasma in the shortest possible time. In fact, if the time lag between tritium use and recovery increases, a larger start-up inventory will be necessary to compensate for delays in tritium availability. Thus, in order to reduce the start-up inventory, the tritium processing time must be minimized, e.g. by replacing batch technologies with continuous technology as explained in [15, 16, 27]. Moreover, a reduction of processing time implies lower inventory held in the various components of the fuel cycle, which is beneficial for safety.

6.4.3.2 The necessity of high fuel cycle reliability to reduce the reserve inventory

In Figs. 6.11 and 6.12 we show the total start-up and reserve inventory for reserve time 0−48 hours and various values of burn fraction and fueling efficiency product. Note we use fraction of fuel cycle that has a failure to be q =25%. The reserve inventory is proportional to the product of t_r and q. Therefore, the reserve inventory for other values of q can be deduced from the figures by using values of t_r that can keep the product $t_r q$ constant. Overall, the total start-up inventory can be <10 kg, if t_r <24 hours and $\eta_f f_b \geq$2%, and <5 kg, if t_r <6 hours and $\eta_f f_b \geq$3%, as seen in Fig. 6.11. Large amounts of tritium reserve inventory to compensate for some major malfunction in the tritium fuel cycle system may be not feasible at low $\eta_f f_b$. For example, ∼9−10 kg of extra tritium are required if we increase the reserve time form 6 hr to 24 hr for $\eta_f f_b$ =1% when the fraction of failure is q =25%. Thus, even though it is desirable to maintain the reactor in operation for as long as possible, when failures are not resolved in a few hours the reactor shutdown seems inevitable, since the reserve inventory magnitude may be too large. Moreover, in case of low availability factors in the early stages of fusion technology development, the reserve inventory is not as meaningful as it is for a mature technology since the reserve time ($t_r \sim hours$) may be orders of magnitude lower than the $MTTR$ ($\sim days - months$). For these situations, the reactor shutdown seems unavoidable and an extra amount of tritium should be obtained to overcome tritium radioactive decay during the repair time (this may be provided by the TBR without the need of purchasing extra tritium outside the reactor). If technology is more mature and reliable, and high $\eta_f f_b$ is reached, it is possible to increase the reserve time and, at the same time, maintain acceptable values of reserve inventory. In Fig. 6.12 we see that the reserve inventory is always lower than 5 kg if $\eta_f f_b$ >2%) even for 24 hours of reserve time. The analysis suggests that the tritium processing systems must be highly reliable in order to increase the overall reactor availability since long reserve times seem not feasible in practice, and lead to unacceptable reserve and start-up inventories requirements. A tritium reserve inventory should however be accumulated by using some of the TBR margin produced within the same reactor.

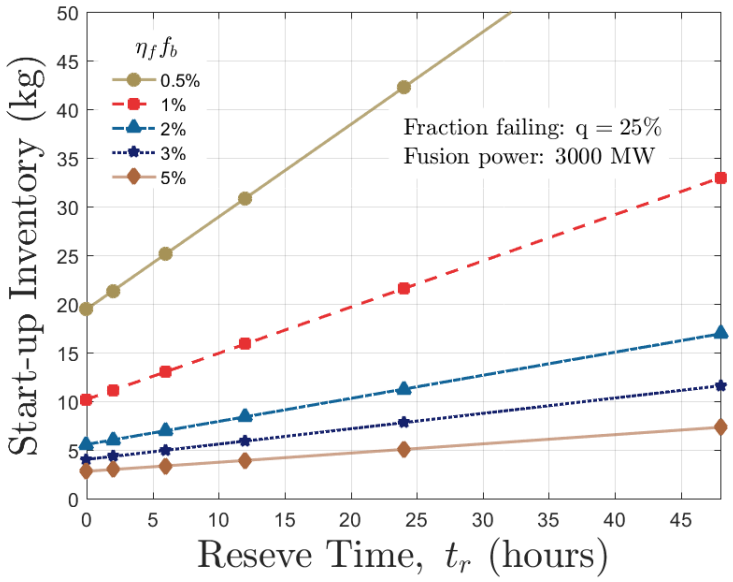

Figure 6.11: Start-up inventory as a function of tritium burn fraction and fueling efficiency product for various reserve times. Parameters used in the analysis: ISS processing time = 4 h, Breeding Zone residence time = 1 day, Tritium Extraction System processing time = 1 day, fusion power = 3 GW, fraction failing = 25%, doubling time = 5 years.

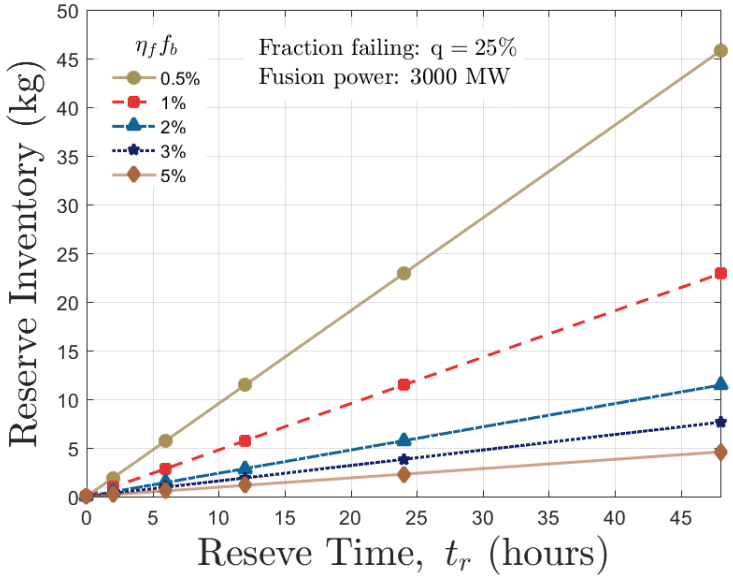

Figure 6.12: Reserve inventory as a function of tritium burn fraction and fueling efficiency product for various reserve times. Parameters used in the analysis: ISS processing time = 4 h, Breeding Zone residence time = 1 day, Tritium Extraction System processing time = 1 day, fusion power = 3 GW, fraction failing = 25%, doubling time = 5 years.

It is worth noticing that the reserve time also affects the required TBR. Figure 6.13 shows the effect of reserve time on required TBR. We note that the increase of the tritium burn fraction narrows the difference in the required TBR for a certain reserve time. One day of reserve inventory with 25% of the fuel cycle failing leads to TBR_R <1.15 when the reactor has $\eta_f f_b$ ~1%. Higher product of burn fraction and fueling efficiency ($\eta_f f_b$ ≥3%) allows a reserve time of 2 days and gives $TBR_R \leq 1.05$, making self-sufficiency very likely. Even though the effect of longer reserve time on required TBR is noticeable, we can conclude that self-sufficiency is possible or possible with high confidence for a wide range of reserve times, especially at mid-to-high burn fraction and fueling efficiency product.

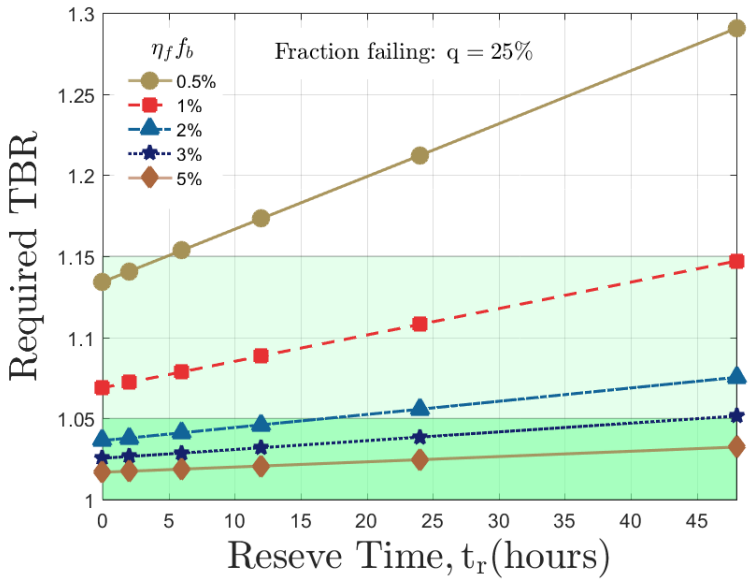

Figure 6.13: Required TBR as a function of tritium burn fraction and fueling efficiency product for various reserve times. Parameters used in the analysis: ISS processing time = 4 h, Breeding Zone residence time = 1 day, Tritium Extraction System processing time = 1 day, fusion power = 3 GW, fraction failing = 25%, doubling time = 5 years.

6.4.3.3 Effect of reactor fusion power on tritium start-up inventory

Thus far we calculated the start-up inventory for fusion power of 3 GW. However, near-term fusion development facilities (e.g. FNSF, VNS, CTF, CFETR) are designed for lower fusion powers. In Fig. 6.14 we explore the effect of the device fusion power on the start-up inventory in the case of 2019 state-of-the-art physics and technology parameters (red lines) and in the case of major advances in physics and technology (blue lines). We found a linear dependency between the tritium start-up inventory and the fusion power. In particular, the tritium start-up inventory for a reactor of 100 MW fusion power is as small as 1 kg at $\eta_f f_b \sim 0.5\%$ or a few hundreds of grams if $\eta_f f_b$ increases, but can be as high as $\sim$30$-$40 kg for 2$-$3 GW reactors at low $\eta_f f_b$. The product $\eta_f f_b$ $\sim$5% is required to obtain a tritium start-up inventory smaller than 5 kg for a mature fusion reactor with a reserve time of 1 day. We present in Fig. 6.15 the start-up inventory for various reactors with different power for $\eta_f f_b$ =1% and 3%. A decrease of the reactor power allows major reductions of the start-up inventory with minimum and maximum of (i) 710 g and 21.18 kg of tritium when $\eta_f f_b$ =1%, and (ii) 260 g and 7.63 kg of tritium when $\eta_f f_b$=3%, for powers of 100 MW and 3000 MW respectively. These values are calculated for fixed values of other parameters, e.g. t_p =4 hr, t_r=1 day, $q = 25\%$.

The results highlight that near-term low power devices require a relatively small and obtainable start-up inventory, i.e. less than a kilogram of tritium. Furthermore, low reactor power is necessary in near term fusion facilities to enable compensation of the shortfall in tritium breeding. Major advances are required to reduce the start-up inventory in higher power reactors, e.g. DEMO and power reactors, which will have powers of 2$-$3 GW and will require several kilograms of tritium.

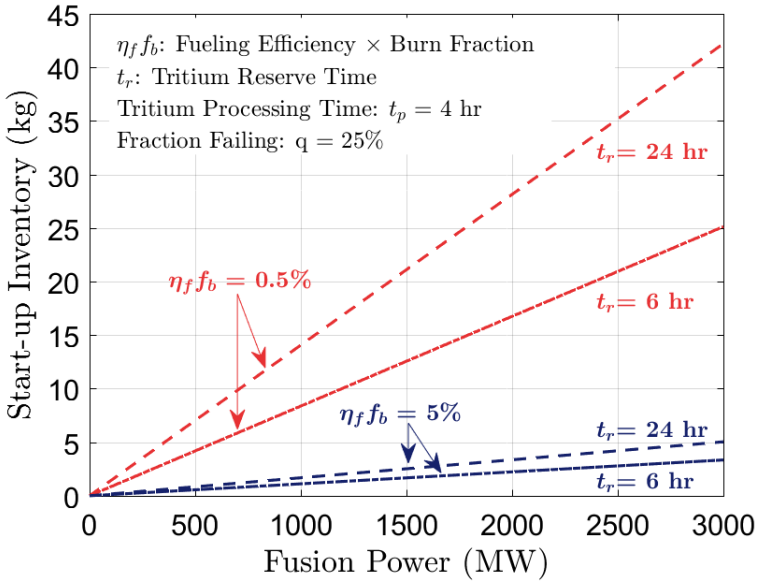

Figure 6.14: Start-up inventory as a function of fusion power for tritium burn fraction and fueling efficiency product of 0.5% and 5%, and reserve time of 6 and 24 hours. Parameters used in the analysis: ISS processing time = 4 h, Breeding Zone residence time = 1 day, Tritium Extraction System processing time = 1 day, fraction failing = 25%, doubling time = 5 years.

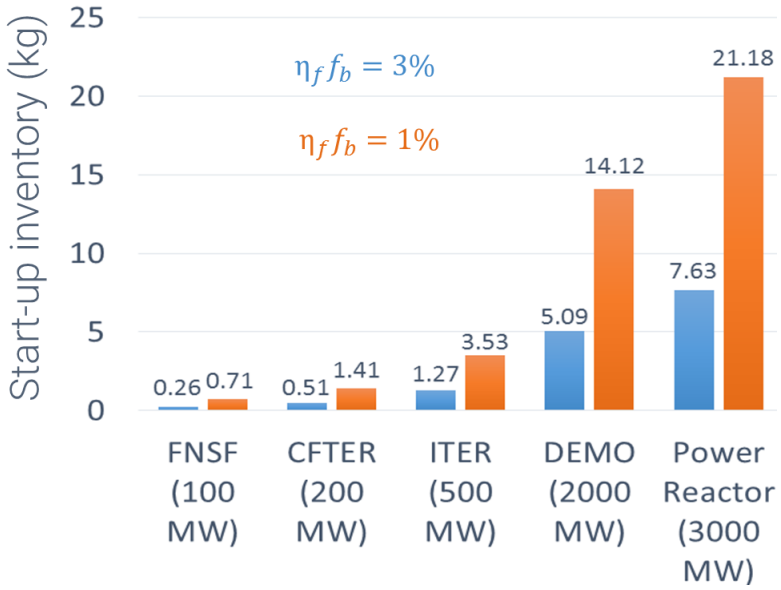

Figure 6.15: Start-up inventory for various fusion reactors (with different power level) and a tritium burn fraction and fueling efficiency product of 1% and 3%. Parameters used in the analysis: ISS processing time = 4 h, Breeding Zone residence time = 1 day, Tritium Extraction System processing time = 1 day, reserve time = 24 h, fraction failing = 25%, doubling time = 5 years.

6.5 Conclusions

In this Chapter a dynamic model representing the overall fuel cycle was derived with the mean residence time method. The model calculates tritium flow rates into and out of components of the fuel cycle, and their inventory build-up. Furthermore, the model is able to simulate different operational scenarios, e.g. availability factor $< 100\%$ due to random failures and scheduled maintenance, or pulsed plasma behavior. The model predicts the required tritium breeding ratio and the initial start-up tritium inventory in function of a wide range of plasma physics and technology parameters.

The analysis shows that the product of fueling efficiency and burn fraction, $\eta_f f_b$, and the availability factor, AF, have major effects on the TBR_R. In general, $\eta_f f_b \geq 2\%$ and $AF \geq 30\%$ are required for tritium self-sufficiency to be achievable. At low $\eta_f f_b$, a reduction in the tritium processing time increases the likelihood of attaining tritium self-sufficiency considerably. We showed in our analysis that the initial start-up inventory of fusion power reactors with fusion power of 3 GW can be as low as a few kilograms (e.g. $\leq$5 kg) if $\eta_f f_b > 3\%$, $t_p \leq 4\ hr$, and $t_r \leq 12\ hr$, but increases tremendously (e.g. >15 kg) when we use current DEMO expected values of $\eta_f = 50\%$ and $f_b = 1.5\%$. High initial inventory is considered a show stopper for fusion technology because of the scarcity of available tritium ($\sim$25 kg), which is projected to be even lower after ITER campaigns (likely <5 kg), the high tritium costs, and the safety implications. Thus, a major effort towards minimizing the start-up inventory (e.g. by increasing $\eta_f f_b$ to at least 2%, and decreasing tritium processing time to less than $2-4$ hours) is required. Reasonable tritium start-up inventories are possible for plasma based experimental facilities which operate at lower power (e.g. $100-500$ MW). Furthermore, several facilities should be built in order for fusion technology to grow at a higher rate. This requires attaining tritium self-sufficiency for low doubling times, which is very challenging in near term facilities due to the expected low availability factors.

To conclude, major advances are needed to improve the stat-of-the-art of fusion technology, attain self-sufficiency, and develop a competitive and attractive technology. Examples of technologies to be pursued are proposed by Loarte and Baylor [30] and Day [15, 16], e.g.

the direct internal recycling concept. The near term facilities must have low fusion power in order to obtain acceptable tritium start-up inventories, and must be able to attain self-sufficiency in order to provide tritium start-up inventories for DEMO and next generation of fusion reactors for short doubling time. This is possible if the fuel cycle is highly reliable, i.e. reaches high availability factor, and fueling efficiency and burn fraction can be increased significantly.

References

1. M. Abdou, "Tritium Fuel Cycle, Tritium Inventories, and Physics and Technology R&D Challenges for: 1) Enabling the startup of DEMO and future Power Plants AND 2) Attaining Tritium self-sufficiency in Fusion Reactors", 13th International symposium on Fusion Nuclear Technology (ISFNT-13) September 25th - 29th, 2017, Kyoto, Japan

2. Muyi Ni, Yongliang Wang, Baoxin Yuan, Jieqiong Jiang, Yican Wu, "Tritium supply assessment for ITER and DEMOnstration power plant", Fusion Engineering and Design, Volume 88, Issues 9-10, 2013, Pages 2422-2426, ISSN 0920-3796.

3. M. Kovari *et al.*, 2018 Nucl. Fusion 58 026010

4. Satoshi Konishi, Ryuta Kasada, Fumito Okino, "Myth of initial loading tritium for DEMO - Modelling of fuel system and operation scenario", Fusion Engineering and Design, Volume 121, 2017, Pages 111-116, ISSN 0920-796.

5. S. Zheng, D.B. King, L. Garzotti, E. Surrey, T.N. Todd, "Fusion reactor start-up without an external tritium source", Fusion Engineering and Design, Volume 103, 2016, Pages 13-20, ISSN 0920-3796.

6. M. Abdou *et al.*, "Deuterium-Tritium Fuel self-sufficiency in Fusion Reactors", Fusion Technology, 9: 250-285 (1986).

7. W. Kuan and M. Abdou, "A New Approach for Assessing the Required Tritium Breeding Ratio and Startup Inventory in Future Fusion Reactors", Fusion Technology, 35: 309-353 (1999).

8. M. Sawan, M. Abdou, "Physics and Technology Conditions for attaining Tritium self-sufficiency for the DT Fuel Cycle", Fusion Engineering & Design, 81 (8-14), 1131-1144 (2006).

9. Abdou, M., Morley, N.B., Smolentsev, S., Ying, A., Malang, S., Rowcliffe, A., Ulrickson, M., "Blanket/First wall challenges and required R&D on the pathway to DEMO", Fusion Engineering and Design, 100: 2-43 (2015).

10. Ni Muyi *et al.* Tritium supply assessment for ITER and DEMOnstration power plant. Fusion Eng. Des. 88 (9-10) 2013, 2422-2426.

11. Hongli Chen, Lei Pan, Zhongliang Lv, Wei Li, Qin, Zeng, "Tritium fuel cycle modeling and tritium breeding analysis for CFETR", Fusion Engineering and Design, 106 (2016) 17-20

12. Lei Pan, Hongli Chen, Qin Zeng, "Sensitivity analysis of tritium breeding ratio and startup inventory for CFETR", Fusion Engineering and Design, 112 (2016) 311-316

13. Yong Song, Qunying Huang, Muyi Ni & Xiaoqiang Chen "Analysis on Initial Tritium Supply for Starting Up Fusion Power Reactor FDS-II", Fusion Science and Technology, 60:3, (2011) 1121-1124, DOI: 10.13182/FST11-A12612

14. M. Coleman, Y. Horstensmeyer, F. Cismondi, "DEMO tritium fuel cycle: performance, parameter explorations, and design space constraints", Fusion Engineering and Design, Volume 141, 2019, Pages 79-90

15. Christian Day, Thomas Giegerich, "The Direct Internal Recycling concept to simplify the fuel cycle of a fusion power plant", Fusion Engineering and Design 88 (2013) 616-620

16. C. Day, "A Smart Architecture for the DEMO Fuel Cycle", 16. C. Day et al., Fusion Engineering and Design 146 (2019) 2462-2468

17. Benedikt Josef Peters, Christian Day, "Analysis of low pressure hydrogen separation from fusion exhaust gases by the means of superpermeability", Fusion Engineering and Design, Volume 124, 2017, Pages 696-699.

18. F. Hernandez, P. Pereslavtsev, Q. Kang, P. Norajitra, B. Kiss, G. Nadasi, O. Bitz, "A new HCPB breeding blanket for the EU DEMO: Evolution, rationale and preliminary performances", Fusion Engineering and Design, Volume 124, 2017, Pages 882-886.

19. Nucl. Fusion 56 (2016) 104001 (7pp)

20. E. Martelli *et al.*, "Advancements in DEMO WCLL breeding blanket design and integration", I NTERNATIONAL JOURNAL OF ENERGY RESEARCH, Int. J. Energy Res. 2018; 42:27-52

21. Abdou et al., Fusion Technology, 29: 1-57 (1996)

22. Alice Ying, H. Zhang, M. Y. Anh, Y. Lee, "Tritium Transport Evolutions in HCCR TBM under ITER Inductive Operations", Fusion Sci. Technol., vol. 68, no. 2, pp. 346-352, Sep. 2015.

23. Alice Ying, Hongjie Zhang, Brad J. Merrill, Mu-Young Ahn, "Advancement in tritium transport simulations for solid breeding blanket system", Fusion Engineering and Design, Volumes 109-111, Part B, 1 November 2016, Pages 1511-1516

24. Alice Ying, Haibo Liu, and M. Abdou, "Analysis of Tritium Retention and Permeation in FW/Divertor Including Geometric and Temperature Operating Features," Fusion Science and Technology, Vol. 64, No. 2, August 2013, Pages 303-308

25. M. Zucchetti, I. Nicolotti, A. Ying, M. Abdou, "TRITIUM MODELING FOR ITER TEST BLANKET MODULE", FUSION SCIENCE AND TECHNOLOGY, VOL. 68 OCT. 2015

26. Alice Ying, Hongjie Zhang, Brad Merrill, Mu-Young Ahn, Seungyon Cho, "Breeding blanket system design implications on tritium transport and permeation with high tritium ion implantation: A MATLAB/Simulink, COMSOL integrated dynamic tritium transport model for HCCR TBS", Fusion Engineering and Design, Volume 136, Part B, 2018, Pages 1153-1160.

27. M. Riva, A. Ying, M. Abdou, M.Y. Ahn, S. Cho, "Impact of Outer Fuel Cycle Tritium Transport on Initial start-up Inventory for Next Fusion Devices", Fusion Science and Technology, 1-9

28. J.G van der Laan *et al.*, "Tritium release data for ceramic breeder materials: compilation of results from EXOTIC-6,-7 and -8", 7th International workshop on Ceramic

Breeder Blanket Interaction, Pelten, 16 September 1998

29. D. Demange *et al.*, "Zeolite membranes and palladium membrane reactor for tritium extraction from the breeder blankets of ITER and DEMO", Fusion Engineering and Design, 88 (2013) 2396-2399

30. M. Abdou, "Challenges and Strategy for Development of FNST: Blanket/FW & Tritium Fuel Cycle", Presentation at the meeting of the NAS Committee for a Strategic Plan for U.S. Burning Plasma Research February 26, 2018 at the General Atomics facility in La Jolla, California

CHAPTER 7

Conclusions and Future Modeling Work

A new methodology to better estimate tritium transport within the Outer Fuel Cycle of fusion systems was presented. It is based on the integration of detailed models, developed in COMSOL Multiphysics, on system-level, with the use of S-Functions blocks within the MATLAB/Simulink environment. Such tool is precious to evaluate the system dynamics and maintain an high degree of accuracy in sub-systems definition. Particularly, the model is being currently developed for the KO-HCCR ITER TBS and will be expanded to consider the KO-HCCR DEMO design as well. The goal of the numerical model is obtaining a more detailed representation of fusion components on system-level and calculate component inventories, tritium permeation to coolant and purge gas loop, tritium molecules partial pressure build-up in coolant and purge gas streams, and losses to buildings with better accuracy. The model is flexible and can be applied to any Test Blanket Module design, and represents a precious tool to be used for design, management and development of test blanket systems. Furthermore, as more detailed design of other fusion components is available, other detailed models can be incorporated in the system-level model.

In parallel, a numerical model describing the overall fuel cycle dynamics for typical fusion reactors was developed. This model includes several features that were not considered in previous researches, e.g. operational scenario, availability factor, random failures, etc. and is useful to identify the critical areas and components of the fusion fuel cycle and provide guidance for future development of fusion technology. The model was used to perform a comprehensive analysis to determine the physics and technology requirements to achieve tritium self-sufficiency and minimize the required tritium start-up inventory. We plan on using the model to estimate the effects of new ideas, concepts, and proposals which aim

to improve the fuel cycle design and to determine the performance of these key fuel cycle components in order to strategically plan fusion R&D. The model is applicable to any fusion reactor fuel cycle design.